Probing Non-covalent Interactions in Biomolecules and Materials: A Gas Phase Laser Spectroscopy Study of N-heterocyclic Aromatic Complexes

A thesis
submitted in partial fulfillment of the requirements
of the degree of
Doctor of Philosophy

By

Sumit Kumar

Roll No. 20093038

INDIAN INSTITUTE OF SCIENCE EDUCATION AND RESEARCH PUNE

(2014)

Dedicated to

My parents

and

My mentor

CERTIFICATE

Certified that the work incorporated in the thesis entitled "Probing Non-covalent Interactions in Biomolecules and Materials: A Gas Phase Laser Spectroscopy Study of N-heterocyclic Aromatic Complexes" submitted by Sumit Kumar was carried out by the candidate, under my supervision. The work presented here or any part of it has not been included in any other thesis submitted previously for the award of any degree or diploma from any other University or Institution.

(Signature)

Dr. Aloke Das
(Supervisor)

Date: 07/11/14

Declaration

I declare that this written submission represents my ideas in my own words and where other's ideas have been included; I have adequately cited and referenced the original sources. I also declare that I have adhered to all principles of academic honesty and integrity and have not misrepresented or fabricated or falsified any idea/data/fact/source in my submission. I understand that violation of the above will be cause for disciplinary action by the Institute and can also evoke penal action from the sources which have thus not been properly cited or from whom proper permission has not been taken when needed.

Date: 07/11/14

Sumit Kumar.

(Signature)

Sumit Kumar
(Name of the student)

Roll No. 20093038

Acknowledgements

Words are not enough for describing my deepest feelings of thanks and gratitude towards my mentor Dr. Aloke Das, for his enormous help, inspiring guidance and morale-boosting words of encouragement when they were needed most during the whole course of the research. Being the first student of my lab, I got all the valuable first-hand experience from my guide which enlightened the path of this journey. I thank him for his meticulous guidance and nurturing care, which helped me in developing my ability to understand research with all its nuances. He helped me to improve my writing skills and also showed the way to deliver presentations. I would like to thank him for his sustained enthusiasm, creative suggestions, motivations and exemplary guidance throughout the course of my doctoral research. Apart from the subject of my research, I have learnt a lot from him, which I am sure will be useful in different stages of my life. I solemnly submit my honest and humble thanks to him for shaping up my dreams into a reality. I offer my deepest gratitude to my guide who, as my academic father, enlightened my ability of thinking and nurtured me as an efficient researcher.

I would like to thank my Research Advisory Committee members Dr. Pankaj Mondal, Dr. Umakant Rapol, and Dr. Sudip Roy for their encouragement, support, valuable suggestions and motivation. Their timely valuable insights really helped me to improve myself.

I would like to thank Dr. Partha Hazra for giving me his valuable suggestions, help and encouragement.

I would like to thank the director of IISER Pune, Prof. Dr. K. N. Ganesh, for providing a very high quality research atmosphere within the hallowed premises of the institution. His gigantic efforts made IISER Pune a very reputed institute within a very short span of time. Within a few years, the institute achieved glorious success because of his painstaking efforts. His continuous efforts made the research quality in the institution far superior to many other institutions in the country.

I would like to thank my group members, Santosh, Jamuna, Neha and Ajay for their continuous support. I thank our new group member Kamal also. They are hard-working as well as helping in nature. I have enjoyed a lot while working with them. I have many sweet memories with them. They have helped me very much during my thesis submission period. I specially want to thank Partha da for sharing his knowledge with me. He helped me very

much during my starting period of my research. I would like to thank Ankita, Vedant, Golu, Sumit Bhatnagar, Murtaza, Deena Dayalan, Pranam and Aman for giving their company at different stages of my work.

I specially thank my friends, Abhigyan and Abhishek for encouraging me during last five years. I feel I had my best time with them, which will be always memorable for me. I want to thank my friends, Moumita, Biplab, Hrishikesh, Krishna, Raj kumar, Sohini, Sweta, Soumya, Arundhati, Tanmay and all my friends for giving me a lot of support without that I would not be able to stay away from my home for such a long time. They filled my life with excitement and joy.

I would like to thank Indian Institute of Science Education & Research (IISER), Pune for funding and Department of Science & Technology and UGC-CSIR for providing research fellowship.

Last but not the least; I want to thank my parents and elder brother for their continuous support throughout my educational career. This journey would not have been possible without their unstinting support. To my family, I extend my deepest thanks for encouraging me in all of my pursuits and inspiring me to follow my dreams. I always knew that they believed in me and wanted the best for me. Thank you for teaching me that my job in life is to learn, understand and be happy so that I could understand others and share my happiness with them as well.

I will really miss my lab, my guide, my lab members, my friends and IISER-PUNE in future……

Sumit Kumar

Table of Contents

List of Abbreviations

1C-R2PI	One color resonantly enhanced two photon ionization
2C-R2PI	Two color resonantly enhanced two photon ionization
Ar	Argon
aVDZ	aug-cc-pVDZ
aVTZ	aug-cc-pVTZ
B3LYP	Becke, three-parameter, Lee-Yang-Parr
BSSE	Basis set superposition error
DFT	Density functional theory
disp	Dispersion
EDA	Energy Decomposition Analysis
Es	Electrostatic
Ex	Exchange
He	Helium
IP	Ionization potential
LMO	localized molecular orbital
MP2	2nd order Moller-Plesset Perturbation Theory
NBO	Natural bond orbital
Pol	Polarization
Rep	Repulsion
RIDIRS	Resonant ion dip infrared spectroscopy
ZPE	Zero point energy
ΔE_e	BSSE corrected Binding Energy
ΔE_0	BSSE + ZPE corrected Binding Energy

List of Figures

List of Tables

SYNOPSIS

Non-covalent interactions are ubiquitous in life starting from its origin to function on day to day basis. These interactions are the backbone of the biomolecular structures and materials as well as biological recognition processes. Thus the quantitative understanding of the nature and strength of these weak interactions may lead to designing of efficient drugs and materials. These interactions can be classified into many different categories. However, the present thesis is mainly focused on hydrogen bonding (strong as well as weak) and π-stacking interactions.

The definition of hydrogen bonding has been reviewed from time to time by many scientists. Recently, Arunan and Scheiner with many other reputed scientists in the IUPAC committee have redefined the hydrogen bonding. Pimentel and McClellan have earlier defined hydrogen bonding and denoted it as; X-H…A, where X-H and A are hydrogen bond donor and acceptor, respectively.[1] There are two types of hydrogen bonding (a) conventional i.e., strong and (b) non-conventional i.e., weak hydrogen bonding interactions. In the case of conventional hydrogen bonding, both X and A are electronegative atoms i.e. N, O, and F. The examples of this hydrogen bonding are N-H…N, O-H…N, O-H…O, etc. In the case of non-conventional hydrogen bonding, the X atom is replaced by a less electronegative atom, carbon, while A is an electronegative atom i.e. O, N, and F. C-H…O, C-H…N, C-H…F hydrogen bonding interactions are examples of this category. Another type of non-conventional hydrogen bonding interaction is π-hydrogen bonding interaction and it is denoted by X-H…π, where the acceptor A is π-electron cloud of aromatic ring. The interaction energy associated with the conventional and non-conventional hydrogen bonding interactions are 5-15 kcal/mol and 2-5 kcal/mol, respectively.

π-stacking interaction is mostly dominated by dispersion forces although electrostatic contribution cannot be neglected. The dispersion interaction originates due to instantaneous dipole-induced dipole interaction, which is based on the fluctuation of electron density distribution in molecules.

Gas phase laser spectroscopy combined with quantum chemistry calculations provides unique information about the nature and strength of these weak intermolecular interactions governing the structures of biomacromolecules and materials. But the quantitative study of these weak interactions using a whole macromolecule is extremely challenging due to the

presence of innumerable interactions there. Thus the study of a whole macromolecule renders only average information about these interactions. Alternatively, as these macromolecules are very often formed by the repetition of a small monomeric unit through backbone of non-covalent interactions, molecular complexes of the building blocks at the dimeric or trimeric levels could be studied to mimic the interactions present in biomolecules and materials.

In fact, there are two popular computational databases, S22 and S66, of molecular complexes comprising of various types of non-covalent interactions. The complexes are classified into three categories; conventional hydrogen bonded complexes dominated by electrostatic interaction, dispersion dominated complexes, and mixed complexes stabilized by comparable magnitude of electrostatic and dispersion interactions. If we carefully look at the mixed complexes in the S22 database, we find that all the complexes except phenol dimer are primarily stabilized by X-H…π (C, N, O) hydrogen bonding interaction consisting of comparable amount of both electrostatic and dispersion energy. It has been demonstrated from both experiment and theory that the phenol dimer has a V-shaped herringbone geometry governed by a delicate balance among conventional hydrogen bond (O-H…O), CH…π, and π…π interactions.[2-8] Thus we have proposed that the phenol dimer is an exception in the class of the mixed complex and this dimer should be considered in a separate category of complex which we have named as "*Special class of mixed complex*".[9] There is a very subtle difference between the "*Special class of mixed complex*" and mixed complex. The "*Special class of mixed complex*" is stabilized due to interplay between conventional (strong) hydrogen bonding and significant magnitude of dispersion bound interactions. On the other hand, only one type of non-covalent interaction (π-hydrogen bonding) comprised of electrostatic and dispersion forces are present in the mixed complexes. Very recently, Hill et al. have renamed the "*Special class of mixed complex*" to "*Special mixed-influence*" (SMI).[10]

It is indeed the fact that the mixed contribution of the electrostatic dominated conventional (strong) hydrogen bonding and dispersion bound interactions govern the structures of the biomolecules and materials as well as biomolecular processes. The very specific shape of these macromolecules is due to interplay or competition between electrostatic and dispersion bound multiple types of non-covalent interactions. Thus gas phase spectroscopic studies of the "*Special class of mixed complex*" stabilized by multiple types of non-covalent interactions reveal unique information on the basic structures of biomolecules and material. But surprisingly, most of the molecular complexes reported in the literature are bound by one

class of non-covalent interaction i.e. strong hydrogen bonding (electrostatics dominated), π-hydrogen bonding (mixed complex) or π-stacking (dispersion dominated) while the gas phase study of the "*Special class of mixed complex*" is scarce in the literature. Thus we have studied selectively those molecular complexes stabilized due to the interplay or competition between multiple types of non-covalent interactions.

Furthermore, it is quite challenging to have accurate determination of the geometry and binding energy of this "*Special class of mixed complex*" from theory as well as experiment as these complexes are stabilized by significant amount of both electrostatic and dispersion interactions.[11-12] From theoretical point of view, study of these complexes is difficult because conventional DFT functionals do not include dispersion interaction while MP2 level of theory overestimates the dispersion interaction. Thus a theoretical method which considers both electrostatic and dispersion interactions with reasonable accuracy as well as handle the quantum calculation of these moderate size complexes within decent time frame has to be used for the study. It is also not straightforward to obtain sufficient amount of signal of this "*Special class of mixed complex*" compared to electrostatic dominated strong hydrogen bonded complexes or dispersion dominated π-stacked complexes in the gas phase spectroscopy experiment.

The aim of the thesis is the following.

1. To understand the interplay between conventional hydrogen bonding and dispersion interactions. Here *our new finding* is "*special class of mixed complex*", which represents the basic structural motifs of biomolecules and materials.

2. To investigate the competition between conventional (strong) hydrogen bonding and π-hydrogen bonding interactions. Can π-hydrogen bonding dominate over the conventional hydrogen bonding while both the possibilities are present in the molecular complexes? We have also asked the question whether the aromatic rings containing heteroatoms can act as effective π-hydrogen bond acceptor.

3. Selective synthesis of the π-stacked complex in the gas phase by suppressing the possibility of the formation of other possible structures of the complex held by conventional hydrogen bonding or π-hydrogen bonding interaction. We have also demonstrated here that hexafluorobenzene (HFB) is a unique building block for building π-stacked architecture in

biomolecules and materials. This π-stacked structural motif is extensively used as a supramolecular synthon for infinite columnar structure in crystal engineering.

4. To study the aromatic-aromatic interactions (dimeric as well as trimeric) in the aromatic side chains of proteins.

We have reported here the study of the complexes of indole with pyridine, furan, thiophene, HFB, imidazole and pyrrole in a supersonic jet. These non-covalently bonded weak complexes have been synthesized in the isolated gas phase using supersonic jet cooling technique. The structures of the complexes have been investigated using resonant two photon ionization (R2PI) and IR-UV double resonance spectroscopic techniques. The presence of single or multiple isomers of the complexes have been confirmed by UV-UV hole-burning spectroscopy. The electronic spectra of the complexes have been measured using the frequency doubled output of a tunable dye laser pumped by a Nd:YAG laser, while vibrational spectra have been recorded using Nd:YAG pumped IR OPO adopting resonant ion dip infrared spectroscopic (RIDIRS) technique. The spectroscopic data obtained from the isolated gas phase experiment are very much suitable to compare with the high level quantum chemistry calculation. The combined spectroscopic and theoretical study reveals the structures of the complexes formed in the experiment.

The thesis has been divided into six chapters and the content of every chapter has been described here briefly.

The 1st chapter deals with the introduction of the thesis. The importance, classification and various definitions of the non-covalent interactions are discussed. The motivation behind study of these interactions as well as the limitation of the study of non-covalent interactions in solution phase and solid phase has also been discussed. A brief review on the aromatic clusters previously studied using gas phase study and quantum chemistry calculations has also been reported. Moreover the aim and scope of the thesis are discussed.

In chapter 2, I have elaborately discussed the experimental setup as well as various spectroscopic techniques used in the present study. The principle of the supersonic jet cooling along with synthesis of the clusters in the gas phase has been described in brief. I have also briefly explained various computational methods as well as different types of calculations used in the study.

In chapter 3, I have reported the subtle interplay between conventional hydrogen bonding and dispersion interactions by studying the complexes of indole and pyridine.[9] Here, our primary goal is to perform the spectroscopic investigation to study the special class of mixed complexes where the geometries of the complexes are determined by the subtle balance between conventional hydrogen bonding as well as dispersion interactions. We have investigated the structure of indole…pyridine dimer in a supersonic jet and reported that the geometry of indole…pyridine dimer is stabilized by conventional hydrogen bonding (N-H…N) as well as CH…π and π…π interactions. The indole…pyridine dimer falls in the category of *special class of mixed complex.*

Competition between conventional hydrogen bonding and π-hydrogen bonding interactions has been reported in chapter 4. We have particularly chosen N-H···π hydrogen bonding for the study because this specific interaction show a wide variation in the interaction energy depending on the molecular systems involved. Sometimes this interaction can have strength comparable to a conventional hydrogen bond. Thus, we have asked the question "can π-hydrogen bonding interaction dominate over conventional hydrogen bonding interaction while there are both the possibilities?" To answer this question, we have studied indole···furan and indole…thiophene dimers, where both π-hydrogen bonded (N-H···π) and N-H···O/N-H…S bound isomers can exist in the experiment.[13-14] Interestingly, we have observed only N-H…π bound isomer in case of both the dimers. Thus these studies demonstrate that "π-hydrogen bonding can win over conventional hydrogen bonding interaction". Further for the improvement of understanding of the effect of heteroatoms on π-hydrogen bonding interactions and to check whether aromatic rings containing heteroatoms can act as an effective π-hydrogen bond acceptor. We have compared the results obtained from the study of complexes of indole with furan, thiophene and pyridine. The study shows that N-H…π bound structure is not formed between indole and pyridine but the similar structure is observed for indole…furan and indole…thiophene dimers.[13-14] It was concluded by Sherrill and coworkers from their theoretical study of benzene...pyridine dimer that aromatic rings containing heteroatoms are poorest π-hydrogen bond acceptors.[15] But our study demonstrates that five membered aromatic heterocycles in contrast to pyridine, a six membered heterocycle, are favorable π-hydrogen bond acceptors.

In chapter 5, we have reported π-stacking interactions by investigating the structure of indole...hexafluorobenzene (HFB) dimer.[16] The gas phase study of the π-stacking interaction is very much limited in the literature because it is quite difficult to synthesize the π-stacked dimer when other competitive non-covalnt interactions are present in the molecular systems. Here, we have suppressed the possibility of formation of π-hydrogen bonded conformer by taking perfluorinated benzene i.e, HFB and hence observed exclusively π-stacked dimer. The observed π-stacked dimer has a unique configuration where the center of the HFB unit is aligned with the center of the shared bond of the indole moiety. This π-stacking interaction which is very often present between aromatic residues (tryptophan and phenylalanine) in proteins, which has not been observed earlier in the gas phase experiment by studying indole...benzene dimer. Further the study of π-stacked dimers containing HFB is particularly interesting because HFB has unique properties in efficient structural control in crystal engineering, medicinal chemistry and biological recognition. The study of this dimer provides useful insight in designing unnatural proteins having strong π-stacking interaction between the tryptophan and phenylalanine residues.

The 6th chapter describes detailed understanding about aromatic-aromatic interactions in the aromatic side chains of proteins.[17-18] These interactions play a crucial role in the stabilization of the specific structures of proteins as well as biological recognition processes. Burley et al. and Esteban et al. have analyzed high resolution crystal structure of proteins and reported that aromatic-aromatic interactions are present in about 50% of the protein.[19-20] Thus we have studied indole…imidazole dimer and indole…$(pyrrole)_2$ trimer, which mimic aromatic-aromatic interaction (dimeric and trimeric) between the aromatic side chain of protein because indole and imidazole are present in the aromatic side chains of tryptophan and histidine amino acids, respectively whereas pyrrole is present in the indole itself. Further motivation behind study of indole…$(pyrrole)_2$ trimer can be highlighted from the review done by Steiner and Koellner on 593 high resolution crystal structures of proteins.[21] They have reported that tryptophan is the most effective π-hydrogen bond acceptor among four amino acid aromatic residues in proteins. But the gas phase studies for the quantitative determination of π-hydrogen bond accepting strength of indole are scarce in the literature whereas in case of indole…$(pyrrole)_2$ trimer, indole is acting as both hydrogen bond donor as well as acceptor. We have found V-shaped structure of the dimer, primarily held by strong N-H···N hydrogen bond and the trimer has a triangular asymmetric cyclic structure. The stability

of the dimer is governed by subtle balance among C-H···π, weak present π-stacking and strong hydrogen bonding interactions. This dimer falls in the category of the "*special class of mixed complex*" which comprises strong hydrogen bonding interaction as well as significant amount of dispersion dominated interactions. The observed trimer is stabilized by three N-H···π and one C-H···π interactions.

List of publications:

1. **Sumit Kumar**, Santosh K. Singh, Camilla Calabrese, Assimo Maris, Sonia Melandri* and Aloke Das*, Structure of saligenin: Microwave, UV and IR spectroscopy studies in a supersonic jet combined with quantum chemistry calculations, *Phys. Chem. Chem. Phys.* **2014**, *16*,17163.

2. S. K. Singh; **Sumit Kumar** and Aloke Das*, Competition between n→π* and conventional hydrogen bonding (N-H…N) interactions: an ab initio study of the complexes of 7-azaindole and fluorosubstituted pyridines, *Phys. Chem. Chem. Phys.* **2014**, *16*, 8819. (**appeared as a front inside cover page**)

3. **Sumit Kumar** and Aloke Das*, Observation of exclusively π-stacked heterodimer of indole and hexafluorobenzene in the gas phase, *J. Chem. Phys.* **2013**, *139*, 104311.

4. **Sumit Kumar**, Ankita Mukharjee and Aloke Das*, Structure of Indole···Imidazole Heterodimer in a Supersonic Jet: A Gas Phase Study on the Interaction between the Aromatic Side Chains of Tryptophan and Histidine Residues in Proteins, *J. Phys. Chem. A* **2012**, *116*, 11573.

5. **Sumit Kumar** and Aloke Das*, Effect of acceptor heteroatoms on π-hydrogen bonding interactions: A study of indole...thiophene heterodimer in a supersonic jet, *J. Chem. Phys.* **2012**, *137*, 094309.

6. **Sumit Kumar** and Aloke Das*, Mimicking trimeric interactions in the aromatic side chains of the proteins: A gas phase study of indole...(pyrrole)2 heterotrimer, *J. Chem. Phys.* **2012**, *136*, 174302.

   (Selected for Virtual Journal of Biological Physics Research, Vol. 23, May 15, 2012, Section: Protein Conformational Dynamics/Folding)

7. **Sumit Kumar**, Vedant Pande, and Aloke Das*, π-hydrogen bonding wins over conventional hydrogen bonding interaction: A jet-cooled study of indole...furan heterodimer, *J. Phys. Chem. A* **2012**, *116*, 1368.

8. **Sumit Kumar**, Indu Kaul, Partha Biswas, and Aloke Das*, Structure of 7-azaindole...2-fluoropyridine dimer in a supersonic jet: Competition between N-H...N and N-H...F interactions, *J. Phys. Chem. A* **2011**, *115*, 10299.

9. **Sumit Kumar**, Partha Biswas, indu Kaul, and Aloke Das*, Competition between hydrogen bonding and dispersion interactions in indole-pyridine dimer and (indole)2-pyridine trimer studied in a supersonic jet, *J. Phys. Chem. A* **2011**, *115*, 7461.

10. **Sumit Kumar**, Santosh K. Singh, Jamuna Vaishnav, and Aloke Das*, Effect of methyl substitution in the π-hydrogen bonded complexes of indole with methylated benzenes: Interplay among electrostatic, dispersion interactions and steric repulsion, (Manuscript under preparation).

11. **Sumit Kumar and Aloke Das,** N-heterocyclic aggregation (Invited perspective from ***Phys. Chem. Chem. Phys.* (2014)**, (Manuscript under preparation).

1. Introduction

1.1. Significance of non-covalent interactions

The realm of non-covalent interactions is spread all over the world, starting from the living species to non-living things.[22-24] These interactions are extremely important as well as responsible for the existence of life on earth, which is mainly possible due to the presence of water in the liquid state. Water remains in the liquid state in ambient conditions because of the presence of multiple hydrogen bonding interactions.[25-26] DNA, the origin of life, is also formed by the association of the nucleic acid bases through hydrogen bonding and π-stacking interactions. These non-covalent interactions are equally important for specific structures of other biomolecules and materials.[24]

In biology, these interactions are key factors for molecular recognition processes such as protein-protein, protein-DNA, drug-DNA interactions. Many other biological processes also depend on these interactions. As for example, we can mention about antigen-antibody interaction,[27] DNA base pair formation,[28] stability of ternary structure of double helix DNA,[29] reversible as well as targeted attack of hormones to the cell membrane, polypeptide chain formation of hemoglobin molecule, distortion of abnormal shaped hemoglobin, etc.[28]

In material science, these non-covalent interactions are backbone of supramolecular assembly, surface adsorption and reactivity, molecular crystal packing, self assembly of nano-materials and catalyst based organic chemical reactions.[30-40] The importance of these interactions can be easily realized from the definition of supramolecular chemistry by J –M Lehn, D. J. Cran and C. D. Pedersen who stated the following: "*the supramolecular chemistry is the science of non-covalent interactions*".[41]

A few selected examples highlighting the significance of the non-covalent interactions are discussed elaborately in the following sections.

1.1.1. Non-covalent interactions in biology

Non-covalent interactions play a major role in the structural stability of DNA and proteins. In DNA, there is selective base pairing between adenine and thymine through double hydrogen bonding (N-H…O and N-H…N) as well as guanine and cytosine through triple hydrogen

bonding (N-H…O, N-H…N, and N-H…O). This base pairing governs the sequences of the counter DNA strands. Apart from the base pairing interactions, the structure of DNA is also stabilized by van der Waals interaction between the bases which is called base stacking. In the case of protein, there are four distinct levels of structure; primary, secondary, tertiary and quaternary structures. The secondary structures of proteins are mostly stabilized by C=O…H-N hydrogen bonding interactions. Some quaternary proteins such as insulin, hemoglobin form a ball-shaped structure whereas keratin forms coiled alpha helical structure. These structures are stabilized by multiple hydrogen bonding and stacking interactions.

π-stacking interactions between aromatic rings have also significant contribution in biological processes. In the case of drug-DNA intercalation, the drug (for example, dopamine) intercalates inside the two base pairs of DNA through minor side. The stabilization force in the intercalation is mostly π-stacking. The distance between two base pairs increases in order to accommodate the drug. Some other examples of π-stacking interaction are as follows: aggregation of porphyrin,[42] activity of anti-tumor drug delivery[43], stability and loading capacity of thermosensitive polymeric micelles for chemotherapeutic drugs,[44] drug-drug interactions in human cytochrome P450 2E1[45], inhibition of the Bcl-2-Bak protein-protein interaction[46] etc.

1.1.2. Non-covalent interactions in materials

Non-covalent interactions have major contribution in self-assembly, selectivity in inclusion compounds (lattice-as well as cavity-type clathrates), solid-state reactions and packing of molecules in crystals. These interactions also govern stereoselectivity, catalytic enantioselectivity in chemical reactions and have a decisive role in several solid-state photoreactions and topochemical polymerization, etc. A few selected examples are mentioned in the following.

Hydrogen bonding has significant importance in the packing of several small sized crystals.[47-49] For example, crystal structures of benzoic acid derivatives,[50] 2'-diemethylgriseofulvin, and griseofulvin,[51] derivatives of uracil monohydrate,[52] etc are stabilized by strong hydrogen bonding interaction. This interaction also helps in stabilization of ferrocene-containing compounds.[53,54] Hydrogen bonding interactions are involved in fullerene convex surface,[55] polymer structure control, organic material design based on polymer crystal engineering,[56]

crystal structure design for topochemical polymerization of 1,3-dienes and di(4-methoxybenzyl)muconate,[57] determination of the structure of clathrates such as molecular chameleon, polycatenanes, oligocatenanes.[58] π-stacking interaction governs the influence of molecular structure on the photoluminescence of 2-methyl benzimidazolium picrate,[59] stabilization of crystals between poly(2-vinyl pyridine) and palladium pincer surfactants.[60] Complexation of Human Dysferlin inner DysF domain, supramolecular assemblies of pyrene-β-cyclodextrin, and the catalytic property of (2-PhInd)(2)Zr elastomeric polypropylene[61] are also stabilizied by stacking interaction. This interaction helps in defining conformation of phenylacetylene macrocycles, the stretching strength of Kevlar,[62] the catalytic formation of elastomeric polypropylene,[61] and several other properties of supramolecular systems.[63-69] The stacking interaction has a significant role in detection of polycyclic aromatic hydrocarbons and influences the conductivity as well as electronic and optical properties of some materials.

Both hydrogen bonding and π-stacking interactions help in host-guest complexation such as encapsulation of guest in organic host molecules, cyclodextrins, cucurbit[n]urils, calixarenes, dendrimers, and cavitands.[70] For example, these interactions govern the guest-induced capsular assembly of calyx-5-arenes and diastereoselectivity of a host-guest complex.[71-72]

1.2. Classification of non-covalent interactions

The importance and applications of these interactions in a large number of fields create a lot of interest among scientists to know about the origin and strength of these interactions. First, it will be informative to compare the strength of these non-covalent interactions with that of covalent bond.

A covalent bond is a chemical bond that involves sharing of electron pairs between atoms and holds multiple atoms together as molecules. Energy of covalent bonds is in the range of 50-200 kcal/mol while generally the strength of the non-covalent interactions is about 1-15 kcal/mol. The importance of non-covalent interactions arises from the ease of formation and breaking, which is only possible because the associated energy is very less as compared to the covalent bond. For example, coiling-uncoiling of DNA as well as folding-unfolding of proteins is possible due to very low energy associated with these processes.

Generally, different types of non-covalent interactions are present between two interacting units in a molecular system. But if we carefully look at the structures of several biomacromolecules e.g. DNA, RNA, proteins and materials, mostly two types of non-covalent interactions are present.[24,73] These interactions are hydrogen bonding and π-stacking interactions.

1.2.1. Hydrogen bonding

The hydrogen bonding could be considered as a special class of dipole-dipole interactions. This bonding is mostly short range interaction and the interaction energy generally varies with the reciprocal of the cube of the distance between the two atoms involved in the hydrogen bonding.

Although the hydrogen bonding was discovered almost a century ago, it is still a topic of interesting scientific research. The reason under this long-lasting interest lies in its ever-growing importance in mineralogy,[74] material science, crystal engineering,[75-79] organic chemistry,[30-40] supramolecular chemistry,[80-84] biochemistry,[73,85-90] and medicinal chemistry.[91-94] The development in the understanding of the hydrogen bonding interaction has substantially influenced the growth of these research areas. Thus we will look at here the sequential growth in the concept of this non-covalent interaction.

1.2.1.1. Various definitions

The journey of the hydrogen bonding started from very beginning of the 1900's when Werner and Hanstzsch used the term Nebenvalenz (in German, "secondary or weak valence") to define the binding condition in the ammonium salts.[95] In 1913, intramolecular hydrogen bonding "Innere Komplexsalzbildung" is introduced by Pfeiffer[96] in the case of 1-hydroxyanthraquinone. Nearly at the same time, Moore and Winmill[97] have investigated the states of amines in the aqueous medium and proposed the word "weak union" while explaining the basic properties of trimethylammonium hydroxide. According to Pauling, Latimer and Rodebush[98] (1920) introduced the term "hydrogen bond" for the first time while discussing the structure of ammonium hydroxide.[98] In his book '*The Nature of Chemical Bond*', Pauling[99] nicely explained hydrogen bonding and concluded that "this bonding has to be electrostatic as it cannot be chemical (covalent) in nature". Thus the concept of hydrogen bonding is composed of the two words "electrostatic" and "chemical".[100] In 1960, Pimentel

and McClellan[1] proposed a very authoritative definition. They stated that "*A hydrogen bond is said to exist when (a) there is evidence of a bond formation (association or chelation), and (b) there is evidence that this bond specifically involves a hydrogen atom already bonded to another atom*."[1] It is noticeable that the definition is made without maintaining any restriction on the chemical nature of donors and acceptor, geometrical orientation and bond formation energy.[101] Thus, as per this definition, the hydrogen bonding can exist between any group X-H and any atom A in the case of intra and intermolecular hydrogen bonding i.e., in the same or different molecule. The hydrogen bonding can be denoted as;

X-H…A

Where X and A can be any atom (C, N, O, P, As, etc) or group. Here X-H and A are the hydrogen bond donor and acceptor, respectively.

Jeffrey and Saenger[102] have classified the hydrogen bonding into two categories, "strong" and "weak" on the basis of this interaction energy and later this classification is expanded by Jeffrey.[103] According to Jeffrey,[103] hydrogen bonding interaction can be divided into three categories; strong, moderate and weak.

Further classification of hydrogen bonding is performed following the definition provided by Linus Pauling based on the electronegativity of "donor" and "acceptor" groups.[104] According to this definition, conventional and non-conventional hydrogen bonding interactions are classified.

Recently, Arunan and Scheiner with many other reputed scientists in the IUPAC committee have redefined the hydrogen bonding.[100] The definition states that "*the hydrogen bond is an attractive interaction between a hydrogen atom from a molecule or a molecular fragment X–H in which X is more electronegative than H, and an atom or a group of atoms in the same or a different molecule, in which there is an evidence of bond formation.*"[100]

1.2.2. Conventional hydrogen bonding

In the last section, hydrogen bonding is already defined as X-H…A, where X-H and A are hydrogen bond donor and acceptor, respectively. In the case of conventional hydrogen bonding, both X and A are electronegative atoms i.e. N, O, and F. The examples are N-H…N, O-H…N, O-H…O, etc. This interaction falls in the category of strong hydrogen bonding which is dominated by electrostatic interaction. The interaction energy associated

with this bonding is in the range of 5-40 kcal/mol. The most versatile example exhibiting strong or conventional hydrogen bonding interaction is water.

1.2.3. Non-conventional hydrogen bonding

In this case, generally the X atom in X-H…A is replaced by a less electronegative atom, carbon, while A is still a traditional electronegative atom i.e. O, N, and F. C-H…O, C-H…N, C-H…F are examples of this non-conventional hydrogen bonding interaction. This class of interaction belongs to weak non-covalent interaction and energy associated with this is 2-5 kcal/mol. This non-conventional hydrogen bonding interaction is widely present in the crystal structures of materials. This interaction has weak electrostatic properties.

Another type of non-conventional hydrogen bonding interaction is denoted by X-H…π, where the acceptor A is π-electron cloud instead of an electronegative atom and X can be O, N, C etc. This non-covalent interaction is called π-hydrogen bonding interaction which is weaker than the conventional hydrogen bonding interaction. The energy associated with this interaction is generally less than 5 kcal/mol. The strength of the π-hydrogen bonding interaction varies depending on the polarity of the X-H group (hydrogen bond donor) as well as π-electron density of the acceptor. In this case, the interaction occurs through dipole-induced dipole forces as the hydrogen bond acceptor could be non-polar i.e. benzene. T-shaped benzene dimer held by C-H…π interaction is a well-known example for π-hydrogen bonding interaction. It is interesting to note that electrostatic as well as dispersion interaction has significant contribution to the stability of the π-hydrogen bonded complexes.

It has been demonstrated from both experimental and theoretical studies that dispersion forces contribute significantly in the stability of π-hydrogen bonding interaction.[13,18,24,105-107] As for example, Shibasaki *et al.* have studied the magnitude and nature of C-H…π interactions in benzene-X (X=acetylene, ethylene, methane, etc) and reported that π-hydrogen bonding consists of both electrostatic and dispersion interactions.[107]

1.2.4. π-stacking interaction

π-stacking interaction is mostly dominated by dispersion forces although electrostatic contribution cannot be neglected. The polarizable nature of the delocalized π-electrons is

responsible for the dispersion interaction.

Dispersion interactions are ubiquitous spanning all areas of science and technology.[108-114] This interaction arises in non-polar molecules due to creation of instantaneous (transient) dipole or multipoles in molecules. This instantaneous dipole is generated due to the fluctuation in the position of electrons in neutral/non-polar molecules. The fluctuation in position of electrons causes the generation of differential electron density. This transient dipole induces the rearrangement of electron density in another non-polar molecule resulting induced transient dipole moment. These two dipoles are opposite in sign and generate attractive force which lowers the potential energy of the pair. In this way, the pair of molecules is always correlated in a direction and the average of instantaneous dipole moments never goes to zero. This instantaneous dipole-induced dipole interaction is termed as dispersion interaction or London dispersion interaction.

The dispersion interaction energy depends upon the polarizability of both the molecules participating in the interaction. The expression for the dispersion energy provided by Fritz Wolfgang London is the following.[115]

$$E_{\text{disp}} = -\frac{3}{2}\left(\frac{I_A I_B}{I_A + I_B}\right)\frac{\alpha_A \alpha_B}{R^6} \qquad (1.1)$$

Here, I_A and I_B are ionization potentials of individual molecules. α_A and α_B are polarizability of individual molecules. The dispersion interaction energy is inversely proportional to the sixth power of distance between two dipoles. Thus, the variation of the interaction energy with distance is faster as compared to the hydrogen bonding and the energy diminishes with the increase of the distance.

This interaction also depends upon physical properties e.g. surface area of molecules. Larger the surface area, larger will be the attractive forces between two molecules and this results increase in the interaction energy. For example, there is a continuous increase in the boiling point with the increase in surface area, going from benzene, naphthalene to anthracene. The boiling points for benzene, naphthalene, and anthracene are 353 K, 490K, and 613 K, respectively. Gonzalez and Lim[116] have performed quantum chemistry study of dimers of benzene, naphthalene, and anthracene. They have found that the parallel displaced (C_{2h})

dimers are mostly dispersion dominated and their binding energies also follow the same trend as the boiling point. The most popular example of π-stacking interaction is base-stacking in DNA. This interaction is also very important in materials, crystal engineering etc.

1.3. Motivation behind the study of the non-covalent interactions

We have already discussed about the importance of the non-covalent interactions present in biomolecules and materials in section 1.1. Different types of non-covalent interactions such as conventional hydrogen bonding, π-hydrogen bonding, π-stacking etc. govern the shape and size of the molecules in materials and biology. Thus understanding of the nature and strength of these interactions are helpful for determining the stereoselectivity in the formation of coordination compounds, conformational equilibrium and enantioselectivity of complexes and selective host-guest interaction. For example, the enantioselectivity in the transfer hydrogenation of aromatic carbonyl compounds catalyzed by chiral η6-Arene-Ruthenium(II) complexes,[117] selective interactions of the aromatic cavity of rigid calix[4]arenes with guests containing acidic CH_3 and CH_2 groups of CH_3CN, CH_2Cl_2, CH_3NO_2, $ClCH_2CN$ and $CH_2(CN)_2$ [118-119] etc. are governed by these non-covalent interactions. Various complexations in the supramolecular chemistry are also held by these interactions. So the study of these interactions can generate profound knowledge in the growth of different shape and size of crystals according to our interest. For example, perfluorobenzene and benzene as a precursor in crystal growth give infinite column like structure due to π-stacking while pure benzene provides herringbone arrangement in the crystal due to C-H…π hydrogen bonding. Thus the arrangement of molecules in the crystal structures is influenced by specific type of interaction present there.

These interactions also play a key role in chemical and biological recognition processes e.g. antigen-antibody, receptor-ligand, DNA-protein, sugar-lectin, RNA-ribosome interactions. These molecular recognition processes are specific interactions between two or more molecules through various non-covalent interactions. The study of the nature and strength of these non-covalent interactions is very significant in understanding the activity of the biological molecules and materials. A few examples are mentioned below.

Kryger and coworkers have designed the drug E2020 (Aricept, donepezil hydrochloride) for the cure of Alzheimer disease on the basis of the binding affinity study between

acetylcholinesterase inhibitor and the drug Aricept.[120] They have pointed out that π-stacking, O-H…π, and other non-covalent interactions are responsible for high binding affinity and selectivity of the drug with the inhibitor. The selective complexation between 7-methylated-GTP (Guanosine-5'-triphosphate) and a messenger RNA 5′-cap-binding protein occurs through stacking interaction.[120] Similarly the complex of d-galactose and d-glucose binding proteins is held by stacking interaction.[121] Another very interesting example of rational drug designing is thrombin inhibitor drug, which counters for blood loss in the body i.e. provides protection against thrombotic disorders.[122] This drug designing is based on π-hydrogen bonding and stacking interaction between the aromatic rings.

The aforementioned examples show that the investigations aimed for quantitative understanding of the non-covalent interactions responsible for the molecular recognitions are of paramount importance for improved drug design. This understanding is also indispensable for synthesis of advanced functional materials.

There are different approaches to study these non-covalent interactions to understand the structural and energetic details of materials, biomolecules and biomolecular processes. These studies can be performed through various spectroscopic techniques, theoretical calculations, mining of crystallographic databases etc. The spectroscopic study can be done in solution phase or in gas phase. Several reports in order to study the non-covalent interactions in various complexes using solution phase spectroscopy and crystallographic study are mentioned below.

1.4. Solution phase study of the non-covalent interactions

There are extensive reports on spectroscopic studies of non-covalent interactions in solution phase. As the detailed description of these studies is beyond the scope of the thesis, it has been discussed here very briefly.

The early indication of hydrogen bonding has been reported by Gordy in 1939.[123] He has performed IR spectroscopy to find the evidence of the C-H…O as well as C-H…N hydrogen bonding interactions of chloroform and bromoform with various solvents such as pyridine, picoline, piperidine, ketones, esters, ethers and amines.[123] In 1963, Allerhand and Schleyer have reported a red-shift of 100 cm^{-1} in the C-H stretching vibration in case of substituted

acetylenes (X-C≡C-H, X=Br, F) with pyridines in CCl_4 solution due to the formation of strong hydrogen bonding between activated C-H groups in alkynes and nitrogen of pyridines.[124] In 1974, Green has contributed a review on C-H…O interaction in various molecular systems.[125] Later, Delaat and Ault have performed IR spectroscopic investigation of C-H…O hydrogen bonding in acetylene-water, acetylene-dimethyl ether and acetylene-acetone systems.[126]

The initial study on π-hydrogen bonding was reported by Wulf et al. in 1936.[127] They have measured the IR absorption spectra for ortho substituted phenols in dilute CCl_4 solution and reported O-H…π hydrogen bonding in case of ortho-phenyl phenols.[127] Intramolecular O-H…π hydrogen bonding has been reported in o-ethynylphenol and o-allylphenol by Prey and Berbalk (1951), Baker and Shulgin (1958), respectively. Further Schleyer et al. have reported O-H…π hydrogen bonding in but-3-yne-1-ol, but-3-ene-1-ol, and 2-cyclopropyl-ethan-1-ol.[128] Joeshten and Schaad have completed several results reported in 1960s in their book on hydrogen bonding.[129] In one of the study performed in 1966, Yoshida and coworkers reported intermolecular O-H…π hydrogen bonding by measuring the υ_{OH} shift in the complexes of phenol with different π-acceptors such as benzene, toluene, mesitylene, naphthalene, ferrocene, cyclopentadiene, etc in CCl_4.[130] Chardin et al. have performed IR spectroscopy of 4-fluorophenol with a series of ortho substituted pyridines.[131] They reported the formation of O-H…N hydrogen bonding between pyridine and 2-tert-butylpyridine. In the case of 2,6-di-tert-butylpyridine and 2,6-di-tert-butyl-4-methylpyridine, formation of O-H..π hydrogen bonding is reported due to unavailability of N atom of pyridine to make O-H…N hydrogen bonding as nitrogen is sterically hindered by bulky substituents at both the ortho positions.

Recently, Boxer and co-workers have studied X-H…π interaction in the complexes of indole, phenol and thiophenol with a number of hydrogen bond acceptors such as benzene, toluene, p-xylene, mesitylene, chlorobenzene, o-dichlorobenzene and m-dichlorobenzene in CCl_4 solution by measuring the IR shift in X-H vibrational frequencies and vibrational stark effect on X-H…π interactions.[132] They have reported that the red-shift in X-H vibrational frequencies increases with the increase in π-electron cloud on the aromatic ring.[132] The red-shift in X-H vibrational frequencies and stabilization energies increases with increase in the

applied electric field. It is also concluded that the strength of the electrostatic interactions of X-H…π interaction decreases in the order of O−H > N−H > S−H.[132]

1.5. Crystallographic studies of various non-covalent interactions

Generally, crystallographic studies are performed for the detailed characterization of the three-dimensional structures of biomolecules like proteins, DNA as well as materials, which are stabilized by various non-covalent interactions. As the literature on the crystallographic studies is vast, only brief description of the early stage investigation of these non-covalent interactions in crystals has been presented here.

Hydrogen bonded crystals are pioneered by Huggins in 1936 in the context of organic compounds in supramolecular chemistry.[133] He reported O-H…O hydrogen bonding patterns in the crystals of aliphatic acids such as oleic acid, stearic acid, formic acid and acetic acid.[133] He has also reported C–H···N hydrogen bonding in the crystals of hydrogen cyanide. In 1936, Robertson and Woodward solved the O-H…O hydrogen bonded crystal structure of oxalic acid dihydrate.[134] Later Dunitz and Robertson analyzed the O-H…O hydrogen bonded crystals of acetylene dicarboxylic acid dihydrate and diacetylene dicarboxylic acid dehydrate.[135] In 1998, Dunitz revisited the topology of the hydrogen bond network in view of the supramolecular concepts and concluded that the crystal packing with hydrogen bonds O–H···O, O–H···N, N–H···O and N–H···N is the basis of crystal engineering.[136-137]

The C-H···O hydrogen bonding in crystals was introduced by Sutor in 1962.[138] He performed systematic study of crystals of purine and pyridine.[138] He confirmed the existence of C-H…O hydrogen bond interaction in caffeine ($d_{C\text{-}H\ldots O}$ = 2.12 Å), theophylline ($d_{C\text{-}H\ldots O}$ = 2.25 Å), and uracil ($d_{C\text{-}H\ldots O}$ = 2.20 Å).[138] Many other analyses have been performed to know the proximity of this weak hydrogen bond interaction. In 1982, Taylor and Kennard have studied 113 high quality organic crystal structures using neutron diffraction.[139] From these exhaustive studies, they have concluded that the geometrical characteristics for the short C-H…O contacts (~ 2.4 Å) are very similar to those of O-H…O and N-H…O strong hydrogen bond interactions. π-hydrogen bonding in crystals is pioneered by Atwood and Suzuki.[140-142] They reported aromatic rings form O-H…π and N-H…π hydrogen bonding with water and ammonia, respectively.[140-142] Malone et al. (1997) and Braga et al. (1998) have performed CSD analysis

of X-H…Ph (X=C, N, O) hydrogen bonds in order to understand the geometrical variability and bond strength of π-hydrogen bonds found in organic and organometallic crystals.[143-145] They have reported that the sequence of donor strength O-H > N-H > C-H.[143-145] Nishio and co-worker have extensively studied C-H…π hydrogen bonded crystals to understand the geometrical orientations of the π-hydrogen bonding in biology as well as materials.[82,84] They reported C-H…π hydrogen bonding in various crystals covering every kind of C-H donor (sp, sp^2, and sp^3-C-H) with various π-acceptors (double bond, triple bond, phenyl, polycyclic aromatic, hetero-aromatic groups, cyclopentadienyl group, fullerene etc).[38] Desiraju and co-workers have analyzed several crystal structures and reported weak hydrogen bonding interactions such as C-H…N, C-H…O, etc.[50,80,104,146-149] They have reported that weakly activated groups such as C-H group can also act as a hydrogen bond donor in molecular and biomolecular systems.[146] They have also reported the several supramolecular synthons having multiple interactions such as O-H…O, N-H…O, C-H…O, etc, which lead to the formation of crystals.[147-149]

The molecular conformations of biological macromolecules such as protein and nucleic acids (DNA, RNA) are primarily determined by crystallography. The double-helical structure of DNA stabilized by hydrogen bonding and π-stacking interactions was reported through crystallographic studies.[28] Trublood, Shefter and Sundaralingam have observed C-H…O hydrogen bonding in crystal structure of nucleobase such as adenosine 3-phosphate dihydrate.[150-151] In 1965, Ramachandran and co-workers have recognized C-H…O and N-H…O hydrogen bonding in crystal structure of collagen and polyglycine.[152-153] McPhail and Sim have reported O-H…π hydrogen bonding in case of cyclic peptides.[154] Baker and Hubbard as well as Jeffrey and Saenger have reported strong hydrogen bonding such as N-H…O, O-H…O, etc in proteins.[155-156] Burley and Petsko, Hunter and co-workers, Lanzarotti et al., have analyzed high resolution crystal structures of proteins and reported aromatic-aromatic interactions between the aromatic side chains of proteins, which are held by hydrogen bonding and π-stacking interactions.[19,157-162] Apart from these groups, Baney, Chakrabarti, Lee, Balaram and many other scientists have also reported aromatic-aromatic interactions in proteins.[19,163-167] Recently, Janiak, Ernst, Desiraju, Nishio, Weck and Zaworotko have highlighted the importance of hydrogen bonding in stabilization of crystals of biomolecules and materials.[45-46,101,168-177]

The study of the non-covalent interactions in the solution and solid phases are very important and useful, but it has certain limitations in the context of molecular level understanding of these interactions. These limitations are discussed in the following section.

1.6. Limitation of the study of the non-covalent interactions in solution and solid phases.

Generally, the study of the non-covalent interactions in solution and solid phases are performed in bulk. In the case of the X-ray crystallography, three dimensional structures of the molecules held by various types of non-covalent interactions are determined with high accuracy. But quantitative information on the physical nature and strength of individual interaction and interplay among different types of non-covalent interactions cannot be obtained using this approach. Similarly, molecular level understanding of these weak interactions in the solution phase using electronic, IR and Raman spectroscopy is not possible due to collisions of molecule of interest among themselves as well as with solvents. Very often, the desired information is lost due to spectral broadening in the solution phase. To obtain in-depth understanding of these non-covalent interactions, it is required to study molecular complexes at the dimeric or higher order level. But it is difficult to stabilize the dimeric or higher order complexes of the building blocks of biomolecules and materials in the solution phase at room temperature while the whole macromolecules are stabilized due to presence of hundreds of non-covalent interactions. On the other hand, dimeric or higher order molecular complexes can be stabilized in the isolated gas phase environment, where there will be no collisions or perturbation with the neighboring molecules and solvent. This isolated gas phase environment can be created using supersonic expansion technique where the internal degrees of freedom of molecules are cooled to a few Kelvin. The ultracold condition of the supersonic jet not only stabilizes the weakly bound complexes but also provides high resolution electronic spectra of molecules and complexes. The principle of the supersonic expansion has been discussed in detail in the method section in chapter 2. In fact, isolated gas phase experiment and quantum chemistry calculations go hand in hand. Thus the results obtained from gas phase experiment match very well with those from quantum calculations. It also becomes possible to check the accuracy of the theoretical method by comparing the theoretical data with the experimental ones.

1.7. Brief review on aromatic complexes studied using isolated gas phase spectroscopy and quantum chemistry calculations.

A brief review on micro-solvated aromatic complexes and aromatic-aromatic complexes studied in the supersonic jet has been reported in the following. Although the study of the aromatic complexes presented in this thesis mostly deals with aromatic-aromatic complexes, it is worth providing here a very brief report on the studies of a few representative micro-solvated aromatic complexes as well.

1.7.1. Micro-solvated aromatic complexes

There are extensive studies in the literature on microsolvated aromatic complexes using supersonic jet spectroscopy as well as quantum chemistry calculations.[178-187] The spectroscopy of the benzene-H_2O complex was pioneered by Suzuki et al using microwave studies in 1992.[188] They have reported rotationally resolved spectra of three isotopic species of 1:1 clusters of benzene with water (H_2O, D_2O, and HDO).[188] Zwier and co-workers have performed the spectroscopic study of benzene…water complex as a prototypical example of aromatic solute…solvent cluster.[189-191] They have reported that benzene and water interact through O-H…π hydrogen bonding at the molecular level, although this aromatic hydrocarbon and polar solvent (water) are generally not miscible.[189-191] They have extended their studies to large water clusters of benzene i.e. benzene-$(H_2O)_{n=1-7}$ and reported that the structural arrangement of the water molecules is similar in $(H_2O)_n$ and benzene-$(H_2O)_n$.[190] $(H_2O)_n$ clusters form O-H…O hydrogen bonded chain, cycles, and three dimensional networks depending upon the number of water molecules.[190] More specifically, $(H_2O)_2$, $(H_2O)_{n=3-5}$, and $(H_2O)_{n=6-7}$ form O-H…O hydrogen bonded chain, cycles and cubes, respectively.[190-191] The only structural difference between $(H_2O)_n$ and benzene-$(H_2O)_n$ is that one of the water molecules in the latter complex is π-hydrogen bonded with benzene.[190] Further Zwier and co-workers have replaced water with methanol as a solvent and studied the spectroscopy of benzene…$(CH_3OH)_{n=1-3}$ complexes.[192] They have reported that $(CH_3OH)_{n=1-3}$ form O-H…O hydrogen bonded chain and O-H group of one of the methanol molecules interacts with benzene through an O-H…π hydrogen bonding. From the study of both benzene…$(H_2O)_{n=1-7}$ and benzene…$(CH_3OH)_{n=1-3}$ complexes using IR-UV double resonance spectroscopy, it has been reported that the red-shift in the stretching frequency of the O-H

group involved in π-hydrogen bonding with benzene increases with the increase in the number of water or methanol molecules.[190,192-193]

Mikami and coworkers have investigated the structures of phenol…$(H_2O)_{n=1-5}$ clusters by analyzing O-H stretching vibrational spectra in ground and excited electronic states using IR-UV double resonance spectroscopy and quantum chemistry calculations.[194] They have reported that the structure of phenol…H_2O complex is stabilized by O-H…O hydrogen bond.[194] The authors have also investigated phenol…$(H_2O)_{n=2-4}$ complexes and observed the presence of O-H…O hydrogen bonded cyclic ring structure involving the O-H group of phenol.[194] They have concluded that the red-shift in phenolic O-H stretching frequency in phenol…$(H_2O)_{n=1-4}$ with respect to the free O-H stretching frequency (3657 cm^{-1}) of phenol increases with the increase of the number of water molecules involved in complex formation in the ground electronic state (S_0).[194] It has been found that the red-shift in the stretching frequency of the O-H group of phenol involved in the O-H…O hydrogen bonding with water in the excited electronic state (S_1) is more in compared to that in the S_0 state.[194] This is because the acidity of phenol in the S_1 state (pK_a=4.0) is more compared to that in the S_0 state (pK_a=9.8).[195]

Mikami and coworkers have also studied hydrogen bonded complexes of phenol with different solvents such as alcohols, ethers, and benzene.[196-198] Complexes of water with difluorobenzene,[183,199] pyridone,[200] tetrazine,[201-202] tropolone,[203] carbazole,[204-205] dimethylaminobenzonitrile,[206] and 2,5-diphenyl-oxadiazole[207-208] have been reported by Levy, Leutwyler and several other groups. Zwier and Sulkes groups have studied 1:1 hydrogen-bonded complexes of indole as well as its analogs with water, ammonia, methanol, tetrahydrofuran, trimethylacetic acid and a few other solvents.[209-212] In one of the studies of indole…$(water)_{n=1-3}$ complexes, Zwier and co-workers have reported that the red-shift in the N-H…O bound N-H stretching frequency increases with the increase in the number of water molecules, which is reminiscent of similar behavior observed in the case of the complexes between benzene and water.[209]

1.7.2. Aromatic-aromatic complexes

Molecular level study of aromatic-aromatic complexes compared to aromatic…$(solvent)_n$ complexes provides more relevant information on the structures of biomolecules and

materials as well as biomolecular processes. Here we have provided a brief review on the aromatic-aromatic complexes studied by experiment as well as theory.

In the literature, mostly nitrogen containing heterocycles are chosen for the study of aromatic-aromatic complexes as these compounds play a key role in the structures and functions of biomolecules like protein, DNA, RNA etc. These heterocylces are also present in several natural signaling compounds such as cyclic nucleotides (e.g., cyclic guanosine monophosphate and cyclic adenosine monophosphate) and plant phytohormone cytokinins and natural biochemical functional pigments such as malenin, hemoglobin, chlorophyll and cytochromes.[213] The study of these complexes provides quantitative understanding of the non-covalent interactions present in the stabilization of the macromolecules in biology and materials. Quantitative study of these weak interactions using a whole macromolecule is extremely challenging due to the presence of innumerable interactions there. Thus the study of a whole macromolecule renders only average information about these interactions. Alternatively, as these macromolecules are very often formed by the repetition of a small monomeric unit through backbone of non-covalent interactions, molecular complexes of the building blocks at the dimeric or trimeric levels could be studied to mimic the interactions present in biomolecules and materials.

In fact, there are two popular computational databases, S22 and S66, of molecular complexes comprising of various types of non-covalent interactions. S22 and S66 databases consist of 22 and 66 model complexes, respectively.[214-215] Most of the complexes present in the computational databases are also studied experimentally. The complexes reported in these databases are classified into three categories; conventional hydrogen bonded complexes dominated by electrostatic interaction, dispersion dominated complexes, and mixed complexes stabilized by comparable magnitude of electrostatic and dispersion interactions. Gas phase studies of these three different types of complexes are reviewed briefly in the following.

1.7.2.1. Hydrogen bonded complexes

Hydrogen bonded complexes are mostly governed by electrostatic interaction. This interaction is highly specific and directional in nature. In the literature, the base pairing in nucleic acids such as DNA and RNA has been investigated in the gas phase by the study of

the dimeric complexes of natural nucleobases such as adenine, guanine, cytosine, thymine and uracil.[216-220] Kleinermanns and coworkers have investigated base pairing between adenine and thymine in the gas phase by studying adenine…thymine dimer using IR-UV double resonance spectroscopy and quantum chemistry calculations.[220] They have reported that the observed dimer has doubly hydrogen bonded configuration.[220]

De Vries and co-workers have studied guanine…cytosine dimer using REMPI spectroscopy and ab initio calculations to understand the base pairing interaction between these two bases.[218,221] The authors have reported a single isomer of the dimer stabilized by triple hydrogen bonding interactions.[218,221] Furthermore they have performed IR-UV and UV-UV double resonance spectroscopy experiments and concluded that the structure of guanine…cytosine dimer is stabilized by three nearly linear hydrogen bonds (N-H…O-H, N-H…N and C=O…H-N).[218,221] Apart from the complexes of the natural nucleobases, some other model complexes, which mimic the base pairing present in DNA, have also been studied in the gas phase.[221-226] Leutwyler and coworkers have studied 2-aminopyridine…2-pyridone dimer using IR-UV double resonance spectroscopy and quantum chemistry calculations.[227-228] They have reported by measuring IR spectra in the C=O and O-H vibrational regions that the dimer is stabilized by N-H…O=C and N-H…N hydrogen bonds. They have performed further IR-UV and UV-UV double resonance spectroscopy experiments and ab initio calculations for 2-pyridone…uracil, 2-pyridone…thymine, and 2-pyridone…5-fluorouracil dimers. It has been found that all of these dimers are stabilized by double N-H…O=C hydrogen-bonding interactions.[229] All of these complexes model the interactions mostly present in adenine…thymine and adenine…uracil base pairs.[229]

There are also a few aromatic complexes of 7-azaindole which have been studied quite extensively in the supersonic jet. In the case of 7-azaindole dimer, a planar double N-H…N hydrogen bonded structure has been reported by several authors.[230] Chakraborty and co-workers have studied 7-azaindole…2-pyridone and 7-azaindole…2-pyrrolidinone complexes using laser induced fluorescence (LIF) spectroscopy.[231-232] They have found that the structures of both the complexes are stabilized by N-H…O and N-H...N double hydrogen bonding interactions.[231-232] Recently, Das and coworkers have performed IR-UV and UV-UV double resonance spectroscopy experiments for investigation of the structure of 7-azaindole···2-fluoropyridine dimer.[233] They have reported that the observed dimer is

stabilized by both N–H···N and C–H···N hydrogen bonding interactions while the less stable isomer with N–H···F and C–H···N interactions was not observed in the experiment.[233]

1.7.2.2. π-stacked complexes

Π-stacked complexes are generally dominated by dispersion interactions although relative contribution of the dispersion and electrostatics in governing the geometry of these complexes is highly debated in the literature.[159,161,234-235] Hunters and Sanders have proposed that it is electrostatics which controls the geometry and magnitude of the π-stacking interaction.[160-161] They have stated that π-stacking interaction between two aromatic rings increases when one of the complexing partners contain an electron withdrawing substituent while the interaction decreases if the substituent at one of the rings is electron donating.[161] This electrostatic model has been proved to be inappropriate as Sherrill and co-workers have proved that π-stacked configuration of the substitiuted benzene dimers is always more stable than that of the benzene dimer irrespective of the electron donating or withdrawing nature of the substituents.[236-244] Thus the electrostatics alone cannot govern the π-stacking interaction rather dispersion plays a significant role for the stability of the π-stacked complexes.

Gas phase studies of the π-stacked dimeric complexes compared to those of hydrogen bonded complexes are very much limited in the literature. In general, a π-stacked isomer compared to a hydrogen bonded (conventional) isomer of a complex is energetically less stable and mostly the latter one is observed in the gas phase experiment. Even if these two types of isomers are comparable in energy, only the hydrogen bonded isomer being the global minimum is observed in the experiment as the interconversion barrier between the higher to lower energy isomer of these complexes is very shallow.

The very first observation of a π-stacked dimer of 1,2-difluorobenzene using microwave spectroscopy has been reported by Goly et al.[245] They have found that the interplanar distance in this dimer is 3.45 Å. Leutwyler and coworkers have studied complexes of nucleic acid base analogues i.e. 2-pyridone (2-PY) and a series of fluorosubstituted benzenes using IR-UV double resonance spectroscopy and quantum chemistry calculations.[246] They have reported that π-stacked structure is observed only for 2-PY…HFB complex while the complexes of 2-PY with other fluorobenzenes (monofluoro, difluoro, trifluoro, tetrafluoro, and pentafluoro benzenes) predominantly form hydrogen bonded structure. De Vries and co-workers have

also explored the base stacking interactions in DNA by studying 9-methyladenine…adenine complex and 3,7-dimethylxanthine dimer in supersonic jet.[247-248] They have found that all of these three complexes form π-stacked structure due to methylation of the hydrogen bonding sites in the nucleic acid bases. Very recently, Patwari and co-workers have studied phenylacetylene dimer as well as complexes of phenylacetylene with pyridine, pyarazine, and triazine using IR-UV double resonance spectroscopy.[249] They have observed π-stacked structure in all the cases. It has been concluded that N-heterocyclic aromatic rings prefer the formation of π-stacked complexes as the substitution of carbon atoms of the benzene ring introduces dipole moment in the molecule and reduces the π-electron density of the ring.

Although gas phase experimental studies of the π-stacked dimers are scarce in the literature, there are extensive theoretical studies on the π-stacking interaction in the aromatic dimers. Till date, the most extensively studied aromatic dimer as a prototype of π-stacking interaction using numerous experimental as well as theoretical investigations is the benzene dimer. The binding energy difference between parallel-displaced π-stacked and T-shaped benzene dimer is very small (about 0.1 kcal/mol) according to highly accurate quantum chemistry calculation at the CCSD(T)/CBS level of theory.[250] Although these two structures of benzene dimer are almost isoenergetic, only the T-shaped structure has been observed in the gas phase study. There are also in-depth theoretical studies on the energetics and structures of the substituted benzene dimers by Hobza and co-workers as well as Sherrill and co-workers.[236-239,251-253] They have reported that the π-stacked configuration is more stable than the T-shaped one in the case of the substituted benzene dimers unlike benzene dimer. Recently there have been numerous theoretical studies to probe the competition between π-stacking and hydrogen-bonding interactions in various aza-aromatic dimers. Sathyamurthy and co-workers have studied non-covalent interactions in homodimers of pyridine, pyrazine and triazine at CCSD(T)/CBS level of theory and reported that both π-stacked and hydrogen-bonded (C-H…N) dimers have comparable binding energies.[254] They have found that the anti-parallel π-stacked structure of pyridine dimer is more stable than the π-stacked benzene dimer by about 6 kJ/mol. Hohenstein, E. G. et al. have performed high level *ab initio* calculations on benzene…pyridine heterodimer as well as pyridine homodimer and reported that the most favorable isomer in both of the cases has parallel-displaced π-stacked structure.[255] Further, very high quality theoretical calculations on heterodimers of benzene

and a few isoelectronic heterocycles by Wang and Hobza indicate that both T-shaped and parallel-displaced structures of each complex are almost isoenergetic.[256]

1.7.2.3. Mixed complexes

Mixed complexes are comprised of significant amount of both dispersion and electrostatic interactions. π-hydrogen bonded complexes, having both electrostatic and dispersion interactions, fall in the category of the mixed complexes and these are widely studied in the supersonic jet.[257-272] Desiraju, Steiner, Fleming, Zukerman-Schpector, Wilcox and many other scientists have investigated the nature of π-hydrogen bonding interaction in detail.[176-177,235,273-276] Nishio has thoroughly reviewed the nature of C-H…π hydrogen bonding and reported that the stabilization energy of the interaction has contribution from both electrostatic and dispersion forces but the latter one is more prominent when sp^2 and sp^3-CH groups act as hydrogen bond donors.[82,84,177]

In the context of the aromatic-aromatic complexes, the T-shaped configuration of the benzene dimer is the prototype example for the π-hydrogen bonding interaction.[251,257-262,277-286] Both the T-shaped and π-stacked isomers of the benzene dimers calculated at the CCSD(T)/CBS level of theory are almost isoenergetic but only the former one bound by C-H…π interaction is observed in the gas phase experiment.[257-262] These benchmark studies on the benzene dimer demonstrate that C-H…π interaction is slightly stronger than the π…π interaction. Indole…benzene dimer has been studied by mass analyzed threshold ionization experiment as well as quantum chemistry calculations.[287-289] It has been found from the CCSD(T)/CBS level of calculation that N-H…π bound T-shaped geometry of the dimer is more stable than the parallel-displaced π-stacked one by about 1.1 kcal/mol.[289] Biswal et al. have reported that only the tilted T-shaped N-H···π bound structure of the indole···benzene dimer with red-shift of the N-H stretch frequency of 46 cm^{-1} is observed in the jet-cooled experiment.[290] The binding energy of this dimer has been found to be 5.21 kcal/mol.[290] Thus it can be concluded from these studies that π-hydrogen bonding is stronger than π-stacking interaction present in aromatic dimers. There are further studies on the N-H···π interaction in various aromatic dimers. Dauster et al. have studied pyrrole dimer in the gas phase using experiment as well as theory.[264] Very strong N-H···π interaction has been observed in the case of pyrrole dimer,

which has a slanted T-shaped geometry with inter-planar angle of 55°.[264] Such a tilted T-shaped geometry compared to the perfect T-shaped one gains maximum stability by effective use of both π-π and N-H···π hydrogen bonding interactions. It has been found that the BSSE corrected binding energy of the pyrrole dimer computed at the MP2 level is about 5.50 kcal/mol while the observed red-shift in the donor N-H stretch is 86 cm^{-1}. Tilted T-shaped N-H···π bound structure has also been observed for 2-pyridone···benzene dimer.[265,291] The dimer shows 56 cm^{-1} of experimental red-shift of the N-H stretching frequency and it has dissociation energy (D_0) of 5.17 kcal/mol calculated at the CCSD(T)/aug-cc-pVDZ level of theory. Similar kind of N-H···π interaction has recently been observed in pyrrole···benzene dimer, where the observed red-shift in the N-H stretch of pyrrole is 59 cm^{-1}.[292] The reported N-H…π bound structure of the pyrrole…benzene dimer has tipping angle of ± 13° in the S_0 state calculated at the SCS-MP2 level of theory and this angle increases to ± 21° in the S_1 state (SCS-CC2 level of theory).[292] The above studies on the π-hydrogen bonded complexes conclude that the associated binding energies can be greater than 5 kcal/mol. These data dictate that the strength of the N-H···π hydrogen bond can be comparable to a conventional hydrogen bond.[265,291-292] Π-hydrogen bonded aniline clusters have also been extensively reported in the literature.[266,268-270,272] Kawamata et al. have measured the N-H stretching frequencies of aniline-pyrrole dimer using IR dip spectroscopy and compared the results with aniline dimer and aniline…benzene dimer.[268-270] They have reported that the red-shifts in the symmetric N-H stretching frequencies of the aniline dimer, aniline…benzene dimer, and aniline…pyrrole dimer are 28 cm^{-1}, 29 cm^{-1} and 29 cm^{-1}, respectively whereas the red-shifts in the antisymmetric N-H stretching frequencies are 42 cm^{-1}, 41 cm^{-1} and 44 cm^{-1}, respectively.[268-270] It has been found that the amount of red-shift in the N-H stretching frequencies for all the three aniline complexes is nearly equal and the shift is due to N-H…π hydrogen bonding.

There are a few theoretical studies in the literature on the effect of the substituents on the T-shaped structures or π-hydrogen bonding interactions in the aromatic dimers.[252,293-298] The effect of the substituents on the T-shaped structures or π-hydrogen bonding interactions is quite different from that on the π-stacking interactions. In this case, the binding energies of the complexes between benzene and substituted benzenes compared to those of the benzene

dimers increase or decrease depending on the nature of the substituents as well as whether the substituents are located on the π-hydrogen bond donor or acceptor moiety. In one of these studies, Kim and co-workers have reported the substitution effect on the T-shaped structure (edge to face interaction) for two conformations (axial and facial) of monosubstituted benzenes at the MP2 level of theory.[298] In case of axial conformation, the para C-H group of substituted benzene forms C-H…π interaction with benzene whereas in case of facial conformation, the C-H group of unsubstituted benzene forms C-H…π interaction with substituted benzene.[298] They have found that electron-withdrawing substituents favor the axial substituent conformation whereas the electron-donating substituents favor facial substituted conformer.[298]

Recently, Sherrill and co-workers have studied the role of nitrogen heteroatom on π-stacking as well as π-hydrogen bonding interactions by studying complexes of pyridine and benzene using very high level quantum chemistry calculations.[299] They have reported that the most favorable configuration for both $(pyridine)_2$ and benzene...pyridine dimer is the parallel displaced π-stacked one unlike the T-shaped one for the benzene dimer.[299] The substitution of the nitrogen atom in the benzene ring reduces the dispersion interaction in the dimer but increases the electrostatic contribution, which plays an important role in stabilizing the parallel displaced configurations. Wang et al. have also studied the complexes of benzene with several N-heteroaromatic systems and concluded that the binding energies of benzene...N-heteroaromatic complexes are higher than that in the benzene dimer.[300] On the other hand, in the case of the T-shaped configurations, it has been found that the aromatic rings containing nitrogen atom are very poor π-hydrogen bond acceptors as the electron density of the rings is pulled away by the electronegative heteroatom.[299] In the case of the benzene…pyridine dimer, the T-shaped structure with pyridine as a π-hydrogen bond acceptor is not stable. But the structure with pyridine as a π-hydrogen bond donor through the C-H group at the para position and benzene as a π-hydrogen bond acceptor is stable.

1.8. Scope of the thesis

1.8.1. Special class of mixed complexes

If we carefully look at the mixed complexes reported in the S22 database, we find that all the complexes except phenol dimer are primarily stabilized by X-H…π (C, N, O) hydrogen

bonding interaction consisting of similar amount of both electrostatic and dispersion energy. It has been demonstrated from both experiment and theory that the phenol dimer has a V-shaped herringbone geometry governed by a delicate balance among conventional hydrogen bond (O-H…O), C-H…π, and π…π interactions.[2-8] Thus we have proposed that the phenol dimer is an exception in the class of the mixed complex and this dimer should be considered in a separate category of complex which we have named as "*Special class of mixed complex*".[9] There is a very subtle difference between the "*Special class of mixed complex*" and mixed complex already defined in the database. The "*Special class of mixed complex*" is defined by the complex stabilized due to interplay between conventional (strong) hydrogen bonding and significant magnitude of dispersion bound interactions. On the other hand, only one type of non-covalent interaction (π-hydrogen bonding) comprised of electrostatic and dispersion forces is present in the mixed complexes. Very recently, Hill et al. have renamed the "*Special class of mixed complex*" to "*Special mixed-influence*" (SMI).[10]

It is indeed the fact that the mixed contribution of the electrostatic dominated conventional (strong) hydrogen bonding and dispersion bound interactions govern the structures of the biomolecules and materials as well as biomolecular processes. The very specific shape of these macromolecules is due to the interplay or competition between electrostatic and dispersion bound multiple types of non-covalent interactions. Thus gas phase spectroscopic studies of the "*Special class of mixed complex*" stabilized by multiple types of non-covalent interactions reveal unique information on the basic structures of biomolecules and material. But surprisingly, most of the molecular complexes reported in the literature are bound by one class of non-bonding interaction i.e. strong hydrogen bonding (electrostatics dominated), π-hydrogen bonding (mixed complex) or π-stacking (dispersion dominated) while the gas phase study of the "*Special class of mixed complex*" is scarce in the literature. Thus we have studied selectively those molecular complexes stabilized due to the interplay or competition among multiple types of non-covalent interactions.

Furthermore, it is quite challenging to have accurate determination of the geometry and binding energy of this "*Special class of mixed complex*" from theory as well as experiment as these complexes are stabilized by significant amount of both electrostatic and dispersion interactions.[11-12] From theoretical point of view, study of these complexes is difficult because conventional DFT functionals do not include dispersion interaction while MP2 level of theory

overestimates the dispersion interaction. Thus a theoretical method which considers both electrostatic and dispersion interactions with reasonable accuracy as well as handle the quantum calculations of these moderate size complexes within decent time frame has to be used for the study. It is also not straightforward to obtain sufficient amount of signal of this "*Special class of mixed complex*" compared to electrostatic dominated strong hydrogen bonded complexes or dispersion dominated π-stacked complexes in the gas phase spectroscopy experiment.

1.8.2. Aim of the thesis

The aim of the thesis is the following.

1. To understand the interplay between conventional hydrogen bonding and dispersion interactions. Here *our new finding* is "*special class of mixed complex*", which represents the basic structural motifs of biomolecules and materials.

2. To investigate the competition between conventional (strong) hydrogen bonding and π-hydrogen bonding interactions. Can π-hydrogen bonding dominate over the conventional hydrogen bonding while both the possibilities are present in the molecular complexes? We have also asked the question whether the aromatic rings containing heteroatoms can act as effective π-hydrogen bond acceptor.

3. Selective synthesis of the π-stacked complex in the gas phase by suppressing the possibility of the formation of other possible structures of the complex held by conventional hydrogen bonding or π-hydrogen bonding interaction. We have also demonstrated here that hexafluorobenzene (HFB) is a unique building block for building π-stacked architecture in biomolecules and materials. This π-stacked structural motif is extensively used as a supramolecular synthon for infinite columnar structure in crystal engineering.

4. To study the aromatic-aromatic interactions (dimeric as well as trimeric) in the aromatic side chains of proteins.

1.8.3. Molecular complexes studied in this work

All the molecular complexes studied in this work contain indole as one of the complexing partners due to its tremendous importance in biology. Indole is present in the side chain of

tryptophan amino acid. It is also present in indole alkaloids.[301] These alkaloids, being a largest class of alkaloids with more than 4000 compounds, have significant physiological and medicinal importance.[301] Our study is also concerned with the N-heterocycilc aggregation at the dimeric and trimeric level, which is prevalent in DNA and proteins.

We have reported here the study of the complexes of indole with a few heterocyclic compounds namely pyridine, furan, thiophene, imidazole and pyrrole as well as HFB in a supersonic jet by employing R2PI, IR-UV, and UV-UV double resonance spectroscopic techniques combined with quantum chemistry calculations. We have investigated the interplay between conventional hydrogen bonding and dispersion interactions from the study of indole…pyridine dimer while competition between conventional hydrogen bonding and π-hydrogen bonding interactions has been explored from the study of indole…furan and indole…thiophene dimers. We have reported observation of an exclusively π-stacked structure of indole…HFB dimer by suppressing the possibility of formation of π-hydrogen bonded isomer. Finally, we have described the study of indole…imidazole dimer and indole…$(pyrrole)_2$ trimer, which mimic the aromatic-aromatic interactions (dimeric as well as trimeric) in the aromatic side chains of proteins.

1.8.3.1. Interplay between conventional hydrogen bonding and dispersion interactions

Gas phase laser spectroscopy in a supersonic jet has been used to study the intermolecular forces present in non-covalently bonded aromatic dimers and higher clusters. Experimental results obtained through isolated gas phase study are also very much suitable to compare with the data available from very high level quantum chemistry calculations. We have discussed in section 1.7.2.3. that the binding energy difference between parallel-displaced π-stacked and T-shaped isomers of benzene dimer and indole…benzene dimer is quite small according to highly accurate quantum chemistry calculations at the CCSD(T)/CBS level of theory.[284] But gas phase supersonic jet studies of both the dimers show the presence of only T-shaped structure stabilized due to π-hydrogen bonding.[257-262] On the other hand, observation of π-stacked dimer from experiment is very scarce.[245,248-249,302-304] Given that there is a competition among conventional hydrogen bonding, π-hydrogen bonding, and π-stacking interactions in aromatic clusters, it is quite challenging to have accurate determination of the structures of the molecular systems or complexes stabilized due to the subtle balance among multiple

types of non-covalent interactions. We have earlier discussed that the strength of the conventional hydrogen bonding could be determined precisely by both experiment and theory but accurate determination of the dispersion interaction is quite difficult.[11-12] It becomes further challenging to investigate the contribution of these two interactions when these are present simultaneously in a molecule or complex to provide its specific structure.

We have investigated the structure of indole…pyridine dimer in a supersonic jet and reported that the geometry of indole…pyridine dimer is stabilized by conventional hydrogen bonding (N-H…N) as well as C-H…π and π…π interactions. The indole…pyridine dimer falls in the category of *special class of mixed complex*. This study is reported in chapter 3.

1.8.3.2. Competition between conventional hydrogen bonding and π-hydrogen bonding interactions

π-hydrogen bonding is defined as X-H...π, where X is generally O, N, S, or C atom. Importance of π-hydrogen bonding in biology as well as materials is already described in detail. Particularly, N-H…π interaction has received much attention quite recently because of its wide variation in the interaction energy depending on the molecular systems involed.[264-265,291,305-307] The prototypical example of this type of non-covalent interaction is present in benzene···NH_3 complex, where the interaction energy is very small (D_0 = 1.84 kcal/mol) and this is even smaller than that of benzene···H_2O complex (D_0 = 2.44 kcal/mol).[305-307] On the other hand, strong N-H···π interaction has been observed in several N-heterocyclic aromatic complexes i.e. pyrrole dimer, 2-pyridone···benzene, indole…benzene and pyrrole…benzene dimers, which are earlier discussed in section 1.7.2.3.[264-265,291] The binding energies of all of these complexes are greater than 5 kcal/mol. It has been concluded from these data that N-H…π hydrogen bond has strength comparable to a conventional hydrogen bond (i.e. N-H…N, N-H…O etc.).[265,291-292] Given this fact, it will be interesting to ask the question whether N-H···π hydrogen bonding can win over conventional hydrogen bonding. To answer this question, one has to choose a molecular complex, which can exist as N-H···π bound conformer as well as conventional hydrogen-bonded conformer. Keeping this in mind, we have studied indole···furan dimer and indole…thiophene dimer, which can exist as both N-H···π bound conformer and N-H···O/N-H…S hydrogen bonded conformer.

We have found that there are extensive experimental and theoretical studies in the gas phase to understand the effect of various hydrogen bond donors (C-H, N-H, O-H and S-H) on the strength of the π-hydrogen bonding interactions.[188,191,251,259,264-265,291-292,305,308-318] But similar studies on the role of the heteroatoms present in the π-acceptor on the π-hydrogen bonding are very much limited in the literature.[299] There are a few theoretical studies on the effect of acceptor heteroatoms on the aromatic dimers containing N-heterocycles.[254,300,303,319] From one of these studies, Sherrill and co-workers have concluded from their theoretical investigation on benzene...pyridine dimer that aromatic rings containing heteroatoms are poorest π-hydrogen bond acceptors.[299,320]

For improved understanding of the effect of the acceptor heteroatoms on the π-hydrogen bonding interaction and to check whether the aromatic rings containing heteroatoms can act as effective π-hydrogen bond acceptor, it is essential to study the complexes of various aromatic heterocycles containing different heteroatoms (O, S) other than nitrogen (N) atom. Thus we have studied the complexes of indole with furan and thiophene and compared the results with that of indole…pyridine dimer. The study is reported in chapter 4.

1.8.3.3. Hexafluorobenzene: A unique building block for π-stacking interaction

Gas phase experimental study of the π-stacking interaction is very much limited in the literature. Generally, it becomes difficult to synthesize the π-stacked dimer in the gas phase when other competitive non-covalent interactions are present in the dimeric systems. There are some reports in the literature to synthesize the π-stacked dimers in the gas phase by methylation of the hydrogen bonding sites present in the complexing partners. It is also possible to synthesize selectively the π-stacked dimers by perfluorination of the π-hydrogen bond acceptor aromatic ring as it decreases the π-electron density in the acceptor ring and hence prohibits the possibility of the formation of the π-stacked conformer. For example, the study of Leutwyler and co-workers[246] on the complexes of 2-pyridone (2PY) with a series of fluorosubstituted benzenes already reported in section 1.7.2.2, demonstrates that only the complex with hexafluorobenzene (HFB) forms the π-stacked structure in the experiment. Here, we have adopted the similar approach to synthesize the π-stacked structure of indole using HFB instead of benzene as the complexing partner.[302] In the case of the indole…benzene dimer reported in the literature, only the observed conformer is the π-

hydrogen bonded one which is suppressed in our study by perfluorination of the benzene ring. The current study of this π-stacked dimer has two motivations. First, both π-stacking and π-hydrogen bonding interactions between the aromatic side chains of tryptophan and phenylalanine residues are present in proteins but only the π-hydrogen bound conformer has been observed earlier by studying indole…benzene complex.[290] Here we are able to observe the π-stacked structure of this complex by perfluorination of the benzene ring. Second, HFB is a very intriguing building block for the formation of more stronger and less parallel displaced π-stacked structure with benzene compared to that in the case of the benzene dimer. Thus the unique π-stacked architecture using HFB provides very efficient structural control in crystal engineering, medicinal chemistry and biological recognition.[321-322]

The study of benzene dimer and benzene...HFB dimer using CCSD(T) level of theory shows that parallel displaced structure of benzene...HFB dimer (interaction energy: -5.38 kcal/mol) is more stable than that of benzene dimer (interaction energy: -2.48 kcal/mol).[323] Generally, the dispersion interaction has major contribution in the interaction energy of the π-stacked dimers but electrostatic contribution plays the decisive role in determining its geometry. The electrostatic interaction is repulsive in the case of the benzene dimer (0.90 kcal/mol) while it is attractive in the case of the benzene...HFB dimer (-1.12 kcal/mol). This is due to equal but opposite quadrupole moment of benzene (- 29 × 10^{-40} Cm^2) and HFB (+ 32 × 10^{-40} Cm^2) (see Figure 1.1).[322] At the same time, the lateral displacement in the case of the parallel displaced conformer of the benzene...HFB dimer (1.0 Å) is significantly smaller than that in the benzene dimer (1.6 Å). This phenyl-perfluorophenyl stacking motif is widely used as a supramolecular synthon in crystal engineering.[321,324-327] This synthon bind alternatively to lead an infinite columnar structure with less lateral displacement between phenyl and perfluorophenyl units.

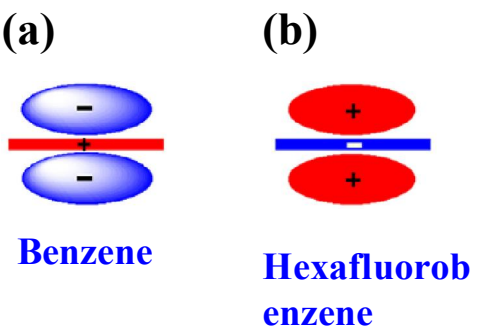

Figure 1.1: Schematic representation of quadrupole moment in (a) benzene and (b) HFB

In the case of the indole…HFB dimer studied here, we have observed a unique π-stacked structure, where the center of the HFB unit is aligned with the center of the shared bond of the indole moiety. This study is reported in chapter 5.

1.8.3.4. Aromatic-aromatic interactions in the aromatic side chains of proteins

Protein is an essential nutrient required by human body for its growth, repair and maintenance. It has also major contribution in the functionality of several organisms combining metabolic reactions and DNA replication. Proteins are biological macromolecules, which consist of multiple long chains of amino acids connected by peptide linkage. This linkage is the backbone of proteins, while the rest other parts are the side chains. These side chains can be aliphatic and aromatic depending upon the amino acid involved in the formation of protein. There are 23 amino acids, in which only four have aromatic side chains. These amino acids are tryptophan, phenylalanine, tyrosine and histidine amino acid, where indole, phenyl, phenolic, and imidazole moieties are present as aromatic chromophores. These aromatic side chains participate in the stabilization of the structures of the proteins apart from the C=O…H-N hydrogen bonding interactions in the backbone which provides specific folding motif. Interaction among these aromatic side chains are popularly known as aromatic-aromatic interaction. These aromatic-aromatic interactions are not only responsible for the structural stabilization of the protein but also govern several other biological recognition processes and drug-DNA intercalation processes.[19,163-165,328-339]

Aromatic-aromatic interactions present in protein are the interesting subject of study since early stage of 1980s. Burley et al. have analyzed high resolution crystal structures of 34 proteins and reported that "about 60 percent of the aromatic side chains in proteins are involved in aromatic pairs, 80 percent of which form networks of three or more interacting aromatic side chains".[340] Esteban et al. have also shown that higher order aromatic clusters (trimers, tetramers etc.) are present in about 50% of the proteins, which have been crystallized to date.[20] For example, they have pointed out a distinctive trimer structure containing tryptophan and two phenylalanine residues[20] in the crystal structure of a protein called L-ribulose-5-phosphate 4-epimerase (PDB ID: 1JDI).[341] In the interior of proteins, aromatic-aromatic interactions occur at the molecular level in the absence of water. Thus quantitative understanding of these non-covalent interactions present in the aromatic side

chains of proteins could be possible through isolated gas phase studies of the complexes between the aromatic residues of proteins.

In spite of the significant importance of these aromatic interactions in the stability of proteins, systematic studies on the molecular level understanding of the non-covalent interactions in the dimeric and higher order complexes of the aromatic side chains of four amino acid residues are scarce in the literature. The most extensively studied aromatic cluster reported in the literature is benzene dimer and trimer, which serves as a model for the interactions among side chains of phenylalanine and probably also tyrosine.[251,257-259,262,278-280,282-283,309,342] In the case of the benzene dimer, C-H…π bound T-shaped structure has been observed in the experiment while the benzene trimer shows C-H…π bound cyclic structure.[343-345] A few more aromatic complexes such as phenol dimer, indole…benzene dimer and pyrrole trimer, representing the interactions between other aromatic amino acid residues, have been reported in the literature.[3-7,287-290,346-349] Phenol dimer mimics the interaction between the aromatic units of tyrosine residue whereas indole···benzene dimer illustrates the aromatic interaction between tryptophan and phenylalanine residues in proteins. Despite these investigations of non-covalent interactions between various aromatic moieties in amino acid residues, surprisingly there are no studies on the interactions between aromatic side chains of tryptophan and histidine aromatic amino acid residues of proteins.

Thus, we have reported aromatic-aromatic interactions (dimeric as well as trimeric) in the aromatic side chains of proteins by studying indole···imidazole dimer and indole…$(pyrrole)_2$ trimer. The indole…imidazole dimer delineates dimeric interaction between tryptophan and histidine residues of proteins while indole…$(pyrrole)_2$ trimer mimics trimeric interaction present among the aromatic side chains of proteins as indole is the aromatic moiety present in the side chain of tryptophan and pyrrole is also the subunit of indole only. This study is reported in chapter 06.

2. Methodology

In this chapter, we have discussed experimental methods and various spectroscopic techniques used to perform the experiments. The experimental setup is also described in detail. A brief description of the quantum chemistry calculations as well as various computational methods has also been provided here.

2.1. Experimental method

2.1.1. Supersonic jet expansion

Supersonic jet expansion technique is the heart of the experiments described in the thesis as it is concerned with the high resolution spectroscopic studies of weakly bound aromatic complexes. This special technique not only enables the measurement of high resolution electronic spectra of molecules but also synthesis of non-covalently bonded complexes of different sizes of interest. This simplification of electronic spectra and study of clusters would not be possible by any other means. Supersonic jet expansion produces cold molecular beam in isolated gas phase where the molecules are in the lowest internal states (rotational, vibrational) without undergoing any collision. This is, indeed, the ultimate dream of high resolution molecular spectroscopists to prepare the samples in well-defined quantum states and measure the interaction with light at the molecular level. Actually it is the marriage between the supersonic molecular beam and advanced lasers to produce high resolution electronic spectra of molecules.

Supersonic jet a high intensity molecular beam source for effective monochromatization of velocities, has been theoretically proposed in 1951 by Kantrowitz and Grey.[350] Prior to this, monochromatization of velocity was achieved by use of rotating sectors or magnetic selection.[351] But applying these procedures, although the desired velocity has been achieved by discarding other velocity components, intensity of the molecular beam is reduced greatly. In contrast, supersonic jet beam provides monochromatization of velocities without sacrifice in intensity. This molecular beam was experimentally achieved by Kistiakowsky & Slichter [351] and Becker & Bier[352]. Later, Levy and coworkers pioneered the spectroscopy of molecules using supersonic jet.[353-355] The principle and application of supersonic expansion technique in molecular spectroscopy have been described in detail in many reviews.[353,355-356]

Supersonic molecular beam is produced when the molecule of interest seeded in a monoatomic carrier gas (e.g. He or Ar) of a few atm of pressure is expanded into a high vacuum (~ 1 x 10^{-6} Torr) through a small orifice. The molecular beam could be supersonic or effusive depending on the relationship between the mean free path of the molecules and diameter of the orifice. If the orifice diameter (D) is much smaller than the mean free path (λ_0) of the molecules i.e. D << λ_0, the gas molecules will escape out from the nozzle without undergoing much collision. This beam is called effusive beam.[357] In this case, there will not be any change in the distribution of velocity as well as internal degrees of freedom of the molecules. The velocity distribution, f(v), of the molecules in an effusive beam is Maxwellian only and this can be calculated from the equation shown below.

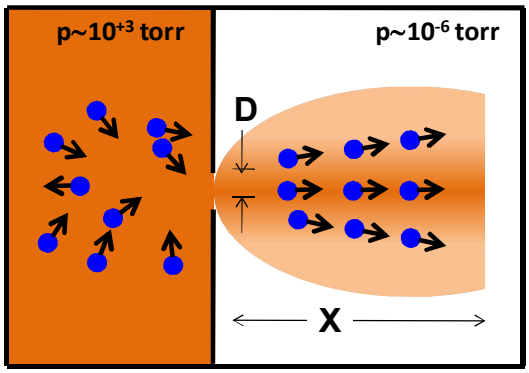

Figure 2.1 schematic diagram of supersonic expansion

$$f(v)=4\pi\left(\frac{M}{2\pi RT}\right)^{3/2}v^2\exp\left(-\frac{Mv^2}{2RT}\right) \qquad (2.1)$$

Where, M is molecular mass, v is speed of molecules, R is universal gas constant, and T is temperature in Kelvin.

In the case of supersonic beam, D >>λ_0.[353] In this condition, the molecules undergo numerous collisions while passing through the orifice and maximum number of collision occurs within a few mm from the orifice in the post-expansion region. These collisions convert the enthalpy of random motion into directed mass flow in the absence of external forces such as viscous forces, heat

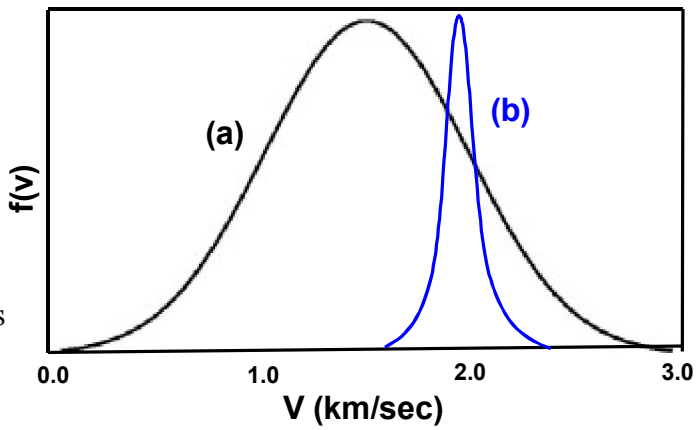

Figure 2.2 Schematic diagrams of velocity distributions in the (a) effusive molecular beam and (b) supersonic beam. Both curves are normalized to unity at the most probable velocity.

conduction and shock waves. It results the mass flow velocity to increase and the velocity-weighted Maxwell-Boltzmann distribution narrows down. Figure 2.2 shows a schematic diagram of velocity distribution in the supersonic beam as well as effusive beam. The translation temperature of molecules in the supersonic beam can be measured from the width of the Maxwell-Boltzmann velocity distribution curve, which shows significant decrease in the translational temperature. This results the velocity of sound to decrease according to the equation, $a = (\gamma kT/m)^{1/2}$, where k is Boltzmann constant, γ, m , T are the ratio of heat-capacity, mass and temperature. Hence the Mach number (M≡ $\frac{v}{a}$) increases. In the case of the supersonic beam, the Mach number is greater than one. The supersonic expansion is isentropic and adiabatic reversible process. Thus the following equation can be used to describe the temperature, pressure, and density in the molecular beam,[353-354]

$$\mathbf{T/T_0} = \left(\mathbf{P/P_0}\right)^{(\gamma-1)/\gamma} = \left(\rho/\rho_0\right)^{\gamma-1} = \left(\mathbf{1} + \mathbf{1/2}\,(\gamma - \mathbf{1})\mathbf{M^2}\right)^{-1} \qquad (2.2)$$

where T_0, P_0 and ρ_0 are the temperature, pressure, and density respectively in the pre-expansion region; T, P, and ρ are the same quantities in the post-expansion region. γ and M are ratio of heat capacities (C_p/C_v) and Mach number, respectively. The equation shows that Mach number increases with the decrease of the T, P and ρ in the mass flow. Thus the degree of translational cooling (defined as T_0/T) also increases with the increase in the Mach number.

The cold translational degrees of freedom act as a bath for cooling of the vibrational and rotational degrees of freedom. The rate of equilibrium between translational and rotational degrees of freedom is relatively fast compared to that between translational and vibrational degrees of freedom. Thus the rotational cooling is quite fast in comparison to the vibrational cooling. The efficiency of cooling of the internal degrees of freedom is in the order of translational > rotational > vibrational.[358] After the expansion, there is formation of a highly non-equilibrium state with the cooling of these internal degrees of freedom. The density of molecules in the beam decreases significantly after a certain distance from the orifice in the post-expansion region and there will not be any further collision until the beam faces any obstruction. Thus the molecules in the supersonic beam will be internally cold and isolated in the gas phase.

By assuming the molecular beam as continuous, the Mach number can be defined in terms of D (orifice diameter) and downstream distance from the orifice (X) as follows,[358]

$$M=A(X/D)^{\gamma-1} \quad (2.3)$$

where A is a constant based on γ. The equation is not valid for a long distance (when X>>D). Thus Anderson and Fenn have proposed a model treating the particles as classical hard spheres and concluded that only finite number of collisions is possible between two hard spheres. Thus Mach number and lowering of temperature approach to a terminal value asymptotically in the flow. The terminal Mach number can be calculated from the following equation,[353]

$$M_T = 2.05\varepsilon^{-(1-\gamma)/\gamma}(\lambda_0/D)^{(1-\gamma)/\gamma} = 133(P_0D)^{0.4} \text{ (for argon)} \quad (2.4)$$

where, ε is collisional effectiveness constant. It is clear from equation 2.4 that the Mach number increases with increasing the backing pressure as well as orifice diameter. But the increase of P_0 and D to obtain efficient cooling demand a very large capacity pumping system to maintain the desired vacuum in the post-expansion region. It is inconvenient to use a vacuum pump of very high pumping speed. On the other hand, pulsed valve with a repetition rate of 10/20 Hz can be used to handle the gas load introduced in the vacuum chamber.

In summary, molecules are cooled far below their melting point without condensation but still remaining in the isolated gas phase using supersonic jet expansion technique. Cooling of the internal degrees of freedom helps in obtaining highly resolved and greatly simplified molecular spectra.[355] This kind of simplified spectra of the sample cannot be achieved from the study performed in the solution phase. In contrast, there is significantly small amount of homogenous and inhomogeneous broadening in the spectral band during measuring the spectra using the supersonic expansion technique but the broadening may be limited by the lifetime of molecule in the excited state.

2.1.2. Resonantly enhanced multiphoton ionization (REMPI) with Time of Flight (TOF) mass spectrometry

Molecules or non-covalently bonded complexes cooled in a supersonic jet are ionized using a tunable UV laser following REMPI technique. Mass selected electronic spectra of molecules

and complexes of different sizes are measured using TOF mass spectrometry. Principles of REMPI and TOF mass spectrometry have been described in the following.

2.1.2.1. REMPI

A schematic diagram demonstrating the principle of REMPI spectroscopy is shown in Figure 2.3. In this figure, S_0, S_1 and D_0 denote ground electronic state, first excited state, and ionization continuum, respectively. A few vibrational levels under different electronic states have also been shown in the figure. REMPI spectroscopy can be classified into one-color resonant two photon ionization (1C-R2PI) and two-color resonant two photon ionization (2C-R2PI) techniques.[359-360] In 1C-R2PI spectroscopy (Fig. 2.3a), jet-cooled molecules are excited

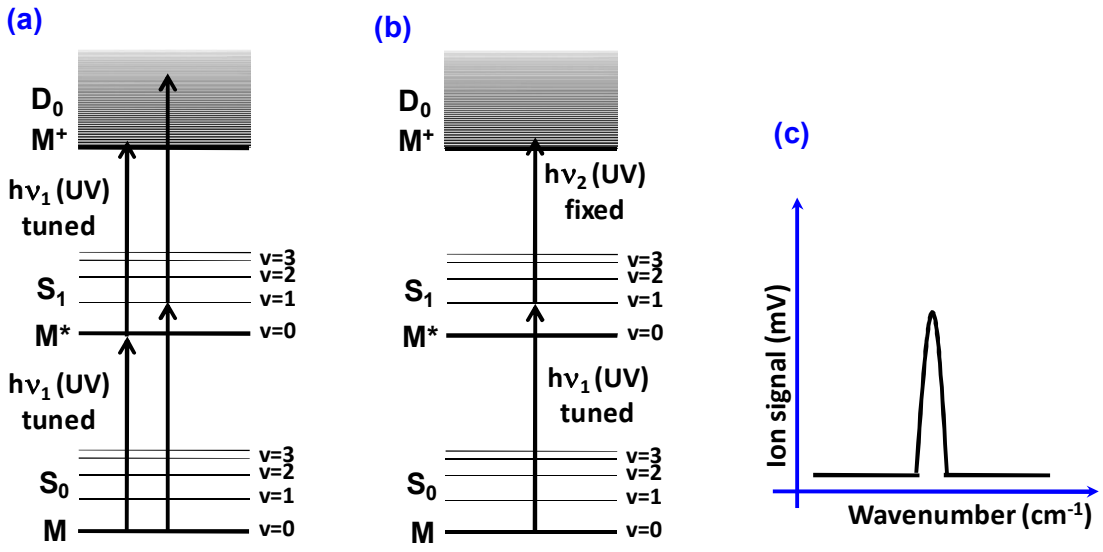

Figure 2.3. Schematic diagram of (a) 1C-R2PI, (b) 2C-R2PI spectroscopy, and (c) REMPI spectrum

to the S_1 state using a tunable UV laser beam and another photon of same energy ionizes the molecules. In this process, more than one photon is absorbed sequentially and hence the total energy absorbed is the sum of the energies of the individual photon absorbed. The ionization of the molecules takes place if the total energy of the photons is greater than the ionization potential of the molecules. If the second photon of different wavelength from a different laser is used to ionize the molecule, the technique is called 2C-R2PI spectroscopy (see figure 2.3b). 2C-R2PI technique is very useful when the sum of the energy of the two photons is less than the ionization potential of the molecule. This technique is also advantageous over

1C-R2PI technique specially for measuring the electronic spectra of non-covalently bonded clusters as the excess energy available in 1C-R2PI can fragment the cluster ions. After the ionization, the molecule loses an electron and a positively charged ion is produced. The mass selection of the ions of different masses is performed using time of flight mass spectrometry. Mass selected electronic excitation spectra of different species are measured in a supersonic jet by varying the laser excitation frequency in the UV region. A typical R2PI spectrum is shown in figure 2.3c. We have coupled jet-cooled REMPI with TOF mass spectrometry for performing various spectroscopy experiments.

2.1.2.2. TOF mass spectrometry

In TOF mass spectrometry, ions of different masses are separated according to their different time of flight. Ions formed through REMPI are accelerated by an electric field of known strength by applying known voltage difference. Here the potential energy experienced by the charged particles is converted to the kinetic energy.

The potential energy (U) of a charged particle in an electric field is directly related to the charge (q) of the particle and applied voltage difference (V):

$$U = qV \qquad (2.5)$$

The kinetic energy (K) of the charged particle directly depends on mass (m) and velocity (v) of the charged particle:

$$K = \frac{1}{2}mv^2 \qquad (2.6)$$

As the potential energy is converted to kinetic energy, $qV = \frac{1}{2}mv^2$ and $v \propto 1/\sqrt{m}$ for the ions having same charge. Thus the velocity of the species is inversely proportional to the mass of the species and hence the heavier mass takes more time of fight to reach the detector than the lighter mass.

In a TOF mass spectrometer, three electrode design given by Wiley and McLaren is used for improved resolution in the mass analysis of molecules and clusters.[361] The Wiley-McLaren design consists of two stage ionization acceleration volume that focuses the ions to the microchannel plate (MCP) detector (see Figure 2.4). The resolution of the mass spectrometer is mainly affected by two factors, velocity spread and spatial spread, which are reduced by using Wiley and McLaren arrangement.

For the acceleration of the charged particles towards the detector in this arrangement, two phase accelerating regions are created by applying differential voltage among the three plates. The first plate is a repeller plate with positive voltage and the second plate is an extraction grid with less positive voltage than the first one while the third plate is an accelerating grid

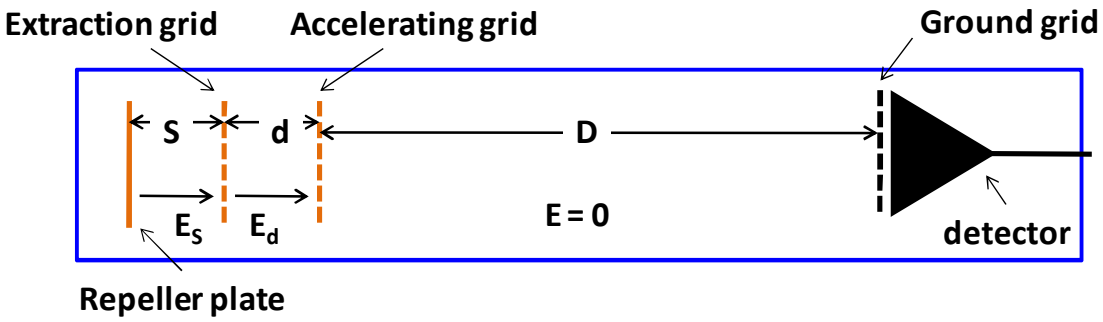

Figure 2.4. Schematic diagram of TOF mass spectrometer

which is grounded. A field free time-of-flight tube is there between the third plate and the detector. The electric field on the detector is terminated by putting a grounded grid near the detector. The distances between repeller plate and extraction grid, extraction grid and accelerating grid, and accelerating grid and detector are s, d and D, respectively. The fields created between first and second accelerating regions are denoted by E_s and E_d. This double-field system gives the privilege to increase the space focusing by adjusting the E_s/E_d ratio. The initial energy of the ions is U_0 which is increased up to a value U.[361]

In this situation,[361]

$U = U_0 + qsE_s + qdE_d$, and time of flight T (total time taken to reach the detector[361]) (2.7)

$= T_s + T_d + T_D$,

where[361] T_s (time taken by ion source to travel the ionization region[361]) (2.8)

$= 1.02\frac{(2m)^{1/2}}{qE_d}[(U_0+qsE_s)^{1/2} \pm (U_0)^{1/2}]$

Here the + and – signs in the T_s show the initial velocity oriented towards the detector and away from the detector.[361]

T_d (time taken by ion source to travel the acceleration region[361]) (2.9)

$= 1.02\frac{(2m)^{1/2}}{qE_d}$ [$U^{1/2}$-(U_0+qsE_s)$^{1/2}$]

and T_D (time taken by ion source to travel field free drift tube[361]) (2.10)

$=1.02(2m)^{1/2}(\frac{D}{2U})^{1/2}$

Thus the adjustment of E_s/E_d provides better mass spectral resolution in experiment by fixing the space spread originating due to physical position of the ions between the plates in the source region.[361]

In our TOF mass spectrometer followed by Wiley-McLaren design, a skimmed supersonic molecular beam is introduced at the center of the repeller plate and accelerating grid which are separated by 1 cm. The molecular beam is ionized by a laser beam which intersects it at right angle. The TOF tube is mutually perpendicular to the axis of molecular beam and laser beam. The ions created are repelled by the repeller plate (VA1) and drawn through the extraction grid (VA2). Typically VA1 and VA2 are 3060 V and 2760 V, respectively. The ions are accelerated further through the ground grid into the field free flight tube of 1 m length. Ions, accelerated from the double accelerating region, are detected by a dual micro channel plate (MCP) detector of 18 mm diameter.

The resolution of a mass spectrometer is expressed in terms of m/Δm, where m is mass of a particular ion and Δm is minimum mass difference of two ions. The resolution of our TOF mass spectrometer is 300 at a mass of 300 amu.

2.1.3. Tunable laser systems used for experiments

2.1.3.1. Dye laser

Dye laser, being from the family of liquid lasers, has a dye dissolved in a liquid solvent (i.e. methanol) as an active material.[362-366] In general, dye molecules should have good photochemical stability, high quantum yield and strong electronic absorption at excitation wavelength as well as minimal intersystem crossing for the effective performance of the laser.[363-366]

We have used frequency doubled UV output of a tunable dye laser (linewidth 0.08 cm^{-1}, ND6000, Continuum) for performing R2PI spectroscopy of molecules or complexes in a

supersonic jet. Generally dye laser covers whole UV-Vis range through use of various dyes and frequency doubling crystals.[363-365] Different dyes used in the laser for measuring electronic spectra of various molecular systems described in this thesis are Fluorescein 548, Rhodamine 590, Rhodamine 610, Rhodamine 590 + Rhodamine 610, DCM, LDS 698, and LDS 750.[363-365] Figure 2.5 depicts a schematic diagram of the optical paths of the dye laser. The working principle of the dye laser is also described here briefly.

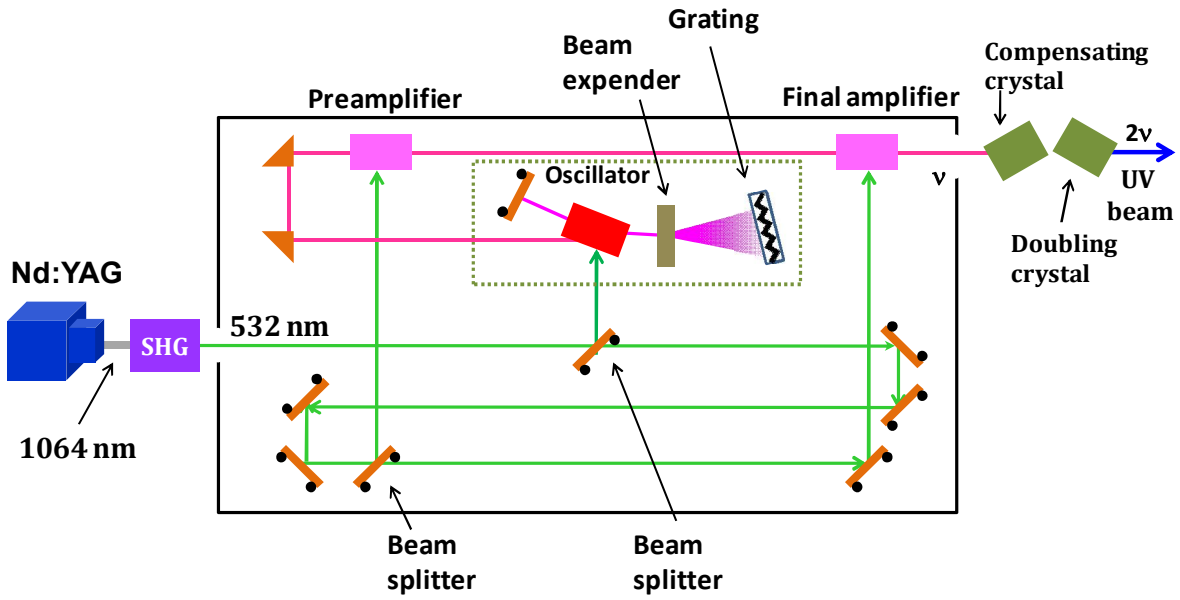

Figure 2.5. Schematic diagram of Nd:YAG pumped dye laser

The dye laser is pumped by the second harmonic (532 nm) output of an Nd:YAG laser (10 ns, 10 Hz, Surelite II-10, Continuum) having pulse energy of 650 mJ at 1064 nm.[367] The dye laser consists of one oscillator and two amplifier cells. Both the oscillator and first amplifier (preamplifier) dye cells are rectangular while the final amplifier is of capillary design. The vertically polarized 532 nm beam (pulse energy 300 mJ) from the Nd:YAG laser (pump laser) strikes the beam splitter which reflects 5% of the total pump energy into the oscillator while the beam with remaining energy is transmitted and falls on another beam splitter. The second beam splitter reflects 10% of the energy into the preamplifier and the residual amount of energy goes to the final amplifier. All these dye cells are pumped transversely by 532 nm pump beam. The dye oscillator contains an improved Moya dye laser cavity, where a beam expander is used to expand the beam and utilize it completely on the grating which has 2400 lines/mm grooving. The grating provides the wavelength selection from the broad output

from the dye. The laser output from the oscillator is amplified using both preamplifier and final amplifier. Finally the UV output is obtained when the visible beam from the dye laser passes through doubling crystal (KD*P) and compensating crystal.

2.1.3.2. IR Optical Parametric Oscillator (OPO)/Optical Parametric Amplifier (OPA) System

IR OPO/OPA system (Laser Vision) provides IR laser beam in the wavelength range of 1.35-5 micron. The IR laser is pumped by 1064 nm output of an unseeded/seeded Nd:YAG laser (10ns, 10Hz, Surelite II-10) of pulsed energy of 510 mJ. Figure 2.6 shows a schematic optical diagram of the IR OPO/OPA system, which works on nonlinear optical processes at multiple stages. At the OPO stage, the non-linear crystal present is KTP (Potassium Titanyl Phosphate, $KTiOPO_4$) while four KTA (Potassium Titanyl Arsenate, $KTiOAsO_4$) crystals are present at the OPA stage. The working principle of the IR OPO/OPA system is described here briefly.

The 1064 nm pump beam from the Nd:YAG laser is focused using a telescope and falls on a beamsplitter which divides the horizontally polarized pump beam into two separate beams. One beam is directed towards the OPO stage after frequency doubling (532 nm) through a

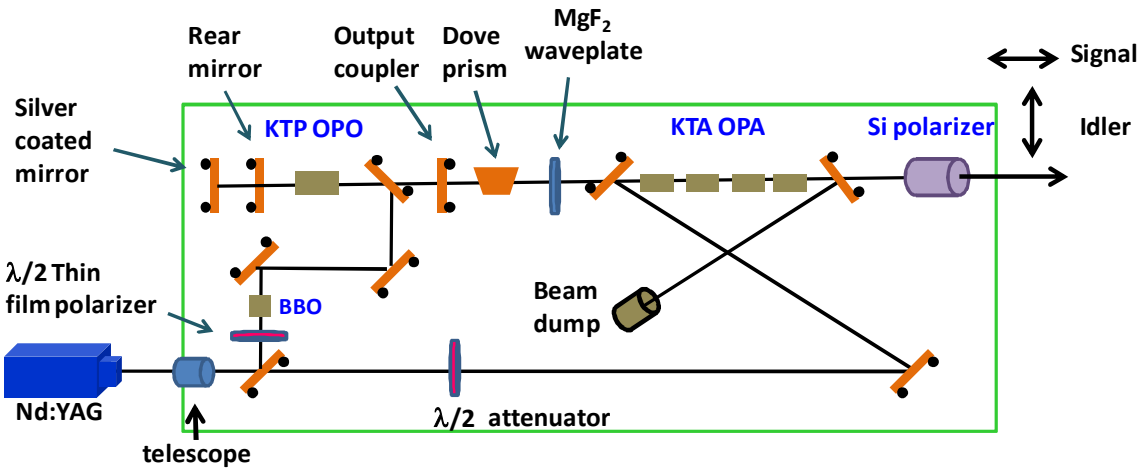

Figure 2.6. Schematic diagram of the Nd:YAG pumped IR OPO/OPA Laser

BBO (β-Barium borate) crystal while another 1064 nm beam is mixed with the idler output from the OPO stage. At the OPO stage, the pump beam (532 nm) passes through the KTP

crystal and the incident photon is converted into two different photons of different frequencies by optical parametric oscillation (OPO) process. According to the energy conversion relationship and phase matching condition, $\omega_p = \omega_i + \omega_s$ and $k_p = k_i + k_s$, where ω_p denotes frequency of a pump photon while ω_i and ω_s denote frequencies of idler and signal photons. In terms of wavelength, the equation can be written as $1/\lambda_p=1/\lambda_i+1/\lambda_s$ and the equation will be $1/(532\text{ nm})=1/\lambda_i+1/\lambda_s$ as $\lambda_p = 532$ nm in this case. The KTP crystal is placed in an optical resonator consisting of two highly reflecting mirrors. An additional mirror with Ag coating is present just behind the rear mirror to reflect back the idler beam leaked through the rear mirror. By varying the angle of the KTP crystal, tunable near IR light (pulse energy = 3-3.5 mJ) in the region of 710 – 885 nm is generated at the OPO stage. A $\lambda/2$ wave plate and variable attenuator are placed in the path of 1064 nm to rotate polarization from horizontal to vertical and to adjust the 1064 nm pump energy delivered to the OPA stage, respectively. The idler light mixes with the 1064 nm beam and the combined beams are directed into the OPA stage, which consists of four KTA crystals. The angles of KTP crystals are optimized to increase the IR energy. Here, the difference-frequency mixing occurs. So, $1/\lambda_i - 1/(1064\text{ nm})=1/\lambda_I$, where λ_I denotes wavelength of idler photons generated after OPA stage. Signal photons are also generated here according to the equation $1/\lambda_S=1/(1064\text{ nm})-1/\lambda_I$, where λ_S is wavelength of signal photon. The idler and signal waves generated after OPA stage are vertically and horizontally polarized, respectively.

At last, a silicon (Si) polarizer is used to isolate either vertically polarized idler or horizontally polarized signal wave from the combined output. In our IR-UV double resonance spectroscopic experiments, we have used vertically polarized idler photons of energy 3-4 mJ. Typical resolution of IR laser used in the experiment is about 2-3 cm^{-1} (about 1 cm^{-1} with seeder pump).

2.1.4. Experimental set-up

A home-built jet-cooled REMPI-TOF mass spectrometer has been used for the experiment and a photograph of the setup has been shown in Figure 2.7. The setup consists of two differentially pumped vacuum chambers connected through a skimmer (Beam Dynamics Inc.) of 2 mm diameter. A pulsed valve (General valve, series 9, rep. rate 10 Hz) with an

orifice diameter of 0.5 mm operated by a pulse driver (IOTA ONE, Parker Instrumentation) is incorporated in the bigger chamber (expansion chamber) pumped by a 10 in. diffstack

Figure 2.7. Photograph of home-built jet-cooled REMPI Time of Flight Mass spectrometer.

diffusion pump (OD250, Hind Hivac) with a pumping speed of 3000 L/s. This diffusion pump is backed by a roughing pump (FD-60, Hind Hivac) having pumping speed of 17 L/s. Another smaller chamber (ionization chamber) is pumped by a 4.5 in. diffstack diffusion pump (OD114, Hind Hivac) with a pumping speed of 280 L/s This small diffusion pump is backed by a roughing pump (ED-21, Hind Hivac) having pumping speed of 6 L/s. The upper wall of the diffusion pumps are cooled by circulating water (temperature = 18°C) from a chiller (Refricon Hvac System). The vacuum chambers are separated from the diffusion pumps by gate valves. Liquid nitrogen traps are used between vacuum chambers and diffusion pumps to get rid of the contamination from the diffusion pump fluid. The pressures in different chambers are measured using cold cathode ionization gauges. A two-stage ion source of Wiley-McLaren design[361] with a 1 m linear time-of-flight (TOF) tube (Jordan TOF Products) is housed in the ionization chamber in the perpendicular direction with respect to

the molecular beam axis. An 18 mm diameter dual Micro Channel Plate (MCP) detector (Jordan TOF Products) is placed at the end of the TOF tube. The detector is housed in a small chamber pumped by a 70 L/s turbomolecular pump (Turbo-V81, Varian). The turbo pump is backed by a dry scroll pump (SH-110, Varian, pumping speed: 1.5 L/s). A TOF power supply (D-603, Jordan TOF Products) has been used to apply voltages at the detector as well as electrodes in the ionization region. The ion signal from the detector is amplified by a preamplifier (SRS, Model SR445A) and sent to a digital oscilloscope (Tektronix, 350 MHz, DPO 4034) interfaced to a PC via a USB port. The data acquisition and laser control are performed using home-built LabVIEW (National instruments, 9.0 version) based programs. Temporal synchronization among the pulsed valve, UV lasers and IR laser is performed using a digital delay generator (BNC, Model 575).

2.1.5. Experimental scheme

A schematic diagram of the experimental setup is shown in Figure 2.8. Generally, the sample of interest (either solid or liquid) having low vapor pressure is put in a stainless steel sample holder placed behind the pulsed valve and heated between 70 - 100°C. On the other hand, a sample having high vapor pressure is taken in a sample holder which is cooled in an appropriate freezing bath and kept outside the chamber. The sample vapor seeded in He or Ar carrier gas at 30 – 40 psig is expanded into vacuum through the pulsed nozzle. Typical operating pressures in the expansion and ionization chambers are 2×10^{-6} and 3×10^{-7} Torr, respectively and the corresponding base pressures of 1×10^{-7} and 8×10^{-8} Torr, respectively. The pulsed valve is operated at 10 Hz with pulse duration of 130-160 μs. The pulsed molecular beam, which is collimated through the skimmer, intersects with the pulsed UV laser beam in the ionization region. The UV beam comes in the perpendicular direction to the molecular beam axis. To have temporal synchronization between the laser beam and molecular beam, the pulsed valve is fired first and the UV laser is delayed by a few hundred μs.

The molecules are ionized by tunable UV laser beam using REMPI technique. The ions are extracted and accelerated by applying typical voltages of +3060 V and +2780 V at the repeller plate (VA1) , the extractor plate (VA2) , respectively. The accelerating plate is held

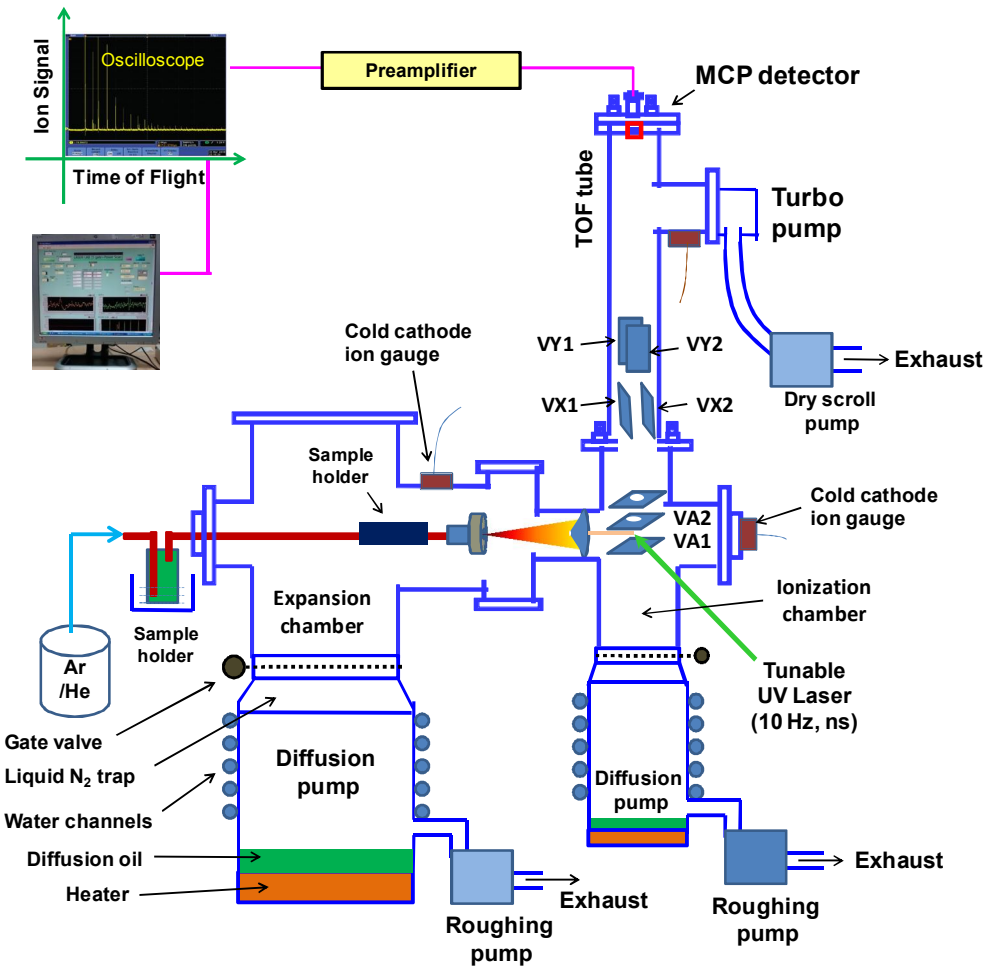

Figure 2.8. Schematic diagram of the experimental setup

at ground potential. Two pairs of deflector plates (X, Y) are also present in the TOF mass spectrometer to correct the ion trajectory of the ions towards the detector. Generally, we keep the voltages of all the deflector plates at zero. The ions of different masses get separated during their travel through the field free TOF tube and are detected at the MCP detector. The ion signal from the detector is amplified (typically 25 or 125 times) using the preamplifier and sent to the oscilloscope interfaced to a PC via an USB port. The data acquisition part has been discussed in the following.

2.1.6. Data Acquisition

A LabVIEW based master software has been written to scan the laser wavelength as well as collect the data from the oscilloscope. The oscilloscope displays ion signals of different masses as a function of the time of flight. The time of flight of different ions is converted to

the corresponding masses using the equation, $\mathbf{T_2}=\sqrt{\frac{m_1}{m_2}}\times\mathbf{T_1}$, already described in the section 2.1.2. The equation is derived using conservation of kinetic energy of the ions of different masses. In this equation, T_1 and m_1 are the time of flight and mass of an unknown molecule, whereas T_2 and m_2 are the time of flight and mass of a reference molecule. The signal of ions as a function of mass at a particular laser wavelength is called TOF mass spectrum. After recording the TOF mass spectrum, all the possible complexes are assigned by taking the addition of the masses of the monomeric units. Thus mass peaks of desired molecules and complexes are identified from the mass spectrum. The mass peak of interest is then gated i.e. the time window for the particular mass channel is selected using the LabVIEW based program. Then the laser wavelength is scanned using the same software to measure the mass selected electronic spectrum. Laser based various spectroscopic techniques used in this work are discussed in the following.

2.1.7. Spectroscopic techniques

Several spectroscopic techniques using UV and IR lasers have been used for our experiment. The mass selected electronic spectra of molecules and complexes have been measured using 1C-R2PI and 2C-R2PI spectroscopy. Presence of a single or multiple isomers of molecules and complexes in the experiment has been confirmed by UV-UV and IR-UV hole-burning spectroscopy techniques. Structures of the molecules and complexes observed in the experiment are determined using resonant ion dip infrared spectroscopy (RIDIRS) and quantum chemistry calculations.

2.1.7.1. 1C-R2PI and 2C-R2PI spectroscopy

These techniques have already been discussed in the section 2.1.2.1.

2.1.7.2. Resonant ion-dip infrared spectroscopy (RIDIRS)

A schematic diagram of RIDIRS has been shown in Figure 2.9a. In this technique, two counter-propagating IR and UV laser beams are spatially overlapped and intersected with the molecular beam at right angle.[368] Typical pulse energy of the IR laser beam used is about 3 - 4 mJ. The IR laser beam is focused using a CaF_2 lens of focal length 185 cm while the UV laser beam used is unfocused and the typical pulse energy is about 0.4 - 0.5 mJ. The IR laser

is fired about 100 ns prior to the UV laser. Figure 2.9b shows delay of 100 ns between the photodiode signal from IR and UV lasers. The IR laser is scanned through the vibrational transitions in the ground electronic state while the UV laser is fixed to a particular transition in the R2PI spectrum of the molecule or complex. Thus the IR spectrum is obtained as depletion of the ion signal whenever the IR laser frequency will be matching with any vibrational transition of the molecule or complex in the ground electronic state. Figure 2.9c shows a typical IR spectrum obtained using RIDIRS.

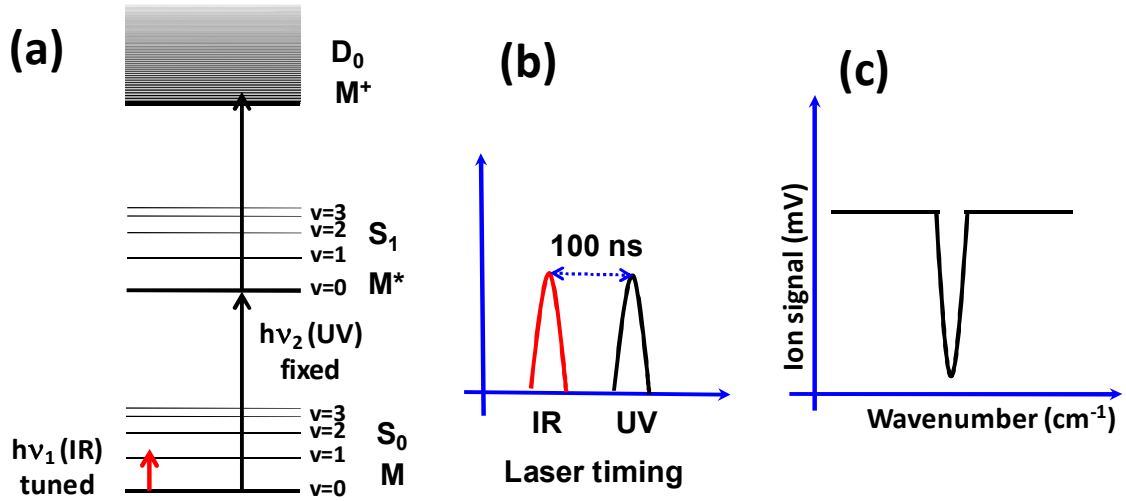

Figure 2.9. Schematic diagram for (a) the principle of RIDIRS, (b) laser timing for RIDIRS, and (c) IR spectrum

2.1.7.3. IR-UV hole-burning spectroscopy

IR-UV hole-burning experiment has been performed to discriminate the transitions in the R2PI spectrum, which belong to different isomers.[368-370] Figure 2.10 shows a schematic diagram of this technique. This technique is similar to RIDIRS, only the difference is that the UV laser instead of IR laser is scanned. The IR laser is kept fixed at a particular vibrational frequency of an isomer of the molecule or complex and the UV laser, which is fired 50-100 ns later from the IR laser, is scanned through the R2PI spectral region. As the IR laser will burn the population of a specific isomer through vibrational excitation, the UV excitation bands of that isomer will show reduced intensity compared to those in the R2PI spectrum. On

the other hand, the intensity of the UV excitation bands of the other isomers in the R2PI spectrum will remain unaltered even in the presence of the IR beam. For example, Figure 2.10d and 2.10e show two IR-UV hole burning spectra when the IR laser frequency is fixed at two different vibrational transitions of two isomers of the molecule or complex. The R2PI spectrum has been shown in Figure 2.10c.

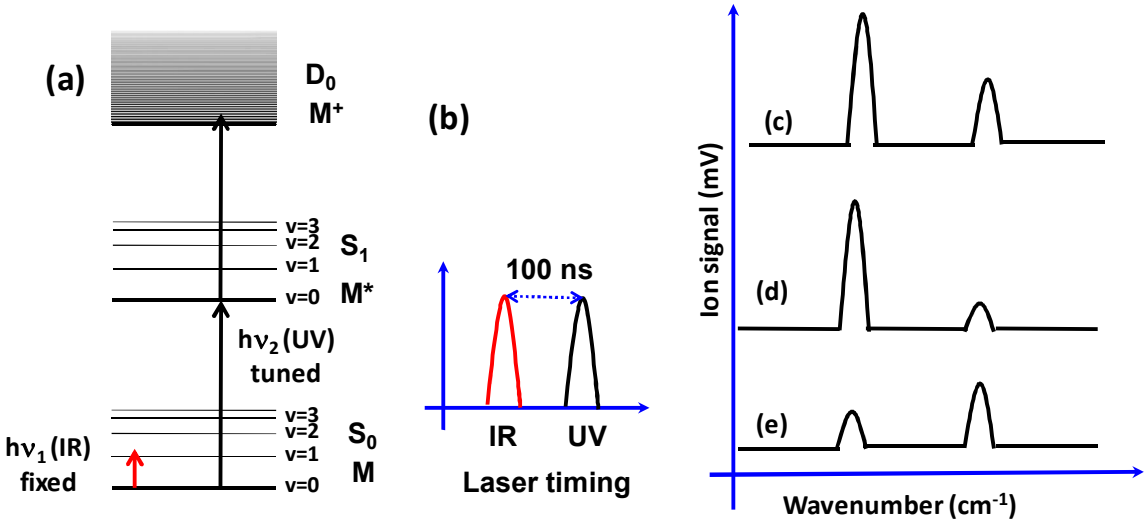

Figure 2.10. (a) Schematic diagram for the principle and (b) laser timing of IR-UV hole burning spectroscopy, (c) schematic diagram of R2PI spectrum, (d-e) schematic diagram of IR-UV hole burning spectra probing at two different IR band positions.

2.1.7.4. UV-UV hole-burning spectroscopy

This technique provides similar information what IR-UV hole-burning spectroscopy gives. A schematic diagram of this technique is shown in Figure 2.11.[369-371] In this spectroscopy, a relatively high power UV laser (hole-burning or pump laser, 10 Hz, pulse energy 0.5-0.6 mJ) is scanned through the wavelength region of the R2PI spectrum of the molecule or complex. A second UV laser (probe laser, 10 Hz, pulse energy 0.2-0.3 mJ) fired 50-100 ns (see Figure 2.11b) after the hole-burning laser is spatially overlapped with the first laser beam and kept fixed at a particular transition in the R2PI spectrum. All vibronic transitions arising from the same ground state will show depletion in the hole-burning spectrum. For example, Figure

2.11d-e shows schematic UV-UV hole-burning spectra while probing two different electronic transitions originating from two different ground electronic states of two isomers. Figure 2.11(d-e) shows depletion in ion signal by fixing the probe laser frequency at two different transitions in the R2PI spectrum shown in Figure 2.11c.

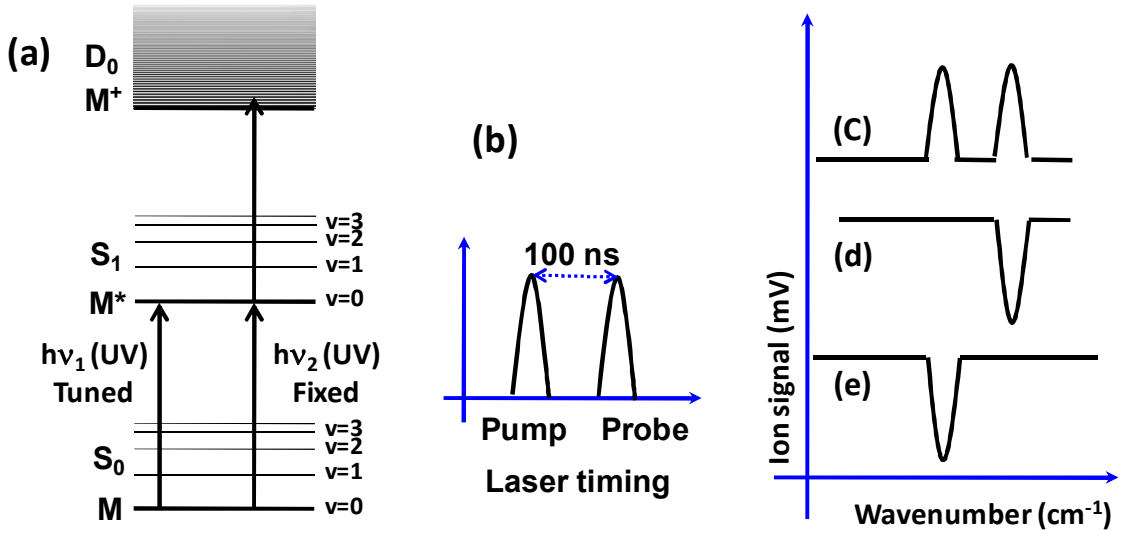

Figure 2.11. Schematic diagram of the (a) UV-UV hole burning spectroscopy (b) laser timing for UV-UV hole burning spectroscopy, (c) schematic diagram of R2PI spectrum, (d-e) schematic diagram of UV-UV hole burning spectra probing at two different UV band positions of the electronic spectrum shown in (c).

2.1.8. Synthesis of non-covalently bonded molecular complexes

The detailed procedure of synthesis of specific complex in the supersonic jet has been

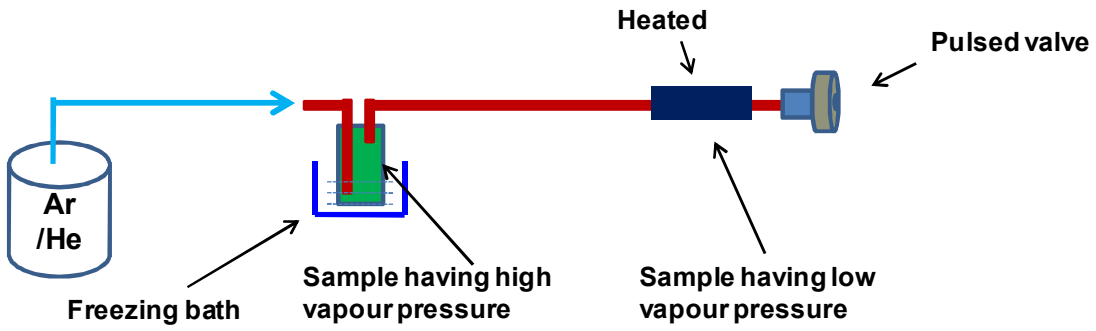

Figure 2.12. Schematic diagram of sample compartments assembly with pulsed valve

provided in individual chapter. Here, we have described only the general procedure used in the synthesis of those non-covalently bonded complexes. Figure 2.12 shows a schematic diagram of the sample compartment assembly along with the pulsed valve. Generally, the samples having low vapor pressure are taken in a stainless steel sample holder placed behind the pulsed valve and heated at 70 - 100 $^{\circ}$C. On the other hand, the samples having high vapor pressure are kept outside the vacuum chamber in a stainless steel container cooled using freezing bath. The buffer gas such as argon or helium at a pressure of about 30-40 psig is bubbled through the liquid sample taken in a stainless steel sample container kept outside the vacuum chamber. The seeded vapor in the buffer gas is mixed with the vapor of another sample kept near the pulsed valve and expanded into vacuum through the pulsed nozzle. The temperatures of the samples are monitored using thermocouple.

The samples indole (≥99%), pyridine (99.8%), furan (98%), thiophene (≥99%), hexafluorobenzene (≥99.5%), imidazole (≥99%), and pyrrole (≥98%) are purchased from Sigma Aldrich and used without further purification.

2.2. Computational methods

2.2.1. Introduction

Data obtained from isolated gas phase laser spectroscopy experiments and quantum chemistry calculations go hand in hand. Thus quantum chemistry calculations are very useful to determine the structures of the molecules or complexes observed in the experiment. Very often, gas phase experimental data are also used to verify the accuracy of the results obtained from quantum calculations. The comparison between these experimental and theoretical data helps the theoreticians to develop or improve different levels of theory. We have performed wave function theory (WFT) as well as density functional theory (DFT) calculations using Gaussian09, NWCHEM, and GAMESS packages.[372-374]

2.2.2. Geometry optimization and frequency calculation

Ground state geometry optimizations and harmonic vibrational frequency calculations of the molecules and complexes are performed at various levels of DFT as well as 2nd order Moller-Plesset Perturbation (MP2) theory.[375-377] Molecular complexes studied in this work are stabilized by electrostatic as well as dispersion interactions. Thus traditional DFT

functional like Becke, three-parameter, Lee-Yang-Parr (B3LYP) which does not include dispersion interaction and MP2 theory which overestimates dispersion interaction is not suitable to determine the structures, energies and vibrational frequencies of these non-covalently bonded complexes.[378] We have mostly performed DFT calculations using dispersion corrected DFT functionals such as B97-D, ωB97X-D, M05-2X, and M06-2X.[379-382] Both Pople type and Dunning's correlation consistent basis sets are used for optimization of the geometries of various possible isomers of the complexes, initial structures are generally made from chemical intuitions. "Ultrafine" numerical integration grid is used to obtain reliable results for the DFT calculations. All the calculations are performed using opt=tight convergence criteria for geometry optimization. The binding energies of various isomers of the dimer have been corrected for basis set superposition error (BSSE) as well as zero point vibrational energy (ZPE). BSSE correction has been done using the counterpoise method given by Boys and Bernardi.[383]

For the determination of the structures of the complexes observed in the experiment, experimental IR frequencies are compared with the theoretical IR frequencies of different possible isomers. Harmonic vibrational frequencies obtained from the quantum calculation using Gaussian program are scaled by a factor obtained from the ratio of experimental and calculated NH stretching vibrational frequencies of the monomer.

2.2.3. Binding energy calculation with BSSE and Zero Point Energy (ZPE) correction

The interaction energy or binding energy [ΔE_{int} (AB)] of a complex AB between monomers A and B can be computed as:

$$\Delta E_{int}(\mathrm{AB}) = E_{AB}^{AB}(\mathrm{AB}) - E_{A}^{A}(\mathrm{A}) - E_{B}^{B}(\mathrm{B}) \qquad (2.5)$$

$E_{AB}^{AB}(\mathrm{AB})$ denotes the energy of the complex AB computed using dimer basis sets and geometry of the dimer. Similarly $E_{A}^{A}(\mathrm{A})$ and $E_{B}^{B}(\mathrm{B})$ denote the energy of the monomer A and B, respectively. The dimer basis sets are the union of the basis sets on A and B. Similarly the energies of the monomers A and B are computed using their own basis sets and geometries.

Next, the binding energies of weakly bound complexes have been corrected for basis set superposition error (BSSE).[383] In the complexes, as the atoms of interacting molecules approach each other, their basis functions overlap and hence one monomer borrows the basis functions from the nearby monomer to increase its effective basis functions. This induces the artificial shortening of intermolecular distances between the atoms and hence strengthens the intermolecular interaction. Thus there occurs an overestimation in calculating the binding energies of the complexes, which is known as "basis set superposition errors" (BSSE).[383]

The counterpoise BSSE corrected binding energy is computed as[383],

$$\Delta E_{int}^{CP}(\mathrm{AB}) = E_{AB}^{AB}(\mathrm{AB}) - E_{A}^{AB}(\mathrm{A}) - E_{B}^{AB}(\mathrm{B}) \qquad (2.6)$$

where E_{A}^{AB}(A) and E_{B}^{AB}(B) denote the energies of the monomers A and B using the dimer basis sets, respectively.

Further Zero Point Energy (ZPE) correction in the binding energy of the complexes are performed using the following equation,

$$\Delta E_{int}^{ZPE}(\mathrm{AB}) = E^{ZPE}(\mathrm{AB}) - E^{ZPE}(\mathrm{A}) - E^{ZPE}(\mathrm{B}) \qquad (2.7)$$

where E^{ZPE}(A) =E^{A}(A) + ZPE, E^{ZPE}(A) denotes the zero point corrected energy.

2.2.4. Energy Decomposition Analysis (EDA)

A localized molecular orbital (LMO) method introduced by Su and Li[384] and implemented in GAMESS has been used for the energy decomposition analysis of the non-covalently bonded complexes studied in this work. Here, a simple but robust basis set insensitive method is used for the decomposition analysis of the interaction energy in the complexes.[384] Kitaura and Morokuma[385], Ziegler and Rauk[386], Hayes and stone[387] have earlier contributed in developing decomposition analysis methods and this LMO-EDA method is an extension in this series.

Using the LMO-EDA method, the total Kohn-Sham (KS) interaction energy of the molecular complexes is decomposed into electrostatic, exchange, repulsion, polarization, and dispersion terms.[384] The electrostatic, exchange, and repulsion contributions to the interaction energy are separated using Hayes and Stone's method.[387] The exchange and dispersion contributions to

the interaction energy are obtained from the change in exchange and correlation functions going from supermolecule to monomer.[384]

In the LMO-EDA method, BSSE correction[383] is also implemented. Thus the monomer can use the basis set of the supermolecule. The geometry distortion, zero point energy, and thermal energy are not considered in this calculation.

2.2.5. Natural bond Orbital (NBO) analysis

NBO program[388] has been developed by Weinhold and co-workers.[389] In the present work, NBO program incorporated in Gaussian09 software has been used to calculate the strength of individual non-covalent interaction present in the complexes. NBO method encompasses a suite of mathematical algorithm that enables the understanding of the fundamental concepts of the localized Lewis-like chemical bonds. The method works to link the elementary valency and bonding concepts into the simplified species such as monoatomic, diatomic and polyatomic.

The aim of the NBO is to formulate a complete orthogonal set of the Natural Atomic Orbitals. First, the input atomic orbital basis set is transformed into natural atomic orbitals (NAOs). Then NAOs is transferred to NBOs through natural hybrid orbitals (NHOs). The results obtained from the NBO analysis are useful in understanding the bonding concepts, such as, bond type (covalent, ionic, dative, σ, π, 2centre-2electron, 3centre-2electron, 3centre-4electron, etc), hybridization, bond order, charge transfer, resonance weights, steric effects as well as spectroscopic descriptors.

In the case of the hydrogen bonded systems, the most significant term is NBO delocalization energy, which is a measure of the strength of hydrogen bonding interaction, is determined by the second order perturbative energy, $E^{(2)}_{i\rightarrow j^*}$, where i and j^* stand for an acceptor and a donor orbital, respectively. Occupancy in the bonding orbital of hydrogen bond donor and antibonding orbital of hydrogen bond acceptor also show the extent of overlap between them in the formation of hydrogen bond. A brief description of NBO analysis has also been provided in individual chapter.

3. Interplay between conventional hydrogen bonding and dispersion interactions: Complexes of indole and pyridine

3.1. Introduction

It has been already discussed in detail in section 1.1 that conventional hydrogen bonding and dispersion bound interactions play a significant role to govern the specific functional structures of biomolecules and materials. The origin of these two types of non-covalent interactions is entirely different. The conventional hydrogen bonding arises mostly from electrostatic interaction while π…π stacking and π-hydrogen bonding interactions are governed by dispersion forces. In fact, conventional hydrogen bonding interaction could be determined precisely by both experiment and theory but accurate determination of dispersion interaction is quite difficult.[11-12] It becomes further challenging to investigate the contribution of these two interactions when these are present simultaneously in a molecule or complex to provide its specific structure. We have discussed in section 1.7.2.3. that the binding energy difference between parallel-displaced π-stacked and T-shaped isomers of benzene dimer as well as indole…benzene dimer is very small according to highly accurate quantum chemistry calculations at the CCSD(T)/CBS level of theory.[284] But gas phase supersonic jet studies show the presence of only the T-shaped structure of benzene dimer and indole…benzene dimer, which are stabilized due to π-hydrogen bonding.[257-262] Thus it can be concluded from these studies that π-hydrogen bonding is stronger than π-stacking interaction present in aromatic dimers. In contrast, observation of π-stacked dimer from experiment is very scarce.[245,248-249,302-304] Given that there is a competition among conventional hydrogen bonding, π-hydrogen bonding, and π-stacking interactions in aromatic clusters, it is quite challenging to study the structures of the molecular systems or complexes stabilized due to the subtle balance among multiple interactions.

In this chapter, we have reported a detailed experimental and theoretical investigation of the structure of a "*special class of mixed complex*", which is already defined in section 1.8.1. These complexes are stabilized by the subtle balance between conventional hydrogen bonding and dispersion interaction. More specifically, we have studied the structures of the complexes of indole and pyridine formed in a supersonic jet by employing R2PI and IR-UV double resonance spectroscopic techniques combined with quantum chemistry calculations.

The most significant finding of the present study is the observation of indole…pyridine dimer which is stabilized by conventional hydrogen bonding (N-H…N) as well as CH…π and π…π stacking interactions. This dimer falls in the category of special class of mixed complex. Moreover the spectroscopic study of complexes of indole and pyridine has specific biological relevance as it mimics protein-enzyme interactions.[390-392]

3.2. Results and discussion

3.2.1. Time of Flight (TOF) mass spectrum.

Figure 3.1 shows TOF mass spectrum of the complexes of indole and pyridine formed in supersonic jet using argon as a buffer gas. The mass spectrum has been recorded at a fixed laser wavelength of 284.16 nm (35191 cm^{-1}), which corresponds to one of the electronic

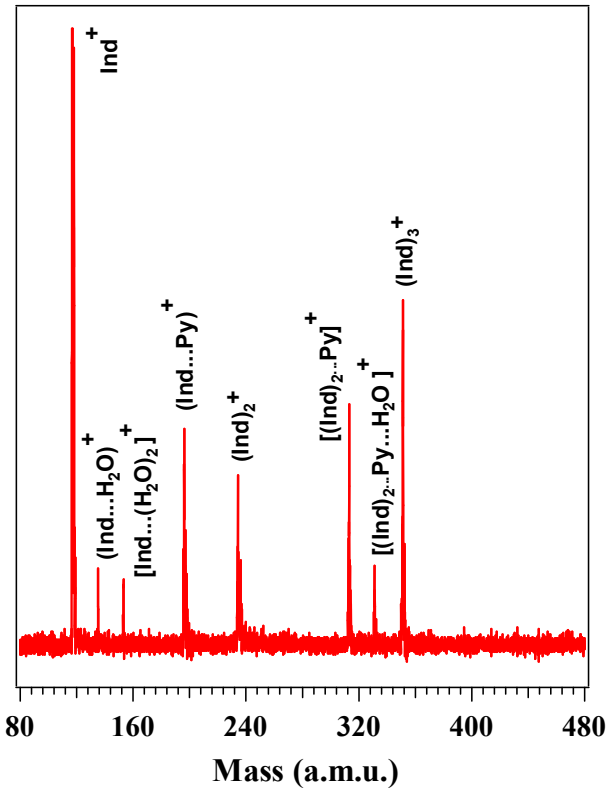

Figure 3.1. TOF mass spectrum of indole in presence of pyridine recorded at laser frequency of 35191cm^{-1}, which corresponds to one of the electronic transition bands of $(indole)_2$…pyridine complex. Ind and Py stand for indole and pyridine, respectively.

transition bands of $(indole)_2$…pyridine complex. The mass peak observed at 196 amu is due to indole…pyridine dimer while the 313 amu mass peak is for $(indole)_2$…pyridine trimer. Higher clusters of indole i.e $(indole)_2$ and $(indole)_3$ are also observed at 234 amu and 351 amu, respectively. Water clusters of indole i.e. indole…$(H_2O)_1$, indole…$(H_2O)_2$ as well as

(indole)$_2$…pyridine…(H_2O) are also observed in the experiment due to presence of water as impurity in the sample and buffer gas.

3.2.2. R2PI spectra

One-color R2PI spectra measured in indole…pyridine dimer and (indole)$_2$…pyridine trimer mass channels are shown in Figures 3.2(b) and 3.2(c), respectively. Pyridine is taken in a stainless steel sample holder maintained at 0°C (using mixture of ice and aqueous solution of NaCl). Vapor pressure of pyridine at 25°C is 20 mmHg.[393] A buffer gas of Ar (40 psig) is

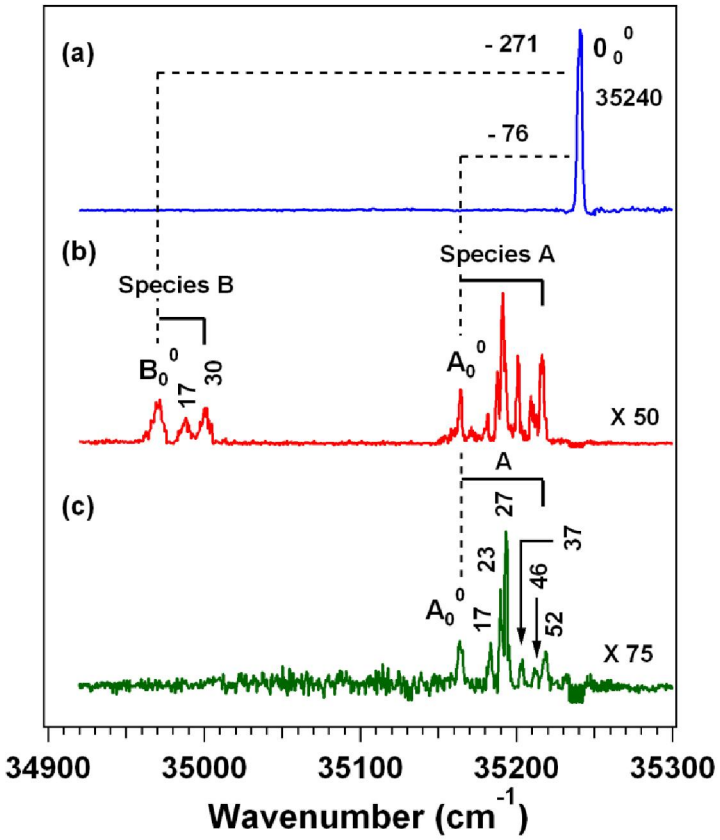

Figure 3.2. One-color R2PI spectra recorded in (a) indole, (b) indole…pyridine dimer, and (c) (indole)$_2$…pyridine trimer mass channels. R2PI signals of the dimer and the trimer are very weak compared to that of the monomer. Thus the dimer and the trimer spectra are magnified by 50 and 75 times, respectively.

flown through pyridine and the vapor seeded in the buffer gas is mixed with the vapor of indole placed behind the pulsed valve heated at 80°C. One-color R2PI spectrum of indole in

absence of pyridine is also shown in Figure 3.2(a) to compare with dimer and trimer R2PI spectra. The origin band (0_0^0) for the $S_1 \leftarrow S_0$ electronic transition of indole appears at 35240 cm^{-1}, which matches well with the previous report.[394] The R2PI spectra of complexes of indole and pyridine are measured by electronic excitation of the indole moiety. R2PI signals of the dimer and the trimer are very weak and thus the dimer and trimer R2PI spectra are magnified by 50, and 75 times, respectively to show in the same Figure with the spectrum of the indole monomer. The R2PI spectrum in the indole…pyridine dimer mass channel shows two different sets of bands originated due to electronic transitions of two different species designated as A and B. When the R2PI spectrum is recorded in $(indole)_2$…pyridine trimer mass channel, all the peaks assigned as species A in the dimer channel also appear in the trimer mass channel. This confirms that the peaks assigned as A do not belong to indole…pyridine dimer, rather it seems that these peaks are originated due to electronic transition of $(indole)_2$…pyridine trimer. These peaks appear in the R2PI spectrum recorded in the dimer mass channel due to efficient fragmentation of the $(indole)_2$…pyridine trimer in the indole…pyridine dimer mass channel. R2PI spectrum in the mass channel of indole in presence of pyridine is also recorded and this indicates the fragmentation of A and B complexes into indole monomer channel as well. But the spectrum in the indole mass channel is complicated due to overlapping of the transitions arise from the fragmentation of other higher clusters of indole. Thus the R2PI spectrum in the indole mass channel in presence of pyridine is not presented here.

In order to avoid the fragmentation of the clusters, generally two-color R2PI scheme is used by fixing the ionization laser frequency just above the ionization threshold. We have tried two-color R2PI of complexes of indole and pyridine but it was not successful probably due to very fast deactivation of the S_1 state. We have also recorded R2PI spectrum in the $(indole)_2$…pyridine…H_2O channel, which is observed in the mass spectrum depicted in Figure 3.1. It is possible that $(indole)_2$…pyridine…H_2O complex may fragment to $(indole)_2$…pyridine trimer and indole…pyridine dimer mass channels. But the R2PI spectrum measured in $(indole)_2$…pyridine…H_2O mass channel shown in Figure 3.3 does not show any peak in the region of the R2PI spectrum of either species A or B. From the R2PI spectra recorded in various observed mass channels, it can be concluded that the species A is

(indole)$_2$…pyridine trimer, which is confirmed in the following sections through IR-UV double resonance spectroscopy and quantum chemistry calculations.

Figure 3.2 shows that the origin band (B_0^0) of indole…pyridine dimer is red-shifted from 0_0^0 band of indole monomer by 271 cm^{-1}. The transitions marked at B_0^0 + 17, and B_0^0 + 30 cm^{-1}

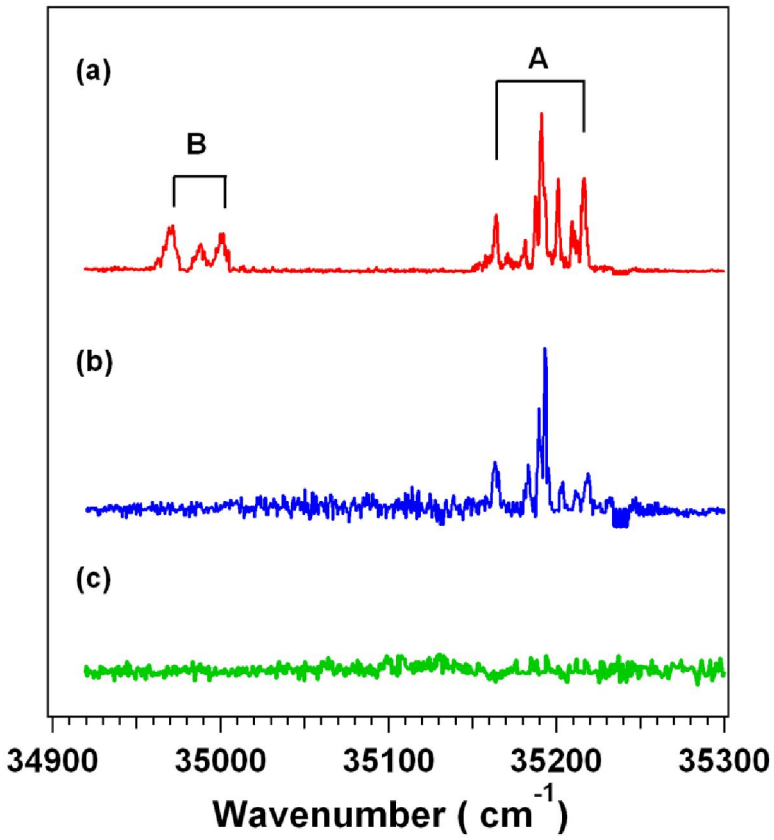

Figure 3.3. One-color R2PI spectra recorded in (a) indole…pyridine dimer (b) (indole)$_2$…pyridine trimer and (c) (indole)$_2$…pyridine…H_2O mass channels.

are assigned as intermolecular vibrations of the mixed dimer. In the case of the (indole)$_2$…pyridine trimer, the origin band (A_0^0) is red-shifted from 0_0^0 band of indole monomer by 76 cm^{-1}. The low frequency vibronic features built off A_0^0 band are assigned as intermolecular vibrations of the trimer. The assignment is confirmed in the following section through RIDIR and IR-UV hole-burning spectroscopy. Intermolecular vibrations of the trimer observed in the R2PI spectrum shown in Figure 3.2(c) are listed in Table 3.1 and a tentative assignment of those vibrations is also provided there. All of the vibronic features in the

spectrum can be tentatively explained as overtone and combination bands of mostly three intermolecular modes of 17 (β), 23 (δ), and 27 (θ) cm^{-1}. Proper assignment of the low frequency vibrations in the R2PI spectrum can be done only by performing excited state frequency calculation of the trimer, which is not possible using our available computational resources. But we have performed the frequency calculation of the trimer in the ground electronic state and 12 intermolecular vibrational frequencies of the most stable isomer of the trimer are listed in Table 3.2. We are aware that the calculated frequencies in the excited state will be different and thus the observed excited state intermolecular vibrational frequencies are not compared with the calculated frequencies in the ground electronic state.

Table 3.1: Tentative assignment of the observed intermolecular vibrations of $(indole)_2$…pyridine trimer

Frequencies (cm^{-1})	Assignment
17	β
23	δ
27	θ
37	2β / β+ δ
46	2δ / β+ θ
52	2θ / 3β / θ+ δ

One characteristic feature of the R2PI spectrum of the trimer is that the 0_0^0 band (A_0^0) is weaker in intensity compared to a few of the low frequency intermolecular vibrations built on it. This indicates that the ground state equilibrium geometry of the trimer is changed significantly upon electronic excitation to the S_1 state and the geometry change of the trimer along 27 cm^{-1} mode is maximum upon electronic excitation. But the excitation spectrum does not show extensive Franck-Condon progressions although multiple intermolecular modes are clearly observed. Absence of further vibrational progressions could be due to the following reason. Actually, few low frequency vibrations beyond 52 cm^{-1} are overlapping with the 0_0^0 band position of indole monomer. The UV laser is blocked in the region of origin band of bare indole to avoid detector saturation due to very strong ion signal of the monomer. This leads to a small dip in the origin band position of indole in the R2PI spectra of the complexes shown in Figure 3.2.

It is interesting to note that the red-shift in the band origin of (indole)$_2$…pyridine trimer with respect to the 0_0^0 band of indole is very less compared to that of indole…pyridine dimer. This indicates that the stabilization of the dimer is more than the trimer in the S_1 state compared to that of the dimer and trimer in the S_0 state relative to the respective monomers. A Similar kind of trend is also observed in case of the phenol dimer and trimer reported in the literature.[3] The red-shifts in the band origins of phenol dimer and trimer are 304 and 146 cm^{-1}, respectively with respect to the 0_0^0 band of phenol monomer. It is also worthy to

Table 3.2. Ground state intermolecular vibrational frequencies (cm^{-1}) of the most stable isomer ((Ind)$_2$ .Py-1) of (indole)$_2$…pyridine trimer at various levels of theory.

M05-2X/6-311++g**	M05-2X/cc-pVDZ
21.4	21.8
29.8	29.8
37	38.7
51.3	52
56	57
59.7	62
62	64
72.5	72
78.8	80.5
89.6	92
104.6	108.4
117.4	118.4

compare the line widths of the transitions in indole…pyridine dimer, (indole)$_2$…pyridine trimer, and bare indole, which can shed light on the photophysics of the complexes of indole in the excited electronic state. The line width of 0_0^0 band of indole monomer is about 3 cm^{-1}, whereas the line widths of the electronic bands in the R2PI spectra of indole…pyridine dimer, (indole)$_2$…pyridine trimer are about 6.5 and 2.5 cm^{-1}, respectively. Line width of transitions and lifetime of the molecules in the excited state are inversely proportional to each other. Thus the dimer has much shorter lifetime in the S_1 state compared to that of bare indole as well as the trimer. This observation is nicely supported by a few investigations reported in the literature. Sobolewski and Domcke have studied the photophysics of hydrogen bonded dimer of indole and pyridine by calculating the potential energy profiles of the ground and lowest excited electronic states of the complex as a function of the NH stretching

coordinate.[395] They have found that there is ultrafast internal conversion between the S_1 (^1L_b) and S_0 states of the hydrogen bonded dimer through the ^{1}CT (charge transfer) state via conical intersection. Hager and Wallace have reported that fluorescence of indole is completely quenched in presence of pyridine in the solution phase and supersonic jet studies.[396] They have explained that the deactivation of the S_1 state is due to either fast internal conversion to the S_0 state or intersystem crossing to the triplet manifold. The fast deactivation of the S_1 state of the dimer can also be explained in terms of efficient energy transfer from the indole moiety to pyridine after electronic excitation of indole as $S_1 \leftarrow S_0$ transition energies of indole and pyridine are close to each other. The excitation energies for 0_0^0 transitions to the S_1 (^1L_b) state of indole and S_1 ($^1B_1$) state of pyridine are 35240 and 34771 cm^{-1}, respectively.[397]

3.2.3. RIDIR spectra

To determine the structures of the indole…pyridine dimer and the (indole)$_2$…pyridine trimer observed in the experiment, IR spectra in the NH stretching frequency region have been recorded by probing several transitions in the R2PI spectrum of the dimer and the trimer. RIDIR spectrum presented in Figure 3.4(a) shows the appearance of NH stretching fundamental of indole monomer at 3526 cm^{-1}, which agrees very well with the previous report.[398] Figure 3.4(b) shows RIDIR spectrum obtained by probing B_0^0 + 30 cm^{-1} band of indole…pyridine dimer. The spectrum shows a single band at 3269 cm^{-1} and this is assigned to the NH stretching vibration of the dimer. The NH stretching vibration of the dimer is red-shifted by 257 cm^{-1} from that of indole monomer. Theoretical IR spectrum of the hydrogen bonded (N-H…N) dimer (HB3) shown with Figure 3.4(b) matches very well with the experimental spectrum. Thus the dimer has hydrogen bonded structure with N-H…N interaction. RIDIR spectrum by probing A_0^0 + 27 cm^{-1} transition of (indole)$_2$…pyridine trimer is depicted in Figure 3.4(c). The spectrum shows a strong band at 3411 cm^{-1} and two other bands at 3281 and 3309 cm^{-1}. Theoretical IR spectra of three probable structures of (indole)$_2$…pyridine trimer are shown with Figure 3.4(c). IR spectra of all the three structures of the trimer reproduce two experimental peaks at 3281 and 3411 cm^{-1} with some variation. Thus, it is assigned that the 3281 cm^{-1} peak is originating from hydrogen bonded (N-H…N) N-H stretch, whereas the 3411cm^{-1} peak is due to π-hydrogen bonded (N-H…π) N-H stretch

in the trimer. The IR peak at 3309 cm^{-1} is assigned to the intermolecular vibration (27 cm^{-1}) of the trimer built off the hydrogen bonded N-H stretching (N-H…N) vibration at 3281 cm^{-1} The 27 cm^{-1} vibration is the most intense intermolecular mode observed in the electronic spectrum of the trimer. Observation of combination bands involving hydrogen bonded N-H or O-H stretch and low frequency intermolecular vibrations of the complexes are extensively

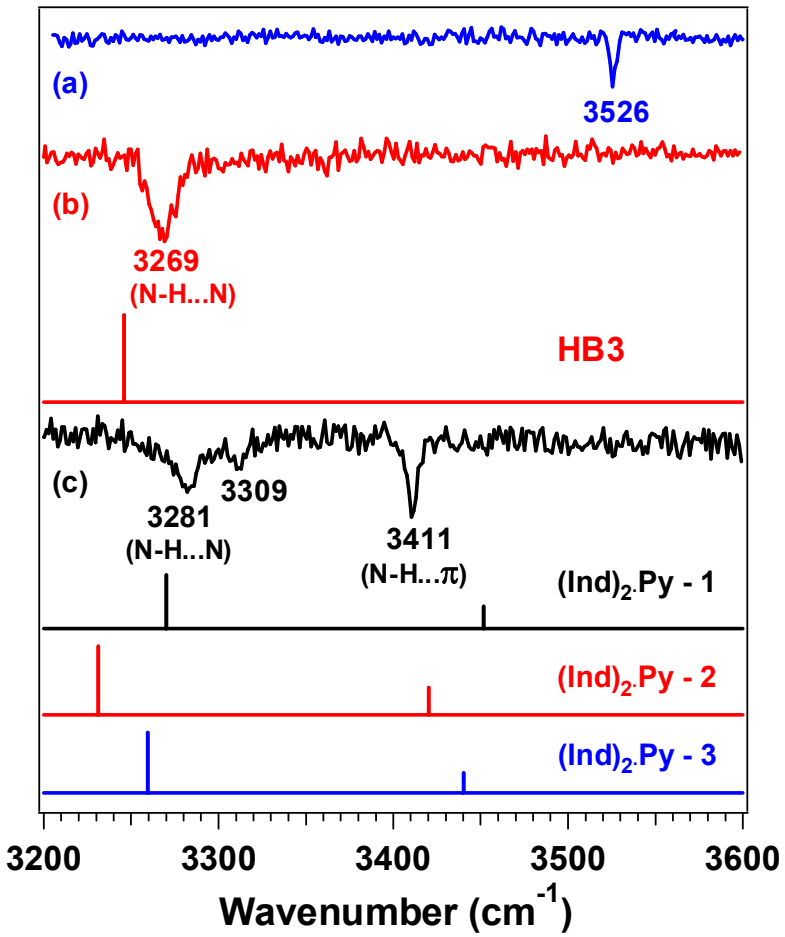

Figure 3.4. RIDIR spectra by probing (a) 0_0^0 band of indole (b) B_0^0 + 30 cm^{-1} band of indole…pyridine dimer, and (c) A_0^0 + 27 cm^{-1} band of $(indole)_2$ …pyridine trimer in the N-H stretching region. Theoretical IR spectra for V-shaped (HB3) isomer of indole…pyridine dimer, and three isomers of $(indole)_2$…pyridine trimer are provided in Figure 3.4(b), and 3.4(c), respectively. Theoretical IR frequencies were scaled using a scaling factor of 0.9566 obtained from the ratio of experimental and theoretical N-H stretch frequencies of the indole monomer.

reported in the literature.[398-401] It is also interesting to point out that the 3309 cm^{-1} band could not be due to C-H stretching modes of either indole or pyridine moieties of $(indole)_2$…pyridine trimer. IR spectra of jet-cooled indole as well as 2-fluoropyridine in the C-H stretching region have been reported in the literature.[398,402] C-H stretching frequencies of indole and 2-fluoropyridine appear in the range of 3000 – 3200 and 3000 – 3100 cm^{-1}, respectively. Gas phase FTIR spectrum of pyridine is also reported in the literature and this shows C-H stretching frequencies in 3000 – 3100 cm^{-1} range.

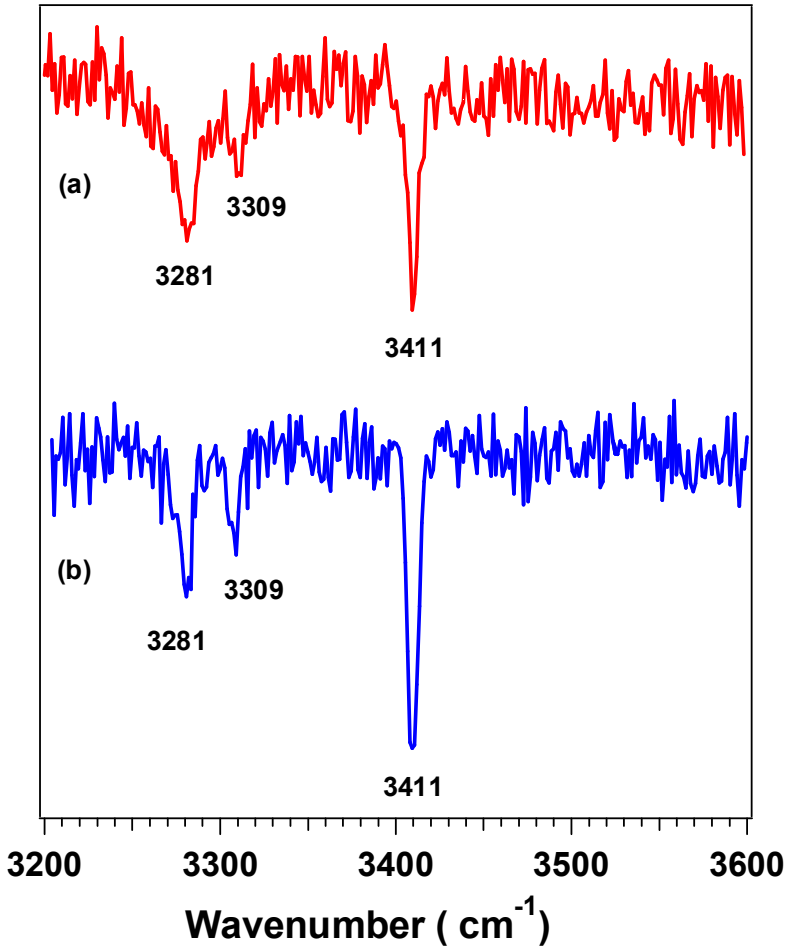

Figure 3.5. RIDIR spectra in the N-H stretching region by probing A_0^0 + 27 cm^{-1} electronic band obtained in (a) $(indole)_2$...pyridine trimer, and (b) indole …pyridine dimer mass channels.

The IR peak at 3309 cm^{-1} can also be assigned as Fermi resonance[303] between one quantum of NH stretch with the two quantum of NH bend. In the case of $(indole)_2$…pyridine trimer, N-H stretching and N-H bend frequencies of $(Ind)_2$.Py-1 are 3269 and 1602 cm^{-1}at M05-2X/6-

311++G** level of theory, respectively. Thus there is a possibility of the Fermi resonance between N-H stretch and NH bend overtone vibrations arising from the one quantum of N-H stretch and two quanta of N-H bend.

The most probable structure of the observed trimer is further determined from the comparison of binding energies and relative energies of the three structures of the trimer and this has been discussed in the theoretical section. Figure 3.5 shows RIDIR spectra by probing $A_0^0 + 27$ cm^{-1} electronic band obtained in (indole)$_2$…pyridine trimer as well as indole…pyridine dimer mass channels. Identical IR spectra have been obtained in both the cases and this confirms that species A is trimer only.

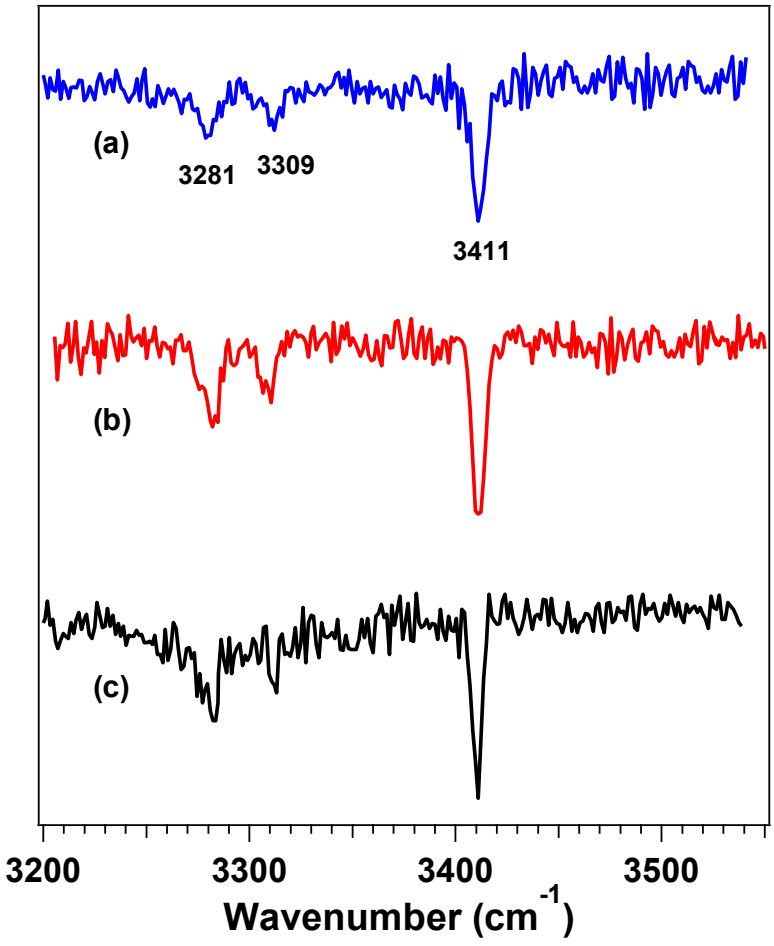

Figure 3.6. RIDIR spectra in the N-H stretching region by probing (a) A_0^0 band, (b) $A_0^0 + 27$ cm^{-1} band, and (c) $A_0^0 + 37$ cm^{-1} band of (indole)$_2$…pyridine trimer obtained in the indole…pyridine dimer mass channel.

The magnitudes of the red-shift in the X-H stretching frequency as well as width of the IR band measure the strength of the hydrogen bond. It is interesting to note that the red-shift in the hydrogen bonded (N-H…N) N-H stretching frequency in the trimer (245 cm^{-1}) is very similar to that in the dimer (257 cm^{-1}). The π-hydrogen bonded N-H stretching frequency in the trimer is red-shifted by 115 cm^{-1}. FWHM of N-H…N bound N-H stretching bands for indole…pyridine dimer and $(indole)_2$…pyridine trimer is about 20 and 12 cm^{-1} respectively, whereas the width of the π-hydrogen bound N-H stretching band is about 8 cm^{-1}. For comparison, we can refer to the FWHM of the free NH stretching band of indole monomer, which is about 4 cm^{-1}. Overall results indicate that N-H…N hydrogen bonding interaction in the dimer is slightly stronger than that in the trimer. As expected, NH…π hydrogen bonding interaction in the trimer is weaker than N-H…N hydrogen bonding interaction observed in the dimer as well as the trimer.

Interestingly, identical IR spectra were obtained by probing most of the electronic transitions of the trimer. Figure 3.6 displays IR spectra by probing A_0^0, A_0^0 + 27, and A_0^0 + 37 cm^{-1} transitions of $(indole)_2$…pyridine trimer observed in the R2PI spectrum recorded in the dimer mass channel and these show similar IR spectral features. This confirms that the lowest energy electronic transition for species A marked as A_0^0 is the origin band of the trimer and all of the higher energy transitions built off A_0^0 are only due to intermolecular vibrations of only one isomer of the trimer. Identical IR spectra were also obtained by probing all the three bands in the R2PI spectrum of the dimer i.e. B_0^0, B_0^0 + 17, and B_0^0 + 30 cm^{-1}. This demonstrates that all these three transitions belong to only one isomer of the dimer.

3.2.4. IR-UV hole-burning spectra

IR-UV hole-burning spectra obtained by probing the vibrational bands of the dimer and the trimer observed in the RIDIR spectra have been shown in Figure 3.7. Figure 3.7(e) shows the R2PI spectrum of the complexes of indole and pyridine in the dimer mass channel, which is identical to the spectrum already shown in Figure 3.2(b). The hole-burning spectrum by exciting the π-bound N-H stretching vibrational band of the trimer at 3411 cm^{-1} is provided in Figure 3.7(a). The spectrum shows depletion in ion signals for all the electronic transitions designated for the trimer while the bands assigned due to the electronic transitions for the

dimer appears with similar intensity as observed in the R2PI spectrum shown in Figure 3.7(e). This clearly demonstrates that all the bands grouped as A belong to same isomer of the trimer. When the σ-bound N-H stretching vibrational band of the trimer at 3281 cm^{-1} is excited, similar hole-burning spectrum like the one in Figure 3.7(a) is observed and the spectrum is shown in Figure 3.7(c). Figure 3.7(b) shows IR-UV hole-burning spectrum by probing the vibrational band of the trimer at 3309 cm^{-1}. The hole-burning spectrum at 3309

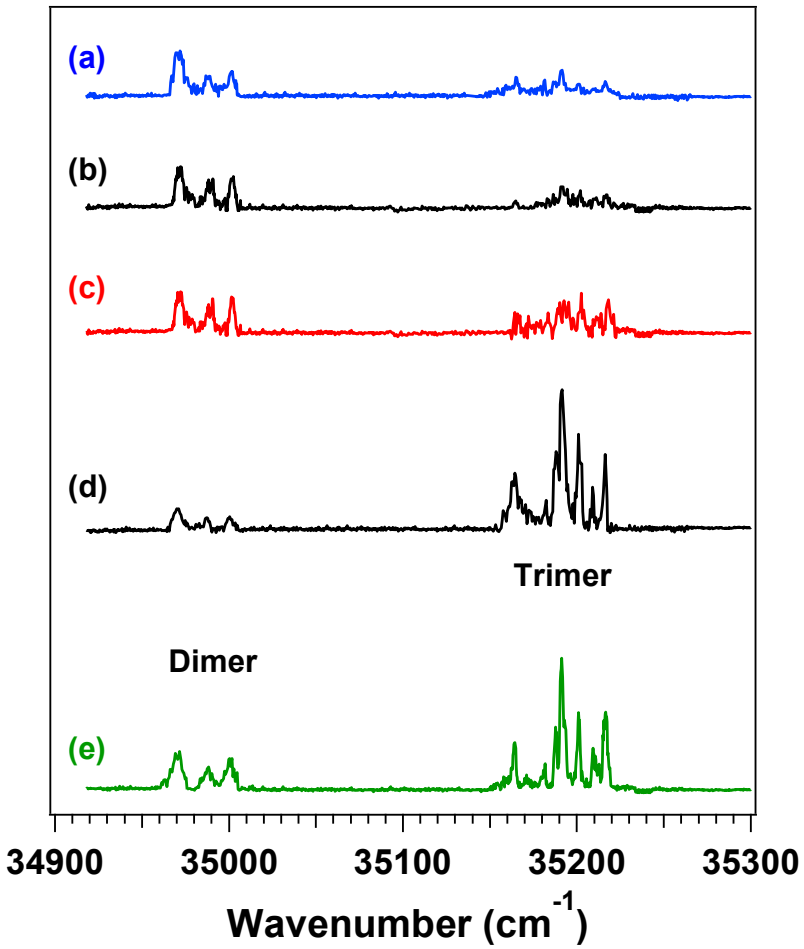

Figure 3.7. IR-UV hole-burning spectra recorded in the indole…pyridine dimer mass channel by pumping the vibrational bands at (a) 3411 cm^{-1}, (b) 3309 cm^{-1}, (c) 3281 cm^{-1}, and (d) at 3269 cm^{-1}. (e) R2PI spectrum in the indole…pyridine dimer mass channel.

cm^{-1} is similar like the spectra shown in Figure 3.7(a) and 3.7(c). Figure 3.7(d) shows the hole-burning spectrum by exciting the N-H stretching vibrational band of the dimer at 3269 cm^{-1}. The spectrum shows dip in the ion signals only for the bands assigned due to the electronic transitions for the dimer while the transitions designated for the trimer appears

with similar intensity as observed in Figure 3.7(e). Thus considering IR-UV hole-burning spectra in Figure 3.7(a)-(d), it is confirmed that each of dimer and trimer shows only one isomer in the experiment.

3.2.5. Theoretical results

3.2.5.1 Structures of indole…pyridine dimer

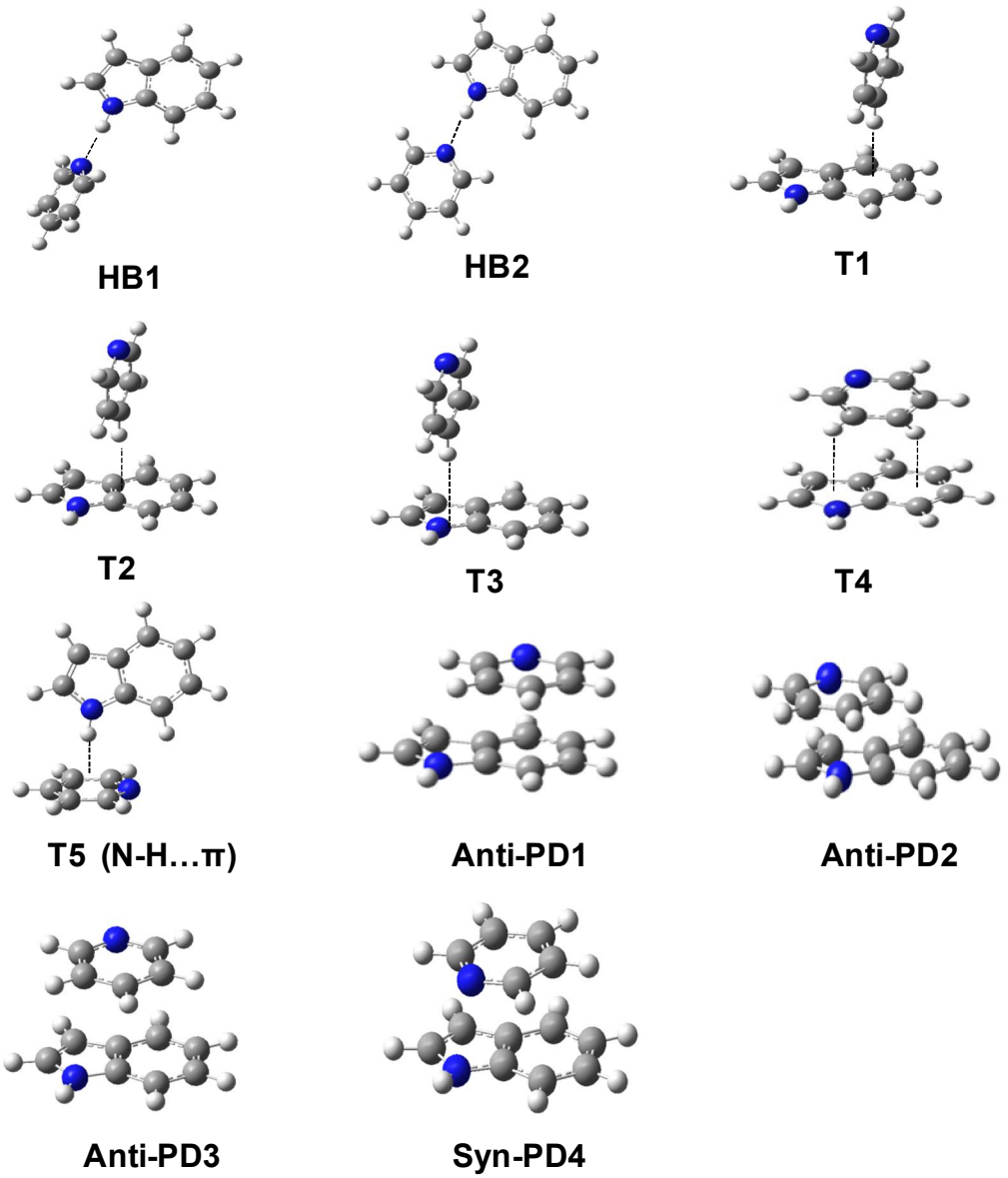

Figure 3.8. Structures of possible isomers for indole…pyridine dimer. These structures are used as initial geometries for optimization.

Several isomeric structures of indole…pyridine dimer with possible different orientations of the two monomer units are shown in Figure 3.8. These structures have been used as starting geometries for optimization. To construct the starting geometries for the dimer, we have

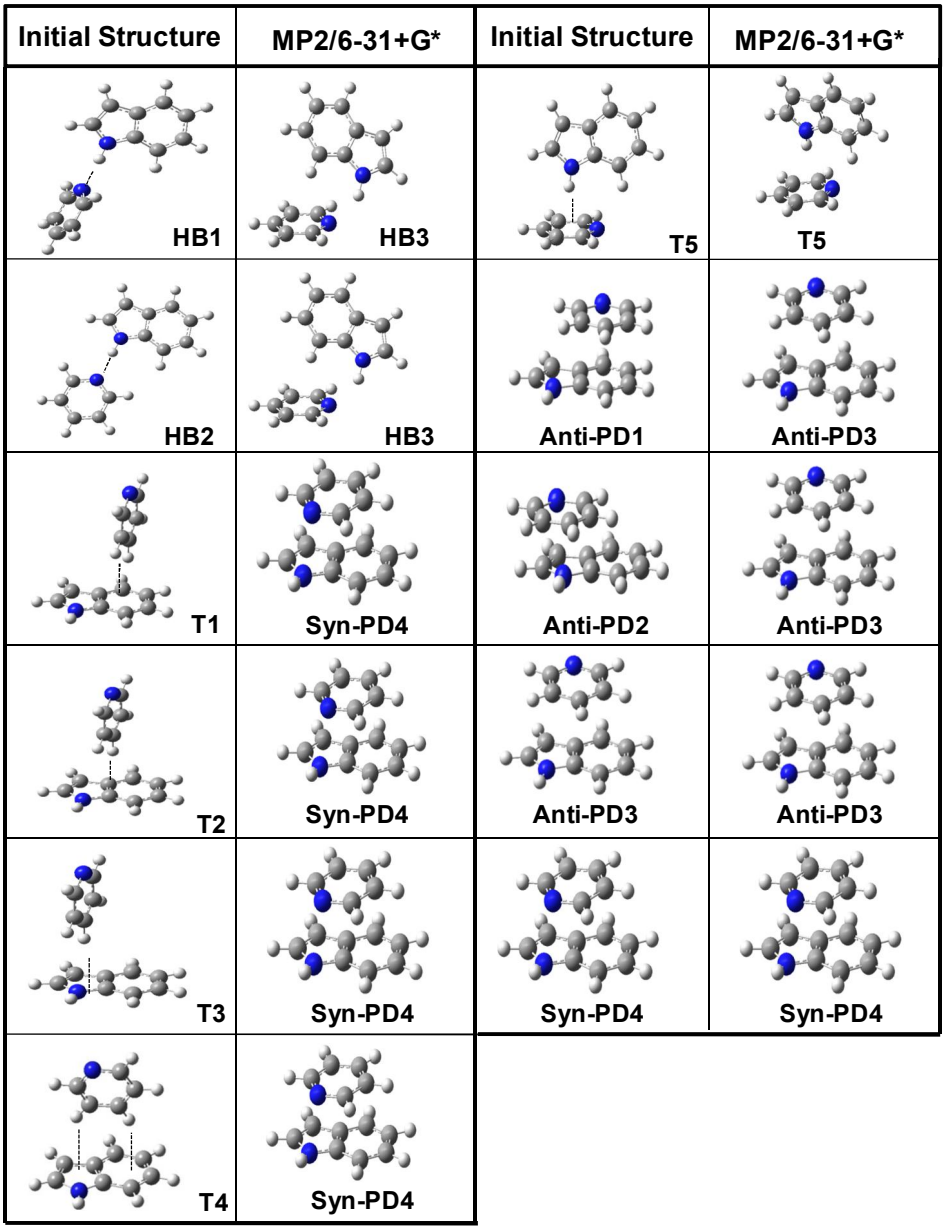

Figure 3.9 Initial and MP2/6-31+G(d) optimized structures of various isomers of indole…pyridine dimer. Eleven different possible structures of the dimer are converted into only four isomers after optimization.

followed the similar scheme adopted by Sickle et al. and Geng et al. for indole…benzene dimer.[289,403] In our case, geometric isomers of indole…pyrdine dimer have been classified mainly into three different categories namely hydrogen bonded (HB), T-shaped (T), and

parallel-displaced (PD). In both HB1 and HB2 structures, there is a strong hydrogen bond between indole NH and nitrogen atom of pyridine. But in the case of the HB1 structure, indole and pyridine are oriented in perpendicular fashion to each other through N-H…N hydrogen bond while indole and pyridine are in the same plane in the HB2 structure. T1, T2, and T3 structures consist of CH…π hydrogen bonding with phenyl group, fused C=C bond, and pyrrole group of indole, respectively, while CH…π hydrogen bonding with both phenyl

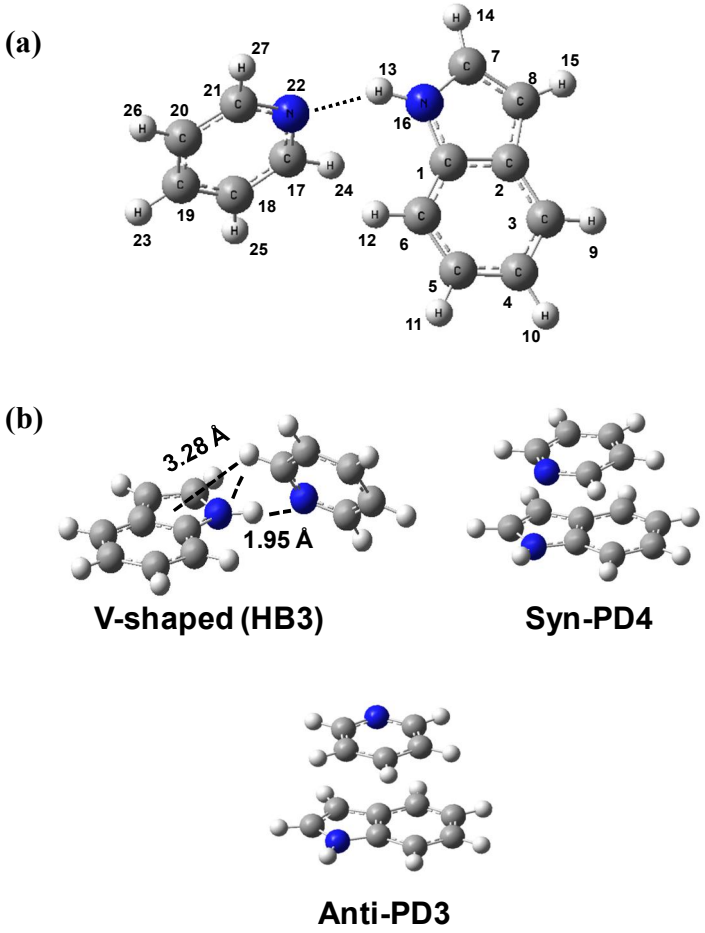

Figure 3.10. (a) Atom-numbering scheme in indole…pyridine dimer, (b) optimized structures of three isomers of indole…pyridine dimer calculated at the MP2/aVDZ level of theory.

and pyrrole groups are present in T4 structure. T5 structure is bound by NH…π hydrogen bonding, where NH group of indole makes hydrogen bonding with the π-cloud of pyridine. Anti-PD1, Anti-PD2, and Anti-PD3 structures have anti parallel-displaced geometry with pyridine placed in the stacked fashion over the phenyl ring, pyrrole ring, and fused C=C bond

of indole, respectively. As indole N-H group and pyridine nitrogen atom are oriented in the opposite side for PD1, PD2, and PD3 structures, those are called anti parallel-displaced stacked. Syn-PD4 structure is obtained by placing pyridine over indole ring in stacking orientation, where indole N-H and pyridine nitrogen atom are facing same side.

Initially geometries of all eleven probable structures of indole…pyridine dimer have been optimized at the MP2/6-31+G(d) level of theory. These structures are further optimized at higher levels of theory. Figure 3.9 shows the initial structures as well as MP2/6-31+G(d) optimized structures of indole…pyridine dimer. After optimization, both HB1 and HB2 structures converge to V-shaped hydrogen bonded structure HB3. Optimization of T1, T2, T3, and T4 structures lead to syn-PD4 structure while anti-PD1, anti-PD2, and anti-PD3 structures converge to anti-PD3 structure. NH…π bound T5 structure gives one imaginary frequency at the MP2/6-31+G* level of calculation. Thus four isomeric structures of the dimer out of eleven probable structures optimized further at various levels of theory with different basis sets (MP2, M05-2X, M06-2X) are HB3, anti-PD3, syn-PD4, and T5 (NH…π). It has been found that the T5 structure provides one imaginary frequency at all levels of theory. Figure 3.10(a) shows atom-numbering scheme used in geometry optimization of indole…pyridine dimer and this numbering scheme is used to compare important calculated geometric parameters of various isomers of the dimer. Figure 3.10(b) shows the structures of the three stable isomers of the dimer optimized at the MP2/aVDZ level of theory. Similar geometries for the three isomers have been obtained at the M05-2X/aVDZ level of theory. For the brevity, optimized structures calculated at all different levels of theory have not been shown here. As MP2 level of calculation overestimates the dispersion interaction, binding energies of different isomers of the dimer have been calculated using DFT/M05-2X and DFT/M06-2X levels theory. It is well-known that traditional DFT functional like B3LYP does not include dispersion interaction. Thus DFT/B3LYP method very often neither accurately computes the interaction energies of dispersion-dominated complexes nor describes their structures properly. But recently developed meta-density functionals M05-2X, and M06-2X by Zhao and Truhlar provide much improved results for non-covalently bonded complexes having dispersion interaction.[404] Sponer et. al. have demonstrated that the mean average error of the interaction energies of stacked complexes of nucleic acid bases computed at DFT/M05-2X level is even smaller than that computed at MP2/CBS level.[405]

The BSSE and zero point energy (ZPE) corrected binding energies for all the three isomers of the dimer calculated at various levels of theory are presented in Table 3.3. Comparison of the binding energies of the isomers at various levels of theory clearly shows that the most stable isomer is the V-shaped (HB3) one. BSSE corrected binding energy of the syn-PD4 isomer at the MP2/aVDZ level is very close to that of the V-shaped isomer (HB3), which clearly demonstrates the overestimation of the dispersion interaction of the stacked isomer at the MP2 level. ZPE correction of the binding energies of the three isomers of the dimer was not done at the MP2/aVDZ level of theory as frequency calculation of the dimer at this level is computationally very expensive. Very recently, Sanders has calculated the binding energies of only π-stacked isomers of indole…pyridine dimer at MP2/aVDZ//MP2-cc-pVDZ level of theory.[390] It is interesting to compare our computed results with these reported values. The binding energies of the syn parallel-displaced π-stacked (Syn-PD4) and anti parallel-displaced π-stacked (Anti-PD3) isomers reported by Sanders are - 8.75 and - 7.03 kcal/mol, respectively, whereas the respective values calculated by us at the MP2/aVDZ level are - 8.39 and - 6.67 kcal/mol. It is obvious that our results agree very well with the reported one.

Table 3.3. BSSE and ZPE corrected Binding Energies (kcal/mol) of three isomers of indole…pyridine dimer at various levels of theory

	M05-2X aVDZ		M06-2X cc-pVDZ		M06-2X aVDZ		MP2 cc-pVDZ		MP2/ aVDZ
	ΔE_e	ΔE_0	ΔE_e	ΔE_0	ΔE_e	ΔE_0	ΔE_e	ΔE_0	ΔE_e
HB3	- 7.44	- 6.48	- 7.55	- 5.94	-7.37	-6.10	-7.45	- 6.52	- 8.70
Syn-PD4	- 4.61	- 4.13	- 5.29	- 4.21	- 6.47	-5.73	- 4.46	-4.08	- 8.39
Anti-PD3	- 2.89	- 2.65	- 4.97	- 3.73	- 4.99	-4.34	- 2.90	- 2.70	- 6.67

ΔE_e: BSSE corrected Binding Energy, ΔE_0: BSSE + ZPE corrected Binding Energy.

A few important geometric parameters of the three stable isomers of the dimer calculated at the MP2/aVDZ level of theory are listed in Table 3.4. Frequencies of the three isomeric structures of indole…pyridine dimer calculated at the MP2/cc-pVDZ level of theory are also provided in the same table. Theoretical harmonic N-H stretching frequency of indole monomer calculated at the MP2/cc-pVDZ level is 3686 cm^{-1}, while experimental N-H

stretching frequency of indole monomer is 3526 cm^{-1}. Thus a scaling factor of 0.9566 is used to correct the theoretical harmonic N-H stretching frequencies of various isomers of the dimer. It has been found that the most stable V-shaped isomer (HB3) of the dimer possesses a strong intermolecular N-H…N hydrogen bond with H…N distance ($d_{H...N}$) of 1.95 Å and N…N distance ($d_{N...N}$) of 2.88 Å. Drastic increase in the N-H bond length (Δr_{N-H} = 0.015 Å) of indole upon formation of dimer with pyridine indicates formation of strong hydrogen bond in the V-shaped isomer. Though the geometry of this isomer is characterized by strong hydrogen bonding interaction, this is stabilized by additional dispersive interactions through weak C-H…π hydrogen bonding and π…π interactions. If we carefully notice, weak C-H…N hydrogen bonding interaction is also present in the HB3 structure. C-H…N hydrogen bonding distance in this structure is 2.72 Å. The presence of C- H…N interaction in the HB3 structure is also indicated by little increase in the C_{17}-H_{24} bond

Table 3.4. Geometrical parameters of the three isomeric structures of indole…pyridine dimer calculated at the MP2/aVDZ level of theory.[a]

	HB3	Syn-PD4	Anti-PD3
$d_{H...N}$ (Å)	1.950	2.970	
$d_{N...N}$ (Å)	2.880	3.170	
Δr_{N-H} (Å)	0.015	0.002	
∠N-H-N	149°	92°	
∠C-H-N	107.5°		
[a]$\angle C_6C_1N_{16}H_{13}$[b]	- 7°	12.6°	-1.71°
Interplanar distance (Å)		3.10	3.11
[a]$\angle C_1N_{16}N_{22}C_{17}$[b]	- 54°		
$d_{C-H...N}$ (Å)	2.72		
$d_{C-H...\pi}$ (Å)	3.28		
$d_{N-H...\pi}$ (Å)			
ν_{N-H} (cm^{-1})	3246	3505	3523

[a]Frequencies of the three isomers calculated at the MP2/cc-pVDZ level of theory are provided here. [b]For atom numbering of the dimer, see Figure 3.10.

length of the pyridine ring compared to the other C-H bonds. C_{17}-H_{24} bond length of the pyridine ring is 1.095 Å, whereas the length of the other C-H bonds in the pyridine ring is 1.093 Å. Thus the indole and pyridine rings in this isomer are not oriented exactly perpendicular to each other through the N-H…N hydrogen bond but these are bent with respect to each other forming a unique V-shaped herringbone structure. The angle between the two rings described by the dihedral angle $C_1N_{16}N_{22}C_{17}$ [see Figure 3.10(a)] is termed as wagging angle and it is – 54°. Similar kind of V-shaped geometry has also been reported for phenol dimer from various experiments and theoretical calculations.[2-8] In case of the phenol dimer, there is a strong O-H…O hydrogen bond with H…O distance of 1.92 Å, O…O distance of 2.88 Å and the angle between the two phenyl rings (wagging angle) is -69.6°.[4] Very recently, Kim and co-workers have performed extensive calculations for phenol dimer at various levels of theory.[8] They have also reported that the V-shaped structure of the phenol dimer is determined by strong hydrogen bonding as well as CH-π and π-π interactions.

There is a striking difference in the geometry of the two parallel-displaced (PD) π-stacked isomers of the dimer. In the case of the syn-PD4 stacked isomer, the N-H group of indole and pyridine nitrogen atom are in the same side having attractive electrostatic interaction leading to shorter H…N distance of 2.97 Å. Due to this electrostatic interaction, the hydrogen atom of NH group of indole goes out of plane to significant extent to point towards the pyridine nitrogen atom. On the other hand, the N-H group of indole and pyridine nitrogen atom of the anti-PD3 stacked dimer are in the opposite side without having any possibility of attractive electrostatic interaction. The planarity of the N-H group of indole is described by the dihedral angle $\angle C_6C_1N_{16}H_{13}$, which is 0°, 12.6°, and - 1.71° for bare indole, syn-PD4 stacked dimer, and anti-PD3 stacked dimer, respectively. The N-H…N hydrogen bonded isomer (HB3) of the dimer also shows non-planarity of the N-H group by - 7° due to the V-shaped geometry. The syn-PD stacked dimer also shows small elongation of the NH bond length by 0.002 Å. It is interesting to mention here that the NH…π hydrogen bonded isomer (T5) of the indole…pyridine dimer is not a stable minimum as frequency calculation of this isomer at various levels of theory with different basis sets provide an imaginary frequency. On the contrary, NH…π hydrogen bonded structure is reported to be the most stable isomer in case of indole…benzene dimer studied by both theory and experiment.[287-289] NH…π

hydrogen bonded isomer of indole…pyridine dimer is unstable probably because aromatic rings with heteroatoms are poor π-hydrogen bond acceptors as reported by Sherrill, and co-workers.[299]

It will be interesting to compare the hydrogen bond strength of the V-shaped isomer (HB3) of indole…pyridine dimer with a few other hydrogen bonded complexes of indole reported in the literature.[398,406] Table 3.5 provides red-shift in N-H stretching frequency, band origin, and Δr_{N-H} of hydrogen bonded complexes of indole with H_2O, Me_2S, NH_3, and pyridine as well as proton affinity[162] of the complexing bases. It is clearly observed that there is a nice correlation of N-H stretching frequency red-shift with Δr_{N-H} in the complex and proton affinity of the acceptors. Proton affinity of both NH_3, and pyridine is much higher than that of H_2O as well as Δr_{N-H} in indole…NH_3 and indole…pyridine complexes is more than double compared to that in indole…H_2O complex. Red-shift in the N-H stretching frequency in these three complexes is consistent with these data. Actually indole…NH_3 complex is very much suitable to compare with indole…pyridine dimer in terms of hydrogen bond strength

Table 3.5. Shift in the N-H stretching frequencies ($\Delta\nu_{N-H}$), and Band origin (ΔE_{BO}) for various complexes of indole, and proton affinity of hydrogen bond acceptors

Hydrogen bond acceptors	Proton affinity[a] (kcal/mol)	indole complexes		
		Δr_{N-H} (Å)	$\Delta\nu_{N-H}$ (cm^{-1})	ΔE_{BO} (cm^{-1})
H_2O[b]	166.5	0.007	- 89	- 132
Me_2S[b]	198.6	0.012	- 158	- 170
NH_3	204.2	0.015[c]	(-321)	- 227[d]
Pyridine	219.6	0.015	- 257 (-280)	- 271

[a] Reference 162. [b] Reference 406. [c] The value calculated in this work at MP2/aVDZ level. The values in the parentheses are theoretical $\Delta\nu_{N-H}$ at MP2/cc-pVDZ level. In case of indole…NH_3 complex, experimental $\Delta\nu_{N-H}$ is not available. [d] References 162,394.

due to the presence of N-H…N hydrogen bond in both the cases. We have performed geometry optimization, and frequency calculation of indole…NH_3 complex at the MP2/aVDZ, and MP2/cc-pVDZ levels, respectively. Both of the indole…pyridine and indole…NH_3 complexes indeed show similar Δr_{N-H} (0.015 Å), and red-shift (more than 250 cm^{-1}) in the N-H stretching frequency. In the case of the indole…NH_3 complex, experimental N-H stretching frequency is not available, thus only theoretical value computed by us has been provided. There is also a linear relationship between band origin shift of indole…solvent complexes with proton affinity of the solvents.[162,394,407] It is interesting to note that band origin shift in the V-shaped indole…pyridine dimer (HB3) is comparable to that of indole…NH_3 complex. Proton affinity values of NH_3 and pyridine are 204 and 219.6 kcal/mol, respectively[162], and band origin shifts of indole…NH_3 complex and indole…pyridine V-shaped dimer are -227, and -271 cm^{-1}, respectively.[162,394] Thus all these data support the assignment of the species B in the R2PI spectrum recorded in the dimer mass channel as V-shaped indole…pyridine dimer (HB3).

3.2.5.2 Structures of $(indole)_2$…pyridine trimer

Initial geometry optimization of various possible isomers of $(indole)_2$…pyridine trimer have been performed at the M05-2X/6-31+G(d) level. Three low energy structures of the trimer obtained from the M05-2X/6-31+G(d) level of calculation were further optimized with higher basis sets at the M05-2X level as well as M06-2X/cc-pVDZ level. Figure 3.11 shows the structures of the three isomers of the trimer optimized at M05-2X/6-311++g(d,p) level. All the three isomers have cyclic structures with a little variation in the orientation of the three monomer units. These three structures are named as $(ind)_2$.py-1, $(ind)_2$.py-2, and $(ind)_2$.py-3. Similar kind of cyclic structures have been reported for naphthalene trimer, phenol trimer, and a few N-heteroaromatic systems like pyridine trimer, pyrazine trimer etc.[3,254,408] All the three structures of $(indole)_2$…pyridine trimer studied here, are stabilized by strong N-H…N hydrogen bond and weak C-H…N electrostatic interactions as well as multiple dispersion interactions between two indole rings as well as pyridine with each of the indole ring. In the $(ind)_2$.py-1 structure, two indole rings are interacting with each other through N-H…π and C-H…π interactions, where N-H group and one C-H group of indole ring are forming hydrogen bonds with the π-clouds of phenyl and pyrrole groups of other indole ring, respectively. On the other hand, two C-H groups of pyridine are forming two C-H…π hydrogen bonds with

pyrrole and phenyl groups of one of the indole rings. In the case of the $(ind)_2$.py-2 structure, similar type of electrostatic and dispersion interactions are present except two indole rings are interacting with each other slight differently. Here, N-H group and one C-H group of indole are interacting with the π-clouds of pyrrole and phenyl groups of other indole ring, respectively. In the case of the $(ind)_2$.py-3 structure, two indole

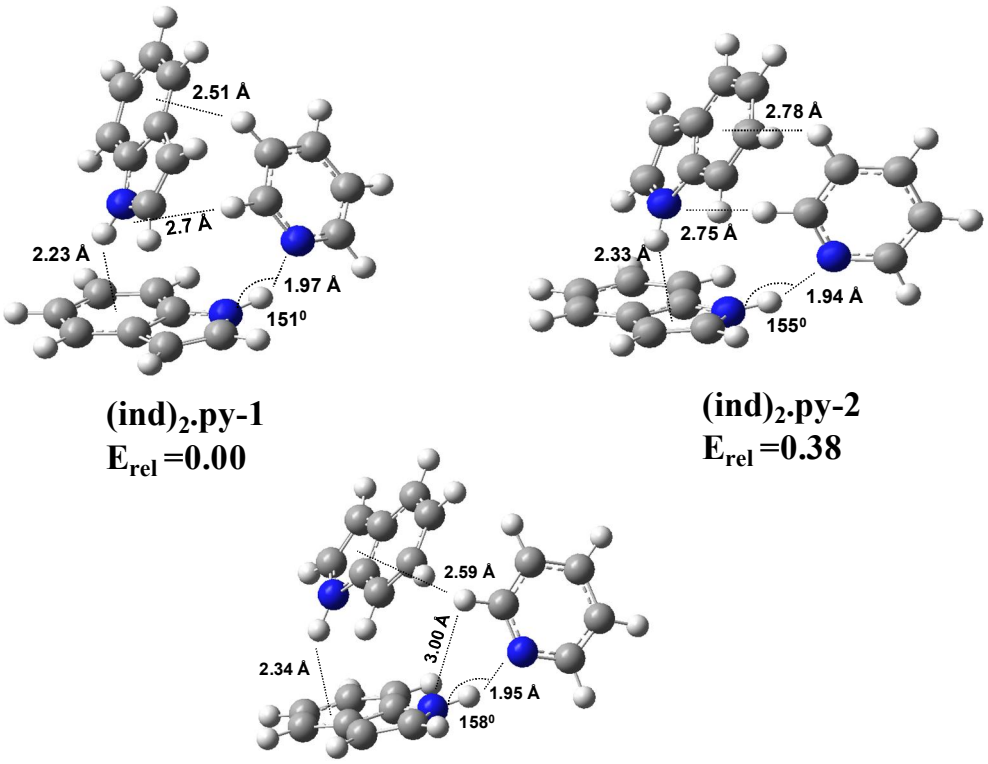

$(ind)_2$.py-1
E_{rel} =0.00

$(ind)_2$.py-2
E_{rel} =0.38

$(ind)_2$.py-3
E_{rel} =1.06

Figure 3.11. M05-2X/6-311++g** optimized structures of three stable isomers of $(indole)_2$…pyridine trimer. E_{rel} is ZPE corrected relative energy of the isomers in kcal/mol.

rings are interacting with each other in a similar fashion like the $(ind)_2$.py-1 structure but interaction between pyridine and the indole rings are different compared to that for the other two trimer structures. There is only one C-H…π interaction between pyridine and the indole rings in the $(ind)_2$.py-3 structure.

BSSE and zero point energy (ZPE) corrected binding energies and ZPE corrected relative energies of the three cyclic structures of the trimer calculated at various levels of theory are presented in Table 3.6. Comparison of binding energies as well as relative energies at

different levels of theory show that $(ind)_2$.py-1 is the most stable trimer structure. Table 3.7 provides theoretical N-H stretching frequencies and Δr_{N-H} (change in N-H bond length in complex formation) of the three isomeric structures of the trimer calculated at the M05-2X/6-311++G(d,p) level of theory. The frequencies presented in the table are corrected with a

Table 3.6. Relative Energies (kcal/mol), ZPE and BSSE corrected Binding Energies (kcal/mol) of three isomers of $(indole)_2$…pyridine trimer calculated at various levels of theory

	M05-2X/6-311++G**			M05-2X/cc-pVDZ			M06-2X/cc-pVDZ		
	ΔE_e	ΔE_0	E_{rel}	ΔE_e	ΔE_0	E_{rel}	ΔE_e	ΔE_0	E_{rel}
$(Ind)_2$ .Py-1	-19.41	-17.63	0.00	-19.00	-17.19	0.00	-20.67	-18.20	0.00
$(Ind)_2$ .Py-2	-18.96	-17.24	0.38	-18.42	-16.63	0.55	-19.76	-17.51	0.70
$(Ind)_2$ .Py-3	-18.22	-16.57	1.06	-17.87	-16.27	0.91	-18.65	-16.49	1.71

ΔE_e: BSSE corrected Binding Energy, ΔE_0: BSSE + ZPE corrected Binding Energy,
E_{rel} : ZPE corrected Relative Energy of the isomers with respect to the most stable isomer.

scaling factor of 0.9430, which is obtained from the ratio of experimental (3526 cm^{-1}) and theoretical (3739 cm^{-1}) N-H stretching frequencies. The strength of the hydrogen bond is

Table 3.7. N-H…N and N-H…π bound N-H stretching frequencies and change in N-H bond lengths of the three isomers of the indole…$(pyridine)_2$ trimer calculated at the M05-2X/6-311++g(d,p) level of theory

	ν_{N-H} (N-H…N) (cm^{-1})	ν_{N-H} (N-H…π) (cm^{-1})	Δr_{N-H} (N-H…N) (Å)	Δr_{N-H} (N-H…π) (Å)
$(ind)_2$.py-1	3270 (734)	3452 (304)	0.016	0.006
$(ind)_2$.py-2	3231 (939)	3420 (373)	0.017	0.008
$(ind)_2$.py-3	3259 (822)	3440 (273)	0.016	0.007

Intensity in km/mol is given in bracket. Frequencies have been scaled by a factor of 0.9388.

generally reflected in the red-shift in the N-H stretching frequency as well as the extent of the lengthening of the N-H bond. The result shows that the experimental red-shift in the σ-bound (N-H…N) N-H stretching frequency of the trimer is 245 cm^{-1} and the lengthening of the corresponding N-H bond length in the three trimeric structures is 0.016-0.017 Å. On the other hand, the π-bound (N-H… π) N-H stretching frequency of the trimer is red-shifted by 115 cm^{-1} and the increase in the corresponding N-H bond length in the three structures of the trimer is 0.006-0.008 Å. It has been found that the theoretical N-H stretching frequencies (N-H…N as well as N-H…π hydrogen bonded) of the three cyclic structures of the trimer corroborate in the similar fashion with the experimental N-H stretching frequencies of the trimer observed in the experiment. But from energetic point of view, $(ind)_2$.py-1 structure is the global minimum and it has also maximum binding energy. Thus the $(ind)_2$.py-1 structure been assigned for the observed trimer.

3.2.5.3 EDA of the dimer and the trimer

For quantitative determination of the various contributions to the stabilization of different isomers of the dimer and the trimer, LMO-EDA procedure introduced by Su and Li is used.[73] Table 3.8 shows the different contributions of the interaction energy of various isomers of the dimer as well as the most stable structure of the trimer $(ind)_2$.py-1. EDA calculations of the dimer and the trimer have been performed at M05-2X/aVDZ, and M05-2X/cc-pVDZ levels, respectively. The result clearly shows that dispersion interaction plays a significant role in

Table 3.8. Interaction Energies (kcal/mol) in various isomers of the dimer and the most stable structure of the trimer, calculated at M05-2X/aVDZ, and M05-2X/cc-pVDZ levels of theory, respectively

	ΔE_{ele}	ΔE_{ex}	ΔE_{rep}	ΔE_{pol}	ΔE_{disp}	ΔE_{tot}
HB3-dimer	-11.10	-6.47	21.57	-3.81	-7.77	-7.57
PD4-dimer	-4.97	-4.76	21.26	-1.60	-14.71	-4.78
PD3-dimer	-2.68	-4.19	19.38	-1.50	-13.89	-2.88
$(ind)_2$.Py-1 trimer	-24.22	-15.55	58.63	-8.44	-30.08	-19.66

the stabilization of the electrostatic dominated dimer HB3. The electrostatic component of the total interaction energy of HB3 dimer is -11.1 kcal/mol, whereas the dispersion component is -7.77 kcal/mol. In case of the dispersion dominated π-stacked dimers, syn-PD4 has indeed more electrostatic contribution in the total interaction energy than the anti-PD3 isomer. This favors for weak N-H…N hydrogen bonding interaction in case of syn-PD4.

EDA analysis of $(ind)_2$.py-1 structure of the trimer shows that the contribution of the dispersion interaction is more compared to the electrostatic interaction in stabilization of the trimer geometry. The electrostatic component of the total interaction energy of the trimer is -24.22 kcal/mol whereas the dispersion component is -30.08 kcal/mol. This supports that the trimer geometry comprises of multiple dispersion interactions i.e. N-H…π and few C-H…π interactions in addition to strong N-H…N and weak C-H…N electrostatic interactions.

3.2.5.4 TDDFT analysis of the dimer and trimer

Single-point TDDFT calculation at the M05-2X/cc-pVDZ level has been performed to compute $S_1 \leftarrow S_0$ transition frequencies of the dimer and trimer. It is known that the absolute value of the electronic transition energy obtained from the TDDFT calculation is quite far away from the experimental vertical excitation energy. But the relative $S_1 \leftarrow S_0$ origin frequencies obtained from the theory are very often useful to assign different species or isomers present in the experiment. The computed transition frequencies of the HB3 isomer of the dimer and the most stable isomer of the trimer, scaled to the experimental band origin of indole, are 300.62 and 292.21 nm, respectively. The corresponding experimental transition frequencies of the dimer and trimer are 285.95 and 284.38 nm, respectively. Thus TDDFT calculation supports the experimental observation that the electronic origin band of the dimer in comparison with the trimer, is more red-shifted from the origin band of the monomer. Comparison of the TDDFT calculated and experimental $S_1 \leftarrow S_0$ transition frequencies of different isomers of isolated molecules as well as complexes has been reported by several authors in the literature.[409-410]

3.3. Conclusions

In summary, we have studied the structures of indole…pyridine dimer and $(indole)_2$…pyridine trimer in a supersonic jet using one-color R2PI, IR-UV double resonance spectroscopic techniques and quantum chemistry calculations. R2PI spectra of the dimer and the trimer have been measured by electronic excitation of the indole moiety. The electronic origin bands of the dimer and the trimer are red-shifted from the 0_0^0 band for the $S_1 \rightarrow S_0$ transition of the indole monomer by 76, 271 cm^{-1}, respectively. The R2PI spectrum obtained in the dimer mass channel exhibits extensive fragmentation from the trimer. RIDIR spectra combined with IR-UV hole-burning spectra confirm the presence of only one isomer in the experiment for both of the dimer and trimer. RIDIR spectra show that there is a large red-shift (-257 cm^{-1}) in the N-H stretching frequency of the dimer compared to that in the indole monomer. MP2 as well as DFT/M05-2X and DFT/M06-2X calculations predict that the observed indole…pyridine dimer has a V-shaped structure stabilized by conventional hydrogen bonding (N-H…N) as well as CH…π and π…π stacking interactions. RIDIR spectra combined with DFT/M05-2X and DFT/M06-2X calculations confirm that the observed trimer has a cyclic structure with N-H…N, N-H…π, C-H…N, and, C-H…π interactions. In future, it will be possible to shed further light on the structures of the dimer and the trimer by using rotational coherence spectroscopy as well as rotationally resolved electronic spectroscopy.

We have introduced a new nomenclature "*special class of mixed complex*" to represent the presence of conventional hydrogen bond and dispersion bound interaction in indole…pyridine dimer. We emphasize that this new category of mixed complex should be incorporated in the computational database of non-covalent interactions. The most important physical insight of this present investigation is that the study of the "*special class of mixed complex*" indeed reveals the unique structural motifs of biomolecules and materials. Thus deeper understanding of the structure of this class of mixed complex may shed light on improved drug design and advanced functional material synthesis. Study of this class of complex is extremely challenging from both experimental and theoretical point of view. In future, a few more complexes of this category are required to study for better understanding

of this "*special class of mixed complex*" using various gas phase spectroscopic techniques as well as high level ab inito calculations.

4. Competition between π-hydrogen bonding and conventional hydrogen bonding interactions: Indole…furan and indole…thiophene dimers

4.1. Introduction

In the last chapter, we have reported the study of the complexes showing the interplay between strong i.e. conventional hydrogen bonding (N-H…N) and dispersion interactions in the stabilization of the observed V-shaped structure of the indole…pyridine dimer. We have introduced the nomenclature "*special class of mixed complex*" to this category of molecular complexes for the first time as these complexes are different from the mixed complexes defined in the S22 database. We have also demonstrated from the study that spectroscopic investigation of "*special class of mixed complex*" can reveal unique information on the basic structures of biomolecules and materials.

π-hydrogen bonding is defined as X-H...π, where X can be C, N, O, or S atom. In particular, N-H…π interaction has received lots of attention quite recently because it has wide variation in the interaction energy depending on the molecular systems involved.[9,17-18,411-418] We have mentioned in section 1.7.2.3 that the interaction energy for benzene…NH_3 dimer is 2.44 kcal/mol whereas the binding energies in the case of pyrrole dimer, pyrrole…benzene dimer, 2-pyridone…benzene dimer and indole…benzene dimer are greater than 5 kcal/mol. It is concluded from these data that N-H…π interaction can have strength comparable to conventional hydrogen bond.[265,291-292] Thus we raised the question whether N-H···π hydrogen bonding can win over conventional hydrogen bonding. To answer this question, we have chosen those molecular systems, where both π-hydrogen bonded and conventional hydrogen bonded conformer can exist. Thus we have studied indole…furan and indole…thiophene dimers. In the case of these dimers, there is a possibility of observation of both N-H···π bound conformer and N-H…O/N-H…S bound conformer in the experiment.

There are extensive experimental and theoretical studies in the gas phase to understand the effect of various hydrogen bond donors (C-H, N-H, O-H, S-H) on the strength of the π-hydrogen bonding interactions.[188,191,251,259,264-265,291-292,305,308-318] But similar studies on the role of the heteroatoms present in the π-acceptor on the π-hydrogen bonding interaction are very rare.[299] Further Sherrill and co-workers from their theoretical study of benzene...pyridine

dimer concluded that six membered aromatic rings containing heteroatoms are poorest π-hydrogen bond acceptors whereas our recent experimental and theoretical studies on indole…pyridine dimer show that the N-H...π hydrogen bonded T-shaped configuration is not even a local minimum and not observed in the gas phase experiment.[320] Hence for improved understanding of the effect of the heteroatoms on the π-hydrogen bonding interactions and to check whether the aromatic rings containing heteroatoms can act as effective π-hydrogen bond acceptor, it is essential to study the complexes of various aromatic heterocycles containing different heteroatoms (O, S) other than nitrogen (N) atom.

Here, we have reported an experimental as well as theoretical study of complexes of indole with furan and thiophene heterodimer respectively by using REMPI based electronic and vibrational spectroscopy in a supersonic jet combined with quantum chemistry calculations. Further we have compared the results obtained from the study of the complexes of indole with furan and thiophene with previously reported results of indole…pyridine dimer to see the effect of heteroatom present in the π-acceptor on the strength of π-hydrogen bonding. The present work on this dimer has also immense biological significance as furan and thiophene derivatives have potential therapeutic applications whereas indole is the chromophore of tryptophan residue in the proteins as well as a precursor of several indole alkaloids.[419-424] Thus understanding the binding motif between indole with furan and thiophene in the heterodimer studied in this work may help in designing of efficient drugs.

4.2. Results and discussion

4.2.1. TOF mass spectra

TOF mass spectrum of the complexes of indole and furan in argon buffer gas recorded at laser frequency of 35192 cm^{-1} (284.16 nm), which corresponds to the electronic origin transition of indole···furan complex, has been shown in Figure 4.1a. The mass peak observed at 185 amu is due to indole···furan dimer whereas the 253 amu mass peak as appears for indole···$(furan)_2$ trimer. The mass spectrum reported in the Figure 4.1a also shows higher clusters of indole i.e $(indole)_2$ and $(indole)_3$ as well as water clusters of indole i.e. indole···$(H_2O)_1$, indole…$(H_2O)_2$ etc.

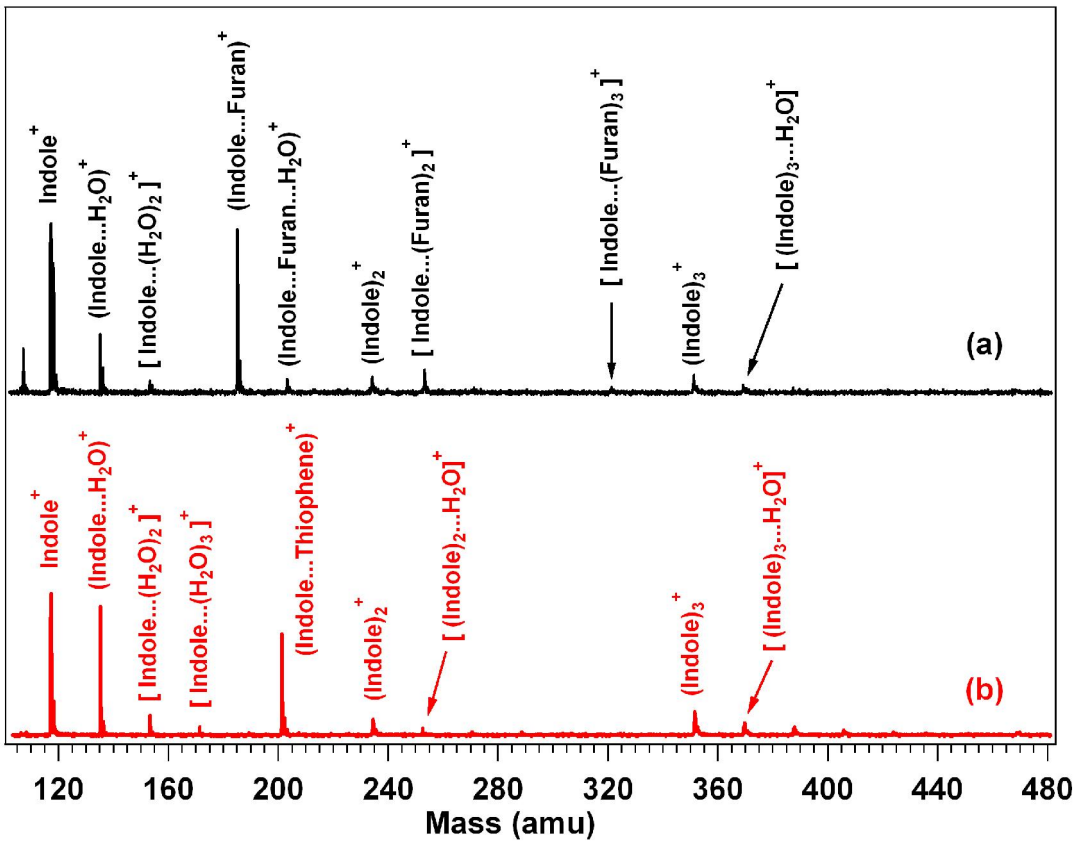

Figure 4.1. (a) TOF mass spectra of complexes of indole and furan and (b) complexes of indole and thiophene recorded at laser frequency of 35192 and 35075 cm^{-1}respectively, which correspond to the origin band position of the dimers. Water has been present as an impurity.

Figure 4.1b shows TOF mass spectrum of the complexes of indole and thiophene in argon buffer gas measured at laser frequency of 35075 cm^{-1}(285.10 nm), which corresponds to the

band maximum of the broad electronic spectrum originated due to the $S_1 \leftarrow S_0$ transition of indole…thiophene dimer. The mass peak of indole…thiophene appears at 201 amu. Like Figure 4.1a, the mass spectrum depicted in Figure 4.1b shows the formation of higher clusters of indole as well as water clusters of indole.

4.2.2. R2PI Spectra

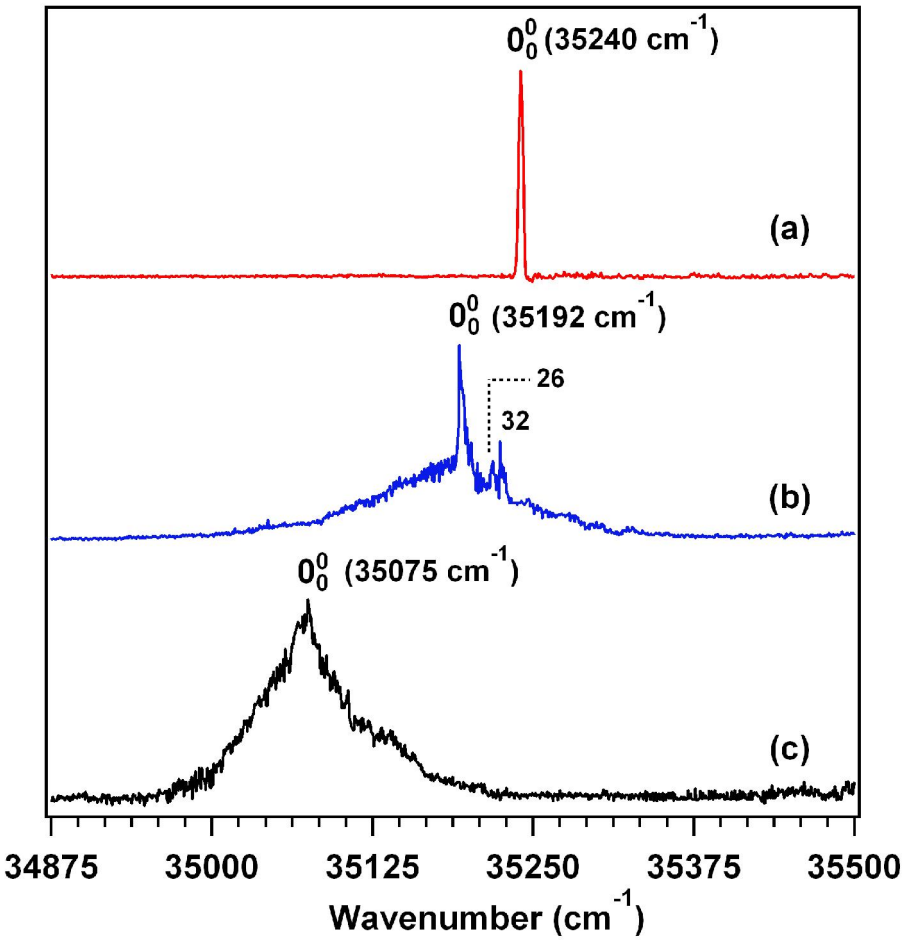

Figure 4.2. One-color R2PI spectra recorded in (a) indole, (b) indole···furan dimer, and (c) indole…thiophene dimer mass channels.

One-color R2PI spectra measured in indole···furan and indole…thiophene dimer mass channels have been shown in Figure 4.2b and 4.2c, respectively. Furan and thiophene are taken in a stainless steel sample holder maintained at -78°C (using dry ice) and -25°C (using mixture of dry ice and aqueous solution of $CaCl_2$), respectively. Vapor pressure of furan and thiophene at 25°C is 599 and 78 mmHg, respectively.[393] A buffer gas of Ar (45 psig) is flown

individually through furan or thiophene and the corresponding vapor seeded in the buffer gas is mixed with the vapor of indole placed behind the pulsed valve heated at 80°C. The R2PI spectrum of indole is also shown in Figure 4.2a to compare with the R2PI spectra recorded in the dimer mass channels. The origin band (0_0^0) for the $S_1 \leftarrow S_0$ electronic transition of indole appears at 35240 cm^{-1}, which matches well with the previous report.[394] The R2PI spectra in indole···furan and indole…thiophene dimer mass channels are measured by electronic excitation of the indole moiety.

The R2PI spectrum (Figure 4.2b) of indole…furan dimer exhibits a strong sharp peak at 35192 cm^{-1}, which is assigned as the origin band for the $S_1 \leftarrow S_0$ electronic transition of the dimer. There are two relatively weak peaks at 0_0^0+ 26 and 0_0^0+ 32 cm^{-1} in the spectrum and these could appear either due to low frequency intermolecular vibrations of the dimer or presence of different isomeric structure of the dimer. The R2PI spectrum of the dimer also shows a very broad background underneath those sharp peaks. On the other hand, the R2PI spectrum of the indole…thiophene dimer provided in Figure 4.2c exhibits a structureless broad band with intensity maximum at 35075 cm^{-1}. The FWHM of the observed electronic band of the dimer is about 80 cm^{-1}. The broad feature observed in the R2PI spectrum of both indole…furan and indole…thiophene dimers could be either due to the origin transitions of multiple isomeric structures of the dimer with their overlapping low frequency intermolecular vibrations or fragmentation of the higher clusters at the dimer mass channel. The broadening of the R2PI spectrum could also be due to shortening of the lifetime of the excited state of the dimer through rapid deactivation. The R2PI spectra obtained in the mass channels of the two dimers have been assigned by measuring RIDIR spectra as well as R2PI spectra in the mass channels of higher clusters and these have been discussed in the following sections.

To verify the contribution of the higher clusters in the broadening of the R2PI spectrum measured in the indole…furan dimer mass channel, we have measured R2PI spectrum in indole…$(furan)_2$ trimer mass channel and the spectra obtained in both the mass channels have been shown in Figure 4.3. Interestingly, the spectrum in the trimer mass channel has similar broad background overlapping with the R2PI spectrum obtained in the dimer mass channel. The sharp peak at 35149 cm^{-1} in the spectrum at the trimer mass is assigned as the origin transition of indole…$(furan)_2$ trimer. Thus comparing the R2PI spectra in the dimer and

trimer mass channels, it is obvious that the broad background observed in the spectrum at the dimer mass channel (Figure 4.3a) is originating mostly from the trimer, which is fragmenting and appearing at the dimer mass channel.

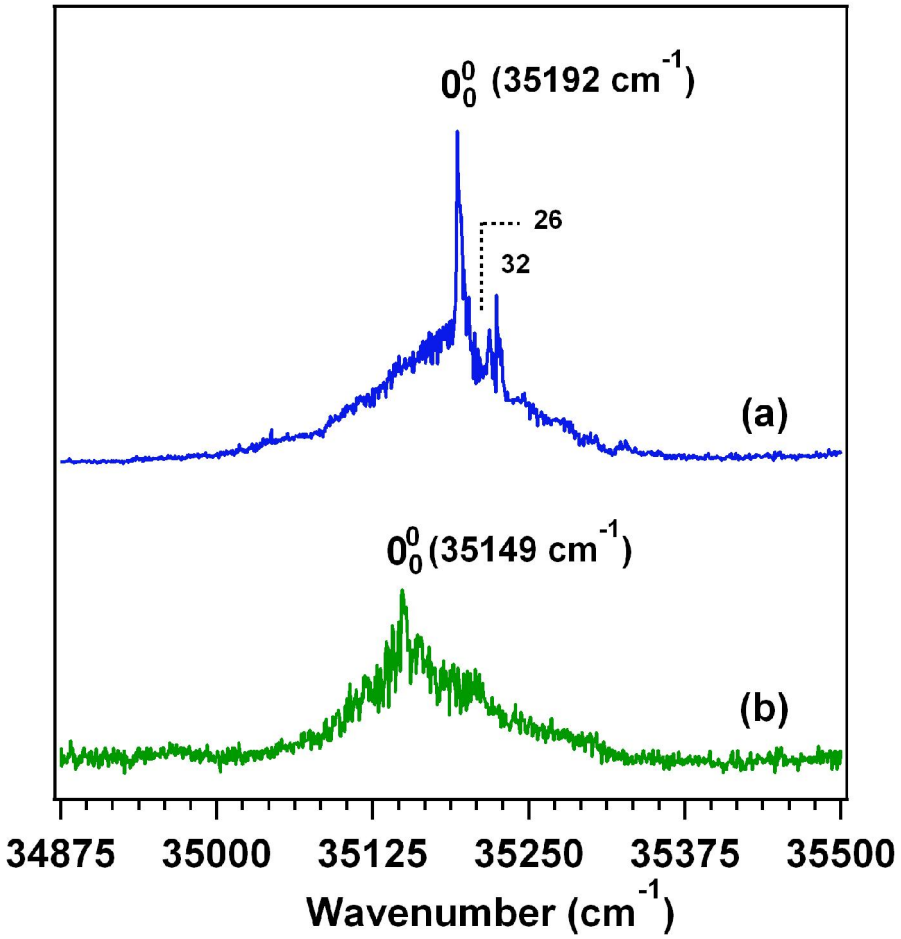

Figure 4.3. 1C-R2PI spectra recorded in (a) indole···furan dimer and (b) indole…(furan)$_2$ trimer mass channels.

The source of the background observed in the R2PI spectrum at the indole…furan dimer mass channel could also be validated by recording the R2PI spectrum upon increasing vapor pressure (temperature) of furan. We have recorded R2PI spectrum of the complex in the dimer mass channel by keeping furan in a bath containing mixture of dry ice and aqueous solution of $CaCl_2$ to maintain temperature at approximately -35°C. The comparison of the R2PI spectra at two different temperatures has been depicted in Figure 4.4, which shows that the relative intensity of the sharp features compared to the background in the R2PI spectrum at the dimer mass channel markedly decreases by increasing the temperature of furan. This

observation reconfirms that the broad background in the R2PI spectrum at the dimer mass channel is mostly due to the higher clusters.

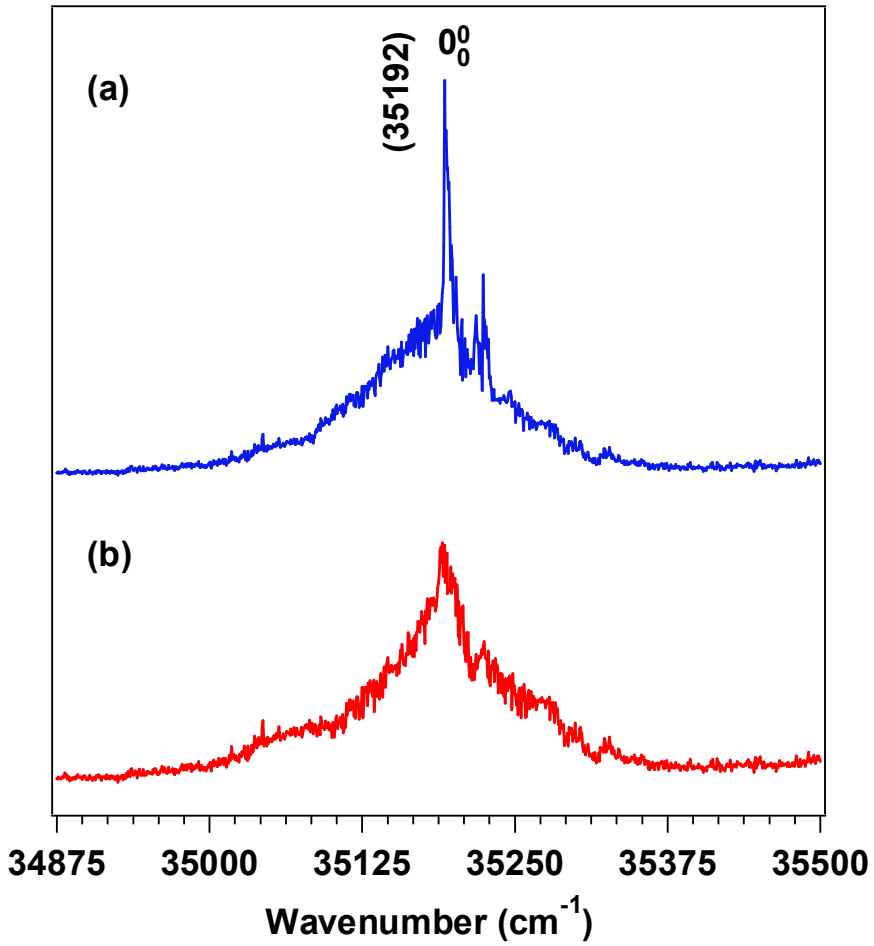

Figure 4.4. One-color R2PI spectra recorded in indole…furan dimer mass channel by keeping furan at (a) -78.5°C (dry ice temperature) and (b) -35°C (mixture of dry ice and aqueous solution of $CaCl_2$).

In the case of the complexes of indole and thiophene, R2PI spectrum has not been measured in the mass channels of the higher clusters as no trace of the complexes larger than the indole…thiophene dimer is observed in the TOF mass spectrum of the mixed vapor of indole and thiophene shown in Figure 4.1b. The source of broadening in the R2PI spectrum of the indole…thiophene dimer has been examined by measuring IR spectra through electronic excitation of several positions of the broad R2PI spectrum. Similarly, multiple IR spectra by probing several positions of the broad background of the indole…furan dimer and indole…$(furan)_2$ trimer R2PI spectra have been recorded. The IR spectra of the complexes of

indole and furan as well as indole and thiophene have been discussed in section 4.2.3. It is quite interesting to compare the red-shift in the band origin of indole···furan dimer and indole…thiophene dimer with respect to the origin band of indole monomer. It is obvious from Figure 4.2 that the red-shift in the band origin of the indole…furan dimer is 48 cm^{-1} while that of the indole…thiophene dimer is 165 cm^{-1}. This difference in the red-shift in the band origin of the two dimers signifies that the S_1 state of the indole…thiophene dimer is more strongly bound than that of the indole…furan dimer compared to the corresponding S_0 states relative to respective monomers.

4.2.3. RIDIR Spectra.

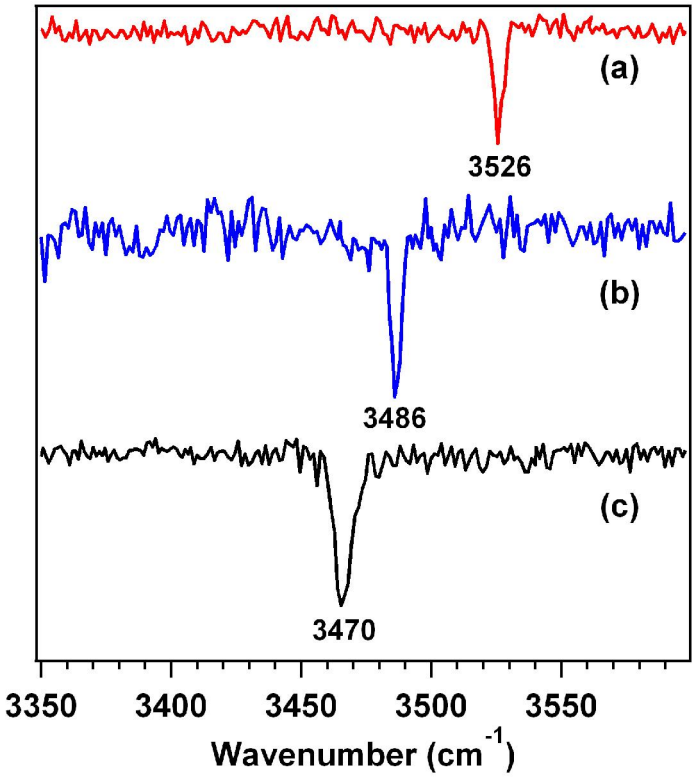

Figure 4.5. RIDIR spectra in the N-H stretching region by probing 0_0^0 band of (a) indole monomer, (b) indole···furan dimer and (c) indole···thiophene dimer.

Figure 4.5 shows IR spectra measured in the indole monomer, indole···furan dimer and indole…thiophene dimer mass channels in the N-H stretching region by using RIDIR spectroscopy. RIDIR spectrum of indole monomer displayed in Figure 4.5a exhibits the N-H stretch fundamental vibration at 3526 cm^{-1}, which agrees very well with the previous

reports.[398,425] Figure 4.5b and 4.5c show RIDIR spectra by probing the electronic origin band of the indole···furan and indole…thiophene dimer, respectively. The N-H stretching vibration in indole…furan dimer appears at 3486 cm^{-1} while that in indole…thiophene dimer occurs at 3470 cm^{-1}. Thus the red-shifts in the N-H stretching vibration in indole…furan and indole…thiophene dimers with respect to that in indole monomer are 40 and 56 cm^{-1}, respectively. This result indicates that the N-H group of indole moiety in both the dimers is involved in non-covalent interaction but the strength of the interaction is slightly higher in the indole…thiophene dimer compared to that in the indole…furan dimer.

Generally the red-shift in the X-H (X = N, O, S) stretching frequency as well as intensity of the vibrational transition indicates the strength of the hydrogen bonding interaction. It is quite intriguing to compare the observed red-shifts in the N-H stretching frequency of the indole…furan and indole…thiophene dimers with those of some relevant complexes reported in the literature. The red-shifts in the N-H and O-H stretching frequencies of a few conventional (strong) hydrogen bonded complexes i.e. indole…H_2O (N-H…O), p-cresol…tetrahydrofuran (O-H…O), indole…Me_2S (N-H…S), and p-cresol…tetrahydrothiophene (O-H…S) are 89, 317, 158, and 280 cm^{-1}, respectively. On the other hand, the red-shifts in the N-H stretching frequencies of a few reported N-H···π hydrogen bonded complexes i.e. indole…benzene, pyridone···benzene, and pyrrole···benzene are 44, 56, 59 cm^{-1}, respectively.[265,290,292] Thus the comparison of the red-shifts in the N-H stretching frequencies of the two dimers studied in this work with those of the complexes described in the literature indicates that the observed structure of both indole…furan and indole…thiophene dimers may be primarily N-H···π hydrogen bonded rather than conventional hydrogen bonded (N-H···O or N-H…S). It has been recently shown by Biswal et al. that the strength of the sulfur hydrogen bond (N-H…S) is comparable with the N-H…O and N-H…N hydrogen bonds.[406] The observed structures of the two dimers in the present study have been confirmed by comparing the experimental results with the theoretical ones and discussed in section 4.2.4. To find out the origin of the two weak sharp bands at 0_0^0+ 26 and 0_0^0+ 32 cm^{-1} in the R2PI spectrum of indole…furan dimer, IR spectra by probing these two bands have been measured and provided in Figure 4.6b-c. The IR spectrum obtained by exciting the 0_0^0 band of the indole…furan dimer has also been reproduced in

Figure 4.6a to compare with the other two IR spectra. Observation of three identical IR spectra in Figure 4.6 confirms that the 0_0^0+ 26 and 0_0^0+ 32 cm^{-1} bands in the R2PI spectrum

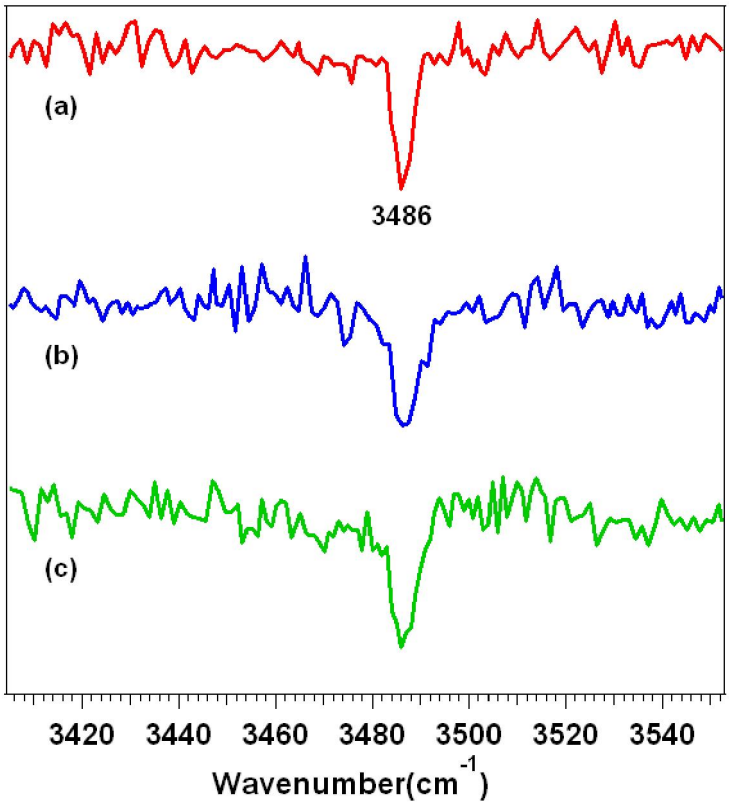

Figure 4.6. RIDIR spectra in the N-H stretching region by probing (a) 0_0^0 band, (b) 0_0^0 + 26 band and (c) 0_0^0 + 32 cm^{-1} band of indole···furan dimer.

(Figure 4.2) are due to low frequency intermolecular vibrations of the indole…furan dimer only.

To shed more light on the origin of the broad background underneath the 0_0^0 band of the indole…furan dimer (Figure 4.2b), we have measured RIDIR spectra by probing several positions on the background of the R2PI spectra in both indole…furan dimer and indole…$(furan)_2$ trimer mass channels. For the brevity, only a few selected RIDIR spectra by probing the background positions have been presented in Figure 4.7. Figure 4.7c and 4.7d show RIDIR spectra by probing 35149 cm^{-1} position of the broad background in indole…furan dimer and indole···$(furan)_2$ trimer mass channels, respectively. The spectrum

in Figure 4.7c shows two bands at 3478 and 3486 cm^{-1}, whereas mostly the 3478 cm^{-1} peak is observed in the spectrum displayed in Figure 4.7d. Thus it is confirmed that 35149 cm^{-1} position of the background obtained in the R2PI spectrum measured in the dimer mass

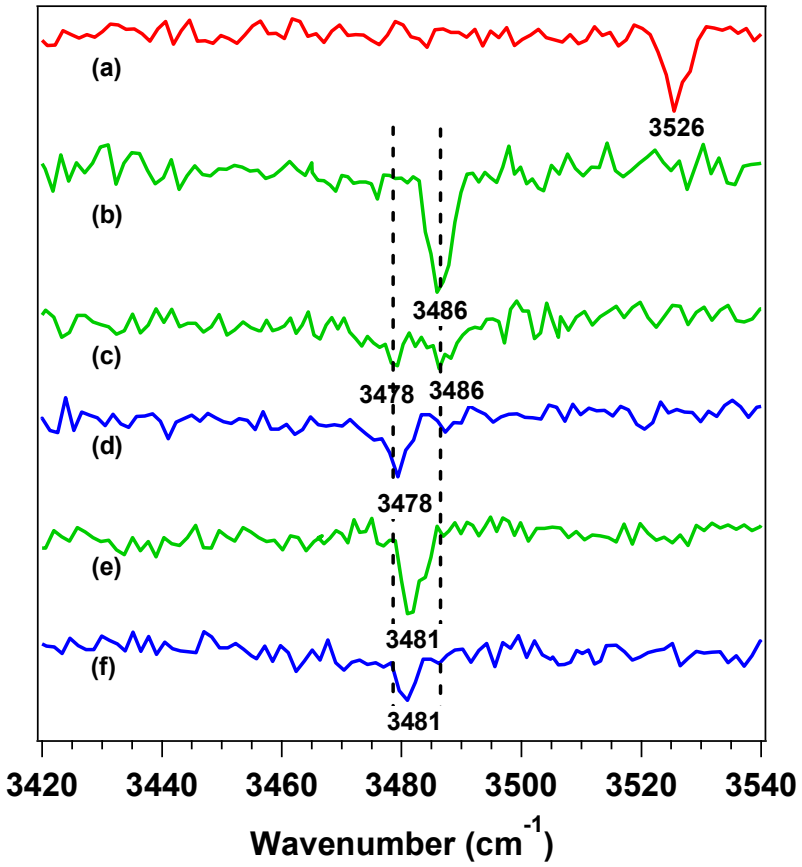

Figure 4.7. RIDIR spectra in the N-H stretching region by probing (a) 0_0^0 band of indole monomer, (b) 0_0^0 band of indole···furan dimer, (c) 35149 cm^{-1} band position in the dimer mass channel, (d) 35149 cm^{-1} band position in indole···$(furan)_2$ trimer mass channel, (e) 35268 cm^{-1} band position in the dimer mass channel, and (f) 35268 cm^{-1} band position in indole···$(furan)_2$ trimer mass channel.

channel originates due to overlapping electronic transitions of both indole···furan dimer and indole···$(furan)_2$ trimer. Similarly, RIDIR spectra are recorded by probing 35268 cm^{-1} position of the background of the R2PI spectra in indole···furan dimer and indole···$(furan)_2$ trimer mass channels and displayed in Figure 4.7e and 4.7f, respectively. As the IR spectra at both the dimer and trimer mass channels show a single peak at 3481 cm^{-1}, the background

observed at 35268 cm^{-1} in the dimer R2PI spectrum could be due to electronic transition of another isomer of indole···$(furan)_2$ trimer.

Similar RIDIR spectra like the ones in Figures 4.7c and 4.7e have been observed by probing many other positions (35160, 35205, 35229, 35255, and 35267 cm^{-1}) on the background of the R2PI spectrum in the dimer mass channel and these have been provided in Figure 4.8.

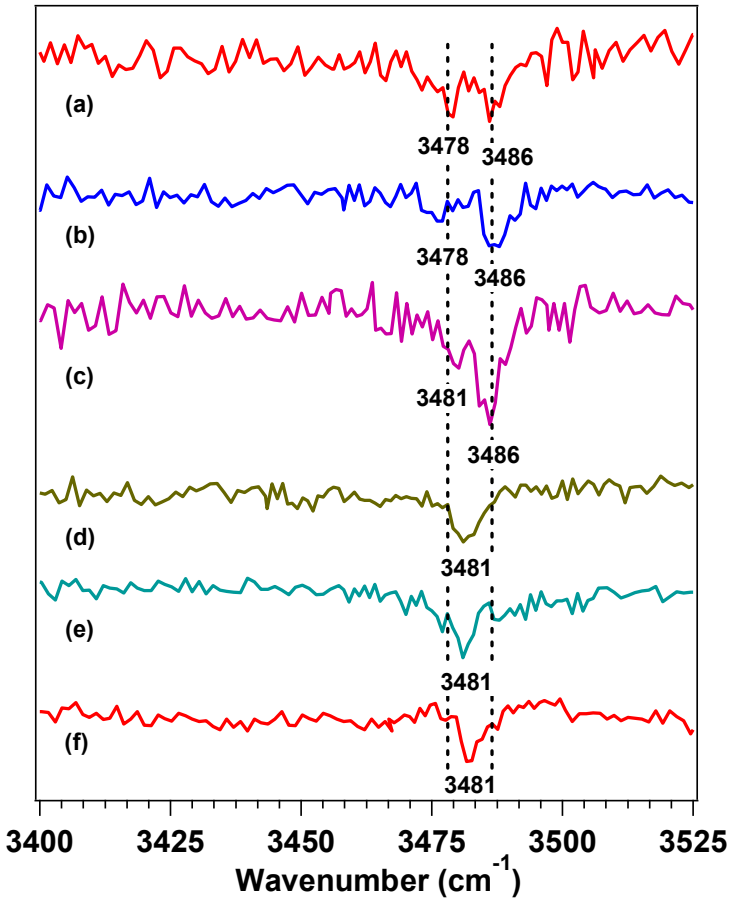

Figure 4.8. RIDIR spectrum in the N-H stretching region by probing several background positions of the R2PI spectrum of indole···furan dimer. (a) 35149 cm^{-1}, (b) 35160 cm^{-1}, (c) 35205 cm^{-1}, (d) 35229 cm^{-1}, (e) 35255 cm^{-1}, and (f) 35267 cm^{-1} UV positions of the dimer R2PI spectrum.

All the RIDIR spectra shown in Figures 4.7 and 4.8 reveal that the broad background of the R2PI spectrum in Figure 4.2b originates due to electronic transitions of multiple isomers of indole···$(furan)_2$ trimer as well as single isomer of indole…furan dimer. Thus it is proved that only one isomer of the dimer is observed in the experiment and the broad background in the

R2PI spectrum of the dimer arises as a result of efficient fragmentation of the indole…$(furan)_2$ trimer at the indole…furan dimer mass channel. Generally UV-UV or IR-UV hole-burning spectroscopies are not very much suitable to determine the presence of multiple isomers when the R2PI spectrum is very broad. There are many reports in the literature where multiple RIDIR spectra are recorded by fixing several UV wavelengths of broad R2PI spectra of the complexes to probe the conformational landscape.[248-249,426] In general, 2-color R2PI spectroscopy is also used to avoid fragmentation of the higher clusters in the dimer mass channel. But we did not obtain any significant amount of 2-color R2PI signal for indole···furan complex.

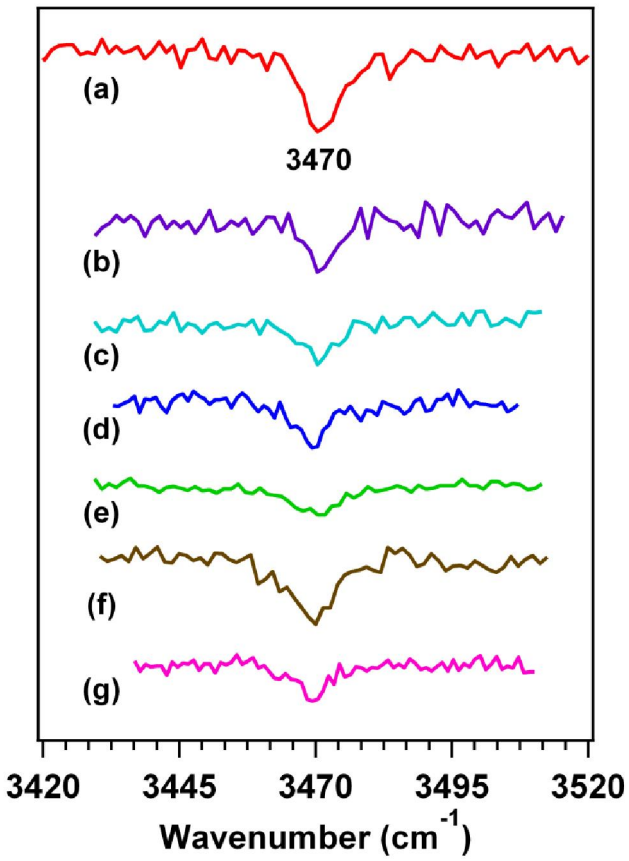

Figure 4.9. RIDIR spectra in the N-H stretching region by probing at (a) 35075 cm^{-1}, (b) 35137 cm^{-1}, (c) 35089 cm^{-1},(d) 35058 cm^{-1} (e) 35052 cm^{-1}, (f) 35039, and (g) 35023 cm^{-1} positions of the broad background of the R2PI spectrum of indole…thiophene dimer.

In a similar fashion, we have measured multiple IR spectra in the N-H stretching region by probing several positions of the broad background in the R2PI spectrum of the

indole…thiophene dimer (Figure 4.2c) to determine the source of broadening of the electronic spectrum. For the brevity, only a few of them have been presented in Figure 4.9. Identical IR spectra obtained by probing most of the positions in the R2PI spectrum confirms that the broad background in the electronic spectrum is due to the presence of only a single structure of the indole…thiophene dimer.

4.2.4. Theoretical results.

4.2.4.1. Structures of indole…furan dimer.

To determine the structure of the observed mixed dimer of indole and furan, DFT calculations of various probable structures of the dimer have been performed at the B97-D level using various basis sets. Figure 4.10 shows six probable structures of the indole···furan dimer, which are used as input geometries for optimization at various levels of theory. It is interesting to note here that most of the structures of the dimer are stabilized due to multiple types of non-covalent interactions. Structure I is named as HB, which is primarily N-H···O hydrogen bonded. This HB structure gets unique V-shaped geometry to maximize the stability through additional C-H···π interaction. Similar kind of V-shaped geometry has been reported for phenol dimer as well as indole···pyridine dimer.[2-5,7,346] This V-shaped structure stabilized by strong hydrogen bonding as well as significant amount of dispersion interactions is named as "*Special class of mixed complexes*". Both structures II and III are N-H···π hydrogen bonded but the former one has right angle T-shaped geometry (T) and the latter one has tilted T-shaped geometry (T′).

It is apparent that the N-H···π bound (T and T′) structures are stabilized through also C-H···O interaction. Structures IV, V, and VI which are parallel-displaced dimers named as syn-PD, syn-PD′, and anti-PD, respectively. In both syn-PD and syn-PD′ structures, indole NH group and oxygen atom of furan are oriented in the same side but the geometry of the former one is nearly parallel while the latter one is tilted parallel-displaced. In the case of the anti-PD structure, indole NH group and oxygen atom of furan are positioned in the opposite side in the parallel fashion.

Initial and final structures of indole…furan dimer optimized at the B97-D/aVDZ level have been provided in Figure 4.11. Both syn-PD and T (right angle T-shaped) structures converge to T′ (tilted T-shaped) structure after optimization at various levels of theory. Thus six probable structures are converged into four structures after optimization.

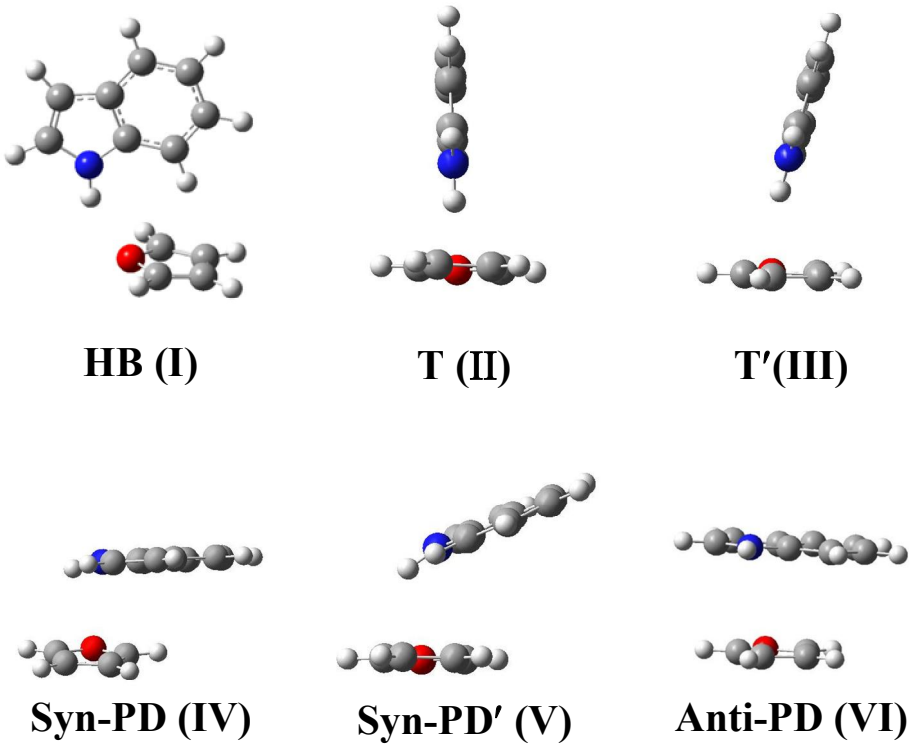

Figure 4.10. Six probable initial structures of indole···furan dimer

Frequency calculations of all four stable structures have been performed to check whether these are true minima. N-H···π bound tilted T-shaped (T′) structure is the most stable isomer of the indole···furan dimer. Figure 4.12 shows both front and side views of the T′ structure optimized at the B97-D/aVDZ level of theory. The tilt angle of the T′ structure calculated is 15° i.e. the angle between the molecular planes of indole and furan is 75°. Similar kind of tilted T-shaped structure has been reported for 2-pyridone···benzene, pyrrole···benzene, indole···benzene, and pyrrole…pyrrole complexes.[264-265,290,418] Tilted T-shaped structure (T′)

becomes more stable compared to the right angle T-shaped one (T) as the former one maximizes the stability through N-H···π with very weak overlap of the two π clouds.

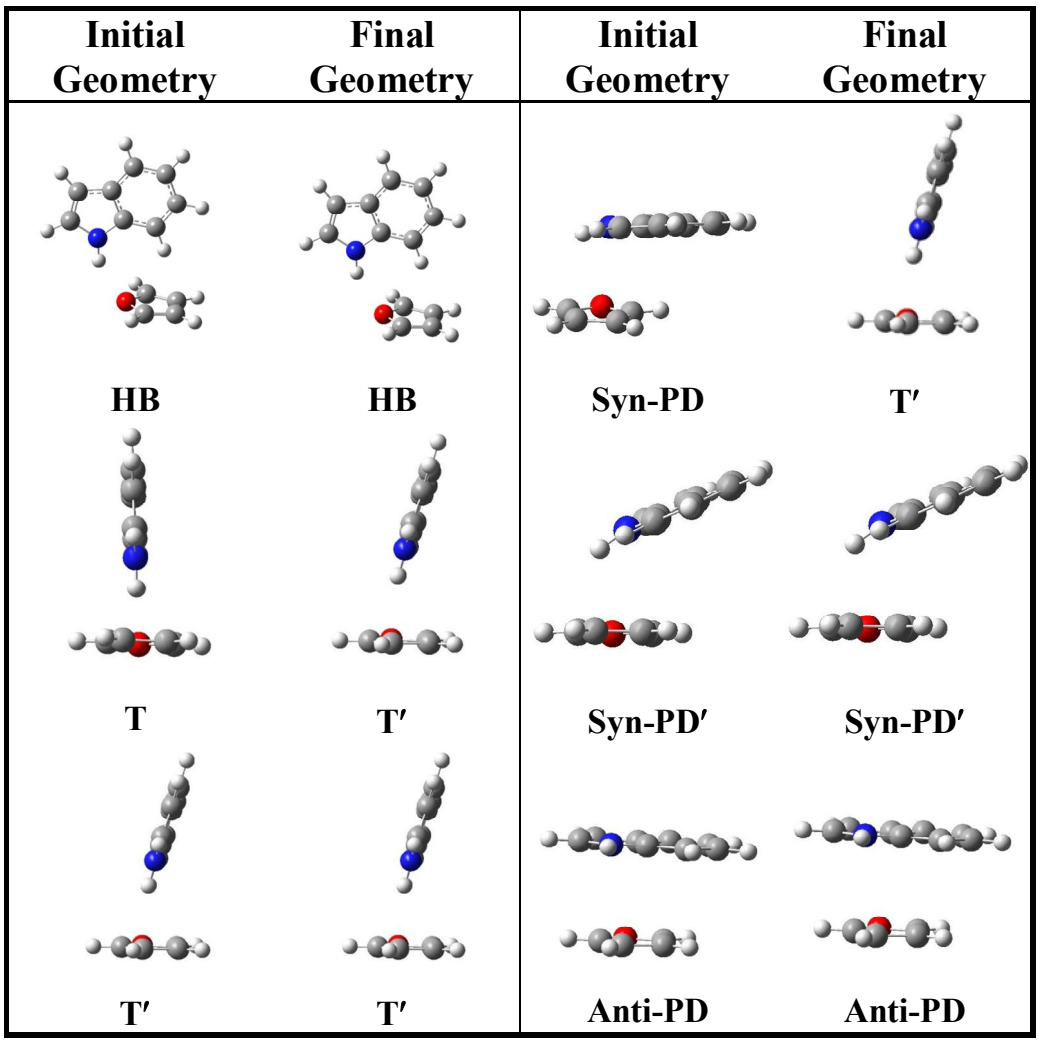

Figure 4.11. Initial and B97-D/aVDZ optimized structures of various isomers of indole···furan dimer. Six different possible structures of the dimer are converged into four isomers after optimization.

A few selected geometrical parameters of the four stable isomers of indole···furan dimer have been provided in Table 4.1. Specially, various types of non-bonding interactions present in most of the isomers are listed in the table. One important geometrical parameter which indicates how strongly N-H group of indole is involved in hydrogen bonding interaction in various isomers of indole···furan dimer is $\Delta r_{N\text{-}H}$ (lengthening of N-H bond). $\Delta r_{N\text{-}H}$ in the HB structure is 0.0015 Å while that in both T′, and syn-PD′ structures is 0.003 Å. These data

clearly points out that hydrogen bonding interaction in the HB structure is weaker compared to that in the N-H···π bound structures of indole···furan dimer.

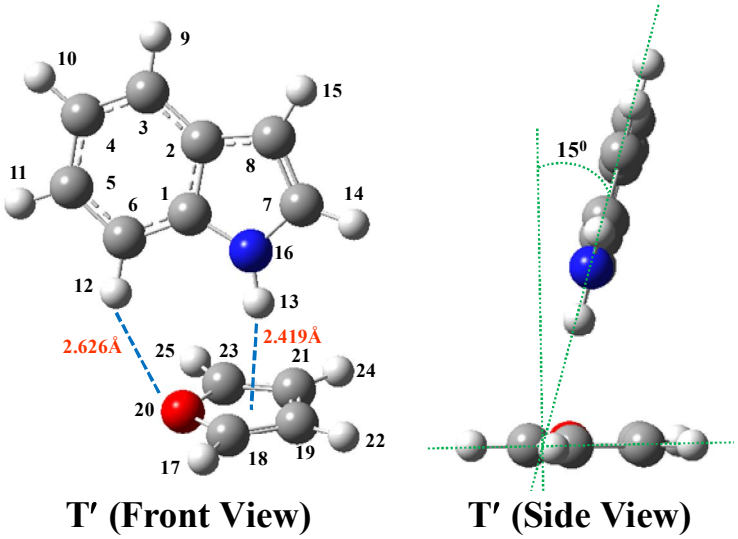

Figure 4.12. Front and side views of the most stable structure (T′) of indole···furan dimer optimized at the B97-D/aVDZ level of theory.

Table 4.1. Selected geometrical parameters of four isomers of indole···furan dimer calculated at the B97-D/aVDZ level of theory

	T′(NH···π)	HB	Syn-PD′	Anti-PD
$d_{N-H\cdots O}$ (Å)	2.84	2.22	2.77	
$d_{N\cdots O}$ (Å)	3.64	3.15	3.26	
Δr_{N-H} (Å)	0.0026	0.0015	0.0030	0.00008
∠N-H…O	135.7°	151.3°	110.4°	
$d_{C-H\cdots O}$ (Å)	2.63	2.90		
∠C-H…O	142.5°	127.0°		
$d_{C-H\cdots\pi}$ (Å)		2.57		
$d_{N-H\cdots\pi}$ (Å)	2.42	3.15	2.53	

Table 4.2 presents BSSE and ZPE corrected binding energies as well as relative energies of all the four stable isomers of the indole…furan dimer calculated at various levels of DFT using different basis sets. As most of the isomers of the indole···furan dimer is stabilized

Table 4.2. BSSE and ZPE corrected binding energies (kcal/mol) as well as N-H stretch frequencies of four Structures of indole···furan dimer calculated at various levels of theory[a]

Methods	Isomers	ΔE_e	ΔE_0	E_{rel}	ν_{N-H}
Expt					3486
B97-D/LP[b]	HB	-4.605	-3.883	0.389	3494
	NH···π (T′)	-4.988	-4.272	0.000	3486
	Syn-PD′	-4.882	-3.960	0.312	3470
	Anti-PD	-3.030	-2.575	1.697	3530
B97-D/cc-pVDZ	HB	-4.549	-3.818	0.427	3496
	NH···π (T′)	-5.001	-4.245	0.000	3485
	Syn-PD′	-4.928	-4.159	0.086	3467
	Anti-PD	-2.582	-2.220	2.025	3530
B97-D/cc-pVTZ	HB	-4.577	-3.888	0.453	3505
	NH···π (T′)	-5.077	-4.341	0.000	3487
	Syn-PD′	-5.015	-4.222	0.119	3475
	Anti-PD	-3.053	-2.677	1.664	3529
B97-D/aVDZ	HB	-4.603	-3.913	0.346	3496
	NH···π (T′)	-4.946	-4.259	0.000	3487
	Syn-PD′	-4.848	-4.117	0.142	3470
	Anti-PD	-2.990	-2.644	1.615	3528

[a]ΔE_e: BSSE corrected binding energy; ΔE_0: BSSE + ZPE corrected binding energy. E_{rel}: ZPE corrected relative energy of the isomer with respect to the most stable isomer. N-H stretch frequency of the experimentally observed isomer of indole…furan dimer is also provided in the Table.

[b]LP stands for 6-311++G (3df, 3pd) basis set.

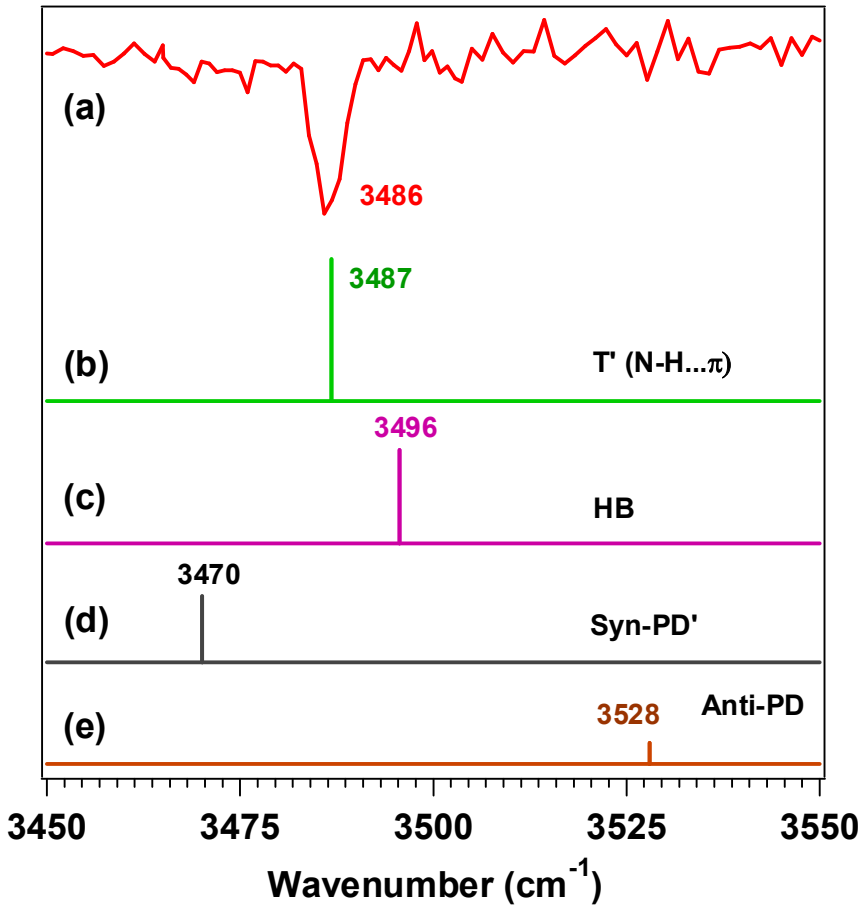

Figure 4.13. (a) RIDIR spectra in the N-H stretching region by probing the origin band of indole···furan dimer. (b)-(e) Theoretical IR stick spectra of four isomers of indole···furan dimer obtained at the B97-D/aVDZ level of theory. Theoretical IR frequencies are scaled by using a scaling factor of 0.9805 obtained from the ratio of experimental and theoretical N-H stretch frequencies of indole monomer.

by electrostatic as well as dispersion interactions, calculations have been performed using B97-D, dispersion corrected DFT functional. By comparing the binding energies and relative energies of the four isomers of the dimer at various levels of theory, it is clear that the N-H···π bound T′ structure of the dimer is the most stable one.

It is important to note that the difference in the binding energies of HB, T′, and syn-PD′ structures is quite small at the level of calculation performed here. Very recently, it has been reported for indole···benzene dimer that the N-H stretch frequency is more sensitive probe for structure determination of the observed isomer of the dimer when multiple isomers are close in energy.[290] We have compared the experimentally observed N-H stretch frequency of

indole···furan dimer with those obtained theoretically for the four isomers and these have been provided in Table 4.2. Theoretical N-H stretch frequencies of the four isomers of the dimer are corrected using a scaling factor obtained from the ratio of the observed and calculated N-H stretch frequency of indole monomer at every level of theory. The result shows that the observed N-H stretch frequency (3486 cm^{-1}) of the dimer matches extremely well with that of the T′ structure calculated at B97-D level of theory using different basis sets. Comparison of the experimental IR spectrum of the observed dimer and theoretical IR stick spectra of four isomers of the indole…furan dimer obtained at the B97-D/aVDZ level of theory has been provided in Figure 4.13. By combining the binding energy as well as N-H stretch frequency values, it is confirmed that the observed indole···furan dimer has N-H···π bound T′ structure. It is quite interesting to note that the observed N-H stretch frequency (3486 cm^{-1}) of indole···furan complex is also in close agreement with the experimental N-H stretch frequency (3479 cm^{-1}) of N-H···π bound T′ structure of indole···benzene complex reported by Biswal et al.[290] This comparison reconfirms our proposed assignment of the structure of the observed indole…furan dimer in the experiment.

A very preliminary results on the indole…furan dimer has been reported earlier in the MS thesis of a student (Vedant Pande) in our laboratoty.[427] The observed geometry of the dimer has not been interpreted correctly in that work. Further an extensive experiment and higher level calculations have been performed to get the energetic and structural details of the dimer.

4.2.4.2. Structures of Indole···thiophene dimer

Geometries of various possible structures of the indole...thiophene dimer have been optimized at different levels of dispersion corrected DFT using various basis sets. To check whether the optimized structures are local minima, frequency calculations have been performed at corresponding level of theory. As per chemical intuition, eight initial structures have been chosen for geometry optimization. A list of possible initial and final structures of the dimer optimized at the M05-2X/6-311++G(2df,2pd) level of theory has been provided in Figure 4.14. Most of the structures are stable at the M05-2X/6-311++G(2df,2pd) level of theory. T-shaped (T1, T2 and T3), SynPD and AntiPD are stable geometries whereas T4 converges to T3 structure and T5 structure gives one imaginary frequency after the

optimization. Figure 4.15 shows only the stable structures of the indole…thiophene dimer optimized at the M05-2X/6-311++G(2df,2pd) level of theory. The structure labeled as T1 is stabilized due to π-hydrogen bonding interaction between the α-CH of furan and π-cloud of the phenyl group of indole, while the sulfur atom is facing towards the pyrrole ring of indole. In the case of the T2 structure, both α-CH and β-CH of furan are hydrogen bonded with the π-clouds of pyrrole and phenyl groups of indole, respectively. T3 structure is mainly stabilized by N-H...π hydrogen bonding interaction but the geometry is tilted T-shaped to get

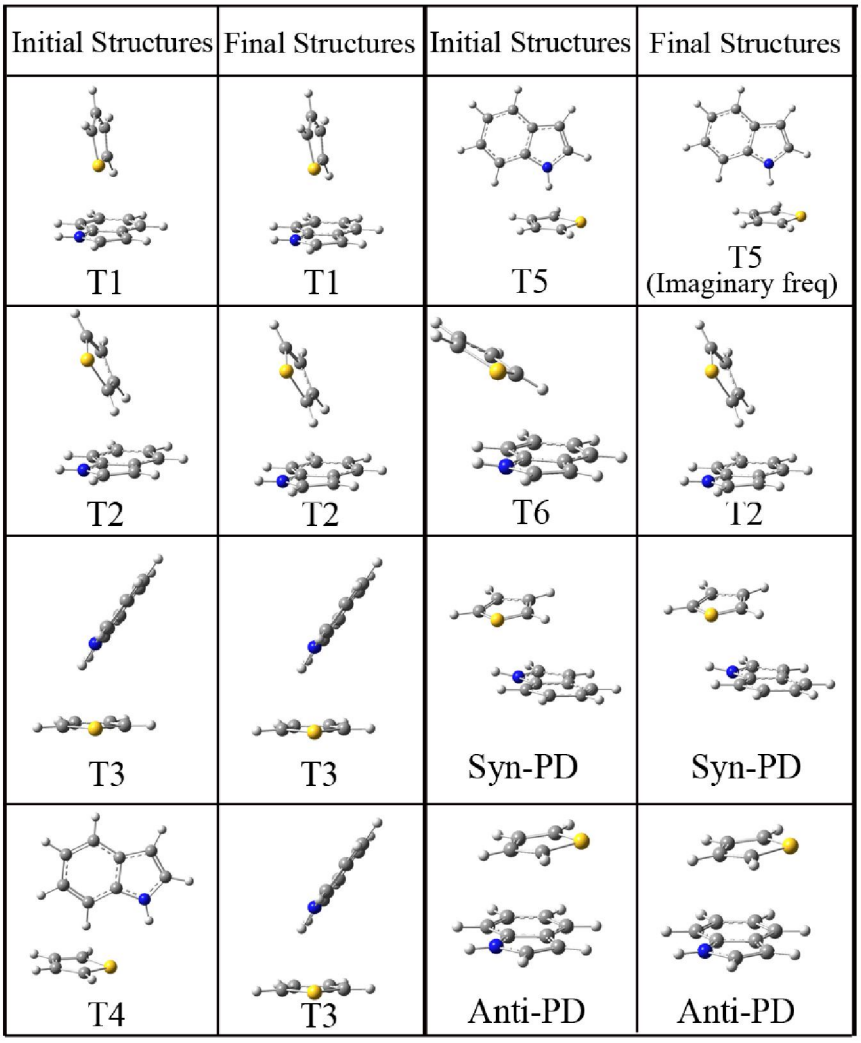

Figure 4.14. A list of all the possible initial and final structures of indole…thiophene dimer optimized at the M05-2X/6-311++G(2df,2pd) level of theory.

additional stability from weak π...π interaction between indole and thiophene moieties. Both syn-PD and anti-PD structures have parallel displaced π-stacked geometry but the orientation

of the N-H group of indole and sulfur atom of thiophene is in the same side in the former structure, while it is in the opposite side in the latter one.

BSSE- and ZPE-corrected binding energies of the stable structures of the indole…thiophene dimer calculated at different levels of theory have been provided in Table 4.3. Comparison of the binding energies shows that the most stable structure of the indole…thiophene dimer is T3, which has a tilted T-shaped geometry with N-H...π hydrogen bonding interaction. We have also calculated the binding energies of various stable structures of the dimer at further

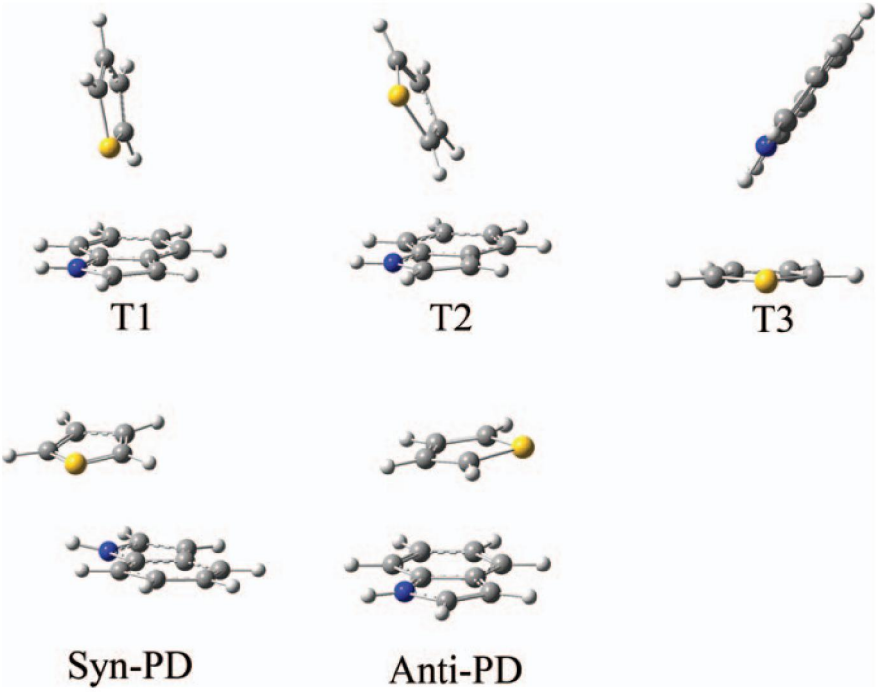

Figure 4.15. Five stable structures of indole···thiophene dimer optimized at the M05-2X/6-311++G(2df,2pd) level of theory.

higher levels of theory (M05-2X/aVDZ, M05-2X/aVTZ, and M05-2X/cc-pVQZ) by performing single point energy calculations on the M05-2X/cc-pVTZ level optimized geometries. BSSE-corrected binding energies of different stable structures of the dimer from these single point energy calculations have been provided in Table 4.4. It is noteworthy that the order of the binding energies of different structures calculated at all levels of theory has similar trend. These results indicate that the observed dimer might have T3 structure. We have confirmed the geometry of the observed indole…thiophene dimer by comparing its N-H as well as C-H stretching frequencies with those of various calculated structures. The

harmonic frequencies for both N-H and C-H stretching vibrations of the dimer calculated at various levels of theory have been scaled by using a factor obtained from the ratio of the experimental (3526 cm^{-1}) and theoretical N-H stretching frequencies of indole monomer at the corresponding level of theory. As N-H stretching frequency is a more sensitive probe than the C-H stretching frequency to determine the structure of the observed dimer in the experiment, theoretical N-H stretching frequencies of the various structures of the dimer calculated at various levels of theory have been presented in Table 4.3. It is quite interesting to note that the N-H stretching frequencies of the five stable structures of the dimer calculated at various levels of theory have similar trend.

Table 4.3. BSSE and ZPE corrected binding energies (kcal/mol) as well as the N-H stretching frequencies of the stable structures of indole···thiophene dimer calculated at various levels of DFT. [a] Calculated N-H frequencies of the dimer are scaled by using a factor obtained from the ratio of the experimental (3526 cm^{-1}) and theoretical N-H stretching frequencies of indole monomer at every level of theory.

Methods	Structures	ΔE_e	ΔE_0	ν_{N-H} (cm^{-1})
Expt.				3470
M05-2X/6-311++G(2df,2pd)	T1	-3.745	-3.230	3524
	T2	-3.798	-3.242	3522
	T3	-4.326	-3.684	3471
	Syn-PD	-4.068	-3.410	3501
	Anti-PD	-2.138	-1.806	3526
M05-2X/6-311++G(3df,3pd)	T1	-3.699	-3.082	3525
	T2	-3.747	-3.022	3523
	T3	-4.417	-3.699	3470
	Syn-PD	-4.103	-3.220	3491
	Anti-PD	-2.069	-1.682	3527
M05-2X/cc-pVTZ	T1	-3.539	-3.152	3522
	T2	-3.630	-3.130	3522
	T3	-4.312	-3.778	3469
	Anti-PD	-1.767	-1.478	3527

[a]Syn-PD structure converges to the T3 structure at the M05-2X/cc-pVTZ level of theory.

Table 4.4. BSSE corrected binding energies of the stable structures of the indole…thiophene dimer at a few higher DFT levels by doing single point energy calculations on M05-2X/cc-pVTZ optimized geometries.

	M05-2X/aVDZ	M05-2X/aVTZ	M05-2X/cc-pVQZ
	ΔE_e	ΔE_e	ΔE_e
T1	-3.738	-3.460	-3.434
T2	-3.883	-3.630	-3.624
T3	-4.463	-4.369	-4.332
Anti-PD	-2.231	-1.856	-1.768

[a]E_e: BSSE corrected binding energy. Syn-PD is not stable at the M05-2X/ccpVTZ level of theory. Thus, single point energy calculation of this structure has not been done.

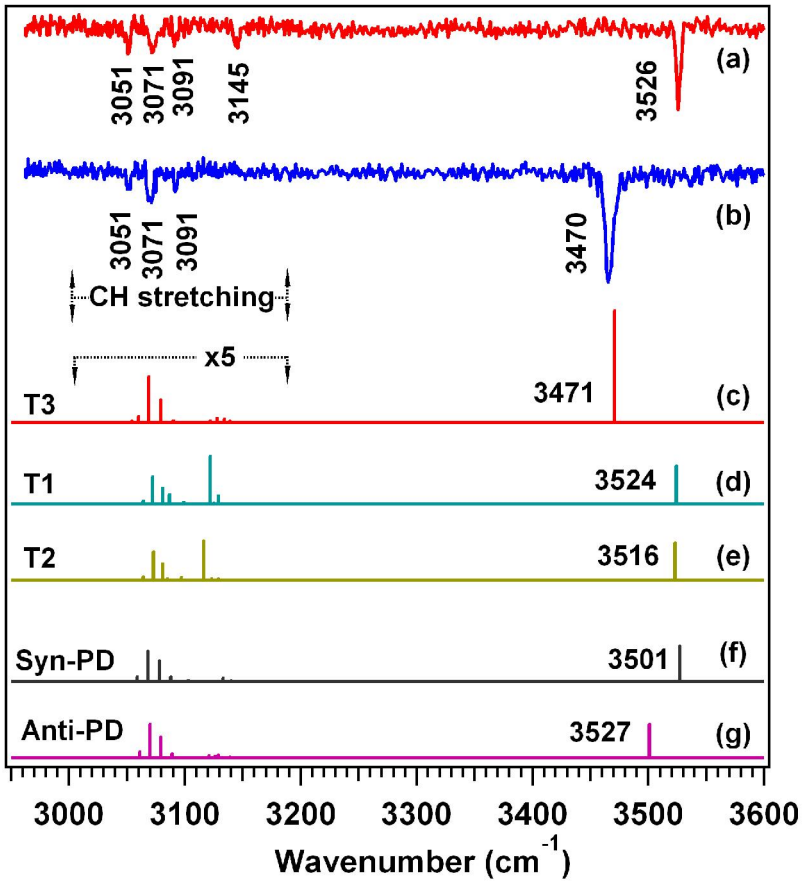

Figure 4.16. Experimental IR spectra by probing electronic origin band of (a) indole, (b) indole…thiophene dimer, and (c-g) theoretical IR spectra of the five stable structures of the indole…thiophene dimer calculated at the M05-2X/6-311++G(2df,2pd) level of theory, in the N-H and C-H stretching regions.

Figure 4.16 shows comparison of the experimental IR spectrum of the observed dimer with the theoretical IR spectra of the five stable structures of the dimer in the N-H and C-H stretching regions calculated at the M05-2X/6-311++G(2df,2pd) level of theory. The IR spectrum in the C-H stretching region of the dimer shown in Figure 4.16b is mostly identical with that of the indole monomer and this indicates that the C-H groups in the dimer are mostly free, whereas the N-H stretch frequency in the dimer is red-shifted from that in the indole monomer by 56 cm^{-1}. The comparison unambiguously confirms that the theoretical IR spectrum of only the T3 structure (N-H...π bound tilted T-shaped) matches very well with the experimental IR spectrum of the observed dimer. Specially, very excellent agreement between the N-H stretching frequency of the observed dimer with that of the T3 structure is noteworthy. This confirms that the observed dimer has an N-H...π bound tilted T-shaped geometry. A complete list of N-H and C-H stretching frequencies of indole and thiophene monomers as well as indole...thiophene dimer along with their assignments obtained at the M05-2X/6-311++G(2df,2pd) level of theory has been provided in Table 4.5. Figure 4.17 shows front and side views of the most stable structure (T3) of the dimer with the atom numbering scheme as well as N-H...π hydrogen bond distance (2.41 Å) and tilt angle (35°) of the dimer obtained at the M05-2X/6-311++G(2df,2pd) level of theory.

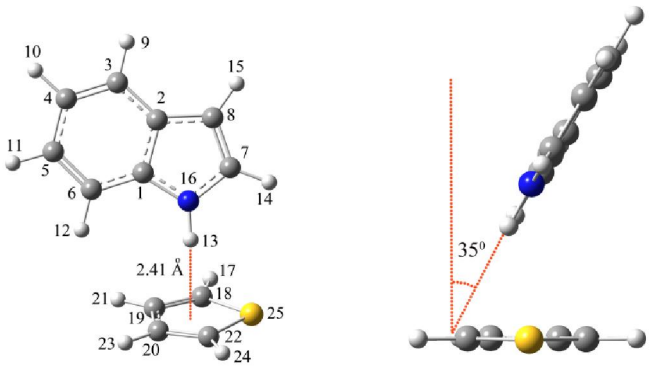

T3 (Front View) T3 (Side View)

Figure 4.17. Front and side views of the most stable structure of indole···thiophene dimer optimized at the M05-2X/6-311++G(3df,3pd) level of theory. Atom numbering scheme has been shown in the front view of the structure. Tilt angle is 35°.

Table 4.5. A complete list of N-H and C-H stretching frequencies (cm^{-1}) of indole and thiophene monomers as well as different structures of indole...thiophene dimer calculated at the M05-2X/6-311++G(2df,2pd) level of theory.[a]

Monomers			Indole…thiophene dimer						Assignment
Indole		Thiophene	Expt. freq.	Calc. freq. (Int)					
Expt. freq.	Calc. freq. (Int)	Calc. freq. (Int)		T1	T2	T3	Syn-PD	Anti-PD	
3526	3526 (93.7)		3470	3524 (92.8)	3522 (91.1)	3471 (273.2)	3501 (81.9)	3526 (87.0)	N-H stretch
3145	3142 (0.7)			3142 (0.3)	3140 (0.2)	3139 (0.7)	3139 (0.5)	3140 (0.6)	Pyrrole C-H SS
		3132 (1.4)		3129 (4.0)	3129 (0.7)	3134 (1.9)	3129 (1.3)	3133 (1.9)	Thiophene C-H SS
		3129 (0.4)		3122 (23.2)	3116 (19.3)	3128 (2.2)	3126 (0.8)	3131 (0.3)	Thiophene C-H AS
	3124 (0.7)			3125 (0.5)	3123 (0.7)	3122 (0.9)	3121 (1.0)	3122 (0.4)	Pyrrole C-H AS
		3102 (1.0)		3099 (1.0)	3097 (1.4)	3103 (0.1)	3103 (0.2)	3103 (0.8)	Thiophene C-H AS
		3090 (2.4)		3087 (4.7)	3085 (0.6)	3090 (1.0)	3089 (1.9)	3088 (2.4)	Thiophene C-H AS
3091	3080 (10.1)		3091	3081 (7.7)	3081 (8.0)	3079 (11.2)	3079 (10.1)	3078 (10.2)	Phenyl C-H SS
3071	3071 (18.1)		3071	3072 (13.3)	3073 (13.9)	3069 (22.6)	3070 (16.6)	3068 (15.1)	Phenyl C-H AS
	3062 (2.0)			3064 (1.6)	3064 (1.7)	3060 (3.0)	3061 (2.9)	3059 (2.3)	Phenyl C-H AS
3051	3055 (0.4)		3051	3057 (0.1)	3057 (0.1)	3054 (0.7)	3055 (0.3)	3053 (0.4)	Phenyl C-H AS

[a]Calculated frequencies are scaled using a factor of 0.94253, which is obtained from the ratio of experimental and theoretical NH stretch frequencies of indole monomer. Pyrrole C-H denotes C-H stretch of pyrrole group of indole, Phenyl C-H denotes C-H stretch of phenyl group of indole, SS = symmetric stretching, AS = Asymmetric stretching. Intensity (Int) is given in km/mol.

It is worthwhile to compare the observed N-H...π bound tilted T-shaped structure of indole...thiophene dimer with those of the relevant complexes reported in the literature. Similar kind of tilted T-shaped N-H...π hydrogen bonded structure has been observed for pyridone...benzene, pyrrole...benzene, indole...benzene, and indole...furan dimers with the red-shifts in the N-H stretching frequency of 56, 59, 44, and 40 cm^{-1}, respectively.[265,290,311,418] The amount of red-shift in the N-H stretching frequency of the indole...thiophene dimer studied in this work is 56 cm^{-1}, which matches well with the reported N-H...π bound dimers. The focus of this work is on the effect of the heteroatoms present in the acceptors on the strength of the π-hydrogen bonding interactions. Thus the above comparison on the red-shift in the N-H stretching frequency reveals that π-hydrogen bonding in the indole...thiophene

dimer is stronger compared to that in the indole...furan[311] as well as indole...benzene[290] dimers. We have reported in chapter 3 that the N-H...π bound indole...pyridine dimer is not observed experimentally and it has been found also from calculation that this dimer is not a minimum energy structure in the potential energy curve.[9] So, five membered aromatic heterocyclic systems (furan, thiophene) are reasonably good π-hydrogen bond acceptor but pyridine is not. Sherrill and co-workers have studied benzene...pyridine dimer theoretically and concluded that aromatic rings containing heteroatoms are poorest π-hydrogen bond acceptors.[299] But our study illustrates that five membered heterocyclic aromatic rings are favorable π-hydrogen bond acceptors.

Comparison of the binding energies of the N-H...π bound T-shaped complexes of indole with several heterocyclic aromatic systems also supports our experimental finding and this has been presented in Table 4.6.[9,311] In the case of the indole...pyridine dimer, we have provided the binding energy of the perfect T-shaped N-H...π bound structure as the optimization of the tilted T-shaped geometry is converged to parallel-displaced structure.

Table 4.6. Comparison of the binding energies (kcal/mol) of the N-H...π bound T-shaped complexes of indole with several heterocyclic aromatic systems.

	M05-2X/aVDZ		M05-2X/cc-pVTZ	
	ΔE_e	ΔE_0	ΔE_e	ΔE_0
Indole…pyridine	-3.823	-3.093	-3.673	-3.114
Indole…thiophene	-4.452	-3.818	-4.315	-3.778
Indole…furan	-4.009	-3.684	-3.937	-3.452

As expected, indole...pyridine dimer has least binding energy among the T-shaped complexes provided in the table. It is also obvious from the comparison that the binding energy of indole...thiophene dimer is higher than that of indole...furan dimer.

4.2.5. Electrostatic potentials of the π-hydrogen bond acceptors

The strength of the π-hydrogen bonding interaction with a specific hydrogen bond donor depends on the extent of the availability of the π-electron clouds of the π-hydrogen bond acceptors. In the case of the heterocyclic aromatic systems as acceptors, there is a role of the

heteroatoms to control the accessibility of the π-electron cloud for hydrogen bonding interactions. Molecular electrostatic potentials of the π-hydrogen bond acceptors can provide quantitative information on this. Figure 4.18 shows electrostatic potential maps of pyridine, furan, and thiophene calculated at the HF/6-311++G(d,p) level of theory. It is quite apparent from the electrostatic potential maps of the heterocyclic systems provided in the Figure that the electrostatic potential or π-electron density in the centre of the ring is most negative for thiophene and least negative for pyridine. This nicely explains the order of the binding energies provided in Table 4.6 as well as strength of the π-hydrogen bonding interactions of the complexes of indole and heterocyclic systems discussed in the Sec. 4.2.4.2. It has been found from the electrostatic potential maps that furan and thiophene unlike pyridine have

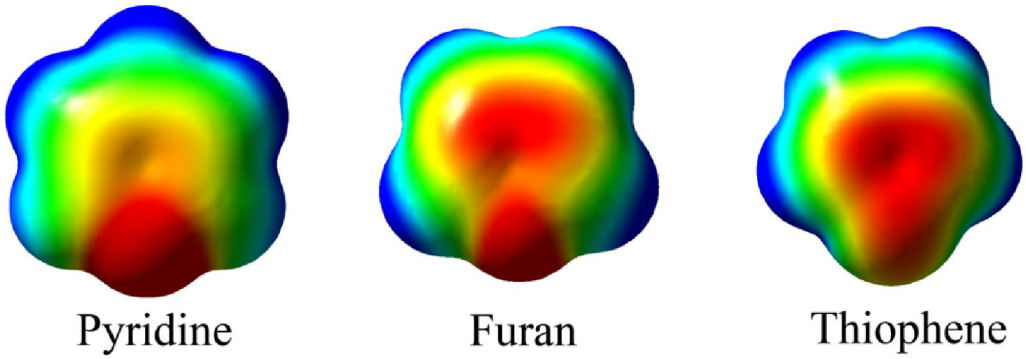

Figure 4.18. Electrostatic potential maps of pyridine, furan and thiophene calculated at the HF/6-311++G(d,p) level of theory. The scale is -16 kcal/mol (red) to 16 kcal/mol (blue).

significant amount of π-electron density in the centre of the ring in spite of the presence of the heteroatoms. In the case of pyridine, nitrogen atom only pulls π-electron density from the ring towards it. But for both furan and thiophene, the p-type lone pair of electrons on oxygen and sulfur atoms, respectively, is delocalized over the rings to participate in their aromaticity and become a part of the π-aromatic system according to Huckel's 4n + 2 π-electrons rule. As electronegativity of oxygen (3.5) is much higher than that of sulfur (2.58), sharing of the lone pair electrons in the aromatic system is less effective in furan compared to thiophene leading to higher π-electron density in the latter than the former one.[428]

4.2.6. NBO analysis

The strength of the hydrogen bonding interaction can be explained more quantitatively with the help of NBO analysis. Figure 4.19 shows comparison of the NBO pictures of the N-H...π

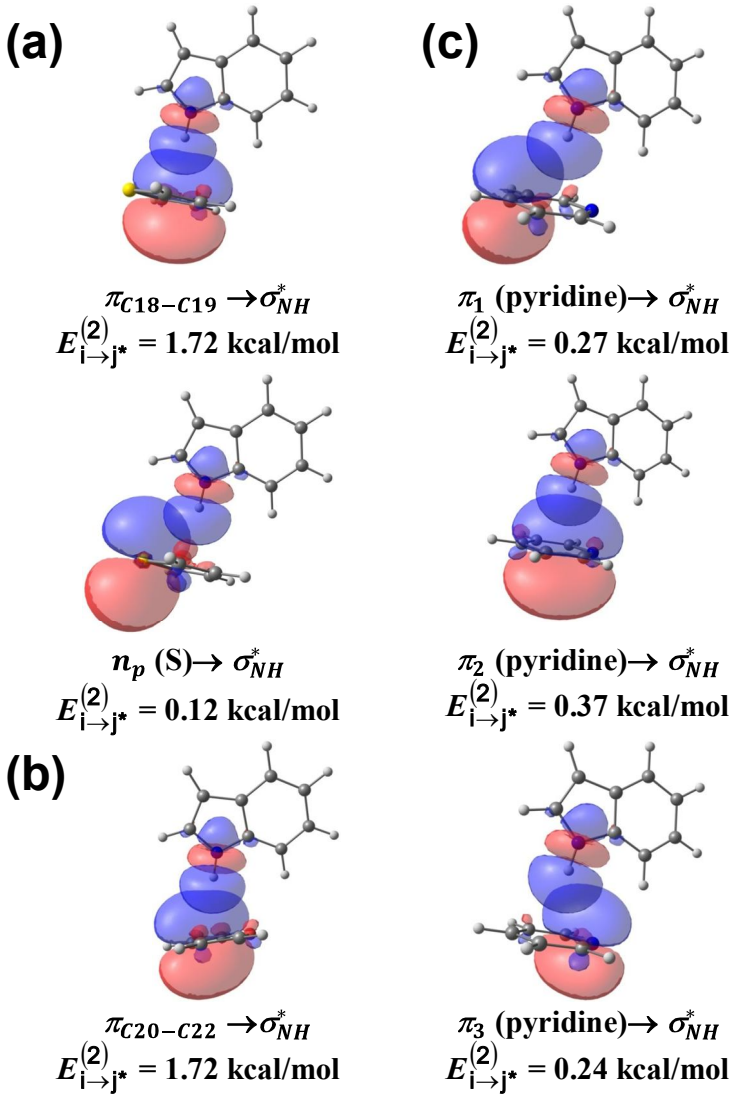

Figure 4.19. Natural bond orbitals of slanted T-shaped N-H...π bound structures of (a) indole...thiophene dimer, (b) indole...furan dimer. (c) Natural bond orbitals of perfect T-shaped N-H...π bound structure of indole...pyridine dimer. For atom numbering, refer to Figure 4.17. Same atom numbering scheme has been followed for both indole…thiophene and indole…furan dimers.

bound structure (T3) of the indole...thiophene dimer with those of indole...furan and indole...pyridine dimers calculated at the M05-2X/cc-pVTZ level of theory. In case of the indole...pyridine dimer, the overlap of the σ^*_{NH} orbital with the three π-orbitals in pyridine is observed. But both indole...thiophene and indole...furan dimers show overlap of the σ^*_{NH} orbital with only one π-orbital in each of thiophene and furan moieties as the interaction with the other π-orbital is negligible. There is small contribution in $E^{(2)}_{i\rightarrow j^*}$ from very weak interaction between p-type lone pair of sulfur and σ^*_{NH} orbital in indole...thiophene dimer and this is absent in indole...furan dimer. This could be explained in terms of lower electronegativity of sulfur in comparison to oxygen leading to more efficient participation of the sulfur lone pair than the oxygen lone pair in aromaticity of thiophene and furan, respectively. The NBO analysis indicate that the $E^{(2)}_{i\rightarrow j^*}$ value for indole...pyrdine dimer (0.88 kcal/mol) is extremely less compared to those for indole...thiophene (1.84 kcal/mol), indole...furan (1.72 kcal/mol) dimers. Thus the NBO result corroborate with the binding

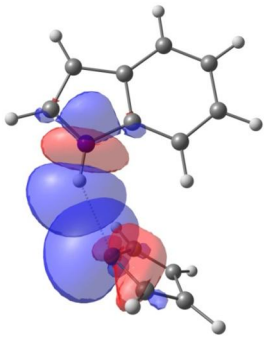

n_{sp2} (O) $\rightarrow \sigma^*_{NH}$

$E^{(2)}_{i\rightarrow j^*}$ = 1.13 kcal/mol

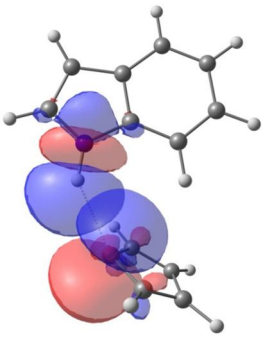

n_p (O) $\rightarrow \sigma^*_{NH}$

$E^{(2)}_{i\rightarrow j^*}$ = 0.46 kcal/mol

Figure 4.20. Natural Bond Orbitals of hydrogen bonded (HB) isomers of indole…furan dimer showing the interactions between hydrogen bond donors and acceptors at M05-2X/cc-pVTZ level of theory.

energies, electrostatic potential maps and red-shifts in the N-H stretching frequencies of the dimers discussed in the Sections 4.2.4.2. and 4.2.5.

In the case of the indole…furan dimer, the interaction of the Natural bond orbitals $n_{sp2}(O) \rightarrow \sigma^*_{NH}$ and $n_p(O) \rightarrow \sigma^*_{NH}$ in the HB structure at M05-2X/cc-pVTZ level of theory has been shown in Figure 4.20. Total $E^{(2)}_{i\rightarrow j^*}$ values for the HB are 1.59 kcal/mol, whereas and $E^{(2)}_{i\rightarrow j^*}$ values for tilted shaped (T′) structure is 1.72 kcal/mol. The NBO results demonstrate that the hydrogen bond interaction in the HB structure is indeed weak. This could be explained due to very small $E^{(2)}_{i\rightarrow j^*}$ value (0.46 kcal/mol) for the $n_p(O) \rightarrow \sigma^*_{NH}$ interaction in the

Table 4.7. Comparison of various NBO parameters of indole···THF dimer and HB as well as T′ structures of indole···furan dimer calculated at the M05-2X/cc-pVTZ Level of Theory.

NBO parameters	Indole···Furan		Indole···THF
	T′ (NH···π)	HB	
$\delta(n_{sp2}(O))_{Furan}$	1.97040	1.96914	1.95729
$\delta(n_p(O))_{Furan}$	1.71806	1.73345	1.93689
$\delta(\pi_{C20-C22})_{Furan}$	1.88442		
$\delta(\sigma^*_{NH})$	0.01968	0.01831	
$E^{(2)}_{i\rightarrow j^*}(n_{sp2}(O)\rightarrow \sigma^*_{NH})$		1.13	
$E^{(2)}_{i\rightarrow j^*}(n_p(O)\rightarrow \sigma^*_{NH})$		0.46	5.92
$E^{(2)}_{i\rightarrow j^*}(\pi_{C20-C22}\rightarrow \sigma^*_{NH})$	1.72		

$E^{(2)}_{i\rightarrow j^*}$ is in kcal/mol; all other values are in a.u. In Furan monomer, $\delta(n_{sp2}(O))_{Furan}$ =1.97042, $\delta(n_p(O))_{Furan}$ = 1.71633. In THF monomer, $\delta(n_{sp2}(O))_{THF}$ =1.96672, $\delta(n_p(O))_{THF}$ =1.92069

HB structure. Actually the availability of the p-type lone pair on the oxygen atom of furan is less for hydrogen bonding as it takes part in the aromaticity of the furan ring. On the other hand, $E^{(2)}_{i\rightarrow j^*}$ value for the $n_p(O) \rightarrow \sigma^*_{NH}$ interaction in the hydrogen-bonded structure of indole···THF dimer and indole…H_2O dimer calculated at the same level of theory (M05/cc-pVTZ) are 5.92 and 11.57 kcal/mol.

Comparison of various NBO parameters of indole···THF dimer and HB as well as T′ structures of indole···furan dimer have also been provided in Table 4.7. In the table, the electron occupancies in sp^2- and p-type lone pair orbitals of O atom of Furan, $\pi_{C20-C22}$ orbitals of furan are denoted by $\delta(n_{sp2}(O))_{Furan}$, $\delta(n_p(O))_{Furan}$ and $\delta(\pi_{C20-C22})_{Furan}$,

respectively while the antibonding orbitals of hydrogen bond donor N-H is designated as δ(σ^*_{NH}). NBO analysis indeed shows that the occupancy of the p-type lone pair on the oxygen atom in furan monomer (1.71633) is very less compared to that in THF monomer (1.92069). Thus the NBO analysis supports the interpretation that the observed indole···furan dimer has N-H···π bound tilted T-shaped geometry.

4.2.7. EDA of the dimers

As various isomers of the dimers studied here comprise of multiple types of non-covalent interactions, it is important to know the contribution of different components of the interaction energies to the stabilization of the complexes. For this purpose, we have used LMO-EDA procedure introduced by Su and Li.[429] For the indole…furan dimer, different components of the total interaction energy along with the ratios of the dispersion to electrostatic interactions (disp/elec) in all the four isomers are provided in Table 4.8. It is quite interesting to note that the dispersion interaction is 1.5 times than the electrostatic one even in the HB isomer of the indole…furan dimer. This result clearly indicates that the hydrogen bonding interaction in the HB isomer is quite weak. Overall we can tell that dispersion wins over electrostatics in the case of the indole···furan dimer.

Table 4.8. Decomposition of Interaction Energies (kcal/mol) in various isomers of the indole···furan dimer calculated at the M05-2X/cc-pVTZ level of thoery

	ΔE_{ele}	ΔE_{ex}	ΔE_{rep}	ΔE_{pol}	ΔE_{disp}	ΔE_{tot}	$\Delta E_{disp}/\Delta E_{ele}$
HB	-4.86	-2.47	11.85	-1.16	-7.45	-4.08	1.53
T′ (NH···π)	-3.84	-2.28	11.30	-1.21	-7.97	-4.00	2.07
Syn-PD′	-3.89	-2.61	11.96	-1.38	-8.05	-3.97	2.07
Anti-PD	-1.45	-2.84	14.25	-1.05	-10.72	-1.81	7.39

Table 4.9 shows comparison of the different components of the total interaction energy in the N-H…π bound T-shaped indole...thiophene, indole...furan, and indole...pyridine dimers calculated at the M05-2X/cc-pVDZ level of theory. The results provided in the Table 4.9 reveal that dispersion plays a much more important role than electrostatic interaction for all the three N-H...π hydrogen bonded complexes of indole with pyridine, furan and thiophene.

Table 4.9. Decomposition of the Interaction Energies (kcal/mol) in N-H...π bound T-shaped indole...thiophene, indole...furan, and indole...pyridine dimers calculated at the M05-2X/cc-pVTZ level of theory.

	ΔE_{ele}	ΔE_{ex}	ΔE_{rep}	ΔE_{pol}	ΔE_{disp}	ΔE_{tot}
Indole…thiophene	-4.28	-2.67	12.40	-1.34	-8.34	-4.22
Indole…furan	-4.06	-2.35	11.28	-1.14	-7.53	-3.79
Indole…pyridine	-3.82	-2.48	11.66	-0.88	-7.97	-3.49

4.3. Conclusions

In conclusion, R2PI and IR-UV double resonance spectroscopy experiments as well as DFT calculations have been performed to study the complexes of indole with furan and thiophene in a supersonic jet. The R2PI spectra of these complexes are measured by electronic excitation of the indole moiety. In the case of the indole…furan complex, the R2PI spectrum obtained in the dimer mass channel shows a broad background with a few sharp features. On the other hand, the R2PI spectrum of the indole…thiophene dimer exhibits very broad and completely structureless electronic band. By measuring R2PI as well as IR spectra at both indole···furan dimer and indole···$(furan)_2$ trimer mass channels, it has been found that the major contribution of the broad background observed in the dimer R2PI spectrum is due to fragmentation of the trimer at the dimer mass channel. Observation of only one isomer of the dimer has also been confirmed by measuring IR spectra at various background positions of the broad electronic spectrum of indole…furan dimer. Similarly, multiple IR spectra have been recorded in the case of the indole…thiophene dimer and it has been established that the broad background in the R2PI spectrum originates from unresolved low frequency intermolecular vibrations as well as very short lifetime of a single isomer of the dimer. Comparison between experimental and theoretical IR spectra confirms that the observed indole…furan and indole…thiophene dimers have a tilted T-shaped N-H···π hydrogen bonded structure.

In the case of both indole…furan and indole…thiophene dimers, there is a possibility of conventional hydrogen bonded structures with N-H…O and N-H…S interactions. But exclusively N-H…π bound structure has been observed in the case of both the dimers. Thus present study demonstrates that π-hydrogen bonding can win over conventional hydrogen bonding interaction. The results obtained in this work manifest the effect of heteroatoms present in the acceptors on the strength of the π-hydrogen bonding interactions. It has been found that N-H…π bound structure is not formed between indole and pyridine but the similar structure is observed for indole…furan and indole…thiophene dimers. It was concluded by Sherrill and co-workers from their theoretical study of benzene...pyridine dimer that aromatic rings containing heteroatoms are poorest π-hydrogen bond acceptors [Hohenstein, E. G. *et al.* J. Phys. Chem. A. **113**, 878 (2009)]. But the current spectroscopic investigation exhibits that

five membered aromatic heterocycles in contrast to pyridine, a six membered heterocycle, are favorable π-hydrogen bond acceptors. Unlike the six membered aromatic heterocycles (pyridine), the lone pair electrons on the heteroatom in five membered aromatic heterocycles (furan, thiophene) participate in aromaticity leading to increased π-electron density in the ring and weak hydrogen bonding interaction through the heteroatom. In this study, it has also been shown that thiophene is a better π-hydrogen bond acceptor than furan as the red-shift in the N-H stretch frequency in the NH…π bound indole…thiophene dimer (56 cm^{-1}) is more than that in the corresponding indole…furan dimer. The present work has immense biological significance as furan and thiophene derivatives have potential therapeutic applications and indole is the chromophore of tryptophan residue in proteins. Thus understanding the binding motif between indole and other hereocycles studied in this work may help in designing efficient drugs.

5. Hexafluorobenzene: A unique building block for π-stacking interaction

5.1 Introduction

In the last chapter, we have discussed the competition between conventional hydrogen bonding and π-hydrogen bonding interaction by studying the complexes of indole…furan and indole…thiophene dimers and shown that non-conventional hydrogen bonding can win over conventional hydrogen bonding depending on the chosen system. Further we have also demonstrated that five membered aromatic heterocycles in contrast to pyridine, a six membered heterocycle, are favourable π-hydrogen bond acceptors.

In the current chapter, we have reported the study of the formation of π-stacked structure of indole...HFB dimer. The gas phase experimental study of the π-stacking interaction is very much limited in the literature.[249,256,303,400,430] This is mostly due to the fact that it is quite difficult to synthesize the π-stacked dimer in the gas phase when other competitive non-covalent interactions are present in the molecular systems. In the current study, we have suppressed the possibility of the formation of π-hydrogen bonded conformer and achieved π-stacked configuration by taking the perfluorinated benzene i.e., HFB as a complexing partner with indole.

We found that the study of the π-stacked indole...HFB dimers containing HFB is particularly interesting because HFB has unique properties in efficient structural control in crystal engineering, medicinal chemistry and biological recognition.[321-322] It has been reported that benzene-HFB is a better building block than benzene-benzene for π-stacking in supramolecular assembly because electrostatic interaction is favourable in the former unlike the latter one, which is already discussed in section 1.8.3.3.[321] Phenyl-perfluorophenyl stacking motif is indeed widely used as a supramolecular synthon in crystal engineering leading to infinite columnar structures with less parallel displacement between phenyl and perfluorophenyl units.[321,324-327] Very recently, Zheng et al. have found that strong face to face stacking interaction between phenyl and perfluorophenyl groups in a designed homodimeric protein α_2D plays a significant role to direct selective protein-protein interactions.[431] Extremely high binding affinity between metalloproteinase stromelysin enzyme and its inhibitor 1,3,4-thiadiazole-2-thione has been reported due to the strong stacking interaction

between phenolic and pentafluorophenyl moieties of the enzyme and inhibitor, respectively.[432] Despite the enormous significance of the π-stacked assembly in many areas starting from materials to biology, experimental study of the molecular complexes containing HFB at the dimeric level for quantitative understanding of the stability as well as strength of the interaction is very much limited.

In this chapter, we have reported a π-stacked heterodimer of indole and HFB in the gas phase by using R2PI and IR-UV double resonance spectroscopy combined with quantum chemistry calculation. The another motivation behind the present study is already discussed in the section 1.8.3.3 that π-stacking interaction which is ubiquitous between aromatic residues (tryptophan and phenylalanine) in proteins has not been observed earlier in the gas phase experiment by studying indole...benzene dimer because the N-H...π hydrogen bonded configuration is always the preferred one. On the other hand, the indole...HFB complex studied here shows exclusively π-stacked structure by inhibiting the formation of the N-H...π hydrogen bonded T-shaped structure. Interestingly, the chosen molecular systems not only eliminate the possibility of formation of N-H...π bound T-shaped dimer but also enable the determination of the structure by probing the N-H group. This kind of π-hydrogen bond inhibition by fluorine substitution of the phenyl ring has also been reported in HFB...H_2O complex, where a new non-covalent interaction namely $n \rightarrow \pi^*$ is switched on.[433-435] The current work mainly focuses on the molecular level understanding on the nature and strength of the π-stacking interaction between indole and HFB. This knowledge, in particular, can help in designing the synthetic proteins having specific aromatic-aromatic interaction between tryptophan and phenylalanine residues.

5.2 Results and discussion

5.2.1. Electronic spectra

The electronic spectra of the indole monomer and indole...HFB dimer measured by 1C-R2PI spectroscopy have been shown in Figures 5.1a and 5.1b, respectively. To synthesize indole...HFB dimer, mixed vapor of indole and HFB seeded in argon carrier gas (about 4 bar)

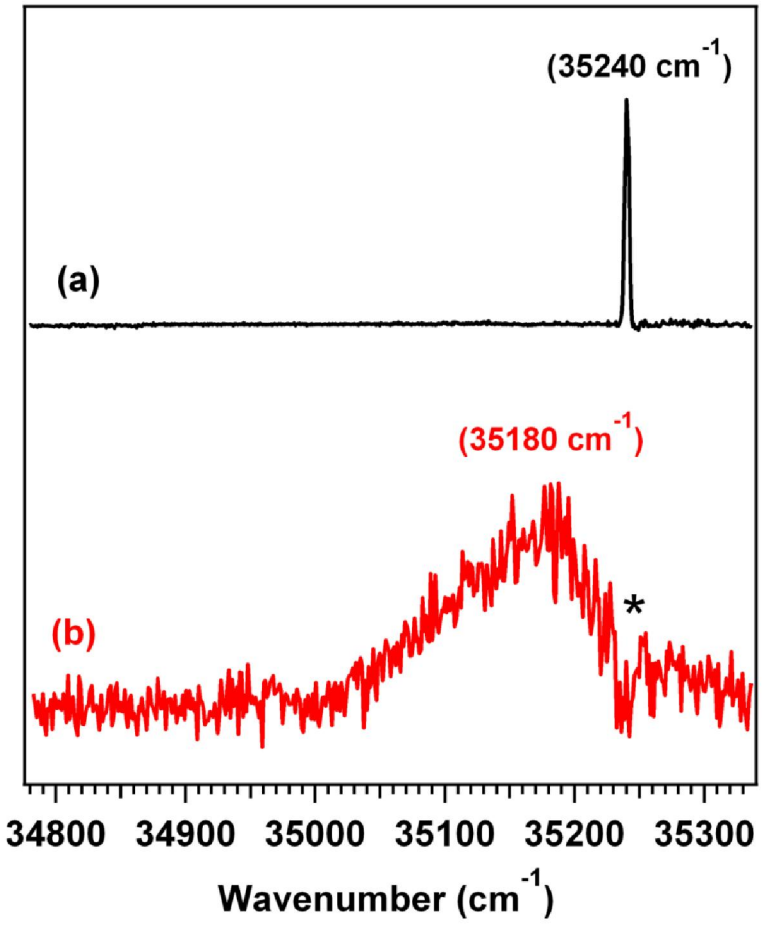

Figure 5.1. Electronic spectra measured at (a) indole and (b) indole...HFB dimer mass channels by using 1C-R2PI. The asterisk (*) in the electronic spectrum of indole...HFB (Figure 5.1b) indicates a dip in the ion signal as the laser beam is blocked at the origin transition of indole at 35240 cm^{-1}.

was expanded into vacuum through the pulsed nozzle. The pulsed valve and a sample holder containing indole was heated at about 80°C while HFB was taken in a separate sample container maintained at -30°C by putting in a bath containing a mixture of dry ice and

aqueous solution of $CaCl_2$. The R2PI spectrum of the indole...HFB dimer has been recorded by electronic excitation of the indole moiety. Figure 5.1a shows the origin band for the $S_1 \leftarrow S_0$ electronic transition of the indole monomer, at 35240 cm^{-1}, which matches well with the previous reports.[212,394,398,436-438] The electronic spectrum of the indole...HFB dimer is very broad (FWHM ~ 300 cm^{-1}) and structureless. The peak position of the broad electronic spectrum of the dimer is red-shifted by about 60 cm^{-1} from the origin band of the indole monomer. Similarly broad electronic spectrum has been observed in the case of many other aromatic dimers studied in the supersonic jet.[246,248-249,303,311,426,439-440]

Generally, the broadening in the electronic spectrum of the dimer in the jet-cooled studies may be due to the presence of multiple isomers or very short lifetime of the dimer in the S_1 state or unresolved low frequency intermolecular vibrations of a single isomer. It has also been observed that the π-stacked dimers very often exhibit broad feature in the electronic spectrum.[248-249,303,409] In the case of the 2-pyridone...n-fluorobenzene complexes, double hydrogen-bonded structure has been observed for n=1-5 and only the 2-pyridone...HFB complex shows π-stacked structure.[409,440] It is reported that the width of the bands (about 60 cm^{-1}) in the electronic spectrum of the π-stacked 2-pyridone...HFB dimer is about 40 times than that of the double hydrogen bonded complexes of 2-pyridone with other fluorobenzenes.[409,440] Incidentally, the electronic spectrum of the π-stacked 2-pyridone...HFB dimer is not completely structureless and the broadening in the electronic spectrum is explained mostly due to the low frequency intermolecular co-planar twisting vibration in the dimer.[409] On the other hand, extremely broad (FWHM > 200 cm^{-1}) and structureless electronic spectra have been reported for the π-stacked structures of the phenylacetylene...pyridine, $(phenylacetylene)_2$, and $(3,7\text{-dimethylxanthine})_2$ complexes.[248-249,303] Such a large broadening in the electronic spectra of these π-stacked complexes has been explained in terms of very short lifetime in the S_1 state due to rapid deactivation and the presence of similar isomeric structures.[248-249,303] In the case of the indole...HFB complex reported here, the broadening (FWHM ~ 300 cm^{-1}) in the electronic spectrum could be due to similar reasons.

To determine whether the origin of the broad electronic spectrum of the dimer studied here is due to the presence of more than one isomeric structure, multiple IR spectra have been

measured by probing various positions of the broad R2PI spectrum of the dimer. For this purpose, conformational landscape of the dimer has also been explored in detail through theoretical calculation. Both of these have been discussed later. In the case of a broad R2PI spectrum, generally multiple IR spectra are measured by fixing the UV laser wavelength at different positions of the R2PI spectrum.[248,311,439]

5.2.2. IR spectra

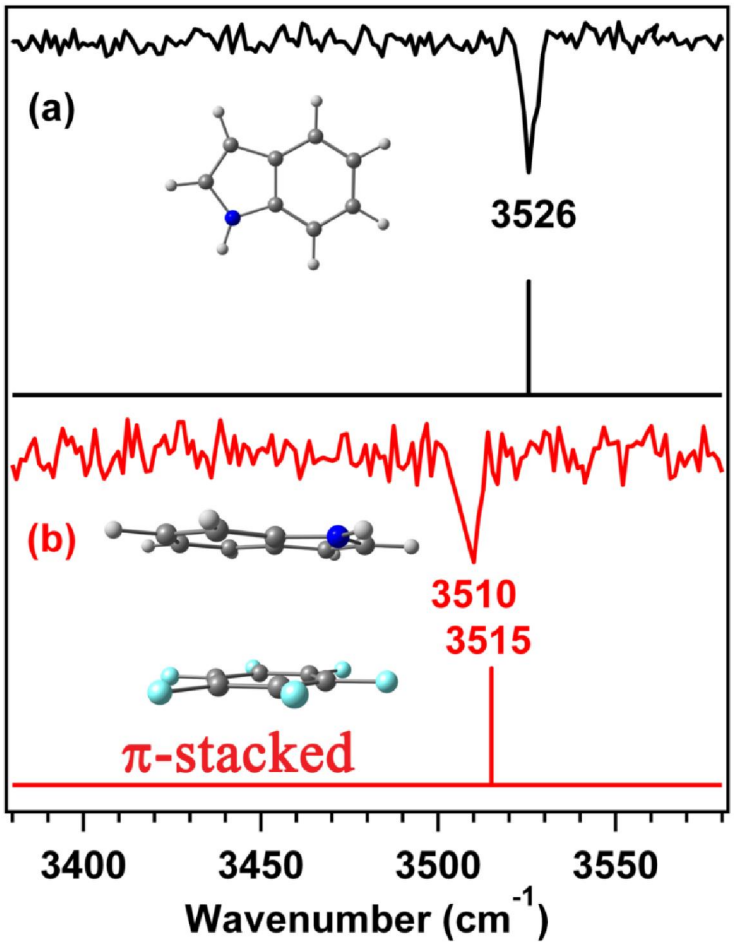

Figure 5.2. The experimental IR spectra in the NH stretching region by probing (a) origin band of indole and (b) band maximum (35180 cm^{-1}) of the broad R2PI spectrum of the indole...HFB dimer. The theoretical IR stick spectra of the indole monomer and π-stacked structure (S3) of the indole...HFB dimer calculated at the M05-2X/cc-pVQZ level of theory are provided with Figure 5.2a and 5.2b, respectively. A scaling factor used to correct the theoretical IR spectra has been discussed in the text.

To determine the structure of the dimer, we have measured IR spectra in the N-H stretching region by fixing the UV laser wavelength at various positions of the broad background of the R2PI spectrum. IR spectrum depicted in Figure 5.2a shows free N-H stretch of the indole monomer at 3526 cm^{-1}, which agrees very well with the previous report.[425] Figure 5.2b shows IR spectrum of the indole...HFB dimer by probing the band maximum at 35180 cm^{-1} of the R2PI spectrum. It is observed that the red-shift in the N-H stretching frequency of the indole...HFB dimer with respect to that in the indole monomer is only 15 cm^{-1}. Theoretical IR spectra of the indole monomer and the most stable structure of the indole...HFB dimer calculated at the M05-2X/cc-pVQZ level of theory have been provided with Figure 5.2a and 5.2b, respectively. Calculated harmonic frequency of the dimer has been scaled with a factor of 0.94325 obtained from the ratio of the experimental and theoretical N-H stretching frequency of the indole monomer.

Table 5.1. N-H stretching frequencies of the indole…HFB dimer calculated using various basis sets at the M05-2X level of theory. All the frequencies are scaled using a factor obtained from the ratio of experimental to calculated N-H stretching frequency (Harmonic) of indole. Experimental N-H stretching frequency of indole is 3526 cm^{-1}.

Methods	Indole…HFB dimer (π-stacked)
	$\nu_{N\text{-}H}$ (cm^{-1})
Expt	3510
M05-2X/cc-pVTZ	3516
M05-2X/cc-pVQZ	3515
M05-2X/aVDZ	3516
M05-2X/aVTZ	3514

Excellent agreement between experimental and theoretical IR spectra of the dimer depicted in Figure 5.2b confirms the presence of the π-stacked structure of the indole...HFB dimer in the experiment. The calculated intensity of the N-H stretching frequency in the complexes also indicates whether the N-H group is free or involved in hydrogen bonding interaction. The

intensity of the N-H stretching frequency calculated at the M05-2X/cc-pVQZ level in the indole monomer and indole...HFB dimer is 86 and 89 km/mol, respectively. Similar intensity of the N-H stretching fundamental transition in both indole monomer and indole...HFB dimer clearly indicates that the N-H group in the dimer is free like that in the monomer. The calculated N-H stretching frequency of the π-stacked indole...HFB dimer using many other different basis sets at the M05-2X level has been provided in the Table 5.1. It is quite intriguing to note that the values for the N-H stretching frequency obtained with different basis sets at the M05-2X level deviate within ± 2 cm^{-1}.

It is worth to discuss about the observed small red-shift (15 cm^{-1}) in the N-H stretching frequency of the indole...HFB dimer. As the π-electron cloud in the HFB ring is highly electron deficient due to the presence of six fluorine groups (electron withdrawing), π-hydrogen bonding through the N-H group of the indole unit is highly unfavoured. In contrast, only the N-H...π hydrogen bonded structure has been found experimentally in the case of the indole...benzene dimer and the observed red-shift in the N-H stretching frequency is 46 cm^{-1}.[290] It has also been reported from the theoretical calculation that the N-H stretching frequency of the π-stacked indole...benzene dimer and indole monomer appears almost at the same position.[290] In the observed π-stacked indole...HFB dimer reported here, very small red-shift (15 cm^{-1}) in the N-H stretching frequency arises due to weak electrostatic interaction between the N-H and C-F groups of indole and HFB, respectively. It can be mentioned here that Leutwyler and co-workers have reported 28 cm^{-1} red-shift in the N-H stretching frequency of the π-stacked 2-pyridone...HFB dimer.[440] Callahan et al. have observed a red-shift of 8 cm^{-1} in the N-H stretching frequency of the π-stacked structure of 3,7-dimethylxanthine homodimer.[248]

To find out whether the broad background observed in the electronic spectrum of the indole...HFB dimer reported here is due to a single isomer or multiple isomers, IR spectra have been measured by probing various positions (35069 cm^{-1}, 35112 cm^{-1}, 35125 cm^{-1}, 35137 cm^{-1}, 35168 cm^{-1}, 35199 cm^{-1}, and 35211 cm^{-1}) of the broad background in the R2PI spectrum and these have been provided in Figure 5.3. Identical IR spectra within the limit of the resolution (~ 2.5 cm^{-1}) of the IR OPO have been obtained for all the probed positions in the electronic spectrum of the indole...HFB dimer. Thus the presence of only a single isomer of the dimer in the experiment has been confirmed. Consequently, it has been concluded that

the broadening in the R2PI spectrum of the dimer is originated mostly due to the very fast deactivation of the S_1 state leading to a significant decrease in the excited state life time as well as unresolved low frequency intermolecular vibrations of a single isomer the dimer

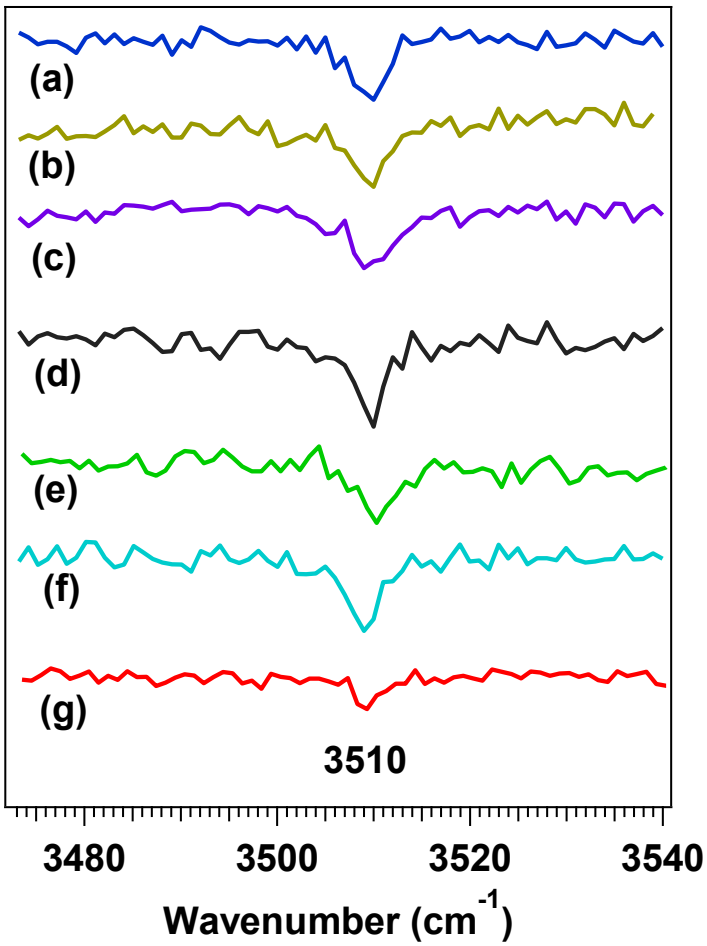

Figure 5.3. RIDIR Spectra in the NH stretching region by probing (a) 35069 cm^{-1}, (b) 35112 cm^{-1}, (c) 35125 cm^{-1}, (d) 35137 cm^{-1}, (e) 35168 cm^{-1}, (f) 35199 cm^{-1}, and (g) 35211 cm^{-1} positions of the broad background of the R2PI spectrum of the indole...HFB dimer.

5.2.3. Structure of the dimer

Various probable initial structures of the indole...HFB dimer have been explored for geometry optimization at the M05-2X/cc-pVTZ level of theory. Figure 5.4 shows different initial structures of the dimer considered for geometry optimization. Three different π-stacked structures of the indole...HFB dimer can be considered and these are named as S1, S2, and S3

where the HFB is stacked over the phenyl, pyrrole, and the middle of the phenyl and pyrrole

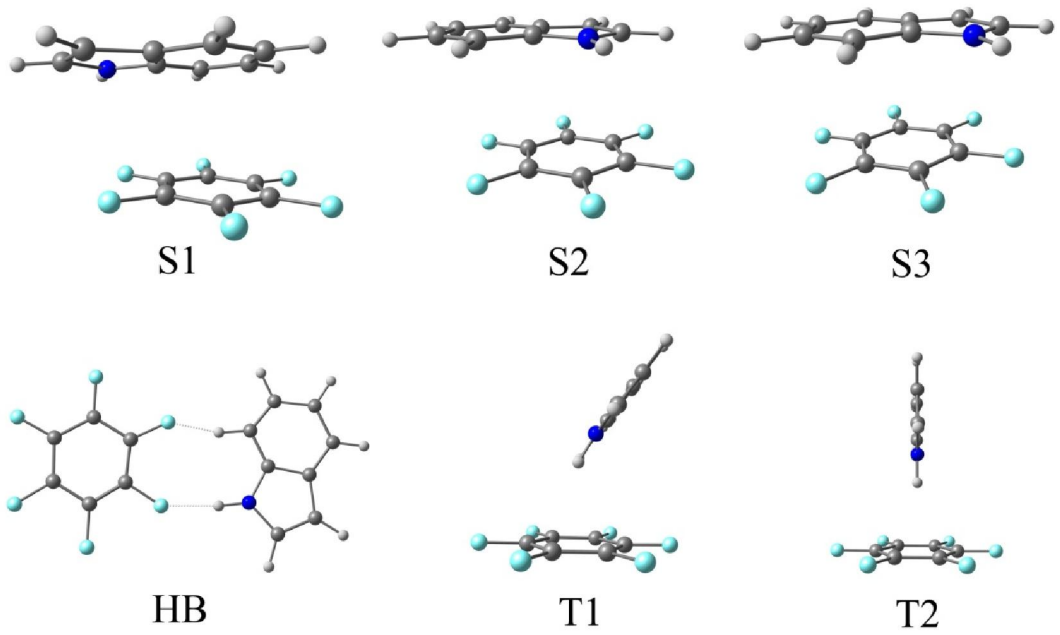

Figure 5.4. Initial structures of the indole...HFB dimer considered for geometry optimization

rings, respectively. Hydrogen bonded (HB) structure of the indole...HFB dimer has a planar geometry with N-H...F and C-H...F hydrogen bonds. Fluorine is actually known as a worst hydrogen bond acceptor.[233,441] Both T1 and T2 structures of this dimer are composed of N-H...π hydrogen bond but the former one is tilted T-shaped while the latter one is perfectly T-shaped. Figure 5.5a shows the six probable initial structures as well as final structures of the indole…HFB dimer after geometry optimization at the M05-2X/cc-pVTZ level of theory. It has been found that all the structures of the indole...HFB dimer except the perfect T-shaped (T2) one are converged to the S3 (π-stacked) structure after geometry optimization at the M05-2X/cc-pVTZ level of theory. The T2 structure has one imaginary frequency and it is not also a stable structure. It is interesting to note that selectively only one structure of the indole...HFB dimer, which is theoretically stable, is observed in the experiment.

Figure 5.5b shows both the side and top views of the only stable structure of the indole...HFB (S3) dimer obtained at the M05-2X/cc-pVQZ level of optimization. It is indeed worth to compare the observed π-stacked structure of the indole...HFB dimer with that of the

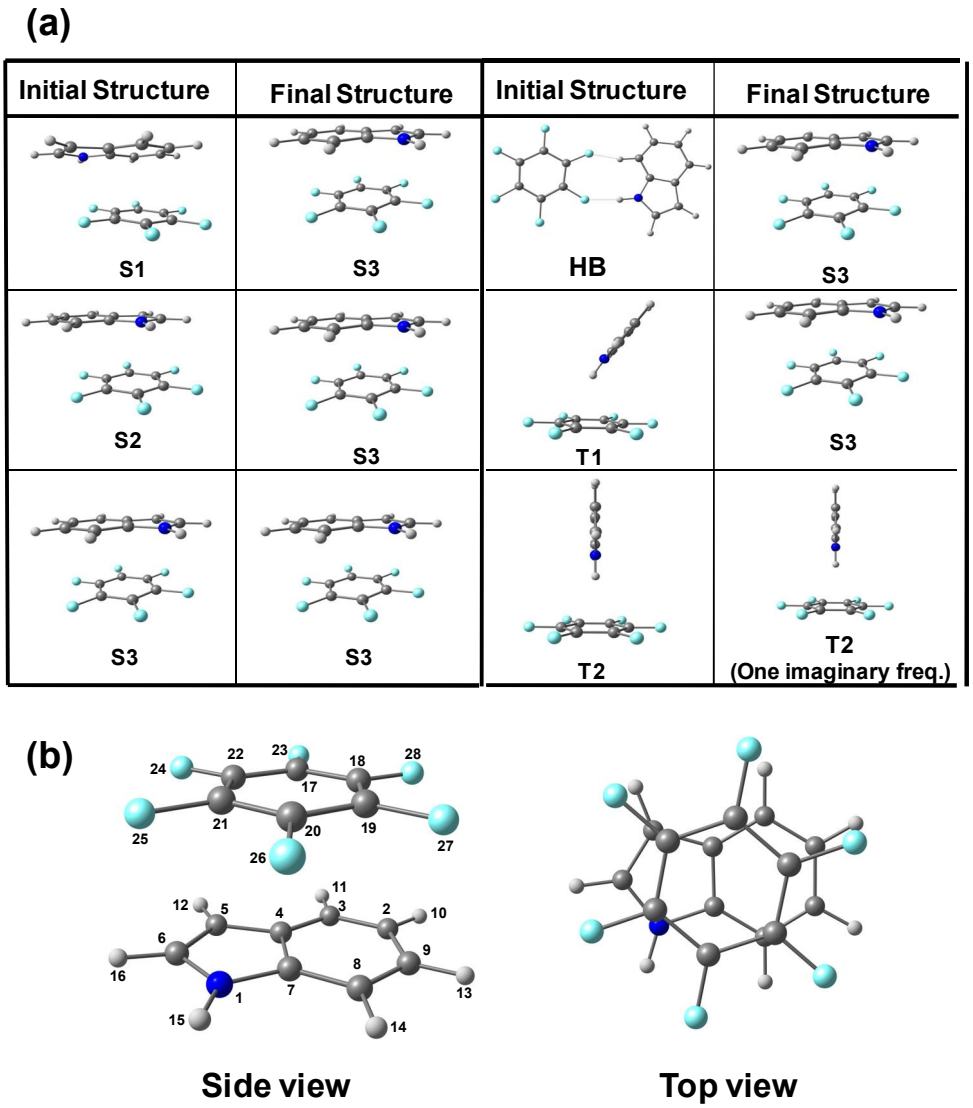

Figure 5.5. (a) Probable initial and final structures of indole…HFB dimer optimized at the M05-2X/cc-pVTZ level of theory and (b) The stable structure of the indole...HFB dimer optimized at the M05-2X/cc-pVQZ level of theory. Both side and top views of the structure are shown in the figure.

indole...benzene dimer reported from the theoretical calculations by Sherrill and co-workers.[289] To describe the π-stacked structure of the indole...benzene dimer, they have defined the parallel displacement of the benzene moiety along the major and minor axes of the indole ring as R_2 and R_3, respectively, in addition to the vertical displacement (R_1). They have considered both the R_2 and R_3 values equal to zero for the configuration where the center of the benzene ring is positioning over the center of the shared bond of the indole moiety. From the three dimensional (3D) potential energy surface scan (simultaneously varying R_2 and R_3 keeping R_1 fixed) at the SCS-MP2/aVDZ level of theory, it has been

reported that the minimum energy π-stacked structure of the indole...benzene dimer has R_2 and R_3 values of +1.3 and -1.8 Å, respectively, while R_1 value is 3.4 Å.[289]

We have followed the same structural definition for the π-stacked indole...HFB dimer, which has been introduced for the π-stacked indole...benzene dimer by Sherrill and co-workers.[289] Figure 5.6a displays the structural definition showing the three important intermolecular distances (R_1, R_2, and R_3) in the π-stacked indole...HFB dimer obtained at the M05-2X/cc-pVQZ level of theory. The interplanar distance (R_1) in the dimer is 3.26 Å while both R_2 and R_3 values (horizontal displacements of the HFB unit) are zero with respect

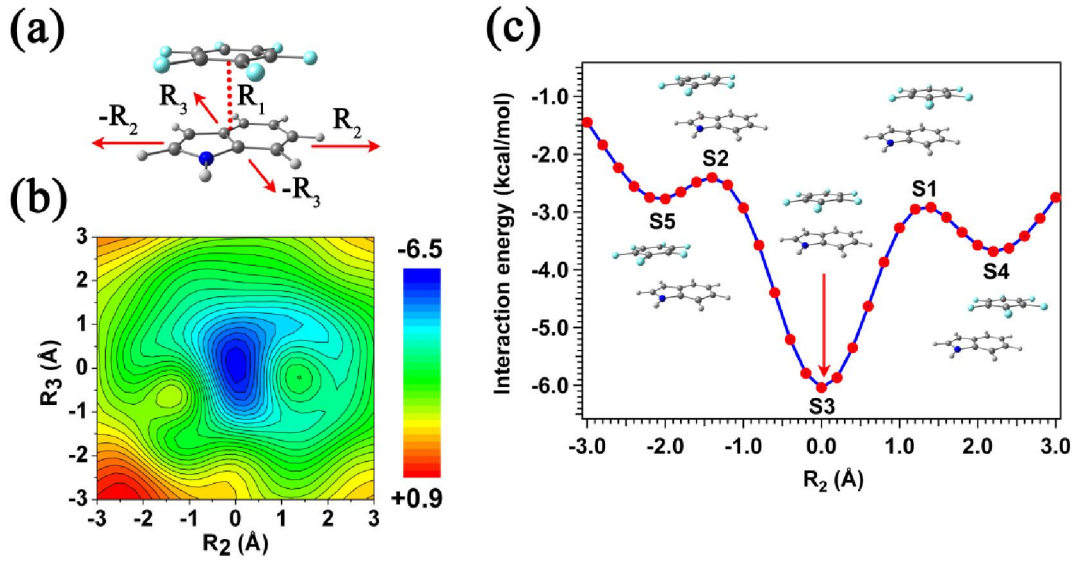

Figure 5.6. (a) Structural definition of the π-stacked structure (S3) of the indole...HFB dimer. R_1 is the interplanar distance between the two monomer units, R_2 and R_3 are defined as the horizontal displacements of the HFB unit of the dimer along the major and minor axes of the indole moiety, respectively. (b) A contour plot showing the 2D projection of the PES obtained from the calculation of the interaction energy of the π-stacked configuration of the dimer for simultaneous variation of R_2 and R_3 at a step size of 0.2 Å while keeping R_1 fixed. $R_2 = R_3 = 0$ has been defined for the configuration where the center of the HFB moiety is perfectly aligned with the center of the shared bond of the indole ring. (c) A slice of the PES along $R_3 = 0$.

to the configuration where the center of the HFB moiety is perfectly aligned with the center of the shared bond of the indole ring. Thus it is revealed that the π-stacked structure of the indole...HFB dimer is much more ordered than that of the indole...benzene dimer as the HFB ring in the former one is just sitting in the middle of the indole ring. A few more selected geometrical parameters of the observed π-stacked structure of the indole...HFB dimer have been provided in Table 5.2. It is obvious from the values of Δr_{N-H} (the lengthening of the N-H bond) and dihedral angle $C_8C_7N_1H_{15}$ defining the planarity of the N-H group of indole that the N-H group in the π-stacked dimer is hardly perturbed with respect to that in the indole monomer. The dihedral angle $C_{17}C_{20}C_7C_4$ defining the angle between the two planes of the monomers in the dimer has been found to be 10° and this indicates that the two monomeric units are quite parallel to each other.

Table 5.2. A few selected geometrical parameters of π-stacked structure of indole…HFB dimer calculated at the M05-2X/cc-pVQZ level of theory.

	Indole…HFB dimer (π-stacked)
d_{N-H} (Å)	1.000
Δr_{N-H} (Å)	0.001
Interplanar distance (Å)	3.26
$\angle C_8C_7N_1H_{15}$	-0.3°
$\angle C_{17}C_{20}C_7C_4$	-10°

[a]For atom numbering of the dimer, see Figure 5.5b. d_{N-H} (Å) (Indole monomer) = 0.99891

To find out the presence of any other stable π-stacked configuration of the indole...HFB dimer apart from the S3 one shown in Figure 5.6b, we have performed 3D potential energy surface (PES) scan by varying R_2 and R_3 simultaneously with a step size of 0.2 Å while keeping R_1 fixed at 3.26 Å. Figure 5.6b presents the 2D projection of the PES of the dimer calculated at the M05-2X/cc-pVDZ level of theory. Different color codes in the figure represent different magnitude of the interaction energy in the dimer i.e. red and blue signifies maximum positive (+0.9 kcal/mol) and maximum negative (-6.5 kcal/mol) values,

respectively. A slice of the PES along $R_3 = 0$ has also been provided in Figure 5.6c which shows a potential energy curve for the variation of R_2. It is obvious from both Figure 5.6b and 5.6c that the S3 structure of the dimer, with both R_2 and R_3 equal to zero, already shown in Figure 5.4b is the most stable. Apart from the global minimum for the S3 structure, there are two higher energy shallow minima (S4 and S5) and two maxima (S1 and S2). In the S1 and S2 structures, the HFB unit is almost sandwiched with the phenyl and pyrrole moieties of the indole ring, respectively and these two structures have already been shown in Figure 5.4. On the other hand, the HFB unit is parallel-displaced with respect to only the phenyl group of indole by 1.09 Å in the case of the S4 structure while the S5 structure shows parallel displacement of the HFB unit with respect to only the pyrrole unit of indole by 0.96 Å. Similar type of sandwich and parallel-displaced (PD) π-stacked structures has been reported for benzene...benzene and benzene...HFB dimers.[323] The PD structure is always more stable than the sandwich one due to the favourable electrostatic interaction in the former one. It is interesting to note here that the parallel displacement reported in the benzene...HFB dimer is 1.0 Å, which is close to that obtained in the case of the S4 structure of the indole...HFB dimer (1.09 Å).[323]

Under the constraint of the R_1 (interplanar distance), the S4 and S5 structures appear to be minima although both of these converge to the S3 structure after geometry optimization. Even if these two could be found as stable structures at very high level of calculation, the barrier to interconversion from the S4 and S5 to the S3 (global minimum) through S1 and S2, respectively, is extremely low (less than 250 cm^{-1}). Thus there is a strong possibility of conformational relaxation of these two high energy isomers into the global minimum during the cooling process in the supersonic expansion. Ruoff *et al*. have reported that conformation relaxation does not occur in presence of any of the carrier gases (He, Ne, Ar, and Kr) used in the expansion if the interconversion barrier is greater than about 350 cm^{-1}.[442] So it can be argued that only the S3 structure of the dimer has been found in our experiment and the observed R2PI spectrum is due to the electronic transition of only this single configuration of the π-stacked dimer.

BSSE as well as zero point energy (ZPE) corrected binding energy of the π-stacked structure (S3) of the indole...HFB dimer calculated at the M05-2X level of theory with various basis sets has been provided in Table 5.3. The result shows that the basis set effect on the binding

energy (D_0) of the dimer (~ -6.5 kcal/mol) obtained at the M05-2X level is minimal. It is worth to compare the binding energy (D_0) value of the π-stacked indole...HFB dimer with that of the indole...benzene dimer available in the literature.[289-290] Reported D_0 values for the parallel-displaced π-stacked indole...benzene dimer calculated at the est. CCSD(T)/CBS and RI-B97-D-CP/TZVPP levels of theory are -4.64 and -3.52 kcal/mol, respectively.[289-290] Although here the comparison of the binding energy between the two similar dimers is done at different levels of theory, the M05-2X level calculation using high quality basis sets (cc-pVQZ, aVTZ) can provide reliable results.

Table 5.3. Binding energies (kcal/mol) of the π-stacked structure (S3) of the indole...HFB dimer calculated at the M05-2X level of theory using various basis sets.

Methods	Indole…HFB dimer (π-stacked)	
	ΔE_e[a]	ΔE_0[b]
M05-2X/cc-pVTZ	-7.08	-6.56
M05-2X/cc-pVQZ	-7.18	-6.59
M05-2X/ aVDZ	-7.42	-6.84
M05-2X/ aVTZ	-7.28	-6.58

[a]ΔE_e: BSSE corrected binding energy. [b]ΔE_0: BSSE + ZPE corrected binding energy.

Sponer *et al.* have indeed shown that the binding energy values of the π-stacked complexes of the nucleic acid bases calculated at the DFT/M05-2X level is more accurate than those calculated at the MP2/CBS level.[405] Thus it is obvious form the comparison here that the indole...HFB dimer is more stable than the indole...benzene dimer. Similarly, binding energy of the π-stacked benzene...HFB dimer (-5.38 kcal/mol) with parallel displacement of 1.0 Å is much higher than that of the benzene dimer (-2.48 kcal/mol) with parallel displacement of 1.6 Å as reported by Tsuzuki et al. from the est. CCSD/CBS level of calculation.[323]

5.2.4. EDA.

It is interesting to look at the different components of the total interaction energy of the dimer calculated by LMO-EDA method at the M05-2X/cc-pVDZ level of theory provided in Table 5.4. The result shows that the ratio of the electrostatic to dispersion component is about 1:2 in the π-stacked (S3) indole...HFB dimer. Thus the electrostatic component of the total interaction energy has a significant contribution in the stabilization of this π-stacked dimer. On the other hand, in the case of the π-stacked indole...benzene dimer presented in the table, the dispersion contribution to the total interaction energy is about five times larger than the electrostatic contribution. There is a literature report on the decomposition of the total interaction energy of the parallel-displaced π-stacked indole...benzene dimer using SAPT method by Sherrill and co-workers.[289] They have found that the ratios of the electrostatic to dispersion contribution for the MP2 PD and SCS-MP2 PD configurations of the indole...benzene dimer are about 1:3.5 and 1:2.5, respectively.[289] Thus the relatively enhanced electrostatic component of the total interaction energy in the case of the π-stacked configuration of the indole...HFB dimer compared to that of the indole...benzene is due to the presence of reverse quadrupole in the HFB with respect to the benzene.

Table 5.4. Decomposition of the interaction energy (kcal/mol) in the π-stacked structure of the indole...HFB (S3) and indole…benzene dimers calculated at the M05-2X/cc-pVDZ level of theory.

	ΔE_{ele}	ΔE_{ex}	ΔE_{rep}	ΔE_{pol}	ΔE_{disp}	ΔE_{tot}
Indole…HFB	-9.66	-8.73	33.77	-1.78	-20.53	-6.92
Indole...benzene	-2.42	-3.95	17.37	-1.45	-12.18	-2.63

5.3. Conclusions

In summary, we have observed exclusively π-stacked heterodimer of indole and hexafluorobenzene by using R2PI and IR-UV double resonance spectroscopy in combination with quantum chemistry calculations. The electronic spectrum of the dimer is extremely broad and structureless. It has been confirmed by measuring several IR spectra by probing many different background positions of the broad electronic spectrum as well as computing the 3D PES of the π-stacked dimer that the broad feature originates due to the shortening of the life time in the S_1 state as well as unresolved low frequency intermolecular vibrations of a single isomer of the dimer. There is an excellent agreement between the experimental and theoretical IR spectra of the dimer in the N-H stretching region. The observed π-stacked dimer has a unique configuration where the center of the HFB unit is aligned with the center of the shared bond of the indole moiety. This π-stacking interaction which is ubiquitous between aromatic residues (tryptophan and phenylalanine) in proteins has not been observed earlier in the gas phase experiment by studying indole...benzene dimer because the N-H...π hydrogen bonded configuration is always the preferred one. We have shown here that it is possible to observe this stacking interaction in the gas phase as well as probe the N-H group using IR spectroscopy by prohibiting the dominant N-H...π hydrogen bonding interaction through making the π-hydrogen bond acceptor highly electron deficient. It is quite interesting to note that the observed π-stacked structure of the indole...HFB dimer is much more ordered than that of the indole...benzene dimer reported from the theoretical calculation. The current knowledge on this specific aromatic complex can be helpful in designing unnatural proteins having strong π-stacking interaction between tryptophan and phenylalanine residues. The present result also demonstrates that hexafluorobenzene is a very efficient building block for π-stacking interaction. Thus, hexafluorobenzene in place of benzene can be used as a better supramolecular synthon for the growth of infinite columnar structure in crystal engineering.

6. Aromatic-aromatic interactions in the aromatic side chains of proteins: Indole…imidazole dimer and Indole…(pyrrole)$_2$ trimer

6.1. Introduction

In chapters 3, we have reported the interplay between conventional hydrogen bonding and dispersion interaction. Competition between conventional hydrogen bonding and π-hydrogen bonding interaction has been discussed in chapter 4. In the last chapter, we have described our study on the selective formation of a unique π-stacked complex. In this case, possibility of the formation of the complex through another non-covalent interaction i.e. π-hydrogen bonding interaction has been suppressed by perfluorination of the benzene ring. In brief, we have studied the interplay or competition between all major types of non-covalent interactions.

In this chapter, we have described our study on the aromatic-aromatic interactions (dimeric and trimeric) present in the aromatic side chains of proteins. The importance of this interaction is already discussed in detail in section 1.8.3.4. More specifically, we have reported here a gas phase spectroscopic study of indole···imidazole dimer and indole…(pyrrole)$_2$ trimer using R2PI, UV-UV, and IR-UV double resonance spectroscopic techniques as well as quantum chemistry calculations. The indole…imidazole dimer delineates the aromatic interaction between tryptophan and histidine residues in the side chains of proteins while indole…(pyrrole)$_2$ trimer mimics the trimeric interactions present among the aromatic side chains of proteins.

In the study of indole…imidazole dimer, we have observed a V-shaped structure stabilized by N-H···N hydrogen bonding, C-H···π, and weak π-stacking interaction. Interestingly, the observed dimer falls in the category of the "*special class of mixed complex*" like indole···pyridine dimer we have reported in chapter 3.[320,349] This class of complexes is stabilized by an interplay between conventional hydrogen bonding and dispersion interaction.[320] The motivation behind the study of this class of complexes has already been discussed in section 1.8.1. In brief, the spectroscopic studies of this type of complexes may give unique information on the basic structures of the building blocks of the biomolecules and materials. For example, the observed V-shaped structure of the indole…imidazole

resembles the aromatic interactions present between tryptophan and histidine residues in the non-fluorescent flavoprotein (PDB ID: 1nfp)[443-444] present in photobacterium leiognathi and barnase (PDB ID: 1brn),[445] a bacterial protein from Bacillus amyloliquefaciens, respectively. Furthermore, the study of this dimer has immense therapeutic significance as imidazole derivatives have a broad range of pharmacological activities.

The most significant finding of the study of the structure of indole···$(pyrrole)_2$ trimer is the direct experimental evidence of the observation of a cyclic asymmetric structure of a heterotrimer of aza-aromatic molecules stabilized by three N-H···π hydrogen-bonding interactions. The major motivation of studying this heterotrimer apart from understanding aromatic trimeric interactions in proteins is the following. It has been observed that π-hydrogen bonding interaction is generally the backbone of the structures of the aromatic trimers observed in the proteins. Steiner and co-workers have reviewed π-hydrogen bonding in proteins based on 593 high resolution crystal structures of proteins in the PDB.[21] From these data analysis, they have found that tryptophan is the most effective π-hydrogen bond acceptor among all the amino acid residues in proteins. It has also been observed that the efficiency of tryptophan as a π-acceptor is maximum with an N-H donor compared to the O-H or S-H donors. Regardless of the major abundance of indole as a π-hydrogen acceptor in the structures of proteins, gas phase studies for the quantitative determination of the π-hydrogen accepting strength of indole is scarce in the literature except the recent studies on the $(indole)_2$···pyridine trimer and indole···H_2S complex.[315,320] Thus we have specifically studied the indole···$(pyrrole)_2$ trimer, where indole acts as π-hydrogen bond donor as well as acceptor. The present spectroscopic study of the complex between indole and pyrrole also models protein-protein interactions as both indole and pyrrole are subunits of the amino acid tryptophan. In addition, the investigation of the structure of the heterotrimer in this study is quite interesting because most of the aromatic trimers reported in the literature are homoclusters having the same monomer units. The study of the complex of pyrrole is also very important as it is present in the building block of heme, chlorophyll, and vitamin B_{12}.

6.2. Results and discussion

6.2.1. Indole...imidazole heterodimer.

6.2.1.1. Experimental results

6.2.1.1.1. 1C-R2PI spectra.

Figure 6.1b shows 1C-R2PI spectrum measured at the indole···imidazole dimer mass channel at 185 amu by electronic excitation of the indole moiety. To synthesize the mixed dimer, both the pulsed valve and sample holder containing imidazole were heated at about 110 ^{0}C while the sample holder containing indole kept behind the imidazole chamber was separately heated at about 85°C. 1C-R2PI spectrum of the indole monomer depicted in Figure 6.1a shows the origin band of the monomer at 35240 cm^{-1} for the $S_1 \leftarrow S_0$ electronic excitation and this corroborates with the previous report.[394]

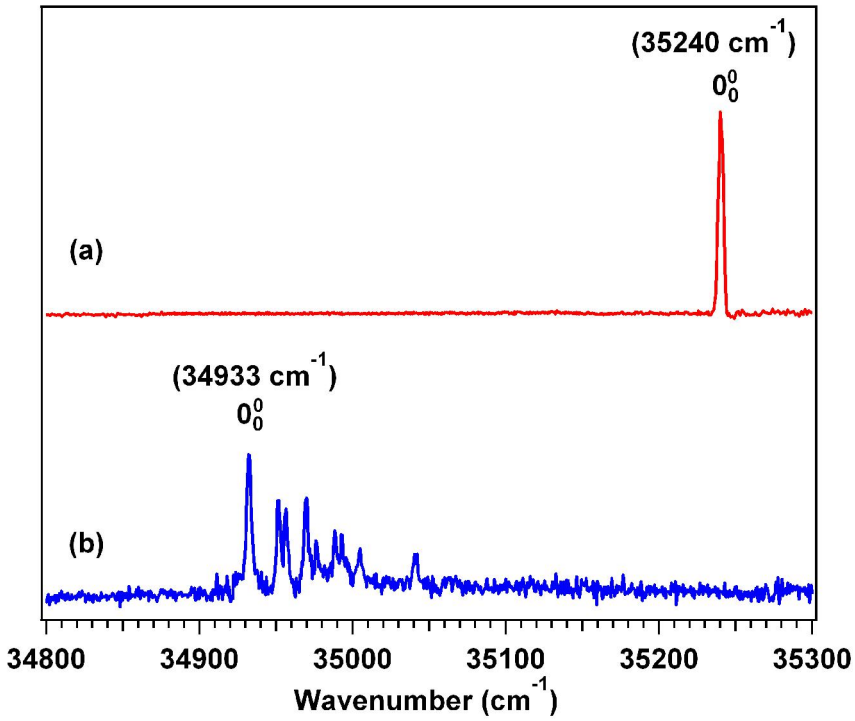

Figure 6.1. 1C-R2PI spectra measured at (a) indole monomer and (b) indole···imidazole dimer mass channels.

The origin band for the $S_1 \leftarrow S_0$ electronic excitation of the indole···imidazole dimer appears at 34933 cm^{-1} and this is red-shifted from the origin band of the indole monomer by 307 cm^{-1}.

The red-shift implies that the S_1 state dimer is more strongly bound than the S_0 state dimer relative to the respective monomers. This is indeed revealed from the comparison of the geometries of the dimer in the S_0 and S_1 states provided in Table 6.6 and Figure 6.7. The comparison shows that the hydrogen bond (N-H...N) present in the S_1 state ($d_{N\text{-}H\ldots N}$ = 1.93 Å) of the dimer is stronger than that in the S_0 state ($d_{N\text{-}H\ldots N}$ = 2.05 Å). The presence of multiple bands within 100 cm^{-1} blue side of the origin band in the R2PI spectrum of the dimer could be due to either low frequency intermolecular vibrations or electronic transitions of isomeric structures of the dimer. To verify this, we have performed UV-UV hole-burning spectroscopy, which has been discussed in section 6.2.1.1.2.

6.2.1.1.2. UV-UV hole-burning spectroscopy.

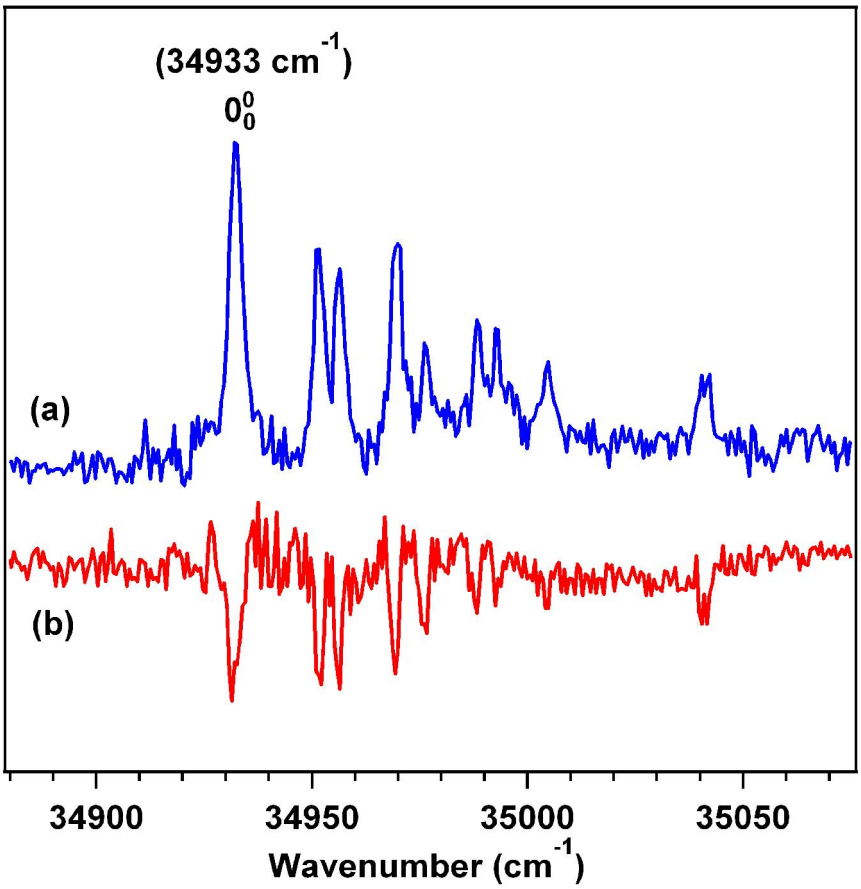

Figure 6.2. (a) 1C-R2PI spectrum of indole···imidazole dimer and (b) UV-UV hole-burning spectrum by probing the electronic origin band of indole···imidazole dimer at 34933 cm^{-1}.

Figure 6.2b depicts a UV-UV hole-burning spectrum by probing the origin band of the indole···imidazole dimer at 34933 cm^{-1} while the pump (hole-burning) laser is scanned through all the electronic transitions observed in the R2PI spectrum of the dimer. The R2PI spectrum of the dimer has been reproduced in Figure 6.2a to compare with the hole-burning spectrum. It is obvious from this comparison that the hole-burning spectrum shows depletion of the ion signal for all the electronic bands present in the R2PI spectrum. This confirms the presence of only one isomer of the dimer in the experiment. Thus the observed electronic bands built off the 0_0^0 band in the R2PI spectrum of the dimer shown in Figure 6.1b are due to low frequency intermolecular vibrations of the dimer. The observed intermolecular vibrations have been assigned by performing the frequency calculation of the dimer in the S_1 state and this has been discussed in the theoretical section 6.2.1.2.

6.2.1.1.3. RIDIR spectra.

IR spectra of the indole monomer and indole···imidazole dimer have been measured in the N-H stretching region by using RIDIR spectroscopy. The IR spectrum of the indole···imidazole dimer presented in Figure 6.3b shows one sharp band of medium intensity at 3516 cm^{-1} and another very strong and relatively broad band at 3270 cm^{-1}. Figure 6.3a depicts IR spectrum of indole monomer showing the N-H stretch fundamental at 3526 cm^{-1}.[425] Free N-H stretching frequency in imidazole monomer is reported at 3518 cm^{-1} from supersonic jet FTIR (Fourier Transform Infrared) spectroscopy and IR laser spectroscopy in helium nanodroplets.[446-447] Interestingly, the free N-H stretching frequency in imidazole dimer is also reported by Choi et al. and this appears at 3516 cm^{-1}.[447] A summary of experimental and calculated N-H stretching frequencies of indole...imidazole dimer and corresponding monomers as well as some relevant dimers has been presented in Table 6.1. Thus the observed 3516 cm^{-1} band in the IR spectrum of the indole···imidazole dimer is easily assigned to the transition due to the free N-H stretching vibration of the imidazole moiety. This clearly indicates that the N-H group of the imidazole unit in the dimer is not engaged in hydrogen-bonding interaction. It is interesting to note that FWHM of the 3516 cm^{-1} band in the dimer IR spectrum is about 4 cm^{-1}, which is similar with that of the N-H stretching band of indole monomer while FWHM of the 3270 cm^{-1} band in the dimer IR spectrum is about 10 cm^{-1}. A

Similarly broad IR band due to the presence of hydrogen bond in the molecular complex has been reported previously for imidazole dimer and indole···H_2O complex.[425,447]

Due to the absence of any band at 3526 cm^{-1} (free N-H stretch of indole) in the dimer IR spectrum, the broad intense band at 3270 cm^{-1} in Figure 6.3b is assigned as the transition due to red-shifted N-H stretch of the indole moiety in the dimer, which is involved in hydrogen-

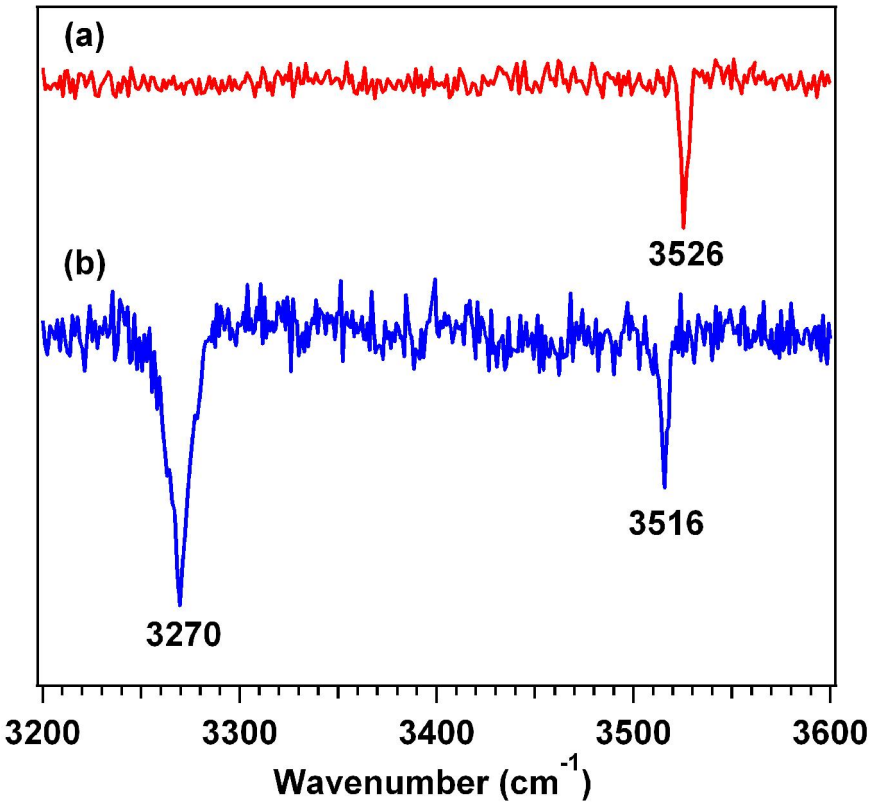

Figure 6.3. RIDIR spectra in the N-H stretching region by probing the origin bands of (a) indole monomer and (b) indole···imidazole dimer.

bonding interaction with the imidazole unit. A significantly large amount of red-shift (256 cm^{-1}) in the N-H stretching frequency indicates the presence of strong N-H···N hydrogen bonding interaction in the dimer. It is worth comparing the red-shifted N-H stretching frequency of the indole moiety in the indole···imidazole dimer with that in a few other N-H···N hydrogen bonded dimer reported in the literature and this has been provided in Table 6.1. [233,320,447-448] In the case of the N-H···N hydrogen bonded indole···pyridine dimer, the N-H

stretching vibration of indole appears at 3269 cm^{-1} (red-shift 257 cm^{-1}).[320] The N-H stretching frequency of 7-azaindole in N-H···N hydrogen bonded 7azaindole···2-fluoropyridine dimer is reported at 3256 cm^{-1} (red-shift 265 cm^{-1}).[233] The red-shift in the N-H stretching frequency in hydrogen bonded (N-H···N) pyrazole dimer is 268 cm^{-1}.[448] This comparison points out that the indole···imidazole dimer observed in this study has an N-H···N hydrogen bonded structure, where the N-H group of indole is in hydrogen bonding interaction

Table 6.1: Experimental as well as calculated vibrational frequencies (S_0 state) and their assignment for indole···imidazole dimer, corresponding monomers and a few relevant dimers[a]

	Exp. freq. (cm^{-1})	Calc. freq. (cm^{-1})	IR intensity (km/mol)	Assignment
Indole...imidazole	3516	3502	47.0	Free NH (imidazole)
	3270	3246	922.5	H-bonded NH (indole)
Indole	3526	3526	51.8	Free NH (indole)
Imidazole	3518[b,c]	3505	34.0	Free NH (imidazole)
Imidazole dimer[c]	3516	3516	81.6	Free NH (imidazole)
	3200	3242	1225.3	H-bonded NH (imidazole)
Pyrazole dimer[d]	3255			H-bonded NH (pyrazole)
Pyrazole[d]	3523			Free NH (imidazole)
Indole...pyridine[e]	3269	3246	1197.2	H-bonded NH (indole)
7-azaindole...2-FP[f]	3256	3253	1242.6	H-bonded NH (7-azaindole)

[a]Frequencies of indole...imidazole dimer as well as indole and imidazole monomers have been calculated at the B97-D/6-311+G(3df,3pd) level of theory. Theoretical harmonic frequencies have been corrected by using a scaling factor of 0.9765 obtained from the ratio of the experimental and theoretical N-H stretching frequencies of indole monomer at 3526 and 3611 cm^{-1}, respectively. [b]Ref 446. [c]Ref 447. [d]Ref 448. [e]Ref 9. [f]Ref 233, 2-FP stands for 2-fluoropyridine.

with the nitrogen atom of the imidazole ring. The detailed structure of the dimer has been determined by comparing the experimental findings with the theoretical results and this has been discussed in the following section.

6.2.1.2. Theoretical results.

6.2.1.2.1. Structures of indole···imidazole dimer.

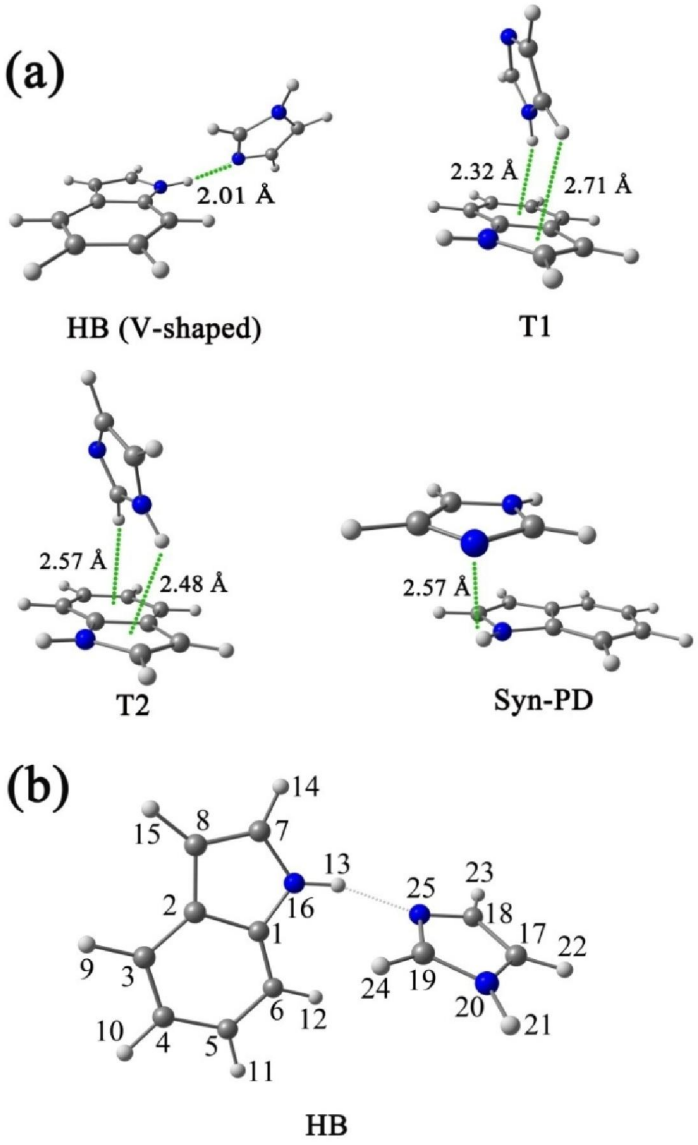

Figure 6.4. (a) Four stable structures of indole···imidazole dimer optimized at the B97-D/6-311+G(3df,3pd) level of theory, (b) Atom numbering scheme has been shown in the HB structure of indole···imidazole dimer.

Geometry optimization of different possible structures of the indole···imidazole dimer has been performed at various levels of theory (M05-2X, M06-2X, B97-D, and MP2) using different basis sets. We have also calculated the frequencies of different structures of the

dimer at all levels of theory to check whether these are stable minimum in the potential energy surface. The stable structures of the dimer optimized at the B97-D/6-311+G (3df, 3pd) level of theory have been shown in Figure 6.4a. The atom numbering scheme in the dimer has been provided in Figure 6.4b. The HB structure has a V-shaped herringbone geometry, which is stabilized by strong N-H···N and weak C-H···π hydrogen bonding interactions as well as weak π···π interaction. T1 and T2 structures have tilted T-shaped geometry with π-hydrogen bonding interactions. In the case of the T1 structure, the N-H and one of the C-H groups of

Table 6.2: Geometrical parameters of four structures of indole···imidazole dimer calculated at the B97-D/6-311+G(3df,3pd) level of theory[a]

Geometrical parameters	HB	T1	T2	Syn-PD
$d_{N16\text{-}H13\ldots N25}$ (Å)	2.01			2.57
$\Delta r_{N\text{-}H}$ (Å)	0.0156	0.0004	0.0005	0.0034
$d_{N16\ldots N25}$ (Å)	2.94			3.28
<N-H-N	153^0			128^0
$<C_6C_1N_{16}H_{13}$	-8^0	-3^0	-3^0	15^0
$<C_1N_{16}N_{25}C_{19}$	-45^0			29^0
$d_{N20\text{-}H21\ldots\pi}$ (Å)		2.32	2.48	
$d_{C17\text{-}H22\ldots\pi}$ (Å)		2.71		
$d_{C19\text{-}H24\ldots\pi}$ (Å)	3.62		2.57	
$d_{C6\text{-}H12\ldots\pi}$ (Å)	3.72			

[a]For atom numbering, refer to Figure 6.4b. $\Delta r_{N\text{-}H}$ is the change in the N-H bond length of the indole moiety in the dimer with respect to the indole monomer.

the imidazole unit make π-hydrogen bonding interaction with the phenyl and pyrrole groups of indole moiety, respectively. On the other hand, the T2 structure is stabilized by π-hydrogen bonds through the interactions of the N-H and C-H groups of imidazole with the π-clouds of the pyrrole and phenyl groups of the indole unit, respectively. Interestingly, another T-shaped structure bound by N-H···π hydrogen bonding interaction through the N-H group of indole and π-cloud of imidazole is not stable and converges to the HB structure. Syn-PD has a tilted parallel displaced π-stacked structure where indole N-H and imidazole nitrogen are

oriented in the same side. Here the PD structure is tilted to get advantage of both π···π stacking and electrostatic interaction between indole N-H group and nitrogen atom of imidazole.

Table 6.3. BSSE and ZPE corrected binding energies (kcal/mol) of four structures of indole···imidazole dimer calculated at various levels of theory[a]

	Structures	ΔE_e	ΔE_0
B97-D/6-311++G(3df,3pd)	HB	-8.87	-7.87
	T1	-7.98	-6.90
	T2	-7.60	-6.56
	Syn-PD	-7.23	-6.07
B97-D/cc-pVTZ	HB	-8.95	-7.95
	T1	-8.11	-7.05
	T2	-7.72	-6.75
	Syn-PD	-7.37	-6.26
M05-2X/cc-pVDZ	HB	-8.41	-7.49
	T1	-7.31	-6.68
	T2	-6.32	-5.63
	Syn-PD	-6.20	-5.45
M05-2X/cc-pVTZ	HB	-8.40	-7.50
	T1	-6.75	-6.01
	T2	-6.45	-5.67
	Syn-PD	-6.41	-5.61
M06-2X/cc-pVDZ	HB	-8.72	-7.81
	T1	-7.39	-6.68
	T2	-7.01	-6.25
	Syn-PD	-7.09	-6.34
MP2/cc-pVDZ	HB	-8.43	-7.45
	T1	-6.42	-5.75
	T2	-6.10	-5.38
	Syn-PD	-5.54	-4.87

[a]ΔE_e: BSSE corrected binding energy; ΔE_0: BSSE + ZPE corrected binding energy.

It is interesting to look at the geometrical parameters of the four stable structures of the indole···imidazole dimer. Table 6.2 lists these geometrical parameters calculated at the B97-D/6-311+G(3df,3pd) level of theory. The HB structure has a strong hydrogen bond with N-

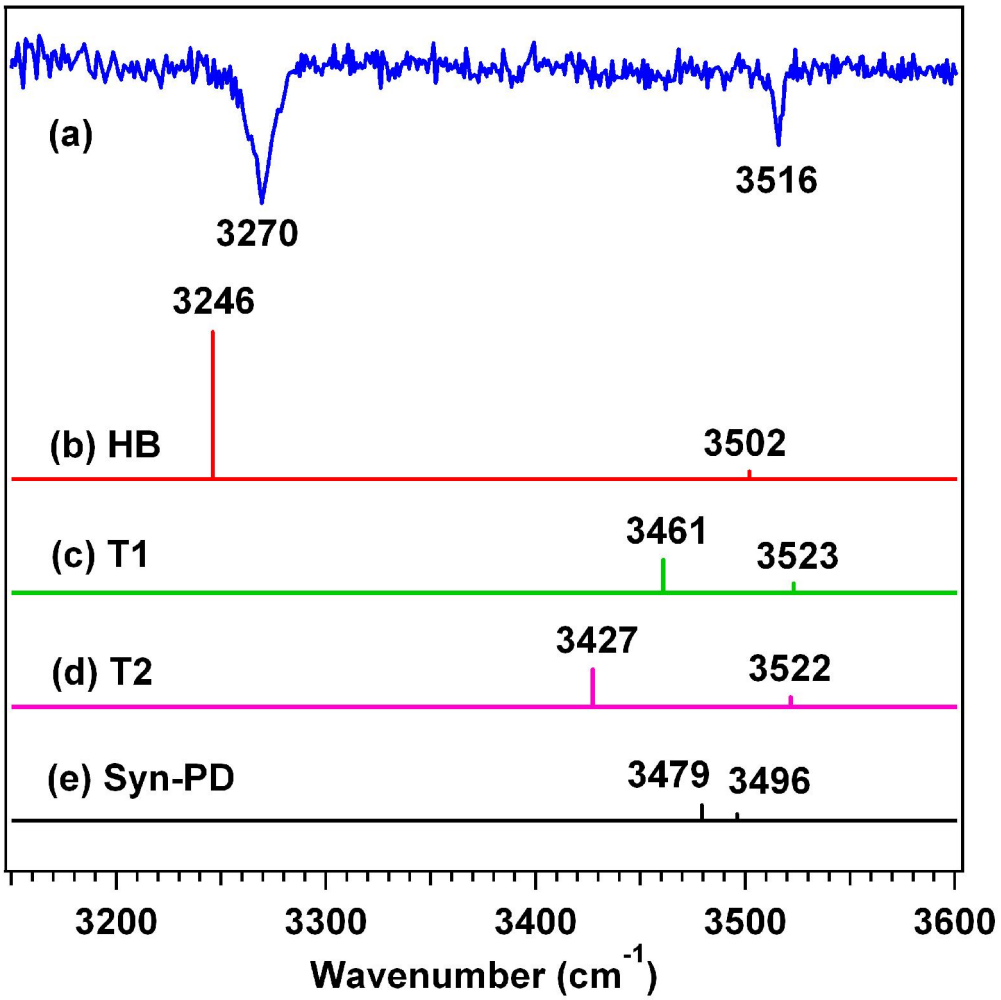

Figure 6.5. (a) RIDIR spectra in the N-H stretching region by probing the origin band of indole···imidazole dimer. (b)-(e) Theoretical IR stick spectra of four structures of indole···imidazole dimer obtained at the B97-D/6-311+G(3df,3pd) level of theory.

H···N distance of 2.01 Å and ∠N-H···N of 153°. Two C-H···π interactions (see Table 6.2) and weak π···π interaction enhance the stability of the HB structure providing a V-shaped geometry. The interplanar angle (wagging angle) between the two rings ($\angle C_1N_{16}N_{25}C_{19}$) in the HB structure is -45^0. Similar type of V-shaped structure has been reported for indole···pyridine and $(phenol)_2$ dimers.[4,320,346] Both T1 and T2 structures show standard N-

H···π, C-H···π distances and are tilted to gain additional stability through weak π···π interaction. The N-H···N hydrogen bond distance in the Syn-PD structure is 2.57 Å and the N-H group of indole is out of plane ($\angle C_6C_1N_{16}H_{13}$) by 15^0. Syn-PD structure is not perfectly parallel and the interplanar angle between the two rings is 29°.

BSSE- and ZPE- corrected binding energies of the four stable structures of the indole···imidazole dimer have been calculated at various levels of theory and provided in Table 6.3. The results presented in the table show that the most stable structure of the dimer is the HB one (hydrogen bonded V-shaped). The comparison of the binding energies indicates that the observed dimer in the experiment has likely to have the V-shaped N-H···N hydrogen bonded structure (HB). It is interesting to note that the T1 structure is slightly more stable than the T2 structure although both of them have N-H···π and C-H···π interactions. The N-H···π interaction in the T1 structure is between the imidazole N-H group and phenyl moiety of indole whereas the corresponding interaction in the T2 structure is between the imidazole N-H group and pyrrole moiety of indole. The N-H···π interaction in pyrrole dimer and pyrrole...benzene complex has been studied by several groups and it has been reported that pyrrole is a stronger π-hydrogen bond acceptor than benzene.[263-264,292] However, the different trend found in the stability of the T1 and T2 structures of the indole...imidazole dimer may be due to the presence of additional C-H···π interaction and different π-hydrogen bond donor i.e. imidazole instead of pyrrole.

Finally, the structure of the indole···imidazole dimer observed in the experiment has been determined by comparing the experimental IR spectrum with the theoretical IR spectra of the four isomeric structures of the dimer in the N-H stretching region. Figure 6.5 shows comparison of the experimental IR spectra of the observed dimer and theoretical IR spectra of the four structures of the dimer calculated at the B97-D/6-311+G(3df,3pd) level of theory. Theoretical frequencies presented in Figure 6.5b-e are scaled using a factor (0.9765) obtained from the ratio of the experimental and theoretical N-H stretching frequencies of indole monomer, which are 3526 and 3611 cm^{-1}, respectively. It is quite obvious from the comparison shown in Figure 6.5 that the theoretical IR spectrum of only the HB structure matches with the IR spectrum of the observed dimer presented in Figure 6.5a. It is interesting

to note that the theoretical IR intensities of the hydrogen bonded indole N-H stretching vibration and free N-H stretching vibration of the imidazole unit in the HB structure of the dimer are 922 and 47 km/mol, respectively. This intensity distribution of the hydrogen bonded and free N-H stretches in the HB structure of the dimer is reflected in the experimental spectrum of the observed dimer. Thus it is unambiguously confirmed that the observed indole···imidazole dimer has a V-shaped N-H···N hydrogen bonded structure (HB).

6.2.1.2.2. EDA.

Table 6.4 shows different components of the interaction energy of four stable structures of the dimer calculated at the M05-2X/cc-pVDZ level of theory using LMO-EDA method. The result shows that the dispersion component (-7.54 kcal/mol) has a significant contribution in the total interaction energy although the electrostatic force (-12.52 kcal/mol) is the dominating one for the stabilization of the HB structure. This finding supports in favor of the presence of the dispersion dominated C-H···π and π···π interactions in the HB structure. As expected, N-H···π and syn-PD structures are dominated by dispersion interaction.

Table 6.4. Decomposition of the interaction energies (kcal/mol) of four structures of indole···imidazole dimer calculated at the M05-2X/cc-pVDZ level of theory using LMO-EDA method.

	ΔE_{ele}	ΔE_{ex}	ΔE_{rep}	ΔE_{pol}	ΔE_{disp}	ΔE_{tot}
HB	-12.52	-6.79	21.97	-3.71	-7.54	-8.58
T1	-6.98	-3.68	16.15	-1.58	-10.54	-6.64
T2	-6.90	-3.91	16.62	-1.91	-10.27	-6.38
Syn-PD	-7.81	-4.46	18.25	-1.43	-11.01	-6.47

At this point, it is very interesting to compare the various contributions to the total interaction energy of the V-shaped HB isomer of the indole…imdazole dimer with that of the indole…pyridine dimer reported in the chapter 03. In the case of both the dimers, $\Delta E_{ele}/\Delta E_{disp}$ ratio is about 1.5 which signifies that the dispersion interaction plays a significant role in the

stabilization of these dimers. Thus from the similarity in the structure as well as interaction energy components of these two complexes, the observed structure of the indole…imidazole dimer could also be put in the category of the "*special class of mixed complex*". Very recently, Hill *et al.* have performed energy decomposition analysis of the indole…pyridine and indole…imidazole dimers using SAPT2+3 method.[10] They have also concluded from their study that these complexes are stabilized due to interplay between conventional hydrogen bonding as well as significant amount of dispersion bound interactions. They have renamed this "*special class of mixed complex*" to "*Special mixed-influence*" (SMI).[10]

6.2.1.2.3. Intermolecular vibrations and geometry of the dimer in the S_1 state.

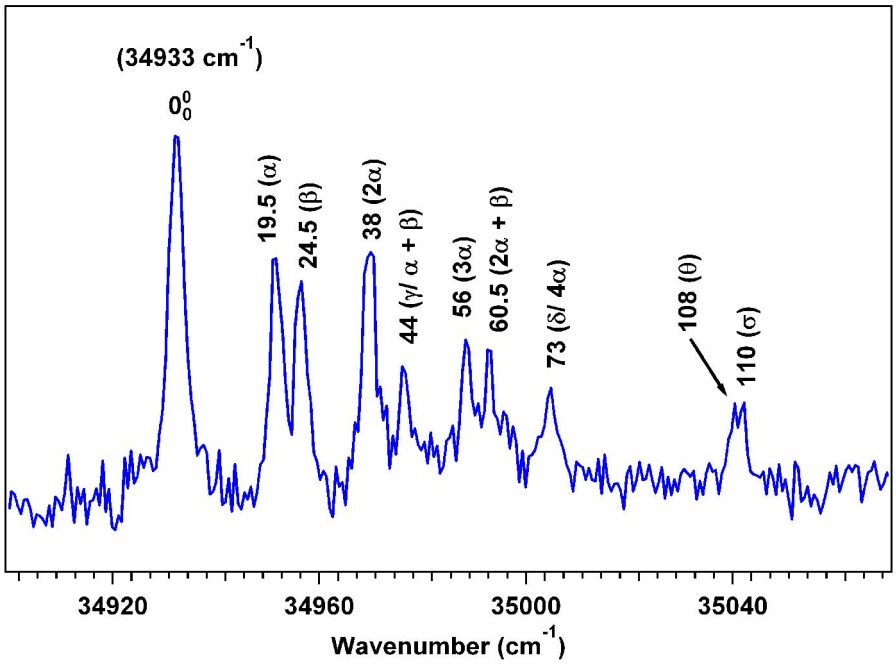

Figure 6.6. 1C-R2PI spectrum of indole···imidazole dimer in an expanded scale with the assignments of the intermolecular vibrations.

To assign the low frequency intermolecular vibrations of the indole…imidazole dimer observed in the R2PI spectrum as well as find out the geometry of the dimer in the S_1 state, we have performed geometry optimization and frequency calculation at the TDDFT level using M05-2X functional and 6-31+G(d) basis set. Figure 6.6 shows the R2PI spectrum of

the dimer in an expanded scale to make the closely spaced electronic bands visible. The assignments of the intermolecular vibrations have been shown in the figure. Table 6.5 presents a comparison of the observed as well as calculated low frequency intermolecular

Table 6.5. Experimental and TD-M05-2X/6-31+G(d) level calculated S_1 state intermolecular vibrational frequencies (in cm^{-1}) of the HB structure of indole··· imidazole dimer

Observed	Calculated	Assignments
19.5	19	α
24.5	30	β
38		2α
44	50	γ / $\alpha + \beta$
56		3α
60.5		$2\alpha + \beta$
73	76	δ / 4α
108	104	θ
110	120	σ

vibrations of the HB dimer and their assignments. The comparison shows that all the electronic bands built off the origin band of the dimer in the R2PI spectrum can be assigned as fundamental, overtone, and combination of hydrogen bond bending and stretching intermolecular modes. It is interesting to note that all the six intermolecular modes of the dimer are observed in the experiment. The highest frequency intermolecular vibration of the dimer at 110 cm^{-1} denoted as σ is assigned as hydrogen bond stretch and rest of the five modes are due to bending of the hydrogen bond. The presence of low frequency intermolecular vibrations in the R2PI spectrum of the dimer points out significant change in the geometry of the dimer upon electronic excitation to the S_1 state. If we look at the vibronic bands of the dimer carefully, it is found that the maximum Franck-Condon activity in the R2PI spectrum occurs due to long progression of the lowest frequency intermolecular mode

denoted as α (buckle) and combination of this mode with another mode β. Thus it is expected that the buckle (α) is the most active mode in the R2PI spectrum and the distortion of the geometry of the dimer in the S_1 state mostly occurs through this intermolecular coordinate.

As the electronic spectrum of the dimer implies the geometry change in the S_1 state, it is intriguing to compare the geometry of the dimer in the S_0 and S_1 states. Table 6.6 shows comparison of a few important geometrical parameters of the HB dimer in the S_0 and S_1 states calculated at the M05-2X/6-31+G(d) level of theory. To obtain the geometry in the S_1 state, TDDFT optimization has been done using the same functional and basis set used for the S_0 state calculation. Geometrical parameters of the dimer in the S_0 state has been reproduced in Table 6.6 but with different level of theory compared to those in the Table 6.2 for the purpose of comparison of those with the S_1 state. The geometries of the HB dimer in the S_0 and S_1 states have been presented in Figure 6.7.

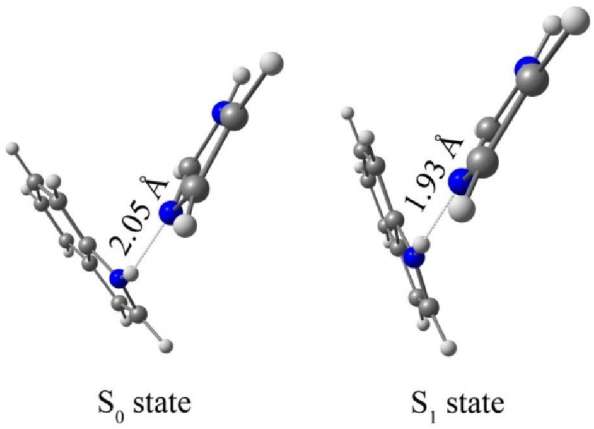

Figure 6.7. M05-2X/6-31+G(d) level optimized geometries of the HB structure of indole···imidazole dimer at the S_0 and S_1 states. TDDFT calculation has been done for the S_1 state. Interplanar angles of the dimer in the S_0 and S_1 states are -55^0 and -39^0, respectively.

The comparison shows that the N-H···N hydrogen bond of the dimer in the S_1 state is stronger than that in the S_0 state. There is also significant decrease in the angle ($\angle C_1N_{16}N_{25}C_{19}$) between the planes of indole and imidazole units in the dimer in the S_1 state compared to that

Table 6.6. Geometrical parameters of S_0 state and TDDFT calculated S_1 state of HB structure of indole···imidazole dimer calculated at the M05-2X/6-31+G(d) level of theory[a]

Geometrical parameters	S_0 state	S_1 state
$d_{N16\text{-}H13\ldots N25}$ (Å)	2.05	1.93
$d_{N16\ldots N25}$ (Å)	2.97	2.90
$\Delta r_{N\text{-}H}$ (Å)	0.0115	0.0149
∠N-H-N	149^0	156^0
$\angle C_6C_1N_{16}H_{13}$	-5^0	-6^0
$\angle C_1N_{16}N_{25}C_{19}$	-55^0	-39^0
$d_{C19\text{-}H24\ldots\pi}$ (Å)	3.67	3.90
$d_{C6\text{-}H12\ldots\pi}$ (Å)	3.78	3.82

[a]For atom numbering, refer to Figure 6.4b. $\Delta r_{N\text{-}H}$ is the change in the N-H bond length of the indole moiety in the dimer with respect to the indole monomer.

in the S_0 state. These results indicate that the interaction energy in the dimer is higher in the S_1 state than that in the S_0 state. Thus significant change in the dimer geometry in the S_1 state compared to that in the S_0 state is revealed from this comparison. So the comparison of the calculated geometries of the dimer in the S_0 and S_1 states nicely explains the observation of the intermolecular vibrations in the experiment. Similar kind of geometry change in the S_1 state compared to the S_0 state has been reported for phenol dimer.[4]

6.2.2. Indole···(pyrrole)$_2$ heterotrimer

6.2.2.1. Experimental results

6.2.2.1.1. 1C-R2PI and 2C-R2PI spectra

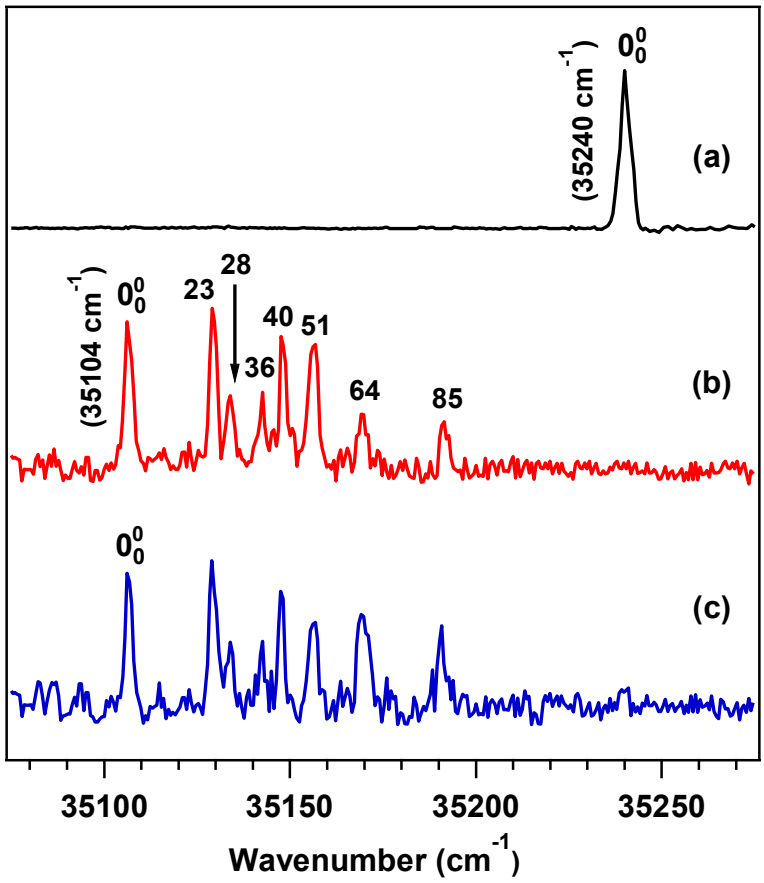

Figure. 6.8. 2C-R2PI spectrum recorded at (a) indole monomer mass channel. (b) 2C-R2PI and (c) 1C-R2PI spectra recorded at indole···(pyrrole)$_2$ trimer mass channel.

Figure 6.8b shows 2C-R2PI spectrum recorded at the indole···(pyrrole)$_2$ trimer mass channel at 251 amu 2C-R2PI spectrum of the indole monomer is shown in Figure 6.8a to compare with the trimer R2PI spectra. The origin band (0_0^0) for the $S_1 \leftarrow S_0$ electronic transition of indole appears at 35240 cm^{-1}, which matches well with the previous report.[394] 1C-R2PI spectrum measured at the indole···(pyrrole)$_2$ trimer mass channel has also been shown in Figure 6.8c. Actually we observed significant fragmentation of the indole···(pyrrole)$_2$ trimer

at the indole···pyrrole dimer channel when we recorded the 1C-R2PI spectra at the dimer channel. Thus we recorded the 2C-R2PI spectrum at the trimer channel by fixing the second photon at longer wavelength (347 nm) to avoid the fragmentation. The R2PI spectrum of the indole···$(pyrrole)_2$ trimer is measured by the electronic excitation of the indole moiety. The lowest energy and the most intense band observed at 35104 cm^{-1} in the spectrum has been assigned to the $S_1 \leftarrow S_0$ origin of the trimer and it is red-shifted from the electronic origin band of the indole monomer by 136 cm^{-1}. Multiple bands observed within 100 cm^{-1} higher energy (blue side) side of the origin band in the R2PI spectrum of the trimer could be due to either low frequency intermolecular vibrations or presence of multiple isomeric structures of the trimer. These have been verified through RIDIR as well as UV-UV double resonance spectroscopic techniques. The results of these experiments have been discussed in detail in the following sections. The presence of only one isomer of the trimer has been confirmed from these experiments. Thus all the bands in the blue side of the 0_0^0 band of the trimer, shown in Figure 6.8b and 6.8c, are only due to low frequency intermolecular vibrations of a single isomer of the trimer. The assignment of the intermolecular vibrations have been done by S_1 state frequency calculation of the trimer and discussed in the theoretical section 6.2.2.2.

6.2.2.1.2. RIDIR spectra

The structure of the observed trimer in the experiment has been determined by measuring the RIDIR spectra in the N-H stretching region by probing several electronic transitions in the R2PI spectrum of the trimer. The RIDIR spectrum depicted in Figure 6.9a shows the appearance of the N-H stretch fundamental of the indole monomer at 3526 cm^{-1}, which matches very well with the previous report.[425] N-H stretch fundamental of pyrrole monomer is also reported at 3531 cm^{-1} from the jet-cooled FTIR (Fourier transform infrared), IR cavity ringdown, and matrix isolation solid state IR spectroscopy.[263-264,449] Figure 6.9b displays RIDIR spectrum by probing the 0_0^0 band of the indole···$(pyrrole)_2$ trimer at 35104 cm^{-1}. The spectrum shows three bands at 3376, 3389, and 3408 cm^{-1}, which are red-shifted from free N-H stretch of the indole monomer by 150, 137, and 118 cm^{-1}, respectively. Absence of any band in the position of the free N-H stretch of either indole or pyrrole clearly indicates that all the three N-H groups present in the indole···$(pyrrole)_2$ trimer are involved in hydrogen

bonding interaction. This is possible only if the observed trimer has an N-H···π bound cyclic structure, where each monomer unit acts as a hydrogen bond donor as well as an

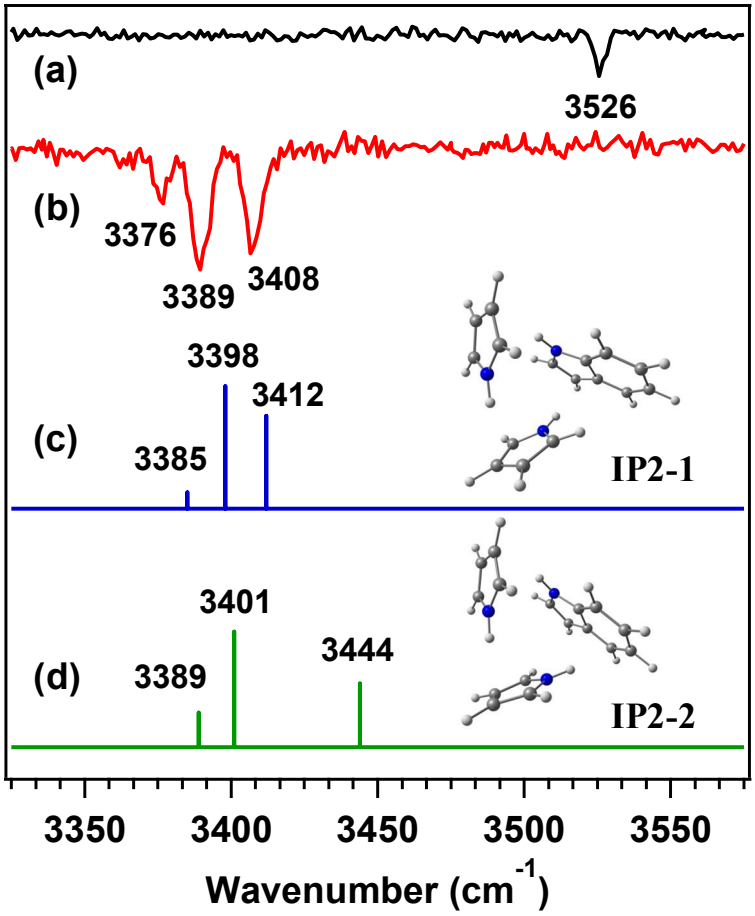

Figure. 6.9. RIDIR spectra in the N-H stretching region by probing the origin bands of (a) indole monomer and (b) indole···$(pyrrole)_2$ trimer. Theoretical IR spectra for the IP2-1 and IP2-2 structures of indole···$(pyrrole)_2$ trimer obtained at the M05-2X/cc-pVTZ level of theory are provided in (c) and (d).

acceptor. Thus the IR spectrum provides a direct evidence of formation of a cyclic trimer in the experiment.

Figure 6.9c and 6.9d present theoretical IR spectra of two probable cyclic structures of indole···$(pyrrole)_2$ trimer designated as IP2-1 and IP2-2 in the N-H stretch region calculated at the M05-2X/cc-pVTZ level of theory. The calculation shows that the three N-H stretching frequencies of the IP2-1 structure of the trimer are very close to those observed in the

experimental IR spectrum. On the other hand, the N-H stretching frequency of the IP2-2 structure at 3444 cm^{-1} is quite far off from the corresponding experimental N-H stretching frequency at 3408 cm^{-1}. Theoretical N-H stretch frequencies are corrected using a scaling factor obtained by taking the ratio of experimental and theoretical N-H stretching frequencies of the indole monomer obtained at 3521 and 3657 cm^{-1}, respectively. It is interesting to note that the agreement between experimental and theoretical frequencies as well as intensity of the IR transitions of the N-H stretching modes of the IP2-1strcuture of the trimer shown in Figure 6.9c is quite excellent. This confirms that the observed trimer has a triangular shaped cyclic geometry (IP2-1) stabilized by three N-H···π hydrogen bonding interactions. The excellent prediction of the intensity pattern of the theoretical N-H stretching transitions of the IP2-1 trimer with that of the experimental one is indeed quite spectacular. Two probable structures of the observed trimer as well as the interactions present therein have been discussed in detail in the theoretical section, vide-infra. IR spectra have also been measured by fixing the UV laser frequency at many of the transitions observed in the R2PI spectrum of the trimer are identical with the one presented in Figure 6.9b by probing the 0_0^0 band of indole···$(pyrrole)_2$ trimer. Thus the measured RIDIR spectra indicate the presence of mostly one isomer of the trimer in the experiment.

6.2.2.1.3. UV-UV hole-burning spectrum

The presence of only one isomeric structure of the indole···$(pyrrole)_2$ trimer in the experiment has further been confirmed by UV-UV hole-burning spectroscopy. Figure 6.10b shows UV-UV hole-burning spectrum by probing the 0_0^0 band of the trimer at 35104 cm^{-1} and scanning another UV laser through the R2PI spectral region of the trimer. The R2PI spectrum of the trimer has been reproduced in Figure 6.10a to compare with the hole-burning spectrum in Figure 6.10b, which shows dip in ion signal for all the electronic transitions in the R2PI spectrum of the trimer. Thus it has been proved that only one isomer of the trimer is observed.

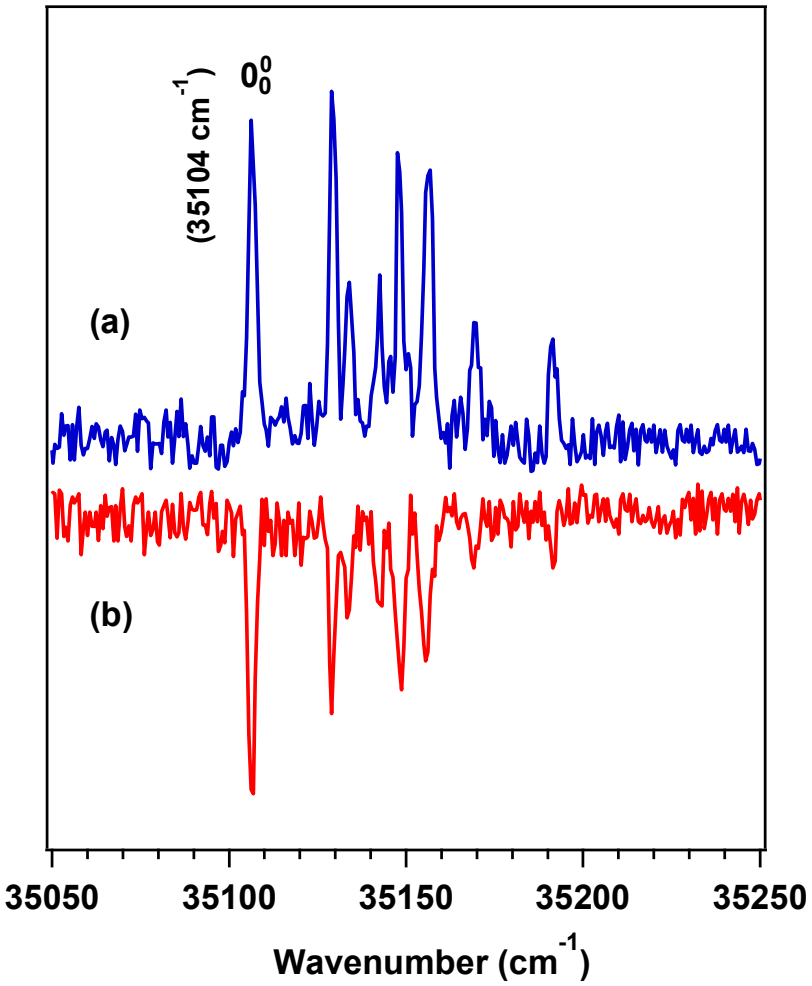

Figure. 6.10. (a) 2C-R2PI spectrum of indole···(pyrrole)$_2$ trimer, and (b) UV-UV hole-burning spectrum by probing the electronic origin band of indole···(pyrrole)$_2$ trimer.

6.2.2.2. Theoretical results

6.2.2.2.1. Structures of Indole···(pyrrole)$_2$ trimer

As the experiment provides a direct evidence that the observed trimer has N-H···π bound cyclic geometry, only two probable cyclic structures of the trimer have been considered for geometry optimization as well as frequency calculation at the DFT level using DFT-D, M05-2X, and M06-2X functionals with various basis sets. Figure 6.11 shows two cyclic structures (IP2-1 and IP2-2) of the indole···(pyrrole)$_2$ trimer optimized at the M05-2X/cc-pVTZ level of theory. Atom numbering scheme in the trimer has also been shown in Figure 6.11. Three

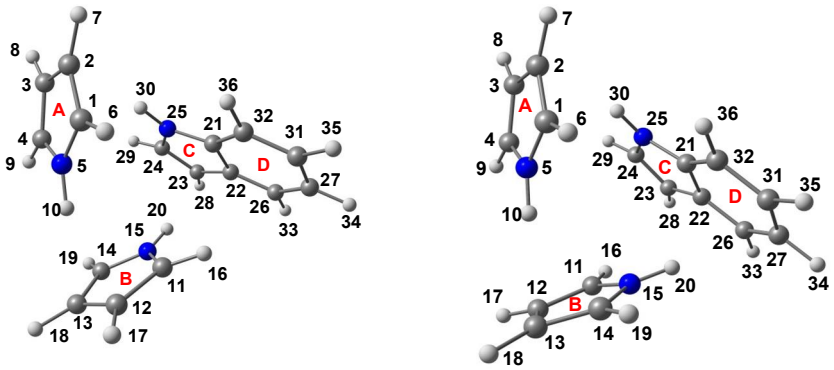

IP2-1 **IP2-2**

indole···(pyrrole)$_2$ trimer

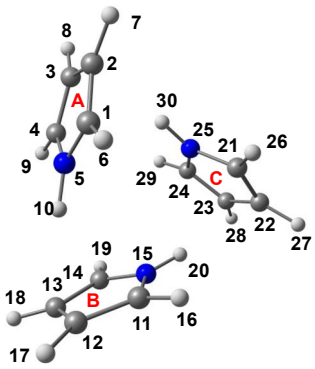

(pyrrole)$_3$

Figure. 6.11. IP2-1 and IP2-2 structures of indole···(pyrrole)$_2$ trimer as well as (pyrrole)$_3$ optimized at the M05-2X/cc-pVTZ level of theory.

pyrrole rings in the trimer has been denoted by A, B, and C while the phenyl ring of indole has been denoted by D. Both of the IP2-1 and IP2-2 trimers have similar triangular cyclic structure held by three N-H···π hydrogen bonds but there is a subtle difference between the two structures. In the case of the IP2-1 structure, one of the pyrrole moieties interact with the π-clouds of pyrrole and phenyl groups of indole through N-H···π and C-H···π hydrogen bonding interactions, respectively. On the other hand, the π-clouds of pyrrole and phenyl groups of indole interacts with one of the pyrrole moieties in the IP2-2 structure through C-H···π and N-H···π interactions, respectively.

Table 6.7. BSSE and ZPE corrected binding energies (kcal/mol) as well as the relative energies (kcal/mol) of IP2-1 and IP2-2 structures of indole···$(pyrrole)_2$ trimer calculated at various levels of DFT[a]

Theory	Indole…$(pyrrole)_2$ trimer					
	IP2-1			IP2-2		
	ΔE_e	ΔE_o	E_{rel}	ΔE_e	ΔE_o	E_{rel}
B97-D/cc-pVTZ	-23.05	-20.51	0.000	-22.96	-20.45	0.049
B97-D/aVDZ	-22.38	-20.02	0.000	-22.16	-19.84	0.140
ωB97X-D/cc-pVTZ	-22.85	-20.54	0.000	-22.46	-20.47	0.079
ωB97X-D / aVDZ	-22.84	-20.69	0.000	-22.39	-20.31	0.372
M05-2X /cc-pVTZ	-20.24	-18.15	0.000	-19.83	-17.92	0.255
M05-2X/aVDZ	-20.29	-18.25	0.000	-19.84	-17.99	0.230
M06-2X /cc-pVTZ	-21.74	-19.46	0.000	-21.25	-19.16	0.304
M06-2X/aVDZ	-22.35	-20.05	0.000	-21.84	-19.69	0.315

[a]ΔE_e: BSSE corrected binding energy; ΔE_0: BSSE + ZPE corrected binding energy; E_{rel}: ZPE corrected relative energy with respect to the most stable structure.

BSSE and ZPE corrected binding energies of the IP2-1 and IP2-2 structures of the trimer calculated at various levels of the DFT using different basis sets have been presented in Table 6.7. Comparison of the binding energies of the two cyclic structures at various levels of the theory reveals that IP2-1 is the most stable structure of the trimer although the energy difference between the two isomeric structures is very small. Table 6.8 provides a few selected geometrical parameters of the IP2-1 structure of the indole···$(pyrrole)_2$ trimer calculated at the M05-2X/cc-pVTZ level of theory. At this point, it will be interesting to compare the cyclic structure of the observed indole···$(pyrrole)_2$ trimer with a few relevant the cyclic structure of $(pyrrole)_3$ trimer reported in the literature.[3,263-264,449-457] A few selected geometrical parameters of the pyrrole trimer have been listed in Table 6.8 as this trimer is the most appropriate one to compare with the observed trimer in our experiment. The optimized structure of the cyclic pyrrole trimer has also been provided in Figure 6.11.

Table 6.8. Geometrical parameters of indole···$(pyrrole)_2$ trimer and $(pyrrole)_3$ calculated at the M052X/cc-pVTZ level of theory[a]

Geometrical parameter	Indole···$(pyrrole)_2$ trimer	$(pyrrole)_3$
	IP2-1	
$\Delta r_{N5\text{-}H10}$ (Å)	0.0094	0.0090
$\Delta r_{N15\text{-}H20}$ (Å)	0.0076	0.0092
$\Delta r_{N25\text{-}H30}$ (Å)	0.0093	0.0091
$\Delta r_{C11\text{-}H16}$ (Å)	0.0009	
[b]<py(A)-py(B)	50.7	61.0
[b]<py(B)-py(C)	52.2	61.0
[b]<py(C)-py(A)	69.4	61.0
$d_{C11\text{-}H16\ldots\pi}$ (Å)	2.96	
$d_{N25\text{-}H30\ldots\pi}$ (Å)	2.30	2.28
$d_{N5\text{-}H10\ldots\pi}$ (Å)	2.28	2.28
$d_{N15\text{-}H20\ldots\pi}$ (Å)	2.41	2.28
μ (Debye)	0.88	0.00

[a] For atom numbering, refer to Figure 6.11. μ denotes dipole moment.

[b]<py(A)-py(B), <py(B)-py(C), <py(C)-py(A) denote the interplanar angles between the pyrrole rings in the trimer. "py" stands for pyrrole. $d_{C\text{-}H\ldots\pi}$, $d_{N\text{-}H\ldots\pi}$: distance between the hydrogen atom, covalently attached to the carbon or nitrogen atom, and the centroid of the aromatic ring.

Pyrrole trimer has a similar cyclic structure with three N-H···π hydrogen bonds like the indole···$(pyrrole)_2$ trimer but the former one is symmetric (C_{3h}) unlike the latter one, which is an asymmetric heterotrimer. The data presented in Table 6.8 indeed point out that the structures of the indole···$(pyrrole)_2$ trimer and the $(pyrrole)_3$ are asymmetric and symmetric, respectively. It is apparent from N-H···π hydrogen bond distances ($d_{N\text{-}H\ldots\pi}$) as well as

lengthening of the N-H bonds (Δr_{N-H}) in the indole···(pyrrole)$_2$ trimer that the three π-hydrogen bonds (N-H···π) present there are of different strength. Here we have defined the $d_{N-H...\pi}$ as the distance between the hydrogen atom, covalently attached to the nitrogen atom, and the centroid of the aromatic ring. The interplanar angles between the monomer units in the IP2-1trimer are also distinctly different (51^0, 52^0, and 69^0) and this clearly indicates that the cyclic structure of this trimer is asymmetric. On the other hand, all the three π-hydrogen bonds in the pyrrole trimer are of similar strength having identical N-H···π hydrogen bond distances (2.28 Å). Three interplanar angles between the monomer units in the pyrrole trimer are also exactly the same (61^0).

The symmetric as well as asymmetric natures of the cyclic structure of a trimer are generally reflected in its IR spectrum recorded in the region of the X-H (X=N, O, C) stretching modes. In the case of the symmetric cyclic structure of (pyrrole)$_3$, only a single IR active band ($E^{/}$) of two-fold degeneracy at 3393 cm^{-1} is observed in jet-FTIR as well as jet IR cavity ringdown spectra due to asymmetric (out-of-phase) stretching of the three N-H bonds.[263-264] The symmetric (in-phase) stretching ($A^{/}$) of the N-H bonds in the pyrrole trimer is IR inactive but strongly Raman active and observed at 3376 cm^{-1} in the jet-Raman spectrum.[264] Here the three equivalent N-H oscillators in the trimer are in resonance via cyclic N-H···π hydrogen bonds or through space and this coupling among the oscillators leads to lifting of their degeneracy resulting into splitting of the symmetric and asymmetric bands. The splitting of these bands in the cyclic trimer is called Davydov splitting[458] and this is 17 cm^{-1} in the pyrrole trimer.[264] Similarly, the phenol trimer has also a symmetric cyclic structure and it shows doubly degenerate ($E^{/}$) very strong IR active bands (3441 and 3449 cm^{-1}) due to out-of-phase stretching of the O-H bonds.[3] The in-phase stretching ($A^{/}$) of the O-H bonds gives IR inactive and Raman active band at 3394 cm^{-1}. On the other hand, the observed IR spectrum of indole···(pyrrole)$_2$ trimer in the N-H stretching region shown in Figure 6.9b exhibits three distinct bands. This clearly indicates that the cyclic structure of the observed trimer in our study is not symmetric unlike those observed for (pyrrole)$_3$ and (phenol)$_3$. It has been already mentioned in the section 6.2.2.1.2. that the theoretical IR spectrum of IP2-1 depicted in Figure 6.9c shows unprecedented agreement with the experimental spectrum in terms of the frequency as well as IR intensity.

Table 6.9. Theoretical frequencies (cm^{-1}), their assignments as well as IR and Raman intensity (km/mol) of the N-H stretching modes of $(pyrrole)_3$ and IP2-1, IP2-2 structures of the indole···$(pyrrole)_2$ trimer calculated at the M05-2X/cc-pVTZ level of theory[a]

	ν_{N-H}		IR intensity	Raman Intensity	Assignment
IP2-1	3412	(3408)	483	105	Asymmetric stretching
	3398	(3389)	638	92	Asymmetric Stretching
	3385	(3376)	81	265	Symmetric Stretching
IP2-2	3444		330	87	Asymmetric Stretching
	3401		602	89	Asymmetric Stretching
	3389		183	232	Symmetric Stretching
$(pyrrole)_3$	3405	(3393)[b]	631	90	Asymmetric Stretching
	3405	(3393)[b]	628	90	Asymmetric Stretching
	3388	(3376)[b]	2	280	Symmetric Stretching

[a]Experimental N-H stretching frequencies are given in the parentheses.

[b]Reference [412]

Theoretical frequencies, their assignments as well as IR and Raman intensity of the N-H stretching modes of $(pyrrole)_3$ and IP2-1, IP2-2 structures of the indole···$(pyrrole)_2$ trimer calculated at the M05-2X/cc-pVTZ level of theory have been provided in Table 6.9. Experimentally observed N-H stretching frequencies of the trimers are also provided in the table for comparison with the corresponding theoretical values. The theoretical data of the pyrrole trimer presented in Table 6.9 nicely reproduce the corresponding experimental values reported by Dauster et al.[264] The calculation nicely shows that the pyrrole trimer has doubly degenerate asymmetric stretch of the N-H bonds with strong IR intensity while the symmetric stretch of the N-H bonds is IR forbidden (intensity ~ 2km/mol). In the case of the

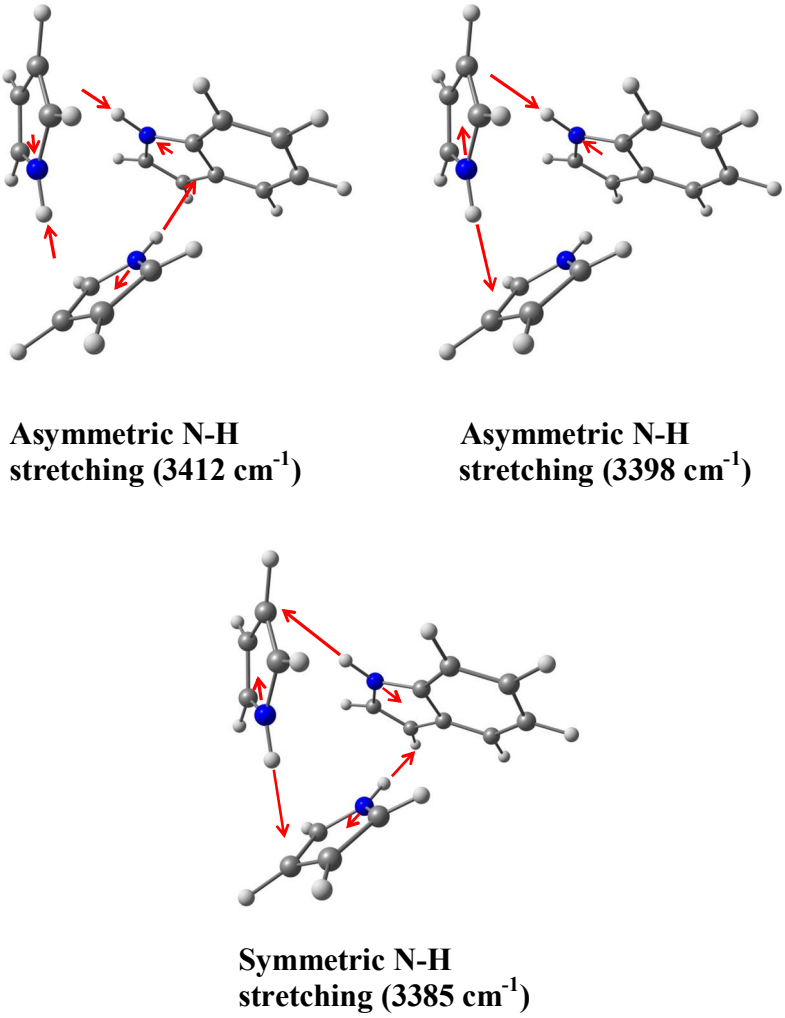

Figure. 6.12. Normal modes of two asymmetric and one symmetric N-H stretches in IP2-1 structure of indole···$(pyrrole)_2$ trimer.

indole···$(pyrrole)_2$ trimer studied in this work, the in-phase stretching of the N-H bonds gives weakly allowed IR active band at 3376 cm^{-1} because of the asymmetric structure of the trimer. Theoretical calculation shown in Table 6.9 indeed shows that the IR band due to the in-phase stretching in indole···$(pyrrole)_2$ trimer is weak and the corresponding Raman band is very strong. Two other strong IR bands of comparable intensity at 3389 and 3408 cm^{-1} shown in Figure 6.9b appear due to splitting of the doubly degenerate out-of-phase N-H stretching vibrations in the trimer. Theoretical calculation also shows that IR intensity of these bands is very high while the corresponding Raman intensity is very low. It is worth mentioning here that the observed N-H stretching frequencies of indole···$(pyrrole)_2$ trimer

(3376, 3389 cm^{-1}) are very similar to those of pyrrole trimer (3376, 3393 cm^{-1}) reported by Dauster et al.[264]

The normal modes of the symmetric and two asymmetric N-H stretches of the IP2-1 structure of indole···$(pyrrole)_2$ trimer have been shown in Figure 6.12. The observed Davydov splitting values between the symmetric (3376 cm^{-1}) and the two asymmetric N-H stretching bands (3389 and 3408 cm^{-1}) are 13 and 32 cm^{-1}. The corresponding theoretical values at the M05-2X/cc-pVTZ level are 13 and 27 cm^{-1}. This indicates an excellent agreement between experimental and theoretical results. Similar experimental evidence has also been obtained in case of the asymmetric cyclic structures of $(CH_3OH)_3$ and $(H_2O)_3$.[450,453]

Finally we would like to point out the theoretical dipole moment values of the trimers listed in Table 6.8, which can provide additional clue about their structures. Exactly zero dipole moment obtained for $(pyrrole)_3$ indicates towards its symmetric cyclic structure. On the other hand, non-zero dipole moment of indole···$(pyrrole)_2$ trimer supports in favor of its asymmetric cyclic structure.

6.2.2.2.2. NBO analysis

NBO analysis could be a very useful tool to shed light on the symmetry and asymmetry in the hydrogen bonded cyclic structures of the complexes as it provides quantitative information about the strength of the individual hydrogen bond present there. In the case of the N-H···π hydrogen bonded cyclic trimer studied here, the hydrogen bond interaction occurs through the delocalization of the π-orbitals of the hydrogen bond acceptor (pyrrole ring) over the antibonding orbital of the hydrogen bond donor (N-H group). The interactions of the donor-acceptor natural bond orbitals (NBOs) through charge delocalization in the IP2-1 structure of indole···$(pyrrole)_2$ trimer calculated at the M05-2X/cc-pVTZ level of theory have been shown in Figure 6.13. As the structure of the trimer is cyclic, each monomer unit acts there as both hydrogen bond donor and acceptor. It has been found that each of the anti-bonding N-H orbitals (σ^*_{NH}) interact with two π-orbitals of each pyrrole unit. Specific NBOs involved in individual hydrogen bonding interaction as well as corresponding NBO delocalization energy have also been provided with the NBO pictures in Figure 6.13. The NBO delocalization energy, which is a measure of the strength of the hydrogen bonding interaction, is determined

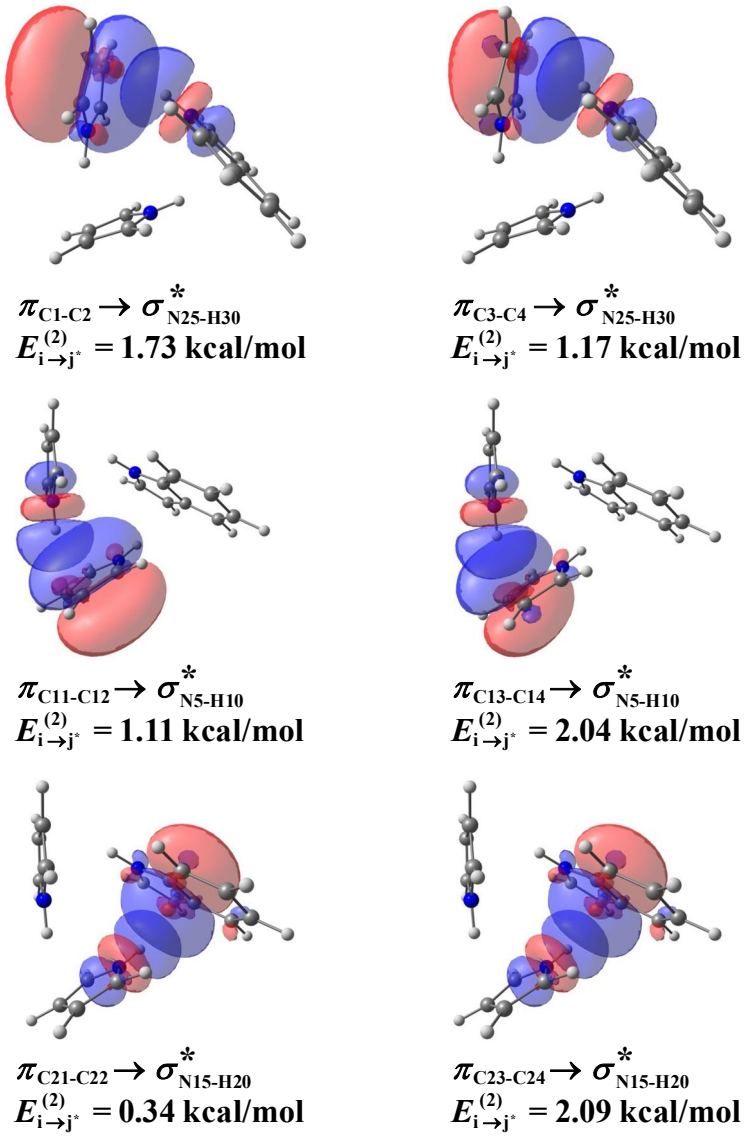

Figure 6.13. Natural bond orbitals of the IP2-1 structure of indole···(pyrrole)$_2$ trimer. The NBO calculations have been performed at the M052X/cc-pVTZ level of theory. For atom numbering, refer to Figure 6.11.

by the second order perturbative energy, $E^{(2)}_{i\rightarrow j^*}$, where i and j* stand for an acceptor and a donor orbital, respectively. Detailed comparison of various NBO parameters of the IP2-1 structure of the indole···(pyrrole)$_2$ trimer and (pyrrole)$_3$ has been shown in Table 6.10. The parameter Δq(H) denotes atomic charges on the H atom of the hydrogen bond donor group N-H while electron occupancies in the π-orbitals of the pyrrole units as well as the antibonding

orbitals of the hydrogen-bond donor N-H are denoted by δ(π), and δ(σ^*_{NH}), respectively. In the IP2-1 structure of the indole···(pyrrole)$_2$ trimer, $E^{(2)}_{i\rightarrow j^*}$ values for the three N-H···π

Table 6.10: Selected NBO Parameters of IP2-1 structure of indole···(pyrrole)$_2$ trimer and (pyrrole)$_3$ calculated at the M05-2X/cc-pVTZ Level of theory[a]

	IP2-1	**(pyrrole)$_3$**
$\Delta q(H)_{pyrrole(A)}$	0.0412	0.0406
$\Delta q(H)_{pyrrole(B)}$	0.0327	0.0406
$\Delta q(H)_{pyrrole(C)}$	0.0390	0.0406
δ($\pi_{C1\text{-}C2}$)	1.8462	1.8470
δ($\pi_{C3\text{-}C4}$)	1.8477	1.8471
δ($\pi_{C11\text{-}C12}$)	1.8434	1.8470
δ($\pi_{C13\text{-}C14}$)	1.8517	1.8471
δ($\pi_{C21\text{-}C22}$)	1.6062	1.8470
δ($\pi_{C23\text{-}C24}$)	1.8611	1.8471
δ($\sigma^*_{N5\text{-}H10}$)	0.0235	0.0234
δ($\sigma^*_{N15\text{-}H20}$)	0.0227	0.0234
δ($\sigma^*_{N25\text{-}H30}$)	0.0246	0.0234
$E^{(2)}_{i\rightarrow j^*}$ ($\pi_{pyrrole(A)}\rightarrow \sigma^*_{N25-H30}$)	2.90 (1.73+1.17)	3.03 (1.49+1.54)
$E^{(2)}_{i\rightarrow j^*}$ ($\pi_{pyrrole(B)} \rightarrow \sigma^*_{N5\text{-}H10}$)	3.15 (1.11+2.04)	3.04 (1.50+1.54)
$E^{(2)}_{i\rightarrow j^*}$ ($\pi_{pyrrole(C)}\rightarrow \sigma^*_{N15\text{-}H20}$)	2.43 (2.09+0.34)	3.04 (1.50+1.54)

[a] $E^{(2)}_{i\rightarrow j^*}$ is in kcal/mol; all other values are in a.u. For atom numbering, refer to Figure 6.11.

interactions i.e. N_5-H_{10}···$\pi_{pyrrole(B)}$, N_{25}-H_{30}···$\pi_{pyrrole(A)}$, and N_{15}-H_{20}···$\pi_{pyrrole(C)}$ are 3.15, 2.90, and 2.43 kcal/mol, respectively. On the other hand, $E^{(2)}_{i\rightarrow j^*}$ values for the three N-H···π

interactions in $(pyrrole)_3$ are same (3.04 kcal/mol). These $E^{(2)}_{i\rightarrow j^*}$ values in both indole···$(pyrrole)_2$ trimer and $(pyrrole)_3$ are exactly in the same line with the relevant geometrical parameters (N-H···π, Δr_{N-H}), listed in Table 6.8, which are discussed in the section 6.2.2.2.1. Thus the NBO analysis reconfirms the asymmetry and symmetry in the cyclic structures of the indole···$(pyrrole)_2$ trimer and $(pyrrole)_3$, respectively.

6.2.2.2.3. EDA of the trimer

The N-H···π bound complexes fall in the category of the mixed complexes, which comprise of comparable amount of electrostatic as well as dispersion interactions as described in the S22 and S66 database of the benchmark calculations.[214,275] For the quantitative determination of these interactions energies in the trimer studied here, we have used LMO-EDA procedure described in the computational section of the methods in chapter 2. EDA of the IP2-1 structure of the indole···$(pyrrole)_2$ trimer and $(pyrrole)_3$ have been performed at the M05-2X/cc-pVDZ level of theory and different components of the total interaction energy have been listed in Table 6.11. The data shown in the table reveal that the contributions of various components of the total interaction energy in both IP2-1 and $(pyrrole)_3$ are similar. The ratio of the dispersion to the electrostatic interactions (ΔE_{disp} /ΔE_{ele}) in the N-H···π bound trimer studied in this work is 1.33, which indeed proves that this trimer belongs to the class of mixed complexes.

Table 6.11. Decomposition of the interaction energies (kcal/mol) of the trimer calculated at the M05-2X/cc-pVDZ level of theory

	ΔE_{ele}	ΔE_{ex}	ΔE_{rep}	ΔE_{pol}	ΔE_{disp}	ΔE_{tot}	$\Delta E_{disp}/\Delta E_{ele}$
IP2-1	-21.86	-13.54	52.13	-8.04	-29.03	-20.34	1.33
$(pyrrole)_3$	-22.20	-13.84	50.72	-8.14	-26.70	-20.17	1.20

6.2.2.2.4. Intermolecular Vibrations of the trimer

We have calculated the vibrational frequencies of the indole···$(pyrrole)_2$ trimer in the S_1 state at the CIS/6-311++G(d,p) level of theory for the assignment of the low frequency intermolecular vibronic bands of the trimer observed in the R2PI spectrum shown in Figure 6.8b and 6.8c. In the case of a trimer, twelve intermolecular vibrations are predicted form theory. Table 6.12 lists the experimentally observed as well as theoretical intermolecular vibrations of the trimer and the assignments of the observed low frequency vibrations in the R2PI spectrum. It is apparent from the table that the low frequency vibronic bands observed in the R2PI spectrum shown in Figure 6.8b and 6.8c could tentatively be assigned to the fundamental transitions of seven intermolecular modes in the trimer. The agreement between the observed and theoretical intermolecular vibrational frequencies is quite remarkable. The observation of these low frequency vibronic bands in the R2PI spectrum indicates that there is a change in the geometry of the trimer along these intermolecular coordinates upon electronic excitation.

Table 6.12. Experimental and CIS/6-311++G^{**} level calculated S_1 state intermolecular vibrational frequencies (in cm^{-1}) of the IP2-1 structure of indole···$(pyrrole)_2$ trimer.

Indole··$(pyrrole)_2$ trimer		Assignments
Observed	Calculated	
	16	
	21	
23	24	α
28	31	β
36	35	γ
40	50	δ
51	52	θ
64	59	ϕ
	70	
	74	
	76	
85	95	σ

6.3. Biological relevance of the observed dimeric and trimeric structures

As already mentioned in the introduction section that aromatic-aromatic interactions at the dimieric, trimeric, and higher order level present in the side chains of the proteins enormously contribute to the stability of its structures while the hydrogen bonding interaction between the –NH and –C=O groups in the backbone provides its specific folding pattern. The observed dimeric structure of indole and imidazole models the aromatic interactions present in the side chains of tryptophan and histidine residues in the proteins. It has been found that the specific V-shaped structure of indole…imidazole dimer is indeed present in a non-fluorescent flavoprotein (PDB ID: 1NFP). Similarly the cyclic trimeric structure like the observed indole…$(pyrrole)_2$ one is present in many proteins and one of them is L-ribulose-5-phosphate 4-epimerase (PDB ID: 1JDI) where the interaction is among tryptophan and two phenylalanine residues.

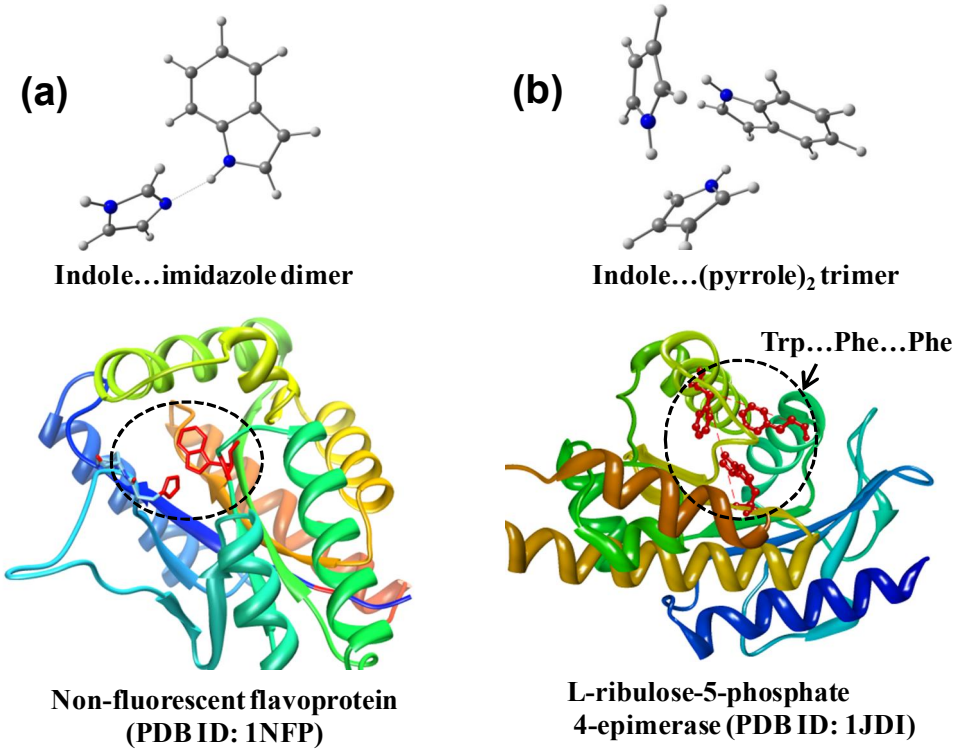

Figure 6.14. (a) A specific V-shaped structure of indole…imidazole dimer has a close structural resemblance with those present between tryptophan and histidine residues in a nonfluorescent flavoprotein (PDB ID: 1NFP) and (b) indole…$(pyrrole)_2$ cyclic trimer has structural similarly with the trimeric structure containing tryptophan and two phenylalanine residues in the L-ribulose-5-phosphate 4-epimerase (PDB ID: 1JDI).

6.4. Conclusions

In this work, aromatic-aromatic interactions present in the side chains of the aromatic amino acid residues have been investigated by studying indole…imidazole dimer and indole…$(pyrrole)_2$ trimer using R2PI, UV-UV, and IR-UV double resonance spectroscopic techniques combined with quantum chemistry calculations. The R2PI spectra of the dimer as well as trimer have been measured by electronic excitation of the indole moiety. It has been found that the red-shift in the band origin of the indole…imidazole dimer with respect to that of the indole monomer is 307 cm^{-1} while the same for indole…$(pyrrole)_2$ trimer is 136 cm^{-1}. In the case of both the dimer and trimer, presence of only one isomer in the experiment has been confirmed by UV-UV hole-burning spectroscopy. The R2PI spectra of the indole…imidazole dimer as well as indole…$(pyrrole)_2$ trimer exhibit a few Franck-Condon active low frequency intermolecular vibrations. This observation indicates that there are significant changes in the geometries of the dimer and trimer in the S_1 state compared to those in the S_0 state after electronic excitation. The comparison of the RIDIR spectra with the theoretical IR spectra of different isomeric structures confirms that the observed dimer has a V-shaped structure primarily held by strong N-H···N hydrogen bond and the trimer has a triangular asymmetric cyclic structure. The stability of the dimer is governed by subtle balance among C-H···π, weakly present π-stacking and strong hydrogen bonding interactions. This dimer falls in the category of the "*special class of mixed complex*" which comprises of strong hydrogen bonding as well as significant amount of dispersion dominated interactions. The observed trimer is stabilized by three N-H···π and one C-H···π interactions. The current spectroscopic investigation on the indole···imidazole dimer and indole…$(pyrrole)_2$ trimer has important biological significance as it mimics the aromatic interactions present in the aromatic side chains of the amino acid residues in proteins. The present study on the indole…imidazole dimer has also immense pharmaceutical significance as it provides molecular level understanding about the binding motifs of the imidazole drugs with proteins.

Concluding remarks

In summary, we have investigated the structures of complexes of indole with pyridine, furan, thiophene, HFB, imidazole and pyrrole in a supersonic jet by employing R2PI, IR-UV, and UV-UV double resonance spectroscopic techniques combined with quantum chemistry calculations. We have investigated the interplay between conventional hydrogen bonding and dispersion interactions from the study of indole…pyridine dimer while competition between conventional hydrogen bonding and π-hydrogen bonding interactions has been explored from the study of indole…furan and indole…thiophene dimers. We have reported observation of an exclusively π-stacked structure of indole…HFB dimer by suppressing the possibility of formation of π-hydrogen bonded isomer. Finally, we have described the study of indole…imidazole dimer and indole…$(pyrrole)_2$ trimer, which mimic the aromatic-aromatic interactions (dimeric as well as trimeric) in the aromatic side chains of proteins.

We have reported the interplay between conventional hydrogen bonding and dispersion interactions from the study of complexes of indole and pyridine dimer. The indole…pyridine dimer has a V-shaped structure stabilized by conventional hydrogen bonding (N-H…N) as well as CH…π and π…π stacking interactions whereas the $(indole)_2$…pyridine trimer has a cyclic structure with N-H…N, N-H…π, C-H…N, and, C-H…π interactions. We have introduced a new nomenclature "*special class of mixed complex*" to represent the presence of conventional hydrogen bonding and dispersion interactions in indole…pyridine dimer. We emphasize that this new category of mixed complex should be incorporated in the computational database of non-covalent interactions. The study of the "*special class of mixed complex*" indeed gives the understanding about the structural motifs of biomolecules and materials. Thus deeper insight of the structure of this class of mixed complex may shed the light on improved drug design and advanced functional material synthesis. Study of this class of complex is extremely challenging from both experimental and theoretical point of view. In future, a few more complexes of this category are required to study for better understanding of this "*special class of mixed complex*" using various gas phase spectroscopic techniques as well as high level *ab initio* calculations.

The competition between conventional hydrogen bonding and π-hydrogen bonding interactions has been reported by studying the indole...furan and indole…thiophene dimer.

The indole…furan and indole…thiophene dimers have a tilted T-shaped N-H···π hydrogen bonded structure. In the case of both dimers, there is a possibility of conventional hydrogen bonded structures with N-H…O and N-H…S interactions. But exclusively N-H…π bound structure has been observed in the case of both the dimers. Thus the study demonstrates that π-hydrogen bonding can win over conventional hydrogen bonding interaction. The results obtained from the study of indole…furan dimer and indole…thiophene dimer also manifest the effect of heteroatoms present in the acceptors on the strength of the π-hydrogen bonding interactions. Our spectroscopic investigation demonstrates that five membered aromatic heterocycles in contrast to pyridine, a six membered heterocycle, are favorable π-hydrogen bond acceptors. It has also been shown that thiophene is a better π-hydrogen bond acceptor than furan.

We have reported exclusively π-stacked heterodimer of indole and HFB. The observed π-stacked dimer has a unique configuration where the center of the HFB unit is aligned with the center of the shared bond of the indole moiety. This π-stacking interaction which is ubiquitous between aromatic residues (tryptophan and phenylalanine) in proteins has not been observed earlier in the gas phase experiment by studying indole...benzene dimer because the N-H...π hydrogen bonded configuration is always the preferred one. The knowledge on this specific aromatic complex can be helpful in designing unnatural proteins having strong π-stacking interaction between tryptophan and phenylalanine residues. The result also demonstrates that HFB is a very efficient building block for π-stacking interaction. Phenyl-perfluorophenyl stacking motif is widely used as a supramolecular synthon in crystal engineering leading to infinite columnar structures with less parallel displacement between phenyl and perfluorophenyl units.

Aromatic-aromatic interactions present in the side chains of the aromatic amino acid residues have been investigated by studying indole…imidazole dimer and indole…$(pyrrole)_2$ trimer. The dimer has a V-shaped structure primarily held by strong N-H···N hydrogen bond and the trimer has a triangular asymmetric cyclic structure. The dimer is governed by the subtle balance among C-H···π, weakly present π-stacking and strong hydrogen bonding interactions. This dimer falls in the category of the "*special class of mixed complex*" which comprises of strong hydrogen bonding as well as significant amount of dispersion dominated interactions.

The observed trimer is stabilized by three N-H···π and one C-H···π interactions. The study of indole···imidazole dimer and indole…$(pyrrole)_2$ trimer has important biological significance as it mimics the aromatic interactions present in the aromatic side chains of the amino acid residues in proteins. The study on the indole…imidazole dimer has also immense pharmaceutical significance as it provides molecular level understanding about the binding motifs of the imidazole drugs with proteins.

Future work

In our lab, we have performed R2PI spectra to get the information about the vibrational levels present in the excited electronic state of the complexes of indole with pyridine, furan, thiophene, hexafluorobenzene and imidazole. However, the assignment of the low frequency intermolecular modes present in the electronic spectra of the non-covalently bonded complexes was very difficult due to inability to perform excited state calculations. At the same time, the problems may arise to assign the geometry obtained in the experiment when more than one isomer has comparable binding energies and vibrational frequencies. Such as in the case of indole...furan dimer and indole...thiophene dimer, the binding energies as well as N-H stretching frequencies of isomeric structures are very close. In such cases the Franck–Condon (FC) simulated electronic spectra of the isomeric structures can be computed and compared with the experimental electronic spectra. Hence Franck-Condon simulation can be performed to confirm the observed structure in the experiment.

In case of indole...furan dimer and indole...thiophene dimer, the analysis of the results has been made on the basis of calculations performed using dispersion corrected density functional theory (DFT-D). The results were matched very well with experimental observation. But at this reported level of B97-D level of theory, the energy difference between the HB structure and the T′ structure in case of indole...furan dimer is not too large and also the difference in the N-H vibrational frequencies. Thus higher level calculation using wave function theory (SCSL-MP2, etc) can be performed to compare the theoretical results with the experimental results so that we can get the much accurate information about the geometry obtained in the experiment.

We have used a standard method to determine the geometrical structure present in the experiment. We have compared the experimentally observed anharmonic vibrational frequencies with theoretically calculated vibrational frequencies using scaling factors. But it has certain limitations depending upon the levels of theory applied for the frequency calculations. Hence, the anharmonic vibrational frequencies can be theoretically calculated to compare with experimentally observed frequencies to identify the geometrical structure and to get the much relevant information about the vibrations present in the experimentally observed isomer.

In case of indole...hexafluorobenzene dimer, we have observed exclusively π-stacked dimer, where the center of the HFB unit is aligned with the center of the shared bond of the indole moiety. This dimer can be the building block of co-crystal of indole and hexefluorobenzene having very less lateral displacement. In future, the crystals can be synthesized taking appropriate molar concentration of parent molecules using multiple heating and cooling processes. These crystals are organized as an array of molecules arranged in a well defined manner. Thus the growth of the crystals can be monitored in a supersonic jet by the stepwise formation of higher order clusters such trimer, tetramer. Thus the structure of trimer, tetramer and higher order cluster can be studied in a supersonic jet. But it may possible that the packing motif of the crystal structure is probably not the most stable structure of clusters of the same size produced in a supersonic jet due to cooperative effects.

We have reported exclusively π-stacked heterodimer of indole and hexafluorobenzene whereas Biswal et al have reported tilted T-shaped isomer in case of indole…benzene dimer from IR-UV double resonance spectroscopy combined with quantum chemical calculations.[16,290] In future, it will be interesting to experimentally observe the change in structure of the dimer of indole and fluorinated benzene with the stepwise fluorination of benzene moiety. The result will shed extra light on the competition between π-hydrogen bonding and π-π stacking interactions.

We have theoretically calculated the binding energies of different isomers of complexes using quantum chemistry calculations. In future, it will be interesting to experimentally determination the dissociation energies of neutral and ionic molecule using photoionization-fragmentation spectroscopy. Figure 7.1a shows the schematic diagram of photoionization-fragmentation spectroscopy. For the calculation of the dissociation energy of the ionic dimer ($\Delta E_{(A...B)^+}$), first the adiabatic ionization energy (AIE) has been obtained by measuring the ion current in the ionic dimer $(A…B)^+$ mass channel with the variation of the two-photon energies. Figure 7.1b shows the ion spectrum measured by the varying the two-photon energies, where the ion current increases when the two-photon energy is more than AIE. Thus the value in terms of two-photon energy corresponding to sudden increase of the ion current in spectrum gives the adiabatic ionization energy (AIE) of the ionic dimer. After that the

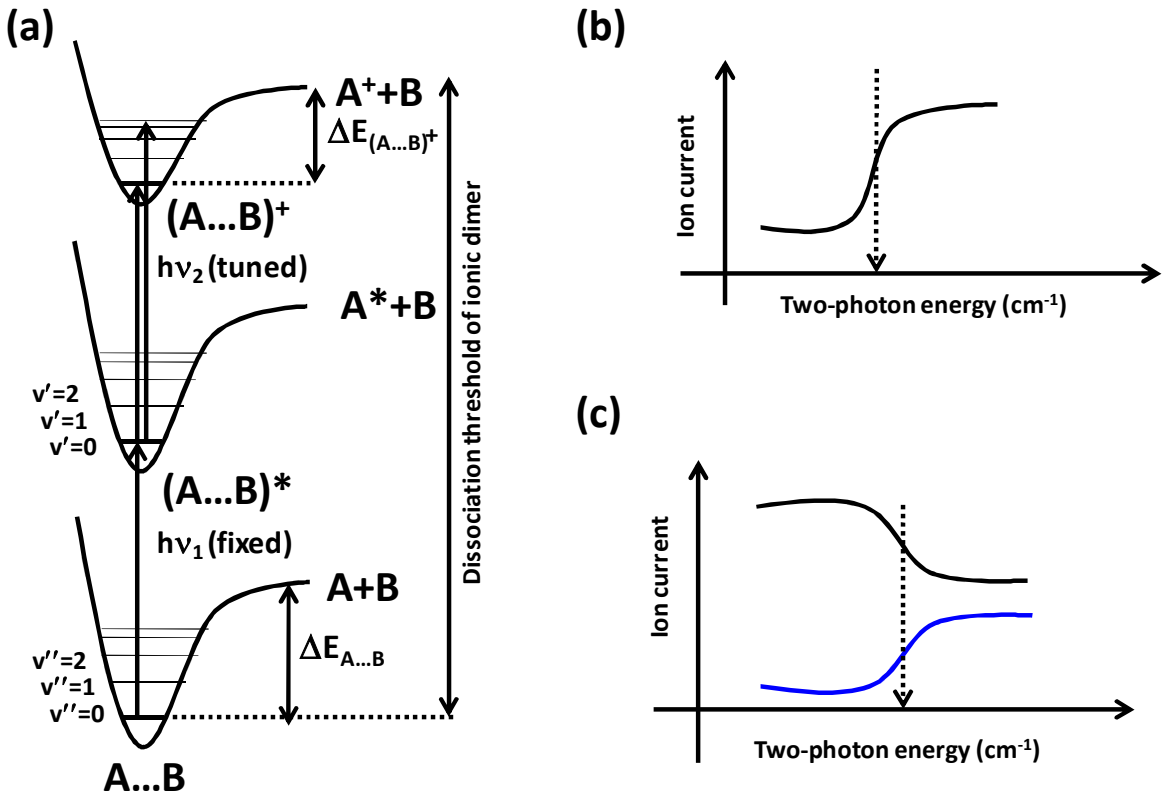

Figure 7.1 Schematic diagram of (a) photoionization-fragmentation spectroscopy, (b) Ion spectrum measured varying the two-photon energies (the arrow in the spectrum corresponds to the adiabatic ionization energy of the ionic dimer) and (c) Threshold ion spectra measured by varying the two-photon energies (black and blue show the threshold ion spectra in the ionic dimer and monomer mass channels, respectively. The arrow in the spectra corresponds to dissociation threshold of the ionic dimer.)

photoionization-fragmentation spectroscopy can be performed to determine the dissociation threshold of the ionic dimer. Here, the threshold ion current of parent molecule and fragmented (daughter) molecules are measured as a function of two-photon energies given by the laser source. The extra energy above dissociation threshold of parent molecule $(A...B)^+$ may lead to the dissociation of the parent molecule $(A...B)^+$ and hence $(A...B)^+$ as well as A^+ forms. The threshold ion current of different masses are recorded in the two different mass channels by varying the two-photon energies provided to the molecule. Figure 7.1c shows the schematic of the threshold ion spectra of ionic dimer measured above the AIE of the dimer. If a certain level of dissociation threshold of the parent molecule $(A…B)^+$ is fixed as a detection

limit, we can measure two-photon energy to reach the particular dissociation threshold of the ionic dimer. At this dissociation threshold of the parent molecule $(A…B)^+$, the ion current in dimer mass channel decreases rapidly whereas the ion current in monomer mass channel increases. Now the difference of dissociation threshold and adiabatic ionization energy (AIE) of the ionic dimer gives the dissociation energy of the ionic dimer. Next, the dissociation energy of the neutral dimer can be measured from the difference of the dissociation threshold of the ionic dimer and energy required for the process $A+B \rightarrow A^+ + B$, which is clear from the schematic diagram presented in Figure 7.1a. The value corresponding to the later process ($A+B \rightarrow A^+ + B$) can be comparable to the adiabatic ionization energy (AIE) of monomer A if the A as well as A^+ are in the ground vibration state after dissociation.

Another way to calculate the adiabatic ionization energy (AIE) is mass analysed threshold ionization (MATI).[288,437,459] The adiabatic ionization energies of dimer and monomer can be measured using mass analyzed threshold ionization (MATI). This method involves detection of zero kinetic energy photoelectron (ZEKE) ions.[460-461] One of the major advantages of MATI over ZEKE is that it provides mass information. In the MATI experiments, the prompt ions, ZEKE electrons, and Rydberg neutrals are formed simultaneously. About few ns (50 ns) after the occurrence of the laser pulses, (ZEKE electrons are gone) and a pulsed electric field of nearly -1.0 V/cm is switched on to reject the prompt ions. After few microseconds (8-10 microseconds) later, a second pulsed electric field of nearly +700 V/cm is applied to field-ionize the Rydberg neutrals. These threshold (MATI) ions are then accelerated and detected by an ion detector.

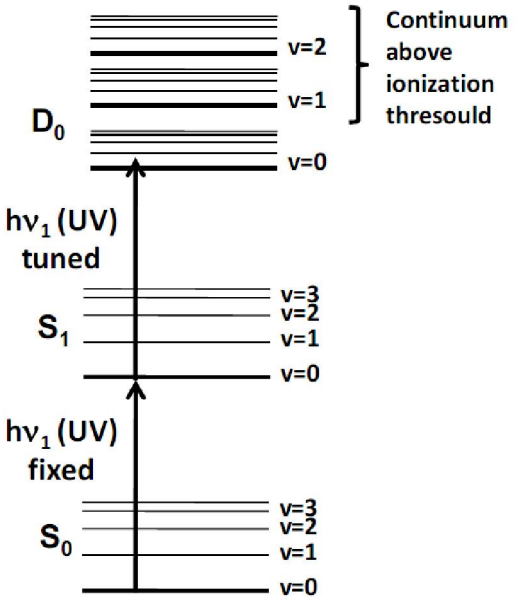

Figure 7.2 Schematic diagram of mass analyzed threshold ionization (MATI) spectroscopy

Figure 7.2 shows the schematic diagram of MATI technique. In this technique, the molecules

are photo-excited to a Rydberg state (high n).[461] The wavelength of first laser is fixed in resonance with the energy of an intermediate state and the wavelength of second laser energy is tuned to the Rydberg manifold of the molecule. The threshold ion spectra of the complexes or monomer have been recorded by fixing the energy of the first laser frequency at origin band of the dimer or monomer while varying the energy of the second laser in the range of high Rydberg states of multiple ionization thresholds. The threshold ion current in monomer as well as complex mass channel has been measured as a function of two-photon energies given by the laser source. The first peak in the spectrum corresponds to the adiabatic ionization energies of complexes or monomer.

Finally, the comparison of the experimental binding energies with theoretical binding energies of possible isomers can give much more confidence regarding the identification of experimentally observed isomers.

References

(1) Pimentel, G. C.; McClellan., A. L. *The Hydrogen Bond*; W. H. Freeman, San Francisco 1960.

(2) Felker, P. M. *J. Phys. Chem.* **1992**, *96*, 7844.

(3) Ebata, T.; Watanabe, T.; Mikami, N. *J. Phys. Chem.* **1995**, *99*, 5761.

(4) Weichert, A.; Riehn, C.; Brutschy, B. *J. Phys. Chem. A* **2001**, *105*, 5679.

(5) Hobza, P.; Riehn, C.; Weichert, A.; Brutschy, B. *Chem. Phys.* **2002**, *283*, 331.

(6) Kolář, M.; Hobza, P. *J. Phys. Chem. A* **2007**, *111*, 5851.

(7) Brause, R.; Santa, M.; Schmitt, M.; Kleinermanns, K. *ChemPhysChem* **2007**, *8*, 1394.

(8) Lee, H. M.; Kumar, A.; Kolaski, M.; Kim, D. Y.; Lee, E. C.; Min, S. K.; Park, M.; Choi, Y. C.; Kim, K. S. *Phys. Chem. Chem. Phys.* **2010**, *12*, 6278.

(9) Kumar, S.; Biswas, P.; Kaul, I.; Das, A. *J. Phys. Chem. A* **2011**, *115*, 7461.

(10) Hill, J. G.; Das, A. *Phys. Chem. Chem. Phys.* **2014**, *16*, 11754.

(11) Müller-Dethlefs, K.; Hobza, P. *Chem. Rev. (Washington, DC, United States)* **2000**, *100*, 143.

(12) Dykstra, C. E.; Lisy, J. M. *J. Mol. Struct.: THEOCHEM* **2000**, *500*, 375.

(13) Kumar, S.; Pande, V.; Das, A. *J. Phys. Chem. A* **2012**, *116*, 1368.

(14) Kumar, S.; Das, A. *J. Chem. Phys.* **2012**, *137*, 094309/1.

(15) Nyadong, L.; Hohenstein, E. G.; Galhena, A.; Lane, A. L.; Kubanek, J.; Sherrill, C. D.; Fernández, F. M. *Anal. Bioanal. Chem.* **2009**, *394*, 245.

(16) Kumar, S.; Das, A. *J. Chem. Phys.* **2013**, *139*, 104311.

(17) Kumar, S.; Mukherjee, A.; Das, A. *J. Phys. Chem. A* **2012**, *116*, 11573.

(18) Kumar, S.; Das, A. *J. Chem. Phys.* **2012**, *136*, 174302/1.

(19) Burley, S. K.; Petsko, G. A. *Science (Washington, D. C., 1883-)* **1985**, *229*, 23.

(20) Lanzarotti, E.; Biekofsky, R. R.; Estrin, D. o. A.; Marti, M. A.; Turjanski, A. n. G. *J. Chem. Inf. Model.* **2011**, *51*, 1623.

(21) Steiner, T.; Koellner, G. *J. Mol. Biol.* **2001**, *305*, 535.

(22) Geim, A. K.; Dubonos, S. V.; Grigorieva, I. V.; Novoselov, K. S.; Zhukov, A. A.; Shapoval, S. Y. *Nat. Mater.* **2003**, *2*, 461.

(23) Autumn, K.; Sitti, M.; Liang, Y. A.; Peattie, A. M.; Hansen, W. R.; Sponberg, S.; Kenny, T. W.; Fearing, R.; Israelachvili, J. N.; Full, R. J. *Proc. Natl. Acad. Sci. U. S. A.* **2002**, *99*, 12252.

(24) Riley, K. E.; Hobza, P. *Wiley Interdisciplinary Reviews: Computational Molecular Science* **2011**, *1*, 3.

(25) Chen, B.; Ivanov, I.; Klein, M. L.; Parrinello, M. *Phys. Rev. Lett.* **2003**, *91*, 215503.

(26) Černý, J.; Hobza, P. *Phys. Chem. Chem. Phys.* **2007**, *9*, 5291.

(27) Watson, J. D.; Baker, T. A. *Molecular Biology of the Gene*; Pearson education, Inc. , 2006.

(28) Watson, J. D.; Crick, F. H. C. *Nature* **1953**, *171*, 737.

(29) Richmond, T. J.; Davey, C. A. *Nature* **2003**, *423*, 145.

(30) Etter, M. C. *J. Phys. Chem.* **1991**, *95*, 4601.

(31) Steiner, T.; Saenger, W. *Acta Crystallogr., Sect. B: Struct. Sci.* **1994**, *B50*, 348.

(32) Rablen, P. R.; Lockman, J. W.; Jorgensen, W. L. *J. Phys. Chem. A* **1998**, *102*, 3782.

(33) Allen, F. H.; Samuel Motherwell, W. D.; Raithby, P. R.; Shields, G. P.; Taylor, R. *New J. Chem.* **1999**, *23*, 25.

(34) Gozzo, F. *J. Mol. Catal. A: Chem.* **2001**, *171*, 1.

(35) Fackler, J. P., Jr. *Inorg. Chem.* **2002**, *41*, 6959.

(36) Kakiuchi, F.; Chatani, N. *Adv. Synth. Catal.* **2003**, *345*, 1077.

(37) Bergman, R. G. *Nature (London, U. K.)* **2007**, *446*, 391.

(38) Nishio, M.; Umezawa, Y.; Honda, K.; Tsuboyama, S.; Suezawa, H. *CrystEngComm* **2009**, *11*, 1757.

(39) Takahashi, O.; Kohno, Y.; Nishio, M. *Chem. Rev. (Washington, DC, U. S.)* **2010**, *110*, 6049.

(40) Auvil, T. J.; Schafer, A. G.; Mattson, A. E. *Eur. J. Org. Chem.* **2014**, *2014*, n/a.

(41) Lehn, J.-M. *Supramolecular Chemistry: Concepts and Perspectives*; John Wiley & Sons, New York, 1996.

(42) Abraham, R. J.; Eivazi, F.; Pearson, H.; Smith, K. M. *J. Chem. Soc., Chem. Commun.***1976**, 699.

(43) Deng, X.; Xu, X.; Lai, Y.; He, B.; Gu, Z. *J. Biomed. Nanotechnol.* **2013**, *9*, 1336.

(44) Shi, Y.; van Steenbergen, M. J.; Teunissen, E. A.; Novo, L.; Gradmann, S.; Baldus, M.; van Nostrum, C. F.; Hennink, W. E. *Biomacromolecules* **2013**, *14*, 1826.

(45) Liu, Y.; Liu, B.-Y.; Hao, P.; Li, X.; Li, Y.-X.; Wang, J.-F. *Proteins: Struct., Funct., Bioinf.***2013**, *81*, 945.

(46) Yusuff, N.; Dore, M.; Joud, C.; Visser, M.; Springer, C.; Xie, X.; Herlihy, K.; Porter, D.; Toure, B. B. *ACS Med. Chem. Lett.* **2012**, *3*, 579.

(47) Frank, N. L.; Baldridge, K. K.; Gantzel, P.; Siegel, J. S. *Tetrahedron Lett.* **1995**, *36*, 4389.

(48) Nagel, N.; Nather, C.; Bock, H. *Acta Crystallogr., Sect. C: Cryst. Struct. Commun.* **1997**, *53*, 79.

(49) Hancock, K. S. B.; Steed, J. W. *Chem. Commun. (Cambridge, U. K.)* **1998**, 1409.

(50) Sharma, C. V. K.; Panneerselvam, K.; Pilati, T.; Desiraju, G. R. *J. Chem. Soc., Chem. Commun.* **1992**, 832.

(51) Lesniewska, B.; Jebors, S.; Coleman, A. W.; Suwinska, K. *Nat. Prod. Commun.* **2012**, *7*, 327.

(52) Srikrishnan, T.; Parthasarathy, R. *Nature (London)* **1976**, *264*, 379.

(53) Ossola, F.; Tomasin, P.; Benetollo, F.; Foresti, E.; Vigato, P. A. *Inorg. Chim. Acta* **2003**, *353*, 292.

(54) Muktha, B.; Srinivas, O.; Amresh, M. R.; Row, T. N. G.; Jayaraman, N.; Sekar, K. *Carbohydr. Res.* **2003**, *338*, 2005.

(55) Suezawa, H.; Yoshida, T.; Ishihara, S.; Umezawa, Y.; Nishio, M. *CrystEngComm* **2003**, *5*, 514.

(56) Matsumoto, A. *Polym. J. (Tokyo, Jpn.)* **2003**, *35*, 93.

(57) Matsumoto, A.; Sada, K.; Tashiro, K.; Miyata, M.; Tsubouchi, T.; Tanaka, T.; Odani, T.; Nagahama, S.; Inoue, K.; Saragai, S.; Nakamoto, S. *Angew. Chem., Int. Ed.* **2002**, *41*, 2502.

(58) Suezawa, H.; Yoshida, T.; Hirota, M.; Takahashi, H.; Umezawa, Y.; Honda, K.; Tsuboyama, S.; Nishio, M. *J. Chem. Soc., Perkin Trans. 2* **2001**, 2053.

(59) Obulichetty, M.; Saravanabharathi, D. *Spectrochim. Acta, Part A* **2014**, *118*, 861.

(60) Davidi, I.; Semionov, A.; Eisenberg, D.; Goobes, G.; Shenhar, R. *Soft Matter* **2012**, *8*, 7393.

(61) Pietsch, M. A.; Rappe, A. K. *J. Am. Chem. Soc.* **1996**, *118*, 10908.

(62) Tanner, D.; Fitzgerald, J. A.; Phillips, B. R. *Angew. Chem., Int. Ed. Engl.* **1989**, *28*, 649.

(63) Adams, H.; Hunter, C. A.; Lawson, K. R.; Perkins, J.; Spey, S. E.; Urch, C. J.; Sanderson, J. M. *Chem. - Eur. J.* **2001**, *7*, 4863.

(64) Zhang, W.; Fukushima, T.; Aida, T.; John Wiley & Sons Ltd.: 2012; Vol. 8, p 3791.

(65) Bloom, J. W. G.; Wheeler, S. E. *Angew. Chem., Int. Ed.* **2011**, *50*, 7847.

(66) Maeda, H. *Bull. Chem. Soc. Jpn.* **2013**, *86*, 1359.

(67) Mooibroek, T. J.; Gamez, P. *Inorg. Chim. Acta* **2007**, *360*, 381.

(68) Ogoshi, T.; Hashizume, M.; Yamagishi, T.-a.; Nakamoto, Y. *Langmuir* **2010**, *26*, 3169.

(69) Sakai, N.; Mareda, J.; Vauthey, E.; Matile, S. *Chem. Commun. (Cambridge, U. K.)* **2010**, *46*, 4225.

(70) Wagner, B. D. *Phys. Chem. Chem. Phys.* **2012**, *14*, 8825.

(71) Frontera, A.; Garau, C.; Quinonero, D.; Ballester, P.; Costa, A.; Deya, P. M. *Org. Lett.* **2003**, *5*, 1135.

(72) Garozzo, D.; Gattuso, G.; Kohnke, F. H.; Malvagna, P.; Notti, A.; Occhipinti, S.; Pappalardo, S.; Parisi, M. F.; Pisagatti, I. *Tetrahedron Lett.* **2002**, *43*, 7663.

(73) Perrin, C. L.; Nielson, J. B. *Annu. Rev. Phys. Chem.* **1997**, *48*, 511.

(74) Borisover, M. D.; Graber, E. R. *Chemosphere* **1997**, *34*, 1761.

(75) Grell, J.; Bernstein, J.; Tinhofer, G. *Crystallogr. Rev.* **2002**, *8*, 1.

(76) Rozenberg, M.; Shoham, G.; Reva, I.; Fausto, R. *Spectrochim. Acta, Part A* **2004**, *60A*, 2323.

(77) Wan, L.; Chen, D.-z.; Lu, Y.-d.; Yu, X.-h. *Gaofenzi Cailiao Kexue Yu Gongcheng* **2004**, *20*, 9.

(78) Lewis, T. C.; Tocher, D. A.; Price, S. L. *Cryst. Growth Des.* **2005**, *5*, 983.

(79) Fink, S. M.; Ojala, W. H.; American Chemical Society: 2010, p CHED.

(80) Allen, F. H.; Howard, J. A. K.; Hoy, V. J.; Desiraju, G. R.; Reddy, D. S.; Wilson, C. C. *J. Am. Chem. Soc.* **1996**, *118*, 4081.

(81) Cooke, G.; Rotello, V. M. *Chem. Soc. Rev.* **2002**, *31*, 275.

(82) Nishio, M. *CrystEngComm* **2004**, *6*, 130.

(83) Sanchez, L.; Martin, N.; Guldi, D. M. *Angew. Chem., Int. Ed.* **2005**, *44*, 5374.

(84) Nishio, M. *Phys. Chem. Chem. Phys.* **2011**, *13*, 13873.

(85) Abraham, M. H. *Chem. Soc. Rev.* **1993**, *22*, 73.

(86) Pratviel, G.; Bernadou, J.; Meuminer, B. *Angew. Chem., Int. Ed. Engl.* **1995**, *34*, 746.

(87) Doherty, A. J.; Serpell, L. C.; Ponting, C. P. *Nucleic Acids Res.* **1996**, *24*, 2488.

(88) Wahl, M. C.; Sundaralingam, M. *Trends Biochem. Sci.* **1997**, *22*, 97.

(89) Gerhard, M.; Lehn, N.; Neumayer, N.; Boren, T.; Rad, R.; Schepp, W.; Miehlke, S.; Classen, M.; Prinz, C. *Proc. Natl. Acad. Sci. U. S. A.* **1999**, *96*, 12778.

(90) Kunkel, T. A.; Bebenek, K. *Annu. Rev. Biochem.* **2000**, *69*, 497.

(91) Gu, M.; Su, Z. G.; Janson, J. C. *Chromatographia* **2006**, *64*, 701.

(92) Laurence, C.; Brameld, K. A.; Graton, J.; Le Questel, J.-Y.; Renault, E. *J. Med. Chem.* **2009**, *52*, 4073.

(93) Kuhn, B.; Mohr, P.; Stahl, M. *J. Med. Chem.* **2010**, *53*, 2601.

(94) Wu, Y.-Q.; Qu, H.; Sfyroera, G.; Tzekou, A.; Kay, B. K.; Nilsson, B.; Nilsson Ekdahl, K.; Ricklin, D.; Lambris, J. D. *J. Immunol.* **2011**, *186*, 4269.

(95) Werner, A. *Justus Liebigs Annalen der Chemie* **1902**, *322*, 261.

(96) Pfeiffer, P.; Fischer, P.; Kuntner, J.; Monti, P.; Pros, Z. *Justus Liebigs Annalen der Chemie* **1913**, *398*, 137.

(97) Moore, T. S.; Winmill, T. F. *J. Chem. Soc.* **1912**, 1635.

(98) Latimer, W. M.; Rodebush, W. H. *J. Am. Chem. Soc.* **1920**, *42*, 1419.

(99) Pauling., L. *The Nature of the Chemical Bond*; Cornell University Press, Ithaca, NY 1960.

(100) Arunan, E.; Desiraju, G. R.; Klein, R. A.; Sadlej, J.; Scheiner, S.; Alkorta, I.; Clary, D. C.; Crabtree, R. H.; Dannenberg, J. J.; Hobza, P.; Kjaergaard, H. G.; Legon, A. C.; Mennucci, B.; Nesbitt, D. J. *Pure Appl. Chem.* **2011**, *83*, 1619.

(101) Nishio, M.; Umezawa, Y.; Fantini, J.; Weiss, M. S.; Chakrabarti, P. *Phys. Chem. Chem. Phys.* **2014**.

(102) Jeffrey, G. A.; Saenger, W. *Hydrogen boning in biological structure*; springer-verlag, Berlin, 1991.

(103) Jeffrey, G. A. *An Introduction to Hydrogen Bonding*; Oxford Univ Press, 1997.

(104) Desiraju, G. R.; Steiner, T. *Oxford University Press, New York,* **1999**.

(105) Kumar, S.; Das, A. *J. Chem. Phys.* **2012**, *137*, 094309.

(106) Tsuzuki, S.; Fujii, A. *Phys. Chem. Chem. Phys.* **2008**, *10*, 2584.

(107) Shibasaki, K.; Fujii, A.; Mikami, N.; Tsuzuki, S. *J. Phys. Chem. A* **2007**, *111*, 753.

(108) Akin-Ojo, O.; Wang, F. *Chem. Phys. Lett.* **2011**, *513*, 59.

(109) Barford, W.; Paiboonvorachat, N.; Yaron, D. *J. Chem. Phys.* **2011**, *134*, 234101/1.

(110) Grimme, S.; Djukic, J.-P. *Inorganic Chemistry* **2010**, *49*, 2911.

(111) Liu, R.-F.; Angyan, J. G.; Dobson, J. F. *J. Chem. Phys.* **2011**, *134*, 114106/1.

(112) Mizuno, H.; Luengo, G. S.; Rutland, M. W. *Langmuir* **2010**, *26*, 18909.

(113) Moellmann, J.; Grimme, S. *Phys. Chem. Chem. Phys.* **2010**, *12*, 8500.

(114) Swart, M.; Sola, M.; Bickelhaupt, F. M. *J. Comput. Chem.* **2011**, *32*, 1117.

(115) Becke, A. D.; Johnson, E. R. *J. Chem. Phys.* **2005**, *122*, 154104.

(116) Gonzalez, C.; Lim, E. C. *J. Phys. Chem. A* **2000**, *104*, 2953.

(117) Yamakawa, M.; Yamada, I.; Noyori, R. *Angew. Chem., Int. Ed.* **2001**, *40*, 2818.

(118) Arduini, A.; Giorgi, G.; Pochini, A.; Secchi, A.; Ugozzoli, F. *Tetrahedron* **2001**, *57*, 2411.

(119) Arduini, A.; Nachtigall, F. F.; Pochini, A.; Secchi, A.; Ugozzoli, F. *Supramolecular Chemistry* **2000**, *12*, 273.

(120) Kryger, G.; Silman, I.; Sussman, J. L. *Journal of Physiology-Paris* **1998**, *92*, 191.

(121) Niedzwiecka, A.; Marcotrigiano, J.; Stepinski, J.; Jankowska-Anyszka, M.; Wyslouch-Cieszynska, A.; Dadlez, M.; Gingras, A.-C.; Mak, P.; Darzynkiewicz, E.; Sonenberg, N. *J. Mol. Biol.* **2002**, *319*, 615.

(122) Betschmann, P.; Sahli, S.; Diederich, F.; Obst, U.; Gramlich, V. *Helvetica Chimica Acta* **2002**, *85*, 1210.

(123) Gordy, W. *J. Chem. Phys.* **1939**, *7*, 163.

(124) Allerhand, A.; Von Rague Schleyer, P. *J. Am. Chem. Soc.* **1963**, *85*, 1715.

(125) Green, R. D.; Green, R. *Hydrogen Bonding by CH groups*; Macmillan London:, 1974.

(126) DeLaat, A. M.; Ault, B. S. *J. Am. Chem. Soc.* **1987**, *109*, 4232.

(127) Wulf, O. R.; Liddel, U.; Hendricks, S. B. *J. Am. Chem. Soc.* **1936**, *58*, 2287.

(128) von R. Schleyer, P.; Trifan, D. S.; Bacskai, R. *J. Am. Chem. Soc.* **1958**, *80*, 6691.

(129) Joesten, M. D.; Schaad, L. J. *Hydrogen bonding*; M. Dekker New York, 1974.

(130) Yoshida, Z.-i.; Osawa, E. *J. Am. Chem. Soc.* **1966**, *88*, 4019.

(131) Chardin, A.; Laurence, C.; Berthelot, M. *J. Chem. Res., Synop.* **1996**, 332.

(132) Saggu, M.; Levinson, N. M.; Boxer, S. G. *J. Am. Chem. Soc.* **2012**, *134*, 18986.

(133) Huggins, M. L. *Angew. Chem., Int. Ed. Engl.* **1971**, *10*, 147.

(134) Robertson, J. M.; Woodward, I. *J. chem. Soc. London* **1936**, *1817*.

(135) Dunitz, J.; Robertson, J. *J. Chem. Soc.* **1947**, 148.

(136) Dunitz, J. D.; Harris, K. D.; Johnston, R. L.; Kariuki, B. M.; MacLean, E. J.; Psallidas, K.; Schweizer, W. B.; Tykwinski, R. R. *J. Am. Chem. Soc.* **1998**, *120*, 13274.

(137) Dunitz, J. D. *Chemistry-A European Journal* **1998**, *4*, 745.

(138) June Sutor, D. *Nature* **1962**, *195*, 68.

(139) Taylor, R.; Kennard, O. *J. Am. Chem. Soc.* **1982**, *104*, 5063.

(140) Atwood, J. L.; Hamada, F.; Robinson, K. D.; Orr, G. W.; Vincent, R. L. *Nature* **1991**, *349*, 683.

(141) Suzuki, S.; Green, P. G.; Bumgarner, R. E.; Dasgupta, S.; Goddard, W. A.; Blake, G. A. *Science* **1992**, *257*, 942.

(142) Rodham, D. A.; Suzuki, S.; Suenram, R. D.; Lovas, F. J.; Dasgupta, S.; Goddard, W. A.; Blake, G. A. *Nature* **1993**, *362*, 735.

(143) F. Malone, J.; M. Murray, C.; H. Charlton, M.; Docherty, R.; J. Lavery, A. *J. Chem. Soc., Faraday Trans.* **1997**, *93*, 3429.

(144) Braga, D.; Grepioni, F.; Desiraju, G. R. *Chem. Rev. (Washington, DC, U. S.)* **1998**, *98*, 1375.

(145) Braga, D.; Grepioni, F.; Tedesco, E. *Organometallics* **1998**, *17*, 2669.

(146) Sarkhel, S.; Desiraju, G. R. *Proteins: Struct., Funct., Genet.* **2004**, *54*, 247.

(147) Desiraju, G. R. *Angew. Chem., Int. Ed.* **1995**, *34*, 2311.

(148) Braga, D.; Grepioni, F.; Desiraju, G. R. *Chem. Rev. (Washington, DC, United States)* **1998**, *98*, 1375.

(149) Desiraju, G. R. *Acc. Chem. Res***1996**, *29*, 441.

(150) Shefter, E.; Trueblood, K. N. *Acta Crystallogr.* **1965**, *18*, 1067.

(151) Sundaralingam, M. *Acta Crystallogr.* **1966**, *21*, 495.

(152) Ramachandran, G. N.; Sasisekharan, V. *Biochimica et Biophysica Acta (BBA) - Biophysics including Photosynthesis* **1965**, *109*, 314.

(153) Ramachandran, G. N.; Sasisekharan, V.; Ramakrishnan, C. *Biochimica et Biophysica Acta (BBA) - Biophysics including Photosynthesis* **1966**, *112*, 168.

(154) McPhail, A.; Sim, G. *Chem. Commun. (London)* **1965**, 124.

(155) Baker, E.; Hubbard, R. *Prog. Biophys. Mol. Biol.* **1984**, *44*, 97.

(156) Saenger, W.; Jeffrey, G.; Springer-Verlag, Berlin: 1991.

(157) Burley, S. K.; Petsko, G. A. *J. Am. Chem. Soc.* **1986**, *108*, 7995.

(158) Burley, S. K.; Petsko, G. A. *Advances in Protein Chemistry* **1988**, *39*, 125.

(159) Hunter, C. A. *Angew. Chem., Int. Ed.* **1993**, *32*, 1584.

(160) Hunter, C. A. *Chem. Soc. Rev.* **1994**, *23*, 101.

(161) Hunter, C. A.; Sanders, J. K. M. *J. Am. Chem. Soc.* **1990**, *112*, 5525.

(162) Hunter, E. P. L.; Lias, S. G. *J. Phys. Chem. Ref. Data* **1998**, *27*, 413.

(163) Chowdhury, S.; Drew, M. G. B.; Datta, D. *Inorg. Chem. Commun.* **2003**, *6*, 1014.

(164) Lee, D.-W.; Flint, J.; Morey, T.; Dennis, D.; Partch, R.; Baney, R. *J. Pharm. Sci.* **2005**, *94*, 373.

(165) Serrano, L.; Bycroft, M.; Fersht, A. R. *J. Mol. Biol.* **1991**, *218*, 465.

(166) Bhattacharyya, R.; Samanta, U.; Chakrabarti, P. *Protein Eng.* **2002**, *15*, 91.

(167) Aravinda, S.; Shamala, N.; Das, C.; Sriranjini, A.; Karle, I. L.; Balaram, P. *J. Am. Chem. Soc.* **2003**, *125*, 5308.

(168) Aakeröy, C. B.; Champness, N. R.; Janiak, C. *CrystEngComm* **2010**, *12*, 22.

(169) Chamayou, A.-C.; Neelakantan, M.; Thalamuthu, S.; Janiak, C. *Inorg. Chim. Acta* **2011**, *365*, 447.

(170) Choe, H.-W.; Kim, Y. J.; Park, J. H.; Morizumi, T.; Pai, E. F.; Krauß, N.; Hofmann, K. P.; Scheerer, P.; Ernst, O. P. *Nature* **2011**, *471*, 651.

(171) Desiraju, G. R. *Cryst. Growth Des.* **2011**, *11*, 896.

(172) Kitaigorodsky, A. *Molecular crystals and molecules*; Elsevier, 2012; Vol. 29.

(173) Nair, K. P.; Breedveld, V.; Weck, M. *Macromolecules* **2011**, *44*, 3346.

(174) Thakur, T. S.; Kirchner, M. T.; Bläser, D.; Boese, R.; Desiraju, G. R. *CrystEngComm* **2010**, *12*, 2079.

(175) Tiekink, E. R.; Vittal, J. J.; Zaworotko, M. *Organic Crystal Engineering*; Wiley Online Library, 2010.

(176) Tiekink, E. R.; Zukerman-Schpector, J. *The importance of pi-interactions in crystal engineering: frontiers in crystal engineering*; John Wiley & Sons, 2012.

(177) Nishio, M.; Umezawa, Y.; Suezawa, H.; Tsuboyama, S. *The importance of Pi-interactions in crystal engineering: frontiers in crystal engineering* **2012**, *1*, 1.

(178) Mikami, N. *Bull. Chem. Soc. Jpn.* **1995**, *68*, 683.

(179) Gerhards, M.; Kleinermanns, K. *J. Chem. Phys.* **1995**, *103*, 7392.

(180) Cheng, B. M.; Grover, J. R.; Walters, E. A. *Chem. Phys. Lett.* **1995**, *232*, 364.

(181) Burgi, T.; Droz, T.; Leutwyler, S. *J. Chem. Phys.* **1995**, *103*, 7228.

(182) Burgi, T.; Droz, T.; Leutwyler, S. *Chem. Phys. Lett.* **1995**, *246*, 291.

(183) Brenner, V.; Martrenchardbarra, S.; Millie, P.; Dedonderlardeux, C.; Jouvet, C.; Solgadi, D. *J. Phys. Chem.* **1995**, *99*, 5848.

(184) Hager, J.; Wallace, S. C. *J. Phys. Chem.* **1984**, *88*, 5513.

(185) Read, W. G.; Campbell, E. J.; Henderson, G. *J. Chem. Phys.* **1983**, *78*, 3501.

(186) Abe, H.; Mikami, N.; Ito, M.; Udagawa, Y. *J. Phys. Chem.* **1982**, *86*, 2567.

(187) Abe, H.; Mikami, N.; Ito, M.; Udagawa, Y. *Chem. Phys. Lett.* **1982**, *93*, 217.

(188) Suzuki, S.; Green, P. G.; Bumgarner, R. E.; Dasgupta, S.; Goddard, W. A.; Blake, G. A. *Science* **1992**, *257*, 942.

(189) Augspurger, J. D.; Dykstra, C. E.; Zwier, T. S. *J. Phys. Chem.* **1992**, *96*, 7252.

(190) Zwier, T. S. *Annu. Rev. Phys. Chem.* **1996**, *47*, 205.

(191) Pribble, R. N.; Zwier, T. S. *Science* **1994**, *265*, 75.

(192) Pribble, R. N.; Hagemeister, F. C.; Zwier, T. S. *J. Chem. Phys.* **1997**, *106*, 2145.

(193) Garrett, A. W.; Severance, D. L.; Zwier, T. S. *J. Chem. Phys.* **1992**, *96*, 7245.

(194) Ebata, T.; Fujii, A.; Mikami, N. *Int. Rev. Phys. Chem.* **1998**, *17*, 331.

(195) Wehry, E.; Rogers, L. *J. Am. Chem. Soc.* **1965**, *87*, 4234.

(196) Abe, H.; Mikami, N.; Ito, M. *J. Phys. Chem.* **1982**, *86*, 1768.

(197) Abe, H.; Mikami, N.; Ito, M.; Udagawa, Y. *J. Phys. Chem.* **1982**, *86*, 2567.

(198) Abe, H.; Mikami, N.; Ito, M.; Udagawa, Y. *Chem. Phys. Lett.* **1982**, *93*, 217.

(199) Martrenchard, S.; Jouvet, C.; Lardeuxdedonder, C.; Solgadi, D. *J. Phys. Chem.* **1991**, *95*, 9186.

(200) Held, A.; Pratt, D. W. *J. Am. Chem. Soc.* **1993**, *115*, 9708.

(201) Young, L.; Haynam, C. A.; Levy, D. H. *J. Chem. Phys.* **1983**, *79*, 1592.

(202) Haynam, C. A.; Morter, C.; Young, L.; Levy, D. H. *J. Phys. Chem.* **1987**, *91*, 2526.

(203) Tomioka, Y.; Ito, M.; Mikami, N. *J. Phys. Chem.* **1983**, *87*, 4401.

(204) Honegger, E.; Bombach, R.; Leutwyler, S. *J. Chem. Phys.* **1986**, *85*, 1234.

(205) Joireman, P. W.; Ohline, S. M.; Connell, L. L.; Felker, P. M. *J. Phys. Chem.* **1993**, *97*, 12504.

(206) Shang, Q. Y.; Bernstein, E. R. *J. Chem. Phys.* **1992**, *97*, 60.

(207) Troxler, T.; Smith, P. G.; Stratton, J. R.; Topp, M. R. *J. Chem. Phys.* **1994**, *100*, 797.

(208) Troxler, T.; Smith, P. G.; Topp, M. R. *Chem. Phys. Lett.* **1993**, *211*, 371.

(209) Carney, J. R.; Hagemeister, F. C.; Zwier, T. S. *J. Chem. Phys.* **1998**, *108*, 3379.

(210) Carney, J. R.; Zwier, T. S. *J. Phys. Chem. A* **1999**, *103*, 9943.

(211) Clarkson, J. R.; Baquero, E.; Zwier, T. S. *J. Chem. Phys.* **2005**, *122*.

(212) Huang, Y.; Sulkes, M. *J. Phys. Chem.* **1996**, *100*, 16479.

(213) Brown, E.; Brown, R. *Ring nitrogen and key biomolecules*; Springer, 1998.

(214) Řezáč, J.; Riley, K. E.; Hobza, P. *J. Chem. Theory Comput.* **2011**, *7*, 3466.

(215) Jurečka, P.; Šponer, J.; Černý, J.; Hobza, P. *Phys. Chem. Chem. Phys.* **2006**, *8*, 1985.

(216) Abo-Riziq, A.; Grace, L.; Nir, E.; Kabelac, M.; Hobza, P.; De Vries, M. S. *Proc. Natl. Acad. Sci. U. S. A.* **2005**, *102*, 20.

(217) Nir, E.; Hünig, I.; Kleinermanns, K.; De Vries, M. S. *Phys. Chem. Chem. Phys.* **2003**, *5*, 4780.

(218) Nir, E.; Janzen, C.; Imhof, P.; Kleinermanns, K.; de Vries, M. S. *Phys. Chem. Chem. Phys.* **2002**, *4*, 732.

(219) Nir, E.; Plützer, C.; Kleinermanns, K.; De Vries, M. *European Physical Journal D* **2002**, *20*, 317.

(220) Plützer, C.; Hünig, I.; Kleinermanns, K.; Nir, E.; De Vries, M. S. *ChemPhysChem* **2003**, *4*, 838.

(221) Nir, E.; Kleinermanns, K.; de Vries, M. S. *Nature* **2000**, *408*, 949.

(222) Abo-Riziq, A.; Crews, B. O.; Compagnon, I.; Oomens, J.; Meijer, G.; Von Helden, G.; Kabeláč, M.; Hobza, P.; De Vries, M. S. *J. Phys. Chem. A* **2007**, *111*, 7529.

(223) Bakker, J. M.; Compagnon, I.; Meijer, G.; Von Helden, G.; Kabeláč, M.; Hobza, P.; De Vries, M. S. *Phys. Chem. Chem. Phys.* **2004**, *6*, 2810.

(224) Brauer, B.; Gerber, R. B.; Kabeláč, M.; Hobza, P.; Bakker, J. M.; Abo Riziq, A. G.; De Vries, M. S. *J. Phys. Chem. A* **2005**, *109*, 6974.

(225) Nir, E.; De Vries, M. S. *Int. J. Mass Spectrom.* **2002**, *219*, 133.

(226) Nir, E.; Kleinermanns, K.; Grace, L.; De Vries, M. S. *J. Phys. Chem. A* **2001**, *105*, 5106.

(227) Müller, A.; Talbot, F.; Leutwyler, S. *J. Am. Chem. Soc.* **2002**, *124*, 14486.

(228) Frey, J. A.; Muller, A.; Frey, H.-M.; Leutwyler, S. *J. Chem. Phys.* **2004**, *121*, 8237.

(229) Mueller, A.; Leutwyler, S. *J. Phys. Chem. A* **2004**, *108*, 6156.

(230) Mukherjee, M.; Bandyopadhyay, B.; Chakraborty, T. *Chem. Phys. Lett.* **2012**, *546*, 74.

(231) Mukherjee, M.; Karmakar, S.; Chakraborty, T. *Chem. Phys. Lett.* **2012**, *519*, 34.

(232) Hazra, M. K.; Samanta, A. K.; Chakraborty, T. *J. Phys. Chem. A* **2007**, *111*, 7813.

(233) Kumar, S.; Kaul, I.; Biswas, P.; Das, A. *J. Phys. Chem. A* **2011**, *115*, 10299.

(234) Kim, E.; Paliwal, S.; Wilcox, C. S. *J. Am. Chem. Soc.* **1998**, *120*, 11192.

(235) Paliwal, S.; Geib, S.; Wilcox, C. S. *J. Am. Chem. Soc.* **1994**, *116*, 4497.

(236) Sinnokrot, M. O.; Sherrill, C. D. *J. Am. Chem. Soc.* **2004**, *126*, 7690.

(237) Sinnokrot, M. O.; Sherrill, C. D. *J. Phys. Chem. A* **2003**, *107*, 8377.

(238) Ringer, A. L.; Sherrill, C. D. *J. Am. Chem. Soc.* **2009**, *131*, 4574.

(239) Arnstein, S. A.; Sherrill, C. D. *Phys. Chem. Chem. Phys.* **2008**, *10*, 2646.

(240) Hohenstein, E. G.; Duan, J.; Sherrill, C. D. *J. Am. Chem. Soc.* **2011**, *133*, 13244.

(241) Wheeler, S. E. *J. Am. Chem. Soc.* **2011**, *133*, 10262.

(242) Wheeler, S. E. *Acc. Chem. Res.* **2012**, *46*, 1029.

(243) Wheeler, S. E.; Houk, K. N. *J. Am. Chem. Soc.* **2008**, *130*, 10854.

(244) Ehrlich, S.; Moellmann, J.; Grimme, S. *Acc. Chem. Res.* **2012**, *46*, 916.

(245) Goly, T.; Spoerel, U.; Stahl, W. *Chem. Phys.* **2002**, *283*, 289.

(246) Leist, R.; Frey, J. A.; Leutwyler, S. *J. Phys. Chem. A* **2006**, *110*, 4180.

(247) Kabeláč, M.; Plützer, C.; Kleinermanns, K.; Hobza, P. *Phys. Chem. Chem. Phys.* **2004**, *6*, 2781.

(248) Callahan, M. P.; Gengeliczki, Z.; Svadlenak, N.; Valdes, H.; Hobza, P.; de Vries, M. S. *Phys. Chem. Chem. Phys.* **2008**, *10*, 2819.

(249) Maity, S.; Patwari, G. N.; Sedlak, R.; Hobza, P. *Phys. Chem. Chem. Phys.* **2011**, *13*, 16706.

(250) Lee, E. C.; Kim, D.; Jurecka, P.; Tarakeshwar, P.; Hobza, P.; Kim, K. S. *J. Phys. Chem. A* **2007**, *111*, 3446.

(251) Hobza, P.; Selzle, H. L.; Schlag, E. W. *J. Am. Chem. Soc.* **1994**, *116*, 3500.

(252) Hobza, P.; Selzle, H. L.; Schlag, E. W. *J. Phys. Chem.* **1996**, *100*, 18790.

(253) Pitonak, M.; Neogrady, P.; Rezac, J.; Jurecka, P.; Urban, M.; Hobza, P. *J. Chem. Theory Comput.* **2008**, *4*, 1829.

(254) Mishra, B. K.; Arey, J. S.; Sathyamurthy, N. *J. Phys. Chem. A* **2010**, *114*, 9606.

(255) Hohenstein, E. G.; Sherrill, C. D. *J. Phys. Chem. A* **2009**, *113*, 878.

(256) Guin, M.; Patwari, G. N.; Karthikeyan, S.; Kim, K. S. *Phys. Chem. Chem. Phys.* **2009**, *11*, 11207.

(257) Henson, B. F.; Hartland, G. V.; Venturo, V. A.; Hertz, R. A.; Felker, P. M. *Chem. Phys. Lett.* **1991**, *176*, 91.

(258) Henson, B. F.; Hartland, G. V.; Venturo, V. A.; Felker, P. M. *J. Chem. Phys.* **1992**, *97*, 2189.

(259) Arunan, E.; Gutowsky, H. S. *J. Chem. Phys.* **1993**, *98*, 4294.

(260) Maxton, P. M.; Schaeffer, M. W.; Ohline, S. M.; Kim, W.; Venturo, V. A.; Felker, P. M. *J. Chem. Phys.* **1994**, *101*, 8391.

(261) Erlekam, U.; Frankowski, M.; Meijer, G.; von Helden, G. *J. Chem. Phys.* **2006**, *124*, 171101.

(262) Erlekam, U.; Frankowski, M.; von Helden, G.; Meijer, G. *Phys. Chem. Chem. Phys.* **2007**, *9*, 3786.

(263) Matsumoto, Y.; Honma, K. *J. Chem. Phys.* **2007**, *127*, 184310.

(264) Dauster, I.; Rice, C. A.; Zielke, P.; Suhm, M. A. *Phys. Chem. Chem. Phys.* **2008**, *10*, 2827.

(265) Ottiger, P.; Pfaffen, C.; Leist, R.; Leutwyler, S.; Bachorz, R. A.; Klopper, W. *J. Phys. Chem. B* **2009**, *113*, 2937.

(266) Nakanaga, T.; Ito, F. *J. Phys. Chem. A* **1999**, *103*, 5440.

(267) Sugawara, K.-i.; Miyawaki, J.; Nakanaga, T.; Takeo, H.; Lembach, G.; Djafari, S.; Barth, H.-D.; Brutschy, B. *J. Phys. Chem.* **1996**, *100*, 17145.

(268) Chowdhury, P. K.; Sugawara, K.; Nakanaga, T.; Takeo, H. *Chem. Phys. Lett.* **1998**, *285*, 77.

(269) Piracha, N. K.; Ito, F.; Nakanaga, T. *Chem. Phys.* **2004**, *297*, 133.

(270) Kawamata, K.; Chowdhury, P. K.; Ito, F.; Sugawara, K.-i.; Nakanaga, T. *J. Phys. Chem. A* **1998**, *102*, 4788.

(271) Ohashi, K.; Inokuchi, Y.; Izutsu, H.; Hino, K.; Yamamoto, N.; Nishi, N.; Sekiya, H. *Chem. Phys. Lett.* **2000**, *323*, 43.

(272) Ohashi, K.; Inokuchi, Y.; Nishi, N.; Sekiya, H. *Chem. Phys. Lett.* **2002**, *357*, 223.

(273) Nishio, M. *Phys. Chem. Chem. Phys.* **2011**, *13*, 13873.

(274) Fleming, I. *Frontier orbitals and organic chemical reactions*; Wiley London, 1976; Vol. 731.

(275) Jurecka, P.; Sponer, J.; Cerny, J.; Hobza, P. *Phys. Chem. Chem. Phys.* **2006**, *8*, 1985.

(276) Desiraju, G. R.; Steiner, T. *The Weak Hydrogen Bond in Structural Chemistry and Biology*; Oxford University Press, New York, 1999.

(277) Han, L.-B.; Zhao, C.-Q.; Onozawa, S.-y.; Goto, M.; Tanaka, M. *J. Am. Chem. Soc.* **2002**, *124*, 3842.

(278) Sinnokrot, M. O.; Valeev, E. F.; Sherrill, C. D. *J. Am. Chem. Soc.* **2002**, *124*, 10887.

(279) Sinnokrot, M. O.; Sherrill, C. D. *J. Phys. Chem. A* **2004**, *108*, 10200.

(280) Sinnokrot, M. O.; Sherrill, C. D. *J. Phys. Chem. A* **2006**, *110*, 10656.

(281) Podeszwa, R.; Bukowski, R.; Szalewicz, K. *J. Phys. Chem. A* **2006**, *110*, 10345.

(282) DiStasio Jr, R. A.; von Helden, G.; Steele, R. P.; Head-Gordon, M. *Chem. Phys. Lett.* **2007**, *437*, 277.

(283) Janowski, T.; Pulay, P. *Chem. Phys. Lett.* **2007**, *447*, 27.

(284) Lee, E. C.; Kim, D.; Jurečka, P.; Tarakeshwar, P.; Hobza, P.; Kim, K. S. *J. Phys. Chem. A* **2007**, *111*, 3446.

(285) Pitoňák, M.; Neogrády, P.; Řezáč, J.; Jurečka, P.; Urban, M.; Hobza, P. *J. Chem. Theory Comput.* **2008**, *4*, 1829.

(286) Grafenstein, J.; Cremer, D. *J. Chem. Phys.* **2009**, *130*, 124105.

(287) Braun, J. E.; Grebner; Neusser, H. J. *J. Phys. Chem. A* **1998**, *102*, 3273.

(288) Braun, J.; Neusser, H. J.; Hobza, P. *J. Phys. Chem. A* **2003**, *107*, 3918.

(289) Geng, Y.; Takatani, T.; Hohenstein, E. G.; Sherrill, C. D. *J. Phys. Chem. A* **2010**, *114*, 3576.

(290) Biswal, H. S.; Gloaguen, E.; Mons, M.; Bhattacharyya, S.; Shirhatti, P. R.; Wategaonkar, S. *J. Phys. Chem. A* **2011**, *115*, 9485.

(291) Pfaffen, C.; Frey, H.-M.; Ottiger, P.; Leutwyler, S.; Bachorz, R. A.; Klopper, W. *Phys. Chem. Chem. Phys.* **2010**, *12*, 8208.

(292) Pfaffen, C.; Infanger, D.; Ottiger, P.; Frey, H.-M.; Leutwyler, S. *Phys. Chem. Chem. Phys.* **2011**, *13*, 14110.

(293) Hobza, P.; Sponer, J. *J. Am. Chem. Soc.* **2002**, *124*, 11802.

(294) Hong, B. H.; Lee, J. Y.; Cho, S. J.; Yun, S. G.; Kim, K. S. *J. Org. Chem.* **1999**, *64*, 5661.

(295) Lindeman, S. V.; Kosynkin, D.; Kochi, J. K. *J. Am. Chem. Soc.* **1998**, *120*, 13268.

(296) Scheiner, S.; Kar, T.; Pattanayak, J. *J. Am. Chem. Soc.* **2002**, *124*, 13257.

(297) Tarakeshwar, P.; Choi, H. S.; Kim, K. S. *J. Am. Chem. Soc.* **2001**, *123*, 3323.

(298) Lee, E. C.; Hong, B. H.; Lee, J. Y.; Kim, J. C.; Kim, D.; Kim, Y.; Tarakeshwar, P.; Kim, K. S. *J. Am. Chem. Soc.* **2005**, *127*, 4530.

(299) Hohenstein, E. G.; Sherrill, C. D. *J. Phys. Chem. A* **2009**, *113*, 878.

(300) Wang, W.; Hobza, P. *ChemPhysChem* **2008**, *9*, 1003.

(301) Kochanowska-Karamyan, A. J.; Hamann, M. T. *Chem. Rev. (Washington, DC, U. S.)* **2010**, *110*, 4489.

(302) Leist, R.; Frey, J. A.; Ottiger, P.; Frey, H.-M.; Leutwyler, S.; Bachorz, R. A.; Klopper, W. *Angew. Chem. Int. Ed.* **2007**, *46*, 7449.

(303) Guin, M.; Patwari, G. N.; Karthikeyan, S.; Kim, K. S. *Phys. Chem. Chem. Phys.* **2011**, *13*, 5514.

(304) Kabelac, M.; Plutzer, C.; Kleinermanns, K.; Hobza, P. *Phys. Chem. Chem. Phys.* **2004**, *6*, 2781.

(305) Rodham, D. A.; Suzuki, S.; Suenram, R. D.; Lovas, F. J.; Dasgupta, S.; Goddard, W. A.; Blake, G. A. *Nature* **1993**, *362*, 735.

(306) Mons, M.; Dimicoli, I.; Tardivel, B.; Piuzzi, F.; Brenner, V.; Millie, P. *Phys. Chem. Chem. Phys.* **2002**, *4*, 571.

(307) Courty, A.; Mons, M.; Dimicoli, I.; Piuzzi, F.; Gaigeot, M.-P.; Brenner, V.; de Pujo, P.; Millié, P. *J. Phys. Chem. A* **1998**, *102*, 6590.

(308) Chipot, C.; Jaffe, R.; Maigret, B.; Pearlman, D. A.; Kollman, P. A. *J. Am. Chem. Soc.* **1996**, *118*, 11217.

(309) Tsuzuki, S.; Honda, K.; Uchimaru, T.; Mikami, M.; Tanabe, K. *J. Am. Chem. Soc.* **2001**, *124*, 104.

(310) Sinnokrot, M. O.; Valeev, E. F.; Sherrill, C. D. *J. Am. Chem. Soc.* **2002**, *124*, 10887.

(311) Kumar, S.; Pande, V.; Das, A. *J. Phys. Chem. A* **2012**, *116*, 1368.

(312) Kumar, S.; Das, A. *J. Chem. Phys.* **2012**, *136*, 174302.

(313) Isozaki, T.; Tsutsumi, Y.-i.; Suzuki, T.; Ichimura, T. *Chem. Phys. Lett.* **2010**, *495*, 175.

(314) Aspiala, A.; Lotta, T.; Murto, J.; Räsänen, M. *Chem. Phys. Lett.* **1984**, *112*, 469.

(315) Biswal, H. S.; Wategaonkar, S. *J. Phys. Chem. A* **2009**, *113*, 12774.

(316) Dickinson, J. A.; Hockridge, M. R.; Kroemer, R. T.; Robertson, E. G.; Simons, J. P.; McCombie, J.; Walker, M. *J. Am. Chem. Soc.* **1998**, *120*, 2622.

(317) Goswami, M.; Arunan, E. *J. Mol. Spectrosc.* **2011**, *268*, 147.

(318) Sherrill, C. D.; Takatani, T.; Hohenstein, E. G. *J. Phys. Chem. A* **2009**, *113*, 10146.

(319) Mignon, P.; Loverix, S.; Geerlings, P. *Chem. Phys. Lett.* **2005**, *401*, 40.

(320) Kumar, S.; Biswas, P.; Kaul, I.; Das, A. *J. Phys. Chem. A* **2011**, *115*, 7461.

(321) Meyer, E. A.; Castellano, R. K.; Diederich, F. *Angew. Chem. Int. Ed.* **2003**, *42*, 1210.

(322) Salonen, L. M.; Ellermann, M.; Diederich, F. *Angew. Chem., Int. Ed.* **2011**, *50*, 4808.

(323) Tsuzuki, S.; Uchimaru, T.; Mikami, M. *J. Phys. Chem. A* **2006**, *110*, 2027.

(324) Ponzini, F.; Zagha, R.; Hardcastle, K.; Siegel, J. S. *Angew. Chem. Int. Ed.* **2000**, *39*, 2323.

(325) Hori, A.; Shinohe, A.; Yamasaki, M.; Nishibori, E.; Aoyagi, S.; Sakata, M. *Angew. Chem. Int. Ed.* **2007**, *46*, 7617.

(326) Coates, G. W.; Dunn, A. R.; Henling, L. M.; Dougherty, D. A.; Grubbs, R. H. *Angew. Chem. Int. Ed.* **1997**, *36*, 248.

(327) Coates, G. W.; Dunn, A. R.; Henling, L. M.; Ziller, J. W.; Lobkovsky, E. B.; Grubbs, R. H. *J. Am. Chem. Soc.* **1998**, *120*, 3641.

(328) Thomas, A.; Meurisse, R.; Charloteaux, B.; Brasseur, R. *Proteins: Struct., Funct., Genet.* **2002**, *48*, 628.

(329) Thomas, A.; Meurisse, R.; Brasseur, R. *Proteins: Struct., Funct., Genet.* **2002**, *48*, 635.

(330) Meurisse, R.; Brasseur, R.; Thomas, A. *Biochim. Biophys. Acta, Proteins Proteomics* **2003**, *1649*, 85.

(331) Meurisse, R.; Brasseur, R.; Thomas, A. *Proteins: Struct., Funct., Bioinf.* **2004**, *54*, 478.

(332) Moreno-Villoslada, I.; Gonzalez, F.; Rivera, L.; Hess, S.; Rivas, B. L.; Shibue, T.; Nishide, H. *J. Phys. Chem. B* **2007**, *111*, 6146.

(333) Uemori, Y.; Takinami, S.; Takahashi, A.; Munakata, H.; Imai, H.; Nakagawa, S.; Kyuno, E. *Inorg. Chim. Acta* **1994**, *224*, 157.

(334) Katagiri, K.; Tohaya, T.; Masu, H.; Tominaga, M.; Azumaya, I. *J. Org. Chem.* **2009**, *74*, 2804.

(335) Shi, J.; Gao, Y.; Yang, Z.; Xu, B. *Beilstein J. Org. Chem.* **2011**, *7*, 167.

(336) Gloaguen, E.; Valdes, H.; Pagliarulo, F.; Pollet, R.; Tardivel, B.; Hobza, P.; Piuzzi, F.; Mons, M. *J. Phys. Chem. A* **2010**, *114*, 2973.

(337) Zhang, Z.-T.; Zhang, X.-L. *J. Chem. Crystallogr.* **2008**, *38*, 129.

(338) Anderson, D. E.; Hurley, J. H.; Nicholson, H.; Baase, W. A.; Matthews, B. W. *Protein Sci.* **1993**, *2*, 1285.

(339) Valdes, H.; Pluhackova, K.; Hobza, P. *J. Chem. Theory Comput.* **2009**, *5*, 2248.

(340) Burley, S. K.; Petsko, G. A. *Science* **1985**, *229*, 23.

(341) Luo, Y.; Samuel, J.; Mosimann, S. C.; Lee, J. E.; Tanner, M. E.; Strynadka, N. C. J. *Biochemistry* **2001**, *40*, 14763.

(342) Erlekam, U.; Frankowski, M.; Meijer, G.; von Helden, G. *J. Chem. Phys.* **2006**, *124*, 171101.

(343) Bornsen, K. O.; Lin, S. H.; Selzle, H. L.; Schlag, E. W. *J. Chem. Phys.* **1989**, *90*, 1299.

(344) Engkvist, O.; Hobza, P.; Selzle, H. L.; Schlag, E. W. *J. Chem. Phys.* **1999**, *110*, 5758.

(345) Henson, B. F.; Venturo, V. A.; Hartland, G. V.; Felker, P. M. *J. Chem. Phys.* **1993**, *98*, 8361.

(346) Kolaski, M.; Kumar, A.; Singh, N. J.; Kim, K. S. *Phys. Chem. Chem. Phys.* **2011**, *13*, 991.

(347) Connell, L. L.; Ohline, S. M.; Joireman, P. W.; Corcoran, T. C.; Felker, P. M. *J. Chem. Phys.* **1992**, *96*, 2585.

(348) Schmitt, M.; Henrichs, U.; Muller, H.; Kleinermanns, K. *J. Chem. Phys.* **1995**, *103*, 9918.

(349) Zhao, Y.; Truhlar, D. G. *J. Chem. Theory Comput.* **2007**, *3*, 289.

(350) Kantrowitz, A.; Grey, J. *Rev. Sci. Instrum.* **1951**, *22*, 328.

(351) Kistiakowsky, G. B.; Slichter, W. P. *Rev. Sci. Instrum.* **1951**, *22*, 333.

(352) Becker, E. W.; Bier, K. *Z. Naturforsch* **1954**, *92*, 975.

(353) Smalley, R. E.; Wharton, L.; Levy, D. H. *Acc. Chem. Res***1977**, *10*, 139.

(354) Levy, D. H. *Annu. Rev. Phys. Chem.* **1980**, *31*, 197.

(355) Levy, D. H. *Science* **1981**, *214*, 263.

(356) de Vries, M. S.; Hobza, P. *Annu. Rev. Phys. Chem.* **2007**, *58*, 585.

(357) Morse, M. D. *Atomic, Molecular, and Optical Physics: Atoms and Molecules. Series: Experimental Methods in the Physical Sciences, ISBN: 9780124759763. Elsevier, vol. 29, pp. 21-47* **1996**, *29*, 21.

(358) Imasaka, T.; Moore, D. S.; Vo-Dinh, T. *Pure Appl. Chem.* **2003**, *75*, 975.

(359) Rademann, K.; Brutschy, B.; Baumgärtel, H. *Chem. Phys.* **1983**, *80*, 129.

(360) Page, R. H.; Shen, Y.; Lee; YT *Phys. Rev. Lett.* **1987**, *59*, 1293.

(361) Wiley, W. C.; McLaren, I. H. *Rev. Sci. Instrum.* **1955**, *26*, 1150.

(362) Sorokin, P.; Lankard, J. *IBM J. Res. Dev.* **1966**, *10*, 162.

(363) Duarte, F. J.; Kelley, P.; Hillman, L. W.; Liao, P. F. *Dye laser principles*; Elsevier Science, 2012.

(364) Ferguson, A. **1991**.

(365) Liao, P. F.; Kelley, P.; Duarte, F. J.; Hillman, L. W. *Dye Laser Principles: With Applications*; Elsevier, 2012.

(366) Sorokin, P.; Lankard, J. *IBM J. Res. Dev.* **1967**, *11*, 148.

(367) Perry, M. D.; Weston, J.; Ettlebrick, R.; Landen, O. L. *Opt. Lett.* **1989**, *14*, 42.

(368) Page, R. H.; Shen, Y.; Lee, Y.-T. *J. Chem. Phys.* **1988**, *88*, 5362.

(369) Crews, B. O. *UV and IR Double Resonance Spectroscopy of Peptides, DNA Bases and Clusters*; ProQuest, 2007.

(370) Schermann, J.-P. *Spectroscopy and Modeling of Biomolecular Building Blocks*; Elsevier, 2007.

(371) Gerhards, M.; Perl, W.; Kleinermanns, K. *Chem. Phys. Lett.* **1995**, *240*, 506.

(372) Frisch, M. J.; Trucks, G. W.; Schlegel, H. B.; Scuseria, G. E.; Robb, M. A.; Cheeseman, J. R.; Scalmani, G.; Barone, V.; Mennucci, B.; Petersson, G. A.; Nakatsuji, H.; Caricato, M.; Li, X. H., H. P.; Izmaylov, A. F. B., J.; Zheng, G.; Sonnenberg, J. L.; Hada, M.; Ehara, M.; Toyota, K.; Fukuda, R.; Hasegawa, J.; Ishida, M.; Nakajima, T.; Honda, Y.; Kitao, O.; Nakai, H.; Vreven, T.; Montgomery, J., J. A.; Peralta, J. E.; Ogliaro, F.; Bearpark, M.; Heyd, J. J.; Brothers, E.; Kudin, K. N.; Staroverov, V. N.; Kobayashi, R.; Normand, J.; Raghavachari, K.; Rendell, A.; Burant, J. C.; Iyengar, S. S.; Tomasi, J.; Cossi, M.; Rega, N.; Millam, N. J.; Klene, M.; Knox, J. E.; Cross, J. B.; Bakken, V.; Adamo, C.; Jaramillo, J.; Gomperts, R.; Stratmann, R. E.; Yazyev, O.; Austin, A. J.; Cammi, R.; Pomelli, C.; Ochterski, J. W.; Martin, R. L.; Morokuma, K.; Zakrzewski, V. G.; Voth, G. A.; Salvador, P.; Dannenberg, J. J.; Dapprich, S.; Daniels, A. D.; Farkas, Ö.; Foresman, J. B.; Ortiz, J. V.; Cioslowski, J.; Fox, D. J. *GAUSSIAN 09, Revision B.01, Gaussian, Inc., Wallingford CT,* **2009**.

(373) Schmidt, M. W.; Baldridge, K. K.; Boatz, J. A.; Elbert, S. T.; Gordon, M. S.; Jensen, J. H.; Koseki, S.; Matsunaga, N.; Nguyen, K. A.; Su, S.; Windus, T. L.; Dupuis, M.; Montgomery, J. A. *J. Comput. Chem.* **1993**, *14*, 1347.

(374) Valiev, M.; Bylaska, E. J.; Govind, N.; Kowalski, K.; Straatsma, T. P.; Van Dam, H. J. J.; Wang, D.; Nieplocha, J.; Apra, E.; Windus, T. L.; de Jong, W. A. In *Comput. Phys. Commun.* 2010; Vol. 181, p 1477.

(375) Head-Gordon, M.; Pople, J. A.; Frisch, M. J. *Chem. Phys. Lett.* **1988**, *153*, 503.

(376) Frisch, M. J.; Head-Gordon, M.; Pople, J. A. *Chem. Phys. Lett.* **1990**, *166*, 281.

(377) Head-Gordon, M.; Head-Gordon, T. *Chem. Phys. Lett.* **1994**, *220*, 122.

(378) Becke, A. D. *J. Chem. Phys.* **1993**, *98*, 5648.

(379) Grimme, S. *J. Comput. Chem.* **2006**, *27*, 1787.

(380) Chai, J.-D.; Head-Gordon, M. *Phys. Chem. Chem. Phys.* **2008**, *10*, 6615.

(381) Zhao, Y.; Schultz, N. E.; Truhlar, D. G. *J. Chem. Theory Comput.* **2006**, *2*, 364.

(382) Zhao, Y.; Truhlar, D. G. *Theor. Chem. Acc.* **2008**, *120*, 215.

(383) Boys, S. F.; Bernardi, F. *Mol. Phys.* **1970**, *19*, 553.

(384) Su, P.; Li, H. *J. Chem. Phys.* **2009**, *131*, 014102.

(385) Kitaura, K.; Morokuma, K. *Int. J. Quantum Chem.* **1976**, *10*, 325.

(386) Ziegler, T.; Rauk, A. *Inorg. Chem.* **1979**, *18*, 1755.

(387) Hayes, I. C.; Stone, A. J. *Mol. Phys.* **1984**, *53*, 83.

(388) Glendening, E. D.; Reed, A. E.; Carpenter, J. E.; Weinhold, F., NBO Version 3.1; online at http://www.gaussian.com/g_tech/g_ur/m_citation.htm.

(389) Glendening, E. D.; Landis, C. R.; Weinhold, F. *Wiley Interdiscip. Rev.: Comput. Mol. Sci.* **2012**, *2*, 1.

(390) Sanders, J. M. *J. Phys. Chem. A* **2010**, *114*, 9205.

(391) Cilento, G.; Tedeschi, P. *J. Biol. Chem.* **1961**, *236*, 907.

(392) Vacca, R. A.; Christen, P.; Malashkevich, V. N.; Jansonius, J. N.; Sandmeier, E. *Eur. J. Biochem.* **1995**, *227*, 481.

(393) McClelland, H. E.; Jurs, P. C. *J. Chem. Inf. Comput. Sci.s* **2000**, *40*, 967.

(394) Hager, J. W.; Demmer, D. R.; Wallace, S. C. *J. Phys. Chem.* **1987**, *91*, 1375.

(395) Sobolewski, A. L.; Domcke, W. *J. Phys. Chem. A* **2007**, *111*, 11725.

(396) Hager, J.; Wallace, S. C. *J. Phys. Chem.* **1984**, *88*, 5513.

(397) Villa, E.; Amirav, A.; Lim, E. C. *J. Phys. Chem.* **1988**, *92*, 5393.

(398) Carney, J. R.; Zwier, T. S. *J. Phys. Chem. A* **1999**, *103*, 9943.

(399) Biswal, H. S.; Wategaonkar, S. *J. Phys. Chem. A* **2010**, *114*, 5947.

(400) Maity, S.; Patwari, G. N. *J. Phys. Chem. A* **2010**, *114*, 8337.

(401) Naresh Patwari, G.; Ebata, T.; Mikami, N. *J. Chem. Phys.* **2002**, *116*, 6056.

(402) Nibu, Y.; Marui, R.; Shimada, H. *J. Phys. Chem. A* **2006**, *110*, 12597.

(403) Van Sickle, K.; Culberson, L. M.; Holzmacher, J. L.; Cafiero, M. *Int. J. Quantum Chem.* **2007**, *107*, 1523.

(404) Zhao, Y.; Truhlar, D. G. *Acc. Chem. Res***2008**, *41*, 157.

(405) Šponer, J.; Riley, K. E.; Hobza, P. *Phys. Chem. Chem. Phys.* **2008**, *10*, 2595.

(406) Biswal, H. S.; Wategaonkar, S. *J. Phys. Chem. A* **2009**, *113*, 12763.

(407) Tubergen, M. J.; Levy, D. H. *J. Phys. Chem.* **1991**, *95*, 2175.

(408) Benharash, P.; Gleason, M. J.; Felker, P. M. *J. Phys. Chem. A* **1999**, *103*, 1442.

(409) Leist, R.; Frey, J. A.; Ottiger, P.; Frey, H.-M.; Leutwyler, S.; Bachorz, R. A.; Klopper, W. *Angew. Chem. Int. Ed.* **2007**, *46*, 7449.

(410) James Iii, W. H.; Müller, C. W.; Buchanan, E. G.; Nix, M. G. D.; Guo, L.; Roskop, L.; Gordon, M. S.; Slipchenko, L. V.; Gellman, S. H.; Zwier, T. S. *J. Am. Chem. Soc.* **2009**, *131*, 14243.

(411) Biswal, H. S.; Wategaonkar, S. *J. Phys. Chem. A* **2009**, *113*, 12774.

(412) Dauster, I.; Rice, C. A.; Zielke, P.; Suhm, M. A. *Phys. Chem. Chem. Phys.* **2008**, *10*, 2827.

(413) Iga, H.; Isozaki, T.; Suzuki, T.; Ichimura, T. *J. Phys. Chem. A* **2007**, *111*, 5981.

(414) Matsumoto, Y.; Honma, K. *Phys. Chem. Chem. Phys.* **2011**, *13*, 13962.

(415) Ottiger, P.; Pfaffen, C.; Leist, R.; Leutwyler, S.; Bachorz, R. A.; Klopper, W. *J. Phys. Chem. B* **2009**, *113*, 2937.

(416) Ottiger, P.; Pfaffen, C.; Leist, R.; Leutwyler, S.; Bachorz, R. A.; Klopper, W. *J. Phys. Chem. B* **2009**, *113*, 2937.

(417) Pfaffen, C.; Frey, H.-M.; Ottiger, P.; Leutwyler, S.; Bachorz, R. A.; Klopper, W. *Phys. Chem. Chem. Phys.* **2010**, *12*, 8208.

(418) Pfaffen, C.; Infanger, D.; Ottiger, P.; Frey, H.-M.; Leutwyler, S. *Phys. Chem. Chem. Phys.* **2011**, *13*, 14110.

(419) Gul, W.; Hamann, M. T. *Life Sciences* **2005**, *78*, 442.

(420) Lalko, J. *Med. Dosw. Mikrobiol.* **1975**, *27*, 1.

(421) Medower, C.; Wen, L.; Johnson, W. W. *Chem. Res. Toxicol.* **2008**, *21*, 1570.

(422) Nguyen, T. L.; Cera, M. R.; Pinto, A.; Lo Presti, L.; Hamel, E.; Conti, P.; Gussio, R.; De Wulf, P. *Mol. Cancer Ther.* **2012**, *11*, 1103.

(423) Sharma, V.; Kumar, P.; Pathak, D. *J. Heterocycl. Chem.* **2010**, *47*, 491.

(424) Zhan, Y.; Wang, X.; Shao, H. *Adv. Chem. Res.* **2012**, *15*, 133.

(425) Carney, J. R.; Hagemeister, F. C.; Zwier, T. S. *J. Chem. Phys.* **1998**, *108*, 3379.

(426) Gengeliczki, Z.; Callahan, M. P.; Kabeláč, M.; Rijs, A. M.; de Vries, M. S. *J. Phys. Chem. A* **2011**, *115*, 11423.

(427) Pande, V. MS Thesis, IISER PUNE, 2011.

(428) Silbey, R. J.; Alberty, R. A. *Physical Chemistry*; 3rd ed.; John Wiley & Sons, Singapore, 2002.

(429) Su, P.; Li, H. *J. Chem. Phys.* **2009**, *131*, 14102.

(430) Maity, S.; Patwari, G. N.; Karthikeyan, S.; Kim, K. S. *Phys. Chem. Chem. Phys.* **2010**, *12*, 6150.

(431) Zheng, H.; Gao, J. *Angew. Chem. Int. Ed.* **2010**, *49*, 8635.

(432) Finzel, B. C.; Baldwin, E. T.; Bryant, G. L.; Hess, G. F.; Wilks, J. W.; Trepod, C. M.; Mott, J. E.; Marshall, V. P.; Petzold, G. L.; Poorman, R. A.; O'Sullivan, T. J.; Schostarez, H. J.; Mitchell, M. A. *Protein Science* **1998**, *7*, 2118.

(433) Gallivan, J. P.; Dougherty, D. A. *Organic Letters* **1999**, *1*, 103.

(434) Danten, Y.; Tassaing, T.; Besnard, M. *J. Phys. Chem. A* **1999**, *103*, 3530.

(435) Amicangelo, J. C.; Irwin, D. G.; Lee, C. J.; Romano, N. C.; Saxton, N. L. *J. Phys. Chem. A* **2013**, *117*, 1336.

(436) Mons, M.; Dimicoli, I.; Tardivel, B.; Piuzzi, F.; Brenner, V.; Millié, P. *J. Phys. Chem. A* **1999**, *103*, 9958.

(437) Hager, J.; Ivanco, M.; Smith, M. A.; Wallace, S. C. *Chem. Phys.* **1986**, *105*, 397.

(438) Brand, C.; Kupper, J.; Pratt, D. W.; Leo Meerts, W.; Krugler, D.; Tatchen, J.; Schmitt, M. *Phys. Chem. Chem. Phys.* **2010**, *12*, 4968.

(439) Kumar, S.; Das, A. *J. Chem. Phys.* **2012**, *137*, 094309.

(440) Bachorz, R. A.; Bischoff, F. A.; Hofener, S.; Klopper, W.; Ottiger, P.; Leist, R.; Frey, J. A.; Leutwyler, S. *Phys. Chem. Chem. Phys.* **2008**, *10*, 2758.

(441) Dunitz, J. D.; Taylor, R. *Chem. – Eur. J.* **1997**, *3*, 89.

(442) Ruoff, R. S.; Klots, T. D.; Emilsson, T.; Gutowsky, H. S. *J. Chem. Phys.* **1990**, *93*, 3142.

(443) Alagona, G.; Ghio, C.; Monti, S. *J. Phys. Chem. A* **1998**, *102*, 6152.

(444) Moore, S. A.; James, M. N. G. *J. Mol. Biol.* **1995**, *249*, 195.

(445) Buckle, A. M.; Fersht, A. R. *Biochemistry* **1994**, *33*, 1644.

(446) Zischang, J.; Lee, J. J.; Suhm, M. A. *J. Chem. Phys.* **2011**, *135*, 061102.

(447) Choi, M. Y.; Miller, R. E. *J. Phys. Chem. A* **2006**, *110*, 9344.

(448) Wassermann, T. N.; Rice, C. A.; Suhm, M. A.; Luckhaus, D. *J. Chem. Phys.* **2007**, *127*, 234309.

(449) Gómez-Zavaglia, A.; Fausto, R. *J. Phys. Chem. A* **2004**, *108*, 6953.

(450) Huisken, F.; Kaloudis, M.; Koch, M.; Werhahn, O. *J. Chem. Phys.* **1996**, *105*, 8965.

(451) Zielke, P.; Suhm, M. A. *Phys. Chem. Chem. Phys.* **2006**, *8*.

(452) Larsen, R. W.; Zielke, P.; Suhm, M. A. *J. Chem. Phys.* **2007**, *126*, 194307.

(453) Pugliano, N.; Saykally, R. J. *Science* **1992**, *257*, 1937.

(454) Liu, K.; Loeser, J. G.; Elrod, M. J.; Host, B. C.; Rzepiela, J. A.; Pugliano, N.; Saykally, R. J. *J. Am. Chem. Soc.* **1994**, *116*, 3507.

(455) Liu, K.; Cruzan, J. D.; Saykally, R. J. *Science* **1996**, *271*, 929.

(456) Schutz, M.; Burgi, T.; Leutwyler, S.; Burgi, H. B. *J. Chem. Phys.* **1993**, *99*, 5228.

(457) Xantheas, S. S. *J. Chem. Phys.* **1995**, *102*, 4505.

(458) Bussi, G.; Ruini, A.; Molinari, E.; Caldas, M. J.; Puschnig, P.; Ambrosch-Draxl, C. *Appl. Phys. Lett.* **2002**, *80*, 4118.

(459) Jouvet, C.; Dedonder-Lardeux, C.; Martrenchard-Barra, S.; Solgadi, D. *Chem. Phys. Lett.* **1992**, *198*, 419.

(460) Johnson, P. M.; Zhu, L. *Int. J. Mass Spectrom. Ion Processes* **1994**, *131*, 193.

(461) Zhang, X.; Smith, J. M.; Knee, J. *J. Chem. Phys.* **1993**, *99*, 3133.